AN INVESTIGATION INTO IMPROVING PERFORMANCE OF CELLULAR CDMA COMMUNICATION SYSTEMS WITH DIGITAL BEAMFORMING

by

A. Mark Earnshaw

A thesis submitted to the
Department of Electrical and Computer Engineering
in conformity with the requirements
for the degree of Doctor of Philosophy

Queen's University
Kingston, Ontario, Canada
October 1997

Abstract

Wireless cellular technology is one of the fields in communications that is currently undergoing phenomenally rapid growth. As the demand for wireless connectivity increases, it is necessary to develop next-generation cellular systems to handle the increased number of users. CDMA (Code Division Multiple Access) is one technique that promises enhanced efficiency of radio spectrum use since it is strictly interference-limited, unlike FDMA (Frequency Division Multiple Access) or TDMA (Time Division Multiple Access).

Total system capacity can be improved by increasing the number of base stations while simultaneously decreasing the size of each cell. However, this is a potentially expensive solution in terms of the equipment required and would also require more frequent hand-offs between adjacent cells. In a CDMA system, an alternative is to reduce multi-user interference, thereby permitting more mobiles to operate within each cell. One method for accomplishing this is through the use of beamforming. By using an array of antenna elements, it is possible to select a suitable set of weighting values so that when the antenna array outputs are summed, the interference from other users is suppressed relative to the desired signal. As a result, it is then possible to accommodate additional mobiles within the same cell.

The IS-95 cellular CDMA standard has been established by Qualcomm and is used within the context of this thesis. Only the reverse link (mobile to base) has currently been investigated due to the fact that beamforming can only be effectively performed at the base station. This communication link is presented and analyzed in detail at the beginning of the thesis. Power control, which has been shown to be necessary for a CDMA cellular system, is then examined. The coding scheme for the IS-95 reverse link is such that a conventional Viterbi decoder produces suboptimal results. A

combined deinterleaver/decoder offering a gain of at least 1 dB over standard Viterbi decoding is presented here.

One of the main areas of beamforming research has been in estimating suitable coefficient weights from the received data. The code-filtering correlation method developed at Stanford [64] [67] [73] [74] has demonstrated promising results, although it cannot be applied directly to IS-95 due to the coding techniques used on the reverse link. This thesis has developed an additional feedback correlation algorithm which provides sufficient gain to estimate accurate beamforming weights. An accompanying error analysis derives the probability distributions of the various estimators and determines the effects of noise and interference on the measurements. This includes an eigenvector perturbation analysis for complex Hermitian matrices. A following analysis into the statistical parameters of various reverse link correlation quantities is used to validate the simulation program.

An investigation into cell capacity improvement through the use of antenna arrays and beamforming is then performed. Simulations are performed with both a PN chip-level method and a more computationally efficient power-level technique which is used to obtain capacity estimates for higher numbers of antenna elements. Predicted capacity values from the system analysis show good agreement with the observed results. Finally, an investigation into multi-service (*e.g.* voice and data) cell capacity is performed, with both simulated and analytical results.

Acknowledgements

I would like to thank my supervisor, Dr. Steven Blostein, for his excellent guidance, encouragement, patience, and support during my time at Queen's. It took longer than originally expected, but we made it.

To all of the friends and colleagues I have had over the past several years, thanks for all of the good times and assistance, both technical and non-technical. I have made some friendships here which should last for the rest of my life.

I would like to thank my parents and other family members for their friendship and encouragement throughout my long academic career. It's nice to have people who believe in you.

The many CPU months put in by the lab computers should be acknowledged. The simulation results contained within this thesis are due to the efforts of cassini, explorer, galileo, huygens, magellan, ranger, surveyor, and ulysses.

This work was supported by the Canadian Institute for Telecommunications Research, the Information Technology Research Centre, the Natural Sciences and Engineering Research Council, and the School of Graduate Studies and Research at Queen's University.

Contents

List of Tables

List of Figures

List of Symbols

α_i	relative phase angle of i^{th} element of array response vector element
β_k	signal envelope for k^{th} mobile at the receiver
γ_i	physical angular location of i^{th} element in a circular antenna array
$\Delta_{\mathrm{R}\mathbf{vv}}$	perturbation of a Hermitian matrix for investigating its effects on the eigenvectors and eigenvalues of the Hermitian matrix
ϵ	path loss exponent
η_k	signal attenuation over the transmission channel for mobile k
θ	direction of propagation of plane wave
θ_{I_k}	in-phase angle used for generating a ± 1 component in the signal
θ_{Q_k}	quadrature angle used for generating a ± 1 component in the signal
Θ	diagonal matrix containing required phase shift values for the complex eigenvectors of a Hermitian matrix in order to generate a strictly real uncorrelated vector
λ	eigenvalue of a matrix
λ_c	wavelength of the carrier frequency
Λ	diagonal matrix with eigenvalues of a covariance matrix along the main diagonal
μ_Υ	mean of summation of sums of squared sin and cos terms when calculating power in a signal from a multi-element antenna array
$(\mu_\Upsilon)_D$	mean of summation of squared sin and cos terms when calculating power in a signal from a multi-element antenna array for data mobiles only
$(\mu_\Upsilon)_V$	mean of summation of squared sin and cos terms when calculating power in a signal from a multi-element antenna array for voice mobiles only
μ_c	mean PN chip correlation value

μ_C	mean of summation of cos terms when calculating power in a signal from a multi-element antenna array
μ_f	mean number of speech active mobiles for a given voice activity factor
μ_F	mean Walsh function correlation value when received signal is correlated with the correct Walsh function
$\mu_{\overline{F}}$	mean Walsh function correlation value when received signal is correlated with the incorrect Walsh function
$\mu_{p(n_s)}$	mean value of $\hat{p}(n_s)$
$\mu_{\mathbf{q}}$	mean vector of normalized mean estimate of array response vector using feedback correlation method
μ_s	mean of the number of frames with the specified number of speech active mobiles
μ_S	mean of summation of sin terms when calculating power in a signal from a multi-element antenna array
μ_V	mean of Gaussian random variable used for predicting expected received power
μ_w	mean Walsh chip correlation value
ν	factor by which transmitted power is reduced when speech is not active
ρ_k	path loss attenuation factor for mobile k
$\hat{\sigma}$	entry in the covariance matrix of the observed $\hat{\mathrm{r}}_{\mathbf{vv}}$ ($\mathrm{C}_{\hat{\mathbf{r}}\mathbf{vv}}$)
σ^2_χ	variance of a χ^2 random variable
σ^2_Υ	variance of summation of squared sums of sin and cos terms when calculating power in a signal from a multi-element antenna array
$(\sigma^2_\Upsilon)_D$	variance of summation of squared sin and cos terms when calculating power in a signal from a multi-element antenna array for data mobiles only
$(\sigma^2_\Upsilon)_V$	variance of summation of squared sin and cos terms when calculating power in a signal from a multi-element antenna array for voice mobiles only
σ^2_c	variance of the PN chip correlation value
σ^2_C	variance of summation of cos terms when calculating power in a signal from a multi-element antenna array
σ^2_f	variance of the number of speech active mobiles for a given voice activity factor
σ^2_F	variance of the Walsh function correlation value
σ^2_n	variance (power) of the background thermal noise
$\sigma^2_{p(n_s)}$	variance of $\hat{p}(n_s)$

σ_s^2	variance of the number of frames with the specified number of speech active mobiles
$\sigma_{\mathcal{S}}^2$	variance of the shadowing random variable
σ_S^2	variance of summation of sin terms when calculating power in a signal from a multi-element antenna array
σ_V^2	variance of Gaussian random variable used for predicting expected received power
σ_w^2	variance of the Walsh chip correlation value
τ_{kp}	time delay of k^{th} mobile's signal relative to p^{th} mobile's signal
Υ	summation of squared sums of sin and cos terms when calculating power in a signal from a multi-element antenna array
ϕ_i	relative phase angle of i^{th} entry of beamforming weight vector
Φ	uniformly distributed random variable representing a phase angle in the interval $[0, 2\pi)$
φ	angle formed within a circular antenna array by two adjacent elements
ψ	mean percentage of time that a user is actually talking (voice activity factor)
$\mathbf{a}_k$	array response vector for k^{th} mobile
b_i	number of known bits at i^{th} Walsh function position in interleaved Viterbi decoding
B	bandwidth of spread signal
$\mathrm{B_C}$	constrained Cramér-Rao Lower Bound for an array response vector estimator
B_E	actual bit error rate
$\hat{B}_E$	observed bit error rate
C	summation of cos terms when calculating power in a signal from a multi-element antenna array
C_F	correlation value for a Walsh function position within a surviving path
$C_{I_k}[r]$	in-phase PN code sequence for k^{th} mobile
$\mathrm{C}_{\mathbf{pp}}$	covariance matrix of feedback correlation method principal eigenvector estimate
$\hat{\mathrm{C}}_{\mathbf{pp}}$	modified covariance matrix of feedback correlation method principal eigenvector estimate
$\mathrm{C}_{\mathbf{qq}}$	covariance matrix of normalized mean estimate of array response vector using feedback correlation method
$\hat{\mathrm{C}}_{\mathbf{qq}}$	modified covariance matrix corresponding to $\mathrm{C}_{\mathbf{qq}}$
$C_{Q_k}[r]$	quadrature PN code sequence for k^{th} mobile

$\mathrm{C}_{\mathbf{uu}}$	covariance matrix of mean vector of feedback correlation estimation method
$\mathrm{C}_{\mathbf{ww}}$	covariance matrix of uncorrelated complex Gaussian random vector
$\mathrm{C}_{\mathbf{vv}}$	covariance matrix for feedback correlation vector as correlated over the length of one Walsh function sequence
$\mathrm{C}_{\mathbf{yy}}$	covariance matrix of uncorrelated real Gaussian random vector
d	distance between correct and incorrect surviving paths in a decoder measured in terms of incorrect Walsh functions
d_{free}	minimum free distance of a convolutional code
d_k	distance from k^{th} mobile to base station
D_i	distance along direction of wave propagation between centre of array and i^{th} antenna element
D_A	spacing between adjacent elements in an antenna array
D_{I_k}	demodulated in-phase signal for k^{th} mobile
D_{Q_k}	demodulated quadrature signal for k^{th} mobile
erf	error function ($\text{erf}(x) = \frac{2}{\sqrt{\pi}} \int_0^x e^{-t^2} dt$)
erfc	complementary error function ($\text{erfc}(x) = 1 - \text{erf}(x)$)
E_b/N_0	ratio of bit energy to noise and interference density
E_{max}	maximum desired squared error between observed and expected distributions of speech active mobiles when calculating confidence intervals
E_T	total squared error between observed and expected distributions of speech active mobiles when calculating confidence intervals
f_c	carrier frequency
F	number of frames included in a power-level capacity estimation simulation run
F_F	number of Walsh functions per frame
$\mathrm{G}_{\mathbf{q}}$	equality constraint for calculating the constrained Cramér-Rao Lower Bound of an array response vector estimator
$G_{\mathbf{v}}$	processing gain obtained by using the feedback correlation method of beamforming
$G_{\mathbf{z}}$	processing gain obtained by using the code-filtering correlation method of beamforming
I	identity matrix
I_p	random variable specifying the interference to mobile p's signal due to other mobiles
J	Fisher information matrix
$\mathcal{M}_P$	surviving path metric for Viterbi decoding

$\mathcal{M}_W$	metric value for a Walsh function in Viterbi decoding
M	metric value for a portion of a surviving path in a Viterbi decoder
$\mathbf{n}$	thermal background noise vector
n	thermal background noise
N	number of output bit errors for a given path in a Viterbi decoder
N_A	number of antenna elements
N_B	number of bits which should be processed to obtain a desired confidence interval for the true BER
N_D	number of data mobiles
$N_f(n_s)$	random variable representing the number of frames which have a specified number of speech active mobiles
N_F	number of Walsh chips in one Walsh function sequence
N_I	number of interferers with active speech
N_M	number of mobiles
N_s	random variable representing the number of speech active mobiles in a given frame
N_S	number of surviving paths retained at each trellis node while Viterbi decoding
N_V	number of voice mobiles
N_W	number of PN chips in one Walsh chip
$\mathbf{p}$	array response vector estimate using the principal eigenvector of the feedback correlation method
$p(n_s)$	probability of observing a specified number of speech active mobiles in a single frame
$\hat{p}(n_s)$	estimated value of $p(n_s)$ from observations
$\mathcal{P}$	surviving path
P	power
P	covariance matrix of complex Gaussian random vector
$\hat{P}$	outage probability – probability that perfect power control will fail for a given number of users
P_B	probability of a bit error
P_{I_k}	interference and noise power for mobile k
$P_{I_{kp}}$	received power in in-phase signal for mobile k when synchronized with mobile p
P_{M_k}	received power from mobile k

$P_{Q_{kp}}$	received power in quadrature signal for mobile k when synchronized with mobile p
P_{T_k}	signal power at transmitter for k^{th} mobile
$\mathbf{q}_{I_p}$	normalized mean vector estimate of array response vector using feedback correlation method
q	probability value for confidence interval
Q	number of standard deviation units for a specified confidence interval with a Gaussian distribution
Q	covariance matrix of expanded complex Gaussian random vector ($\mathbf{v}$)
$\mathrm{Q}_{\mathbf{q}}$	adjustment matrix when calculating the constrained Cramér-Rao Lower Bound for an array response vector estimator
$\hat{\mathrm{r}}_{\mathbf{vv}}$	vector formed by stacking the columns of the $\hat{\mathrm{R}}_{\mathbf{vv}}$ correlation matrix
R	real component of covariance matrix of complex Gaussian random vector
R_k	Rayleigh amplitude fading multiplicative attenuation for mobile k
R_A	radius of a circular antenna array
R_B	data bit rate (number of data bits per second)
$\mathrm{R}_{\mathbf{n}}$	autocorrelation of background noise
$\mathrm{R}_{\mathbf{uu}}$	correlation matrix of mean vector of feedback correlation estimation method
$\mathrm{R}_{\mathbf{vv}}$	correlation matrix for feedback correlation vector as correlated over the length of one Walsh function sequence
$\hat{\mathrm{R}}_{\mathbf{vv}}$	correlation matrix of feedback correlation vector estimated from observed values
$\mathrm{R}_{\mathbf{xx}}$	correlation matrix of signal vector correlated over one PN chip
$\mathrm{R}_{\mathbf{zz}}$	correlation matrix of signal vector correlated with PN chip values over the length of one Walsh chip
S	imaginary component of covariance matrix of complex Gaussian random vector
S	summation of sin terms when calculating power in a signal from a multi-element antenna array
$\mathcal{S}_k$	shadowing multiplicative attenuation for k^{th} mobile
t	current time
T	transfer function of the convolutional encoder
T_c	period of one PN chip
$\mathbf{u}$	unit vector specifying direction of wave propagation
$\mathbf{u}_{I_p}$	summation of feedback correlation vectors over an entire frame

U	matrix whose columns contain the eigenvectors of a covariance matrix
$U_{C_p}[r]$	PN chip correlation for mobile p
$U_{F_p}[r]$	Walsh function correlation for mobile p
$U_{I_p}[r]$	in-phase signal correlated over one PN chip for p^{th} mobile
$U_{Q_p}[r]$	quadrature signal correlated over one PN chip for p^{th} mobile
$U_{W_p}[r]$	Walsh chip correlation for mobile p
$\mathbf{v}$	eigenvector of a matrix
$\mathbf{v}$	expanded complex Gaussian random vector with real and imaginary components being considered as two separate strictly real vectors
$\hat{\mathbf{v}}$	observed feedback correlation vector as correlated with the reconstructed Walsh chip values over the length of one Walsh function sequence
$\delta\mathbf{v}$	perturbation in observed feedback correlation vector
$\mathbf{v}_{I_p}$	$\mathbf{z}_{I_p}$ correlation vectors correlated with Walsh chip values over one Walsh function sequence
V	matrix whose columns contain the eigenvectors of a correlation matrix
V	Gaussian random variable used for predicting expected received power
w	current Walsh chip value
$\mathbf{w}$	uncorrelated complex Gaussian random vector
w_i	i^{th} entry of beamforming weight vector
$\mathbf{w}_{I_p}$	summation of feedback correlation vectors over an arbitrary period of time scaled such that the expected value has a constant magnitude
$w_k(t)$	current Walsh chip value for the k^{th} mobile
$\mathbf{w}_p$	vector of beamforming weights for mobile p
W	confidence interval width
$W_n[\cdot]$	sequence of Walsh chips corresponding to the n^{th} Walsh function
$\mathbf{x}$	received signal vector
$\mathbf{x}$	complex Gaussian random vector
x_{I_k}	in-phase component of signal for k^{th} mobile
$\mathbf{x}_{I_p}$	in-phase signal vector for the p^{th} mobile correlated over one PN chip
x_{Q_k}	quadrature component of signal for k^{th} mobile
$\mathbf{x}_{Q_p}$	quadrature signal vector for the p^{th} mobile correlated over one PN chip
X	received signal

$\mathbf{y}$	real component of complex Gaussian random vector
$\mathbf{y}$	uncorrelated real Gaussian random vector
Y_{I_k}	binary random variable (± 1) representing in-phase multiplied PN code values
Y_{Q_k}	binary random variable (± 1) representing quadrature multiplied PN code values
$\mathbf{z}$	imaginary component of complex Gaussian random vector
$\mathbf{z}_{I_p}$	$\mathbf{x}_{I_p}$ received signal vectors correlated with PN chip values over one Walsh chip

Chapter 1

Introduction

1.1 Motivation

There is a growing trend in the communications market towards wireless systems. The removal of the physical link between a user and the remainder of the communication system permits greater user mobility and requires less physical infrastructure, which thereby reduces the overall system cost. Next-generation cellular phone systems will be of a digital form for an improved quality of service. Since there is a finite amount of the radio spectrum available for cellular purposes, it is desirable to accommodate as many users as possible within that bandwidth, while not compromising the level of performance.

CDMA (Code Division Multiple Access) is one technique by which a given portion of the radio spectrum can be shared among multiple users. TDMA and FDMA are two other multiple access techniques which provide separate time slots or frequency bands, respectively, for different users. The major disadvantage of both TDMA and FDMA is that they are both limited to a specific maximum number of users by the number of available time slots or frequency channels. In addition, adjacent cells cannot share the same channel allocations due to mutual interference. Conversely, in CDMA, all of the users share the same bandwidth with each mobile's signal being spread by a unique individual PN (pseudo-noise) chip sequence. By correlating the received signal at the base station with each user's known sequence, the original data can be recovered. Unlike the other two methods, CDMA is limited only by interference

(which arises mainly from other users). Thus, instead of having a sharp cut-off point in cell capacity, it is possible to continue adding users to the system by gradually reducing everyone's level of performance. Lee [48] provides a good introduction to the concept of cellular CDMA and illustrates how this multiple-access scheme is more suitable for the cellular environment than are TDMA and FDMA, in terms of providing greater system capacity. Pickholtz, Milstein, and Schilling [80] [81] provide tutorial introductions to spread-spectrum communications which describe the basic nature of spread-spectrum CDMA and investigate how it can share the same frequency band with narrow-band users. A basic introduction to spread-spectrum techniques has also recently been given by Flikkema [24]. Finally, Qualcomm [85] provides an in-depth introduction to the use of CDMA in digital cellular communication systems, including many of the necessary implementation details.

Since CDMA provides the prospect of significantly increased capacity for a given amount of bandwidth, a substantial amount of research has gone into finding methods by which the multiple access interference (MAI) can be reduced. If it is possible to do this, individual cell capacity can be further increased. By increasing capacity, the same area can be covered with fewer base stations, thereby reducing the overall cost of the cellular communications system. In addition, by avoiding the need for subdividing cells, the logistical problems of performing hand-offs between adjacent cells as users move around are reduced.

One popular method for reducing interference from other users is termed *beamforming*. In this situation, an array of antenna elements is used at the base station to receive signals. Each element will receive a phase-shifted version of the same signals. By determining a suitable set of complex coefficients for a desired mobile, it is possible to obtain a weighted sum of the antenna outputs in which the desired signal adds constructively (due to phase alignment) and, on average, the interfering signals tend to add destructively (due to random relative phases). That is, unless an interfering signal's direction of arrival is the same as for the mobile of interest, beamforming will tend to suppress the interfering signal relative to the desired signal. In this way, it is possible to reduce the interference seen by a given user with the only requirement

being for some additional processing power at the base station. Also, incorporating beamforming into an existing CDMA standard such as Qualcomm's IS-95 can be performed quite simply since the beamforming layer is essentially transparent to the remainder of the coding/decoding system so it is not necessary to modify the currently-defined protocol.

To this point in time, beamforming has mainly been analyzed via theoretical analyses and computer simulations, although some physical experiments have also been performed. Of course, it is usually more practical and less expensive to predict expected system performance via analytical and simulation-based methods before actually constructing an actual prototype for testing. To aid in the investigations performed in this thesis, a comprehensive PN chip-level simulation program adhering to the IS-95 standard has been developed [15]. The chip-level data was required for performing beamforming simulations and verifying any simplifying assumptions which might be made. To the best of the author's knowledge, simulations with this level of detail have not yet been used by other researchers.

There are a number of important aspects of beamforming which require investigation in order to aid in accessing the physical feasibility of this technique. In real life, it will not be possible to estimate the optimum beamforming weights exactly, so the effects of estimation error should be determined. It is also necessary to evaluate both the quality of the estimates obtained and the corresponding effect on system performance.

1.2 Summary of Contributions

This section briefly summarizes the primary contributions of this thesis. A more detailed summary may be found at the end of the thesis in Section 8.2.

- A comprehensive simulation platform for the IS-95 reverse link and capable of operating at the PN chip level was developed for conducting most of the simulations contained in this document. This level of detail significantly reduces the number of simplifying assumptions which must be made.

- A combined deinterleaver/decoder for the IS-95 reverse link which provides superior performance as compared to Viterbi decoding with deinterleaved soft-decision bit metrics has been proposed.

- Using feedback correlation of the decoded data to increase the gain factor of the beamforming coefficient estimator significantly improved the accuracy of these weighting estimates. A detailed error analysis of this estimation method allows the statistical parameters of the various estimators to be predicted quite accurately.

- An error analysis of the IS-95 reverse link also allowed the operation of the simulation program to be validated.

- Various methods are used for estimating cell capacity, including the actual transmission of PN chip values through the system, and a more computationally-efficient power-level capacity estimation method was also developed.

- In addition, it is also possible to predict cell capacity values from the equations derived in this thesis.

- Finally, an investigation into multi-service operation (*i.e.* data and voice) is made through the use of simulations and predictions.

1.3 Thesis Outline

The following chapters examine various aspects of a CDMA reverse link (mobile to base), all of which ultimately cohere together to permit accurate estimation of cell capacity and the improvements that can be attained through beamforming in such a communication system. As a consequence, relevant background material and literature reviews of previous research are primarily covered at the beginning of each individual chapter, as this structuring is more appropriate for the format of this thesis.

Chapter 2 examines the reverse link of the IS-95 cellular CDMA system and covers such aspects as data encoding, transmission channel parameters, and the effective modelling of such a communication system for simulation purposes. Power control is

an important component of a CDMA system in order to maintain multi-user interference at an acceptable level, and this topic is covered in Chapter 3. Due to IS-95's data encoding format, a standard Viterbi decoder must be modified in order to function efficiently. Chapter 4 examines existing techniques for decoding reverse link data in IS-95 and then presents a combined deinterleaver/decoder which offers an enhanced level of performance due to improved path metrics. User capacity in a CDMA system can be improved by reducing interference. One method of accomplishing this is through beamforming as examined in Chapter 5 which presents a suitable beamforming technique for IS-95 and includes a complete error analysis of the estimation process for beamforming weights. On a related note, the following chapter contains an error analysis of the simulated IS-95 system which is useful for system validation purposes. Chapter 7 presents techniques for predicting and estimating cell capacity via analysis and simulation, and shows the improvements that can be attained when beamforming at the base station is used. Finally, Chapter 8 summarizes the contributions and findings of this thesis and presents a number of areas in which further research work could be performed.

Chapter 2

The IS-95 Reverse Link

2.1 Introduction

Qualcomm [86] has developed the IS-95 cellular CDMA standard which defines the complete implementation protocol for such a communication system. A number of researchers [6] [37] [69] [71] have adopted this standard for their research. In addition, considering an existing CDMA system design is more appropriate than defining a new coding and transmission protocol.

Within the context of this thesis, only the reverse link (mobile to base) of the IS-95 communication system has been studied. It is not realistically practical to implement beamforming at the mobiles due to the necessary antenna arrays and processing requirements. Therefore, beamforming is used only at the base station, and the reverse link situation is more suited to this task since the received signal data can be directly processed to obtain the required beamforming information. In addition, cell capacity is usually limited by the reverse link. However, beamforming at the base transmitters can also be implemented on the forward link by using feedback information from the mobiles [27].

In order to aid in conducting detailed investigations of system performance, a comprehensive PN chip-level simulator of the IS-95 reverse link has been developed [15]. This program includes such features as complete reverse link modelling, multiple independent mobiles, and possible multi-cell situations. However, it is first necessary to examine the actual communication system and how it may be modelled effectively

and efficiently.

This chapter examines the reverse link of IS-95 and includes the issues of data encoding for transmission, transmission channel parameters, and processing of the received data. Two aspects of the IS-95 reverse link, power control and data decoding, are examined in greater detail in the two following chapters. The contents of this chapter are based on the IS-95 standard which may be found in [86], although much of the actual analysis within this chapter is original work.

2.2 Encoding Reverse Link Data

The source data is assumed to consist of sequences of random bits representing compressed voice signals which are generated as required. In order to provide protection against errors, the data bits are sent through a multi-level encoding process as shown in Figure 2.1.

It is assumed that acceptable voice quality data can be transmitted at a bit rate $R_B = 9600$ bps which includes overhead. The IS-95 standard [86] also includes defined protocols for fractional data transmission rates such as 4800, 2400, and 1200 bps, although these particular rates have not been addressed in this thesis.

The bits to be transmitted are divided into frames with 50 frames per second and 192 total bits per frame. The first 184 bits represent actual data (including a CRC (cyclical redundancy check) value), and the remainder are tail bits which are all zero.

The frame bits are initially passed through a rate 1/3 convolutional encoder with a constraint length of 9. This produces 576 encoded bits per frame.

The next stage involves block interleaving the encoded bits using a 32×18 interleaver matrix. Bits are written into successive columns of this array and then read out row by row. Although the interleaving step is part of the IS-95 specification and is essential for dealing with correlated fading, it is an optional process in the simulator so that its effects on system performance can be studied.

The resulting bits are then grouped into sets of 6 to form binary numbers which select one of $2^6 = 64$ different Walsh functions. This yields a total of 96 Walsh functions per frame.

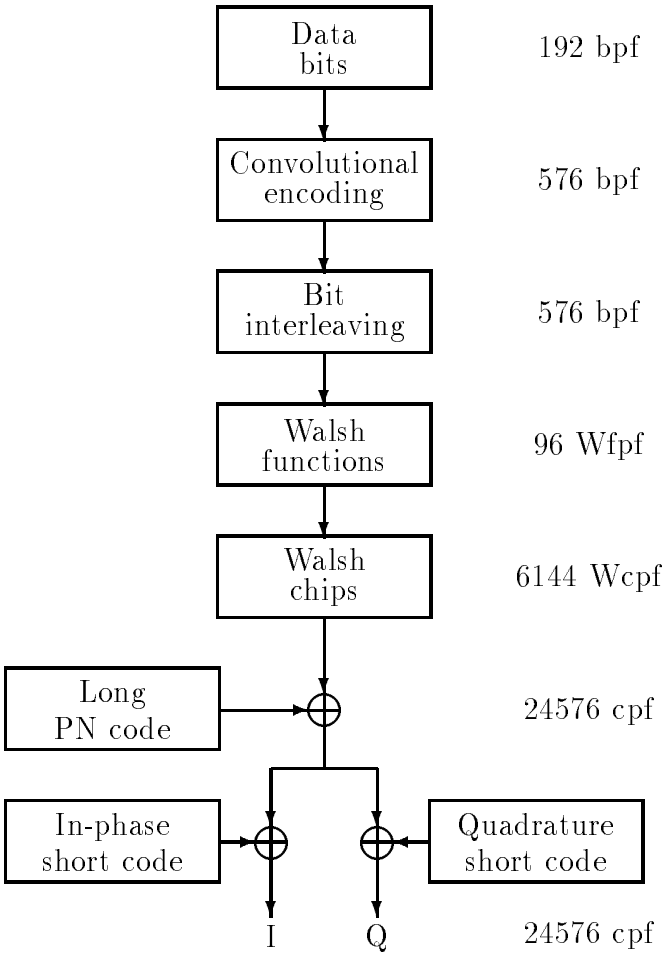

Figure 2.1: IS-95 reverse link data encoding process showing "per frame" throughput

Each Walsh function has a sequence of 64 chips associated with it which results in a total of 6144 Walsh chips per frame. These sequences are constructed so that a given sequence is orthogonal to each of the other 63 Walsh chip sequences.

Finally, pseudo-noise (PN) sequences are used to spread the signal by a factor of 4. A long code with a period of $2^{42} - 1$ is first used to spread the Walsh chips. The resulting signal is then split into in-phase and quadrature components with each component being further encoded by a different short code sequence, each with a period of 2^{15} chips. The long and short code chips are of the same length.

The in-phase and quadrature components are modulated using BPSK (Binary Phase Shift Keying) with a carrier frequency of f_c Hz. A typical value for f_c in a terrestrial cellular environment might be 2 GHz. Giannetti [28] also investigated the capacity improvements resulting from using a higher carrier frequency in the 63-64 GHz band. In this situation, intercell interference is significantly reduced to signal absorption by atmospheric oxygen and thus cell capacity increases. However, increased transmitter power is also necessary due to the absorption phenomenon.

2.3 Transmission Channel Parameters

This section details how the reverse link transmission channel between the mobiles and base station is modelled. This mainly involves quantities specifying signal attenuation over the transmission channel such as path loss, shadowing, and Rayleigh fading.

2.3.1 Path Loss

The amount of power in a signal falls off as a function of the distance from the transmitter. A generally accepted model of this path loss is:

$$\rho_k = d_k^{-\epsilon} \tag{2.1}$$

where d_k is the distance between the k^{th} transmitter and the receiver, and ϵ is the path loss exponent. Typical values for ϵ range between 2 and 5 depending upon the local environment, and a commonly used value for testing purposes is 4. A larger path loss exponent corresponds to greater path loss attenuation as would be the case in a built-up urban environment.

Xia *et al* [116] investigated path loss using actual measured data from various urban, suburban, and rural areas. Path loss was found to be significantly higher for non-LOS (Line Of Sight) paths than for LOS paths. Consequently, cell shape was found to depend on the orientation of the LOS paths, with circular cells in rural areas, elliptical cells in suburban regions, and linear cells in built-up urban areas. Harley [33] also performed actual measurements of signal attenuation for carrier frequencies of 900 MHz and 1.8 GHz over distances of less than 1 km, which represent typical cell sizes for a microcell system.

Note that ρ_k dictates how the power of the signal falls off as a function of distance. Therefore, the amplitude of the signal envelope should be multiplied by $\sqrt{\rho_k}$. The path loss quantity is updated dynamically as mobiles move within the cell.

2.3.2 Shadowing

Shadowing is caused by various obstacles such as trees and buildings in the transmission path of a mobile. As a mobile moves around, the degree of shadowing will vary. However, for the results considered in this thesis, this quantity currently remains constant for the duration of a call since Rayleigh fading is assumed to affect the signals much more dramatically. In addition, dynamic motion is often simulated by moving a mobile to a new location and beginning another call with a new shadowing value. This should, however, be modified when further experiments are performed.

A commonly accepted shadowing model is to use a lognormal random variable such as:

$$\mathcal{S}_k = 10^{\xi/10} \tag{2.2}$$

where ξ has a $N(0, \sigma_{\mathcal{S}}^2)$ distribution. The value typically used for $\sigma_{\mathcal{S}}$ is 8 dB.

A new value of $\mathcal{S}_k$ is chosen for each mobile at the start of each call by that mobile, and $\mathcal{S}_k$ currently remains constant for the duration of each call.

2.3.3 Rayleigh Fading

Although only a single resolvable path is considered for each mobile, Rayleigh fading due to multipath propagation is incorporated into the channel model. This type of

fading can be modelled as either uncorrelated or correlated. Ricean fading would include a line of sight component, but Rayleigh fading was selected to represent the worst-case scenario. An introduction to the characteristics of and methods for overcoming Rayleigh fading in mobile digital communication systems may be found in the recent pair of tutorial articles by Sklar [94] [95].

2.3.3.1 Uncorrelated Rayleigh Fading

The simplest fading model is to consider Rayleigh-distributed random amplitude factors which are mutually uncorrelated. This multiplicative quantity is calculated as:

$$R_k = \sqrt{(G_1)^2 + (G_2)^2} \tag{2.3}$$

where G_1 and G_2 are $N(0,1)$ Gaussian random variables.

A new Rayleigh fading parameter is calculated for each mobile at a maximum of every 48 PN chips. This roughly corresponds to the time required to transmit the equivalent of one data bit (46 PN chips), but was rounded up since 48 divides evenly into the power control period of 1536 PN chips, thereby simplifying the simulation process. This parameter can also be changed at a faster rate such as every 24 or 16 PN chips.

2.3.3.2 Correlated Rayleigh Fading

For moving mobiles, time-correlated Rayleigh fading represents a more realistic fading environment. For the simulations presented here, the third-order Butterworth filter fading model discussed in [56] and [36] was used. In this model, pairs of Gaussian random numbers form the inputs to a filter whose parameters depend on the mobile's current velocity. The filter outputs are correlated Gaussian random variables which may then be used in equation (2.3) to generate correlated fading values. Actual illustrative examples of correlated fading may be found in Section 3.5.

2.3.3.3 Amplitude Fading

As can be seen from the above paragraphs, the fading models used within this thesis only consider the effect of Rayleigh fading on the amplitude of the signal. However,

in reality, there would also be a perturbation in the carrier phase due to the multipath propagation. This would likely degrade the performance of the beamforming algorithms to some extent, but it is not clear what level of impact would be observed without further investigation via both analysis and simulations as discussed in Section 8.4.

2.3.4 Overall Channel Attenuation

The transmission power and, hence, the signal amplitude or envelope originating from each mobile is known. As the signal travels to the base station, its strength is attenuated by the previously discussed factors. Thus, the envelope is multiplied by the following value to determine its magnitude as observed at the base station.

$$\eta_k = \sqrt{\rho_k \mathcal{S}_k} R_k \tag{2.4}$$

The path loss and shadowing terms affect the power of a signal, so it is necessary to take the square root of these terms when considering the signal amplitude.

2.4 Antenna Array Processing

This section briefly introduces the concept of beamforming with adaptive antenna arrays which is discussed in more detail in Chapter 5.

2.4.1 Array Response Vector Calculation

If a multi-element antenna array is used at the base station, it is necessary to determine the array response vector $\mathbf{a}$ for a signal arriving from a given direction. This vector specifies the relative phases of the signal waveform at each of the antenna elements. Each entry in $\mathbf{a}$ is a unit magnitude complex number whose phase specifies the relative phase of the signal at the corresponding antenna element. Currently, it is assumed that identical copies of the signal, subject to this relative phase shift and independent background noise, are observed at each antenna element.

The antenna array is assumed to be in a circular form with N_A representing an arbitrary number of elements which are omnidirectional with equal gains. Adjacent

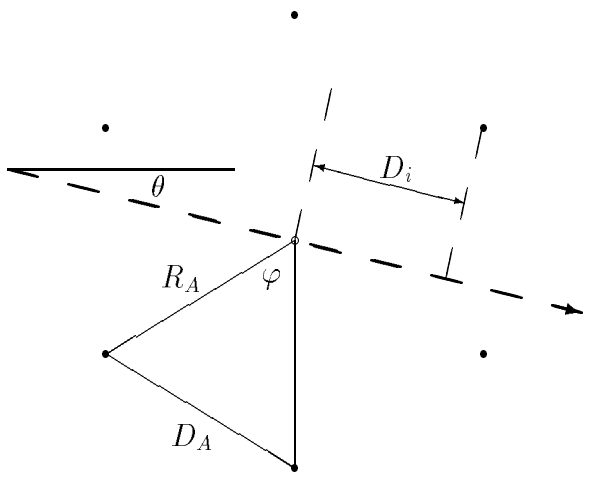

Figure 2.2: Array response vector calculation for a multi-element circular antenna array

elements are assumed to have one-half wavelength ($\lambda_c/2$) spacing between them. This analysis can be easily adapted for a linear array, although circular arrays were chosen since they are less directional in nature. In terms of antenna arrangements other than circular and linear designs, Liang and Paulraj [54] investigated several different array topologies and the resulting improvements in coverage.

Refer to Figure 2.2 for the definition of quantities used in this derivation. If the inter-element spacing is $D_A = \lambda_c/2$, then the corresponding radius of the circular antenna array can be calculated as follows [62, pp. 65].

$$\varphi = \frac{2\pi}{N_A} \tag{2.5}$$

$$\sin(\varphi/2) = \frac{D_A/2}{R_A} \tag{2.6}$$

$$R_A = \frac{D_A/2}{\sin(\varphi/2)} = \frac{D_A}{2\sin(\pi/N_A)} = \frac{\lambda_c}{4\sin(\pi/N_A)} \tag{2.7}$$

Let γ_i represent the angle at which the i^{th} $(0 \leq i \leq N_A - 1)$ element is located on the circle. Without loss of generality, it can be assumed that $\gamma_0 = 0$. Then:

$$\gamma_i = i\left(\frac{2\pi}{N_A}\right) \tag{2.8}$$

The position of the i^{th} antenna element in Cartesian coordinates can thus be written

as:

$$x_i = R_A \cos(\gamma_i) \tag{2.9}$$

$$y_i = R_A \sin(\gamma_i) \tag{2.10}$$

Now assume that a plane wave with frequency f_c and propagating in the direction θ is impinging upon the antenna array as shown by the dashed arrow in Figure 2.2. A unit vector in the direction of wave propagation can be written as:

$$\mathbf{u} = \begin{bmatrix} \cos(\theta) & \sin(\theta) \end{bmatrix} \tag{2.11}$$

It is now simply necessary to take the dot product of this vector with the Cartesian coordinates of each antenna element in order to find D_i. This represents the distance along the direction of wave propagation between the centre of the array and the i^{th} antenna element.

$$\begin{aligned} D_i &= x_i \cos(\theta) + y_i \sin(\theta) \\ &= R_A \cos(\gamma_i)\cos(\theta) + R_A \sin(\gamma_i)\sin(\theta) \\ &= R_A \cos(\theta - \gamma_i) \end{aligned} \tag{2.12}$$

Let α_i represent the relative phase delay for the i^{th} element. The centre of the circle is taken to be the reference point with a phase delay of zero. Consequently, the phase at the i^{th} element can be calculated as:

$$\begin{aligned} \alpha_i &= 2\pi \left(\frac{D_i}{\lambda_c}\right) \\ &= \frac{2\pi R_A \cos(\theta - \gamma_i)}{\lambda_c} \\ &= \frac{2\pi \cos(\theta - \gamma_i)}{\lambda_c} \left(\frac{\lambda_c}{4\sin(\pi/N_A)}\right) \\ &= \frac{\pi \cos(\theta - \gamma_i)}{2\sin(\pi/N_A)} \end{aligned} \tag{2.13}$$

It is interesting to note that the relative phase is independent of the carrier frequency since the inter-element spacing is a function of this frequency value. Due to this latter consideration, it is necessary to design the antenna array according to the carrier frequency to be used.

2.4.2 Beamforming

Digital beamforming can be utilized to increase the capacity of a cell [64] [67] [73] [74]. By using a multi-element antenna array at the base station and a suitable set of beamforming coefficients, it is possible to take a weighted sum of the antenna element outputs which maximizes the ratio of the desired mobile's signal power to the noise and interference power. This is essentially a form of spatial filtering that reduces interference from other mobiles and thus boosts overall cell capacity. This process is only covered briefly here to show how it affects the reverse link signals. Beamforming is investigated and analyzed in much greater detail later in Chapter 5.

In a simulation or analysis, the true array response vector $\mathbf{a}_k$ can be determined for each of the mobiles in the system as shown in Section 2.4.1. For a multi-element base station array, the received signal vector $\mathbf{x}(t)$ can be calculated as:

$$\mathbf{x}(t) = \sum_{k=1}^{N_M} \beta_k(t)\mathbf{a}_k + \mathbf{n}(t) \tag{2.14}$$

where $\beta_k(t)$ represents the signal strength from the k^{th} mobile and $\mathbf{n}(t)$ represents wide-sense stationary zero-mean Gaussian white noise with autocorrelation:

$$\mathrm{R}_{\mathbf{n}}(\tau) = \begin{cases} \sigma_n^2 \mathrm{I} & \tau = 0 \\ 0 & \tau \neq 0 \end{cases} \tag{2.15}$$

It is necessary to reduce the complex vector $\mathbf{x}$ to a scalar quantity that can be used in the remainder of the decoding process. This can be accomplished by taking a weighted sum of the elements of $\mathbf{x}$.

$$x_p = \mathbf{w}_p^* \mathbf{x} \tag{2.16}$$

Each entry in the beamforming weight vector $\mathbf{w}_p$ induces a phase shift in the corresponding entry of the signal vector $\mathbf{x}$ and may also scale that quantity. If $\mathbf{w}_p = \mathbf{a}_p$, then the phase shifts introduced by the antenna array and the beamforming process will cancel each other out for mobile p. However, if the signal from another mobile with a different array response vector is considered, the entries from each antenna element will not be in phase with each other when they are summed in equation (2.16). Typically, interfering signals will not add constructively, and thus the interference from other mobiles will be greatly reduced by the beamforming process.

If the interference is assumed to be spatially white, which will be the case for a large number of mobiles [82], then the optimal (in terms of maximizing the output signal-to-noise-ratio) choice of beamforming weights for the p^{th} mobile is to let $\mathbf{w}_p$ equal the true array response vector $\mathbf{a}_p$. However, in reality $\mathbf{a}_p$ is not known exactly so it is necessary to estimate suitable values for $\mathbf{w}_p$ from the received signal data as shown in Chapter 5.

2.5 Demodulation and Correlation

There are a number of processing steps required at the base station receiver in order to recover the original data bits. These include demodulation, correlation, and data decoding. This latter process is considered later in Chapter 4 due to the level of detail required in the presentation. Note that a rectangular chip pulse shape is assumed throughout this thesis.

2.5.1 Demodulation

After taking the inner product of the signal vector from the antenna array with the vector of beamforming weights, the result is a scalar complex quantity x_p as shown in (2.16) which can then be demodulated. It is simpler to consider the demodulation of the signal from a single antenna element first and then to generalize this result to a multi-element antenna array.

2.5.1.1 Single Element Demodulation

Consider the BPSK modulated in-phase and quadrature signal components originating from the k^{th} mobile:

$$x_{I_k}(t) = \cos(2\pi f_c t + \theta_{I_k}(t)) \tag{2.17}$$

$$x_{Q_k}(t) = \sin(2\pi f_c t + \theta_{Q_k}(t)) \tag{2.18}$$

where $\theta_{I_k}(t)$ and $\theta_{Q_k}(t)$ are the phase angles used to modulate the carrier signal and are limited to the following values:

$$\theta_{I_k}, \theta_{Q_k} \in \{0, \pi\} \tag{2.19}$$

Note that there should also be a scaling factor representing the signal amplitude, but for simplicity this quantity can be ignored for the purposes of this analysis.

The combined signal can be written as:

$$\begin{aligned} X_k(t) &= x_{I_k}(t) + x_{Q_k}(t) \\ &= \cos(2\pi f_c t + \theta_{I_k}(t)) + \sin(2\pi f_c t + \theta_{Q_k}(t)) \end{aligned} \tag{2.20}$$

Now introduce a random time delay τ_k which will cause a phase shift. This quantity is due to the lack of time synchronization between the mobiles on the reverse link and is assumed to be uniformly distributed over the interval $[0, T_c)$.

$$\begin{aligned} X_k(t) &= \cos(2\pi f_c(t-\tau_k) + \theta_{I_k}(t-\tau_k)) \\ &\qquad + \sin(2\pi f_c(t-\tau_k) + \theta_{Q_k}(t-\tau_k)) \end{aligned} \tag{2.21}$$

θ_{I_k} and θ_{Q_k} have a much lower frequency than f_c, so their dependence on time and the effects of the delay τ_k on these terms can be ignored during this analysis.

$$\begin{aligned} X_k(t) &= \cos(2\pi f_c(t-\tau_k) + \theta_{I_k}) + \sin(2\pi f_c(t-\tau_k) + \theta_{Q_k}) \\ &= \{\cos(\theta_{I_k})\cos(2\pi f_c(t-\tau_k)) - \sin(\theta_{I_k})\sin(2\pi f_c(t-\tau_k))\} \\ &\qquad + \{\sin(\theta_{Q_k})\cos(2\pi f_c(t-\tau_k)) + \cos(\theta_{Q_k})\sin(2\pi f_c(t-\tau_k))\} \\ &= \{\cos(\theta_{I_k}) + \sin(\theta_{Q_k})\}\cos(2\pi f_c(t-\tau_k)) \\ &\qquad + \{-\sin(\theta_{I_k}) + \cos(\theta_{Q_k})\}\sin(2\pi f_c(t-\tau_k)) \end{aligned} \tag{2.22}$$

Equation (2.22) can also be written in phasor format to simplify the remainder of the analysis.

$$\begin{aligned} X_k(t) &= \mathrm{Re}\Big\{\big[\{\cos(\theta_{I_k}) + \sin(\theta_{Q_k})\} - j\,\{-\sin(\theta_{I_k}) + \cos(\theta_{Q_k})\}\big] \\ &\qquad\qquad \exp(j2\pi f_c(t-\tau_k))\Big\} \\ &= \mathrm{Re}\Big\{[\cos(\theta_{I_k}) - j\cos(\theta_{Q_k})]\exp(j2\pi f_c(t-\tau_k))\Big\} \\ &= \mathrm{Re}\Big\{[\cos(\theta_{I_k}) - j\cos(\theta_{Q_k})]\exp(-j2\pi f_c\tau_k)\exp(j2\pi f_c t)\Big\} \end{aligned} \tag{2.23}$$

Note that the sin terms in (2.23) will evaluate as zero due to the constraints given in (2.19) and can therefore be dropped from the equation. The cos terms will evaluate as ± 1.

To demodulate the in-phase component, equation (2.23) is multiplied by $\cos(2\pi f_c t)$ and low-pass filtered. In complex exponential form:

$$\cos(2\pi f_c t) = \frac{1}{2}\Big\{\exp(j2\pi f_c t) + \exp(-j2\pi f_c t)\Big\} \tag{2.24}$$

This yields the final in-phase demodulated result:

$$\begin{aligned} D_{I_k}(t) &= \mathrm{Re}\Big\{[\cos(\theta_{I_k}) - j\cos(\theta_{Q_k})]\exp(-j2\pi f_c\tau_k)\exp(j2\pi f_c t) \\ &\qquad \Big[\frac{1}{2}\{\exp(j2\pi f_c t) + \exp(-j2\pi f_c t)\}\Big]\Big\} \\ &\overset{\text{LPF}}{=} \mathrm{Re}\Big\{\frac{1}{2}[\cos(\theta_{I_k}) - j\cos(\theta_{Q_k})]\exp(-j2\pi f_c\tau_k)\Big\} \\ &= \frac{1}{2}\cos(\theta_{I_k})\cos(2\pi f_c\tau_k) - \frac{1}{2}\cos(\theta_{Q_k})\sin(2\pi f_c\tau_k) \end{aligned} \tag{2.25}$$

If the time delay τ_k is such that the effective phase due to the time delay is a multiple of 2π, it will be possible to recover the in-phase signal exactly. Otherwise, the quadrature signal will contribute interference.

To demodulate the quadrature component, equation (2.23) is multiplied by $\sin(2\pi f_c t)$ and low-pass filtered where:

$$\sin(2\pi f_c t) = -j\frac{1}{2}\Big\{\exp(j2\pi f_c t) - \exp(-j2\pi f_c t)\Big\} \tag{2.26}$$

This yields the demodulated quadrature signal:

$$\begin{aligned} U_{Q_k}(t) &= \mathrm{Re}\Big\{[\cos(\theta_{I_k}) - j\cos(\theta_{Q_k})]\exp(-j2\pi f_c\tau_k)\exp(j2\pi f_c t) \\ &\qquad \Big[-j\frac{1}{2}\{\exp(j2\pi f_c t) - \exp(-j2\pi f_c t)\}\Big]\Big\} \\ &\overset{\text{LPF}}{=} \mathrm{Re}\Big\{\frac{1}{2}[j\cos(\theta_{I_k}) + \cos(\theta_{Q_k})]\exp(-j2\pi f_c\tau_k)\Big\} \\ &= \frac{1}{2}\cos(\theta_{I_k})\sin(2\pi f_c\tau_k) + \frac{1}{2}\cos(\theta_{Q_k})\cos(2\pi f_c\tau_k) \end{aligned} \tag{2.27}$$

Similarly, there will be interference from the in-phase component unless the phase shift due to the time delay is an integral multiple of 2π.

Note that equations (2.25) and (2.27) only represent the demodulation of a signal from a single mobile. Consequently, it is necessary to sum the demodulation results for each mobile in the system in order to obtain the total demodulated signal (including interfering signals from other users). If mobile p is the user of interest, then $\tau_p = 0$ but τ_k will be a uniformly distributed random variable for $k \neq p$.

2.5.1.2 Multiple Element Demodulation

Consider a received signal from mobile k in the form of (2.23).

$$X_k(t) = \mathrm{Re}\Big\{ [\cos(\theta_{I_k}) - j\cos(\theta_{Q_k})] \exp(-j2\pi f_c \tau_k) \exp(j2\pi f_c t) \Big\} \quad (2.28)$$

For the i^{th} antenna element, there is a known phase offset α_{ki} relative to the centre of the array. This phase offset depends on the direction of arrival of the signal and the geometry of the antenna array, and the value of this quantity comes directly from the array response vector which was derived in Section 2.4.1. Thus, with this additional phase offset the received signal at the i^{th} array element can be written as:

$$\begin{aligned} X_{ki}(t) = \mathrm{Re}\Big\{ & [\cos(\theta_{I_k}) - j\cos(\theta_{Q_k})] \\ & \exp(-j\alpha_{ki}) \exp(-j2\pi f_c \tau_k) \exp(j2\pi f_c t) \Big\} \end{aligned} \quad (2.29)$$

Let w_{pi} be the i^{th} entry in the beamforming weight vector for the p^{th} mobile which is the mobile of interest. This represents a phase shift of the corresponding element of the signal vector, so w_{pi} can be written as:

$$w_{pi} = \exp(-j\phi_{pi}) \quad (2.30)$$

$$w_{pi}^* = \exp(j\phi_{pi}) \quad (2.31)$$

Thus, by combining equations (2.16), (2.29) and (2.31), the final complex quantity to be demodulated can be obtained as:

$$\begin{aligned} X_p(t) &= \sum_{i=1}^{N_A} w_{pi}^* \sum_{k=1}^{N_M} X_{ki}(t) \\ &= \sum_{i=1}^{N_A} \sum_{k=1}^{N_M} \mathrm{Re}\Big\{ [\cos(\theta_{I_k}) - j\cos(\theta_{Q_k})] \\ &\qquad \exp(j\phi_{pi}) \exp(-j\alpha_{ki}) \exp(-j2\pi f_c \tau_{kp}) \exp(j2\pi f_c t) \Big\} \\ &= \sum_{i=1}^{N_A} \sum_{k=1}^{N_M} \mathrm{Re}\Big\{ [\cos(\theta_{I_k}) - j\cos(\theta_{Q_k})] \\ &\qquad \exp(j(\phi_{pi} - \alpha_{ki} - 2\pi f_c \tau_{kp})) \exp(j2\pi f_c t) \Big\} \end{aligned} \quad (2.32)$$

X_p represents the received signal vector containing signals from all of the mobiles after having undergone beamforming with the weights for the p^{th} mobile. τ_{kp} represents the relative time delay of the k^{th} mobile's signal when τ_{pp} is assumed to be zero.

Referring to equations (2.25) and (2.27), it is easy to see that the demodulated in-phase and quadrature components should be:

$$\begin{aligned} D_{I_p}(t) &= \frac{1}{2}\sum_{i=1}^{N_A}\sum_{k=1}^{N_M}\beta_k w_k(t)\Big\{\cos(\theta_{I_k})\cos(\phi_{pi}-\alpha_{ki}-2\pi f_c\tau_{kp}) \\ &\qquad + \cos(\theta_{Q_k})\sin(\phi_{pi}-\alpha_{ki}-2\pi f_c\tau_{kp})\Big\} \qquad (2.33) \\ &= \frac{1}{2}\sum_{i=1}^{N_A}\sum_{k=1}^{N_M}\beta_k w_k(t)\Big\{C_{I_k}\cos(\alpha_{ip}-\phi_{ki}-2\pi f_c\tau_{kp}) \\ &\qquad + C_{Q_k}\sin(\alpha_{ip}-\phi_{ki}-2\pi f_c\tau_{kp})\Big\} \\ D_{Q_p}(t) &= \frac{1}{2}\sum_{i=1}^{N_A}\sum_{k=1}^{N_M}\beta_k w_k(t)\Big\{-\cos(\theta_{I_k})\sin(\phi_{pi}-\alpha_{ki}-2\pi f_c\tau_{kp}) \\ &\qquad + \cos(\theta_{Q_k})\cos(\phi_{pi}-\alpha_{ki}-2\pi f_c\tau_{kp})\Big\} \qquad (2.34) \\ &= \frac{1}{2}\sum_{i=1}^{N_A}\sum_{k=1}^{N_M}\beta_k w_k(t)\Big\{-C_{I_k}\sin(\phi_{pi}-\alpha_{ki}-2\pi f_c\tau_{kp}) \\ &\qquad + C_{Q_k}\cos(\phi_{pi}-\alpha_{ki}-2\pi f_c\tau_{kp})\Big\} \end{aligned}$$

where β_k is the received signal strength as included in equation (2.14), $w_i(t)$ is the current Walsh chip value for the k^{th} mobile, and C_{I_k} and C_{Q_k} represent the current in-phase and quadrature PN chip values which are ± 1.

2.5.2 Correlation

The basic unit of time correlation is one PN chip (T_c). It is necessary to integrate equations (2.33) and (2.34) over this time period, multiply by the current known PN chip value for the p^{th} mobile, and add the results together in order to obtain a PN chip correlation value.

For the in-phase and quadrature signal components, the correlation values over one PN chip can be evaluated as:

$$\begin{aligned} U_{I_p}[r] &= \frac{1}{2}C_{I_p}[r]\sum_{i=1}^{N_A}\sum_{k=1}^{N_M}\beta_k w_k(t)\Big\{C_{I_k}[r]\cos(\phi_{pi}-\alpha_{ki}-2\pi f_c\tau_{kp})(T_c-\tau_{kp}) \\ &\qquad + C_{I_k}[r-1]\cos(\phi_{pi}-\alpha_{ki}-2\pi f_c\tau_{kp})\tau_{kp} \qquad (2.35) \\ &\qquad + C_{Q_k}[r]\sin(\phi_{pi}-\alpha_{ki}-2\pi f_c\tau_{kp})(T_c-\tau_{kp}) \\ &\qquad + C_{Q_k}[r-1]\sin(\phi_{pi}-\alpha_{ki}-2\pi f_c\tau_{kp})\tau_{kp}\Big\} \end{aligned}$$

$$
\begin{aligned}
U_{Q_p}[r] &= \frac{1}{2} C_{Q_p}[r] \sum_{i=1}^{N_A} \sum_{k=1}^{N_M} \beta_k w_k(t) \Big\{ C_{I_k}[r] \sin(\phi_{pi} - \alpha_{ki} - 2\pi f_c \tau_{kp})(T_c - \tau_{kp}) \\
&\quad + C_{I_k}[r-1] \sin(\phi_{pi} - \alpha_{ki} - 2\pi f_c \tau_{kp}) \tau_{kp} \\
&\quad + C_{Q_k}[r] \cos(\phi_{pi} - \alpha_{ki} - 2\pi f_c \tau_{kp})(T_c - \tau_{kp}) \\
&\quad + C_{Q_k}[r-1] \cos(\phi_{pi} - \alpha_{ki} - 2\pi f_c \tau_{kp}) \tau_{kp} \Big\}
\end{aligned} \tag{2.36}
$$

Adding (2.35) and (2.36) together yields the correlation value for the r^{th} PN chip of mobile p.

$$
U_{C_p}[r] = U_{I_p}[r] + U_{Q_p}[r] \tag{2.37}
$$

In the IS-95 standard, the quadrature chip values are actually delayed by half a chip period. This feature is incorporated into the simulation methodology but is not included here since it does not affect the basic results of the analysis.

The correlation value for each Walsh chip is found by summing the $N_W = 4$ correlation values for the PN chips corresponding to the current Walsh chip.

$$
U_{W_p}[r] = \sum_{m=0}^{N_W - 1} U_{C_p}[r N_W + m] \tag{2.38}
$$

If $W_n[\cdot]$ represents the chip sequence of the n^{th} Walsh function, then the correlation value of the r^{th} Walsh function position with the n^{th} Walsh function for mobile p is:

$$
U_{F_p}[r, n] = \sum_{m=0}^{N_F - 1} U_{W_p}[r N_F + m] W_n[m] \tag{2.39}
$$

The correlation quantities given by the above expression are suitable for inputs to the decoding process as described in Chapter 4.

2.5.2.1 Background Noise Term

For simplicity, equations (2.35) and (2.36) did not include a background noise component. The integrated thermal noise will have a zero-mean Gaussian distribution. The variance of this distribution is relatively easy to find [76, pp. 209].

$$
\begin{aligned}
E\left[n^2[r]\right] &= \int_0^{T_c} \int_0^{T_c} E\left[n(t_1) n(t_2)\right] dt_1 dt_2 \\
&= \int_0^{T_c} \int_0^{T_c} \mathrm{R}_n(t_1, t_2) dt_1 dt_2
\end{aligned} \tag{2.40}
$$

where the autocorrelation of n in this situation is:

$$\mathrm{R}_n(t_1, t_2) = \begin{cases} \sigma_n^2 & t_1 = t_2 \\ 0 & t_1 \neq t_2 \end{cases} \tag{2.41}$$

Substituting yields:

$$E\left[n^2[r]\right] = \int_0^{T_c} \sigma_n^2 dt = T_c \sigma_n^2 \tag{2.42}$$

This variance must be scaled by $1/2$ to account for the effects of demodulation. As a result, it is only necessary to add a $N(0, N_A T_c \sigma_n^2/2)$ random variable to both (2.35) and (2.36) to completely model the demodulation and correlation processes. The scaling factor of N_A is included to account for the use of multiple element antenna arrays.

2.6 Summary

This chapter has presented components of the IS-95 reverse link required for the system simulation model including data encoding, transmission channel parameters, and demodulation and correlation of the received signal. Expressions for the PN and Walsh chip correlation values were derived, including the consideration of background noise and beamforming with multi-element antenna arrays. Additional aspects of the communication model are covered in Chapters 3 (power control) and 4 (data decoding). A brief introduction to beamforming with antenna arrays was included with further details being reserved until Chapter 5.

Additional details on the actual chip-level simulation platform and implementation process can be found in [15].

Chapter 3

Power Estimation and Control

3.1 Introduction

Power control is an important component of a CDMA communication system. If the ratio of the received power from a given mobile to the corresponding interference power is too low, an unacceptably large number of errors in the data flow will occur. Conversely, if this ratio is too high, the mobile will generate excessive interference for other users. Therefore, it is necessary to measure the received signal power and interference power for each user, and then to control the transmission power level for each mobile so that a state of relative equilibrium in the system can be maintained.

This chapter outlines how the received signal and interference power levels are estimated for each mobile. Two types of power control methods, perfect and imperfect, each with different advantages, are explained. The importance of power control in the presence of correlated fading is then illustrated. Finally, the initialization of a mobile's call, including the initialization of its transmission power, is considered.

3.2 Related Research

Research by other individuals which is briefly reviewed here may be divided into two basic areas. One involves developing effective and efficient power control algorithms, whereas the other investigates the effects of imperfect power control on system performance, which is usually, but not always, defined in terms of maximum cell capacity.

3.2.1 Power Control Techniques

Although the power control algorithm for IS-95 has already been defined in the standard (as discussed in Section 3.4.2), it is worth reviewing some of the work that has been performed in this particular area in order to identify any limitations of the present design.

Zander [122] investigated the performance of optimum transmitter power control in a cellular system to reduce cochannel interference. This method was eigenvector-based and determined the optimum power vector which maximized the number of successful users out of all of the mobiles who were requesting access. If the desired carrier-to-interference ratio for a specific link could not be achieved, that link was deemed to be inactive. Thus, this control method may really be better suited for a TDMA or FDMA system, rather than CDMA where system performance can degrade gracefully by relaxing the power requirements, although it could provide an upper bound for performance in this situation. A distributed power control algorithm was then proposed in [121] in which each base station was responsible for its own power control, rather than using a centralized controller for the entire system. This latter design was somewhat unrealistic and infeasible for real-time operation. Leung [53] developed a distributed power control algorithm which included Zander's method as a special case, but which both converged more quickly and was less sensitive to measurement errors. Finally, Wu, Wu, and Zhou [115] applied the algorithms originally introduced by Zander to CDMA and compared outage probabilities obtained from simulations for the different power control techniques.

Hanly [32] developed a decentralized algorithm for determining the optimum allocation of mobiles to base stations in order to maximize system capacity. Each base station was responsible for measuring the interference it received from all users and then broadcasting this value to the mobiles over a control channel. In addition, if a particular cell became congested with heavy traffic, its physical size could be reduced and some of its mobiles handed off to adjacent base stations.

Power control and base station assignment were integrated into one algorithm by Yates and Huang [117]. While maintaining a desired CIR (carrier-to-interference ratio) for each mobile, it is still possible to have many different feasible assignments

of users to base stations. Their MPA (Minimum Power Assignment) algorithm was developed to be optimum in terms of minimizing the total transmitted uplink power.

Ariyavisitakul and Chang [3] investigated a feedback power control method which allowed transmission power to be updated at a higher rate than that of multipath fading. In a sequel paper, Ariyavisitakul [2] proposed a uplink power control algorithm which depended on the signal-to-interference ratio (SIR). Simulation results showed that when cell capacity was exceeded, users with low SIR values suffered while most of the other mobiles were relatively unaffected. Cell capacity could only be effectively increased by reducing the desired power control threshold for all users.

3.2.2 Effects of Imperfect Power Control

In reality, of course, it will not be possible to control the transmission power of each mobile perfectly so that users interfere with each other only to the desired amount. Due to measurement noise and feedback delays, the performance of the power control algorithms will be degraded from their theoretical optimum levels. As a result, a significant amount of research has gone into investigating the effects of imperfect power control on system performance.

Prasad, Kegel, and Jansen [83] demonstrated the need for power control on the reverse link of a CDMA system. This was accomplished by deriving expressions for the outage probability and determining the maximum number of users which could be accommodated with an outage probability of less than 1%. The cases of no power control, perfect power control, and imperfect power control with an assumed log-normal distribution of received power and varying standard deviations were considered. A significant increase in cell capacity was observed when either of the two power control methods were compared against the case of no power control. When no power control feedback was used, the *near-far effect* resulted in nearby users generating more interference than far away mobiles which increased the latters' error rates and thus decreased maximum system capacity.

Naguib [65] studied the effect of closed-loop power control on system performance when base-station antenna arrays were used. It was found that this type of power control could eliminate most of the channel variations. In addition, closed-loop power

control was found to perform better with multiple antennas when the correlation between the antenna elements decreased.

Cameron and Woerner [4] performed an analytical investigation into the effects of imperfect power control on system capacity. This used the probability distribution for multiple-access interference originally derived in [50] and [49], and thus did not require the use of a Gaussian approximation which is less accurate. By comparing imperfect and perfect power control results, it was shown that standard deviations of 1, 1.4, and 2 dB in the E_b/N_0 values corresponded to capacity reductions of 15%, 30%, and 60%, respectively.

Panicker and Kumar [75] evaluated the BER performance of an indoor multipath CDMA system with imperfections in power control, channel parameter estimation, and PN code phase estimation. Power control imperfections were modelled by considering the received signal power to have a log-normal distribution. Variances of 1 and 2 dB in the received power were found to correspond to capacity reductions of 12.5% and 25%, respectively.

The effects of imperfect power control on system performance were investigated by Jansen and Prasad in [39]. They found that the system was quite sensitive to small power control errors with capacity reductions of 50-60% for a power control error of 1 dB. This seems to be excessive when compared to other researchers' results [4] [75].

Kim and Lee [44] examined the effects of imperfect power control on PN sequence acquisition. Determining the mean time for synchronization with a user's PN sequence is important, especially in a packet data type system or when hand-offs are occurring between adjacent cells. Their analytical and simulation results showed that a standard deviation in the power of more than 1 dB resulted in a significant increase in the mean acquisition time.

3.3 Power Measurement

3.3.1 Power Estimation

In order to perform power control, it is necessary to estimate or measure the signal power originating from each mobile. In addition, the interference power resulting from

all of the other mobiles in the system must be estimated. A base station antenna array with N_A elements is assumed here since the results of this derivation can be reduced to the single element case simply by setting $N_A = 1$.

Recall equations (2.33) and (2.34), which give the demodulated in-phase and quadrature components of the received signal for the p^{th} mobile.

$$D_{I_p}(t) = \frac{1}{2}\sum_{i=1}^{N_A}\sum_{k=1}^{N_M}\beta_k w_k(t)\Big\{C_{I_k}\cos(\alpha_{ip}-\phi_{ki}-2\pi f_c\tau_{kp}) + C_{Q_k}\sin(\alpha_{ip}-\phi_{ki}-2\pi f_c\tau_{kp})\Big\} \tag{3.1}$$

$$D_{Q_p}(t) = \frac{1}{2}\sum_{i=1}^{N_A}\sum_{k=1}^{N_M}\beta_k w_k(t)\Big\{-C_{I_k}\sin(\phi_{pi}-\alpha_{ki}-2\pi f_c\tau_{kp}) + C_{Q_k}\cos(\phi_{pi}-\alpha_{ki}-2\pi f_c\tau_{kp})\Big\} \tag{3.2}$$

β_k is the received signal strength as included in equation (2.14), $w_i(t)$ is the current Walsh chip value for the k^{th} mobile, and C_{I_k} and C_{Q_k} represent the current in-phase and quadrature PN chip values which are ± 1.

From the above equations, the received power values for the in-phase and quadrature components of the k^{th} mobile when the beamforming coefficients for the p^{th} mobile are used can be easily shown to be:

$$P_{I_{pk}} = \frac{1}{4}\beta_k^2\left\{\left[\sum_{i=1}^{N_A}\cos(\phi_{pi}-\alpha_{ki}-2\pi f_c\tau_{kp})\right]^2 + \left[\sum_{i=1}^{N_A}\sin(\phi_{pi}-\alpha_{ki}-2\pi f_c\tau_{kp})\right]^2\right\} \tag{3.3}$$

$$P_{Q_{pk}} = \frac{1}{4}\beta_k^2\left\{\left[\sum_{i=1}^{N_A}\sin(\phi_{pi}-\alpha_{ki}-2\pi f_c\tau_{kp})\right]^2 + \left[\sum_{i=1}^{N_A}\cos(\phi_{pi}-\alpha_{ki}-2\pi f_c\tau_{kp})\right]^2\right\} \tag{3.4}$$

where β_k^2 is the received signal strength. For notational simplicity, the following term may be defined:

$$\Upsilon_{pk} = \frac{1}{2}\left\{\left[\sum_{i=1}^{N_A}\sin(\phi_{pi}-\alpha_{ki}-2\pi f_c\tau_{kp})\right]^2 \tag{3.5}$$

$$+ \left[\sum_{i=1}^{N_A} \cos(\phi_{pi} - \alpha_{ki} - 2\pi f_c \tau_{kp}) \right]^2 \Bigg\}$$

Note that $P_{I_{pk}}$ and $P_{Q_{pk}}$ are equal. Since the in-phase and quadrature signal components are independent due to the differing short code PN sequences, the total received power from mobile p will simply be the sum of the two power values.

$$P_{M_p} = P_{I_{pp}} + P_{Q_{pp}} = \Upsilon_{pp}\beta_p^2 \tag{3.6}$$

The corresponding total interference power for the p^{th} mobile will be:

$$P_{I_p} = \sum_{k \neq p} \left(P_{I_{pk}} + P_{Q_{pk}} \right) = \sum_{k \neq p} \Upsilon_{pk}\beta_k^2 \tag{3.7}$$

The power levels will vary between frames due to the updating of the beamforming weights which affects the Υ_{pk} values, and will also vary within a frame due to dynamic Rayleigh fading which affects the received signal envelopes (β_k).

3.3.2 E_b/N_0 Ratio

In a CDMA communication system, the standard unit of power measurement is termed the *bit energy to interference and noise density ratio* which, for the p^{th} mobile, is defined as:

$$\left(\frac{E_b}{N_0} \right)_p = \frac{P_{M_p}/R_B}{P_{I_p}/B + N_A\sigma_n^2} \tag{3.8}$$

where the signal and interference powers are defined in (3.6) and (3.7), respectively. R_B is the data bit rate, B is the bandwidth of the spread CDMA signal, N_A is the number of antenna elements in the event that beamforming at the base station is being performed, and σ_n^2 is the power of the background noise. The noise term must be multiplied by the number of antenna elements to compensate for the use of an antenna array. In addition, the scaling factors of 1/2 (from the demodulation process) and 2 (from considering both the in-phase and quadrature components) which affect the background noise cancel each other and have therefore not been included in the denominator of (3.8).

It is generally desirable to adjust the transmission power of each mobile so that this ratio is maintained at a given value. For a given coding algorithm, the expected BER

(Bit Error Rate) for a given E_b/N_0 can easily be found. Hence, once an acceptable BER for the intended application has been defined (such as 10^{-3} for voice calls), the corresponding desired E_b/N_0 value will be known.

3.3.3 Voice/Data Transmission Activity Factor

In voice applications, users typically spend less than 50% of their time actually talking. The actual percentage of time when speech is active is defined as the voice activity factor (ψ) and is generally assumed to have a value between 0.35 and 0.45. For data transmission applications, ψ can be set to 1.0 to simulate full loading.

During periods of voice inactivity, there is less data to transmit since there is no voice signal to encode and send. Thus, the data transmission rate can be reduced by a factor of ν ($\nu = 8$ for IS-95) when speech is inactive, while still maintaining the communication link. At the same time, the transmission power level is reduced by a factor of ν so that the same E_b/N_0 ratio is maintained. This feature has the effect of reducing the average interference power to other mobiles. As a result, the net capacity of a cell will increase.

In this thesis, periods of speech activity and inactivity are assumed to have exponentially distributed lengths with mean values specified for each of these two quantities. Usually, it is simplest to use the same mean value for both lengths so that a voice activity factor of 0.5 results.

3.4 Power Control Methods

In this section, two different power control methods are discussed. They each have their own advantages and disadvantages for analysis and simulation purposes, as will become evident.

3.4.1 Perfect Power Control

In perfect power control, each mobile's transmission power is set so that its corresponding E_b/N_0 is exactly the desired value. In actuality, since dynamic Rayleigh fading is used, the transmission power levels are chosen such that the observed E_b/N_0

averaged over time will equal the desired value. This is accomplished by using the mean of a squared Rayleigh random variable to represent the average effect of fading on the power levels.

Since the E_b/N_0 ratio depends on both the power received from the desired mobile and the interference power from other mobiles, it is necessary to solve a simultaneous system of N_M linear equations with N_M unknowns in order to determine the appropriate transmission levels for each mobile. It is usually necessary to do this at the beginning of each frame, since channel conditions typically vary from frame to frame.

From (3.8), E_b/N_0 for the p^{th} mobile can be calculated as:

$$\left(\frac{E_b}{N_0}\right)_p = \frac{P_{M_p}/R_B}{P_{I_p}/B + N_A\sigma_n^2} \tag{3.9}$$

where the mobile and interference powers are defined in (3.6) and (3.7), respectively.

Each $(E_b/N_0)_p$ in (3.9) can be set to the exact desired value. This ratio is generally the same for each mobile so the subscript will be dropped. By rearranging this equation, the following expression can be obtained.

$$\left(\frac{E_b}{N_0}\right)\left(\frac{P_{I_p}}{B} + N_A\sigma_n^2\right) = \frac{P_{M_p}}{R_B} \tag{3.10}$$

Substituting (3.6) and (3.7) into (3.10) and taking the expectation yields:

$$\frac{1}{R_B\ (E_b/N_0)}\Upsilon_{pp}E\left[\beta_p^2\right] - \frac{1}{B}\sum_{k\neq p}\Upsilon_{pk}E\left[\beta_k^2\right] = N_A\sigma_n^2 \tag{3.11}$$

If P_{T_p} is the transmission power of the p^{th} mobile, then the expected squared received signal strength from this mobile will be:

$$E\left[\beta_p^2\right] = 2\rho_p\mathcal{S}_pE\left[R^2\right]P_{T_p} \tag{3.12}$$

where the effects of the channel parameters (path loss, shadowing, and Rayleigh fading) on the signal power have been taken into account. P_{T_p} represents the unknown quantity which must be determined. Substituting (3.12) into (3.11) produces the following equation for the p^{th} mobile:

$$\frac{1}{R_B\ (E_b/N_0)}\Upsilon_{pp}\rho_p\mathcal{S}_pE\left[R^2\right]P_{T_p} - \frac{1}{B}\sum_{k\neq p}\Upsilon_{pk}\rho_k\mathcal{S}_kE\left[R^2\right]P_{T_k} = N_A\sigma_n^2 \tag{3.13}$$

There are N_M unknowns (P_{T_p},P_{T_k}) in each equation and p can take on N_M different values. The result is a system of N_M equations with N_M unknowns which can be easily solved using Gaussian elimination.

In this system of equations, quantities are known exactly so the only perturbations in the coefficients are due to the limits of numerical representation within the computer. Consequently, the solution should not be affected by parameter measurement noise which does not exist within the simulation environment. Of far greater importance is whether or not an acceptable solution actually exists.

Either an infinite number of or no solutions will exist if there is any dependence among the above equations. However, Υpk, ρ_k and $\mathcal{S}_k$ are all random quantities in (3.13). Consequently, it is extremely unlikely in practice that one or more of the equations will be linearly dependent on the others.

When all of the equations are linearly independent, a single unique solution to the system of equations will exist. If the obtained transmission power values are positive, an acceptable solution has been found. Conversely, if the solution consists of negative power levels, then the capacity of the cell has been exceeded and the desired level of performance cannot be maintained for all of the mobiles.

Of course, perfect power control does not reflect reality. However, this facility does provide a useful testing scenario for verifying error analyses that assume perfect power control, and also permits significant computational simplifications to be made for simulation purposes.

3.4.2 Imperfect Power Control

A more realistic power control model which is imperfect in nature involves estimating the power received from each mobile over a set period of time, comparing this to the measured noise and interference power, and then instructing each mobile to either raise or lower its transmitted signal strength by some set amount based on whether the observed E_b/N_0 ratio is below or above a specified threshold, respectively. If the number of mobiles does not exceed the capacity of the cell, a situation of relative equilibrium in the power levels can be attained. This method of closed-loop feedback power control is the technique defined in the IS-95 standard and is used here in

simulation experiments. Chang and Ariyavisitakul [5] also described a similar type of power control method for a CDMA system and investigated how the characteristics of a fading multipath channel affected the signal-to-interference ratio. In addition, there is an open-loop power control algorithm included in IS-95 based on the downlink signal strength which is designed to combat slow fading, although it is not considered within this thesis due to the greater importance of the closed-loop feedback. The effects of open-loop power control on capacity were investigated in [7] and [8] for Ricean and Rayleigh fading, respectively.

The feedback control algorithm described above is imperfect in two senses. Firstly, the average E_b/N_0 ratios will not be exactly the desired value due to the quantization of the power adjustment step size. Secondly, there is a time delay involved in the control process. The received power levels must initially be estimated over a period of time. Some additional time is then required to process this data and transmit the appropriate control directions back to each mobile. Thus, there is a definite time lag before a mobile will actually react to its power levels being too low or too high. In addition, there is a nonzero probability that a power control bit (which specifies whether the transmission power should be raised or lowered) will have its value flipped due to transmission noise.

In IS-95, the step sizes for power level adjustments have a fixed value in terms of decibels. Thus, the power levels can only be adjusted at a constant rate, regardless of how quickly the channel parameters are varying. An alternative is to use an adaptive power step size such as in the power control technique proposed by Lee and Steele [46]. In this method, previous power control bits are saved so that the mobile can determine how quickly and in which direction the power levels are changing. If the power levels are remaining relatively constant, the step size is small, so as not to deviate significantly from the desired E_b/N_0 ratio. Conversely, if the power levels are constantly decreasing or increasing, the power adjustment step size is increased in magnitude so that convergence to the desired E_b/N_0 value is achieved more quickly.

As a result of this imperfect power control algorithm, the observed E_b/N_0 ratios for each mobile will tend to vary about the desired value. The degree of this variation depends on the particular fading model which has been selected.

Within the context of this thesis, the received power levels are measured over the length of one power control period. Since there are 16 of these periods in each frame for IS-95, each period has a length of 1536 PN chips. A new power control bit is generated and transmitted at the end of each of these periods.

3.5 Fading and Power Control

When correlated Rayleigh fading is considered at the PN chip-level, it is preferable to use imperfect power control since it is better able to track the changing received power level within the time period of a frame. When a mobile goes into a fade, it is necessary to instruct it to increase its transmission power to reduce the BER. Conversely, if a mobile comes out of a fade, it must decrease its transmission power so that it does not cause excessive interference to the other users in the system. The use of perfect power control with correlated fading is less desirable since it is computationally expensive to solve for the mobile transmission power levels more often than once per frame. Thus, perfect power control cannot track correlated fading values within a frame.

Figures 3.1 through 3.4 and 3.5 through 3.8 show sample received power levels for correlated fading at various mobile velocities for imperfect (closed-loop) power control methods A and B, respectively. Method A has no feedback delay and zero probability of feedback error for the power control bits, whereas method B delays the power control bits by one power control period (1536 PN chips) with a probability of feedback error of 10%. Note that for a given user velocity, the fading pattern is the same for both power control methods in these examples for comparison purposes. By comparing the two power control figures for the same mobile speed, it can be seen that slightly larger deviations from the desired mean value (as shown by the dashed lines) are obtained for method B relative to method A. For both of these methods, the transmitted power was adjusted up or down by 0.5 dB in each power control period. Figures 3.9 through 3.12 show sample power control for method C which is identical to method A except that the power control step is 1 dB. As can be seen, there appears to be little significant difference between the results for methods A and C. Hence, a power control step of 0.5 dB is used almost primarily throughout the

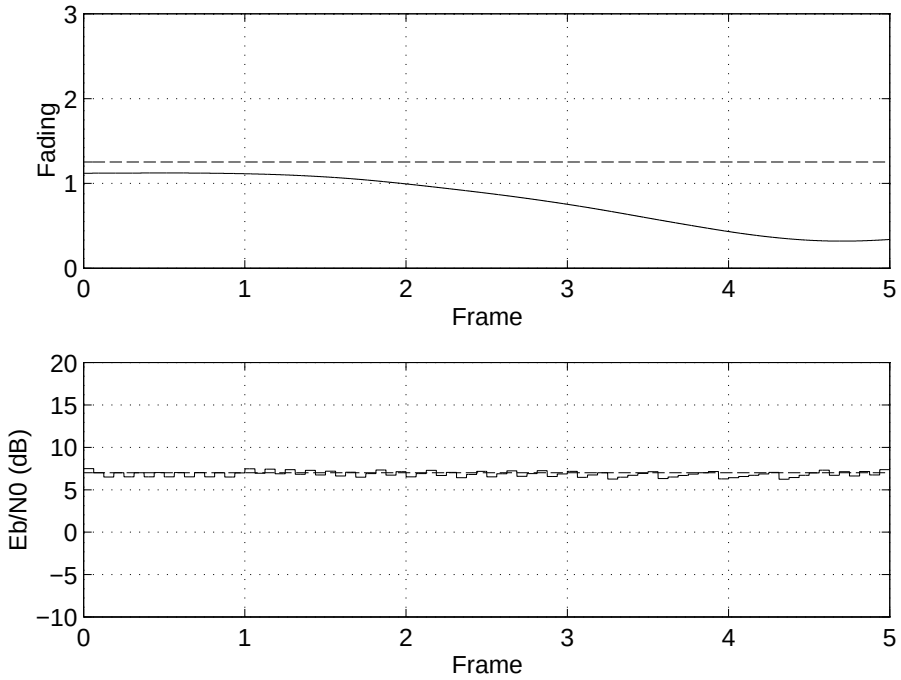

Figure 3.1: Correlated fading and feedback power control at 1 m/s (imperfect power control method A)

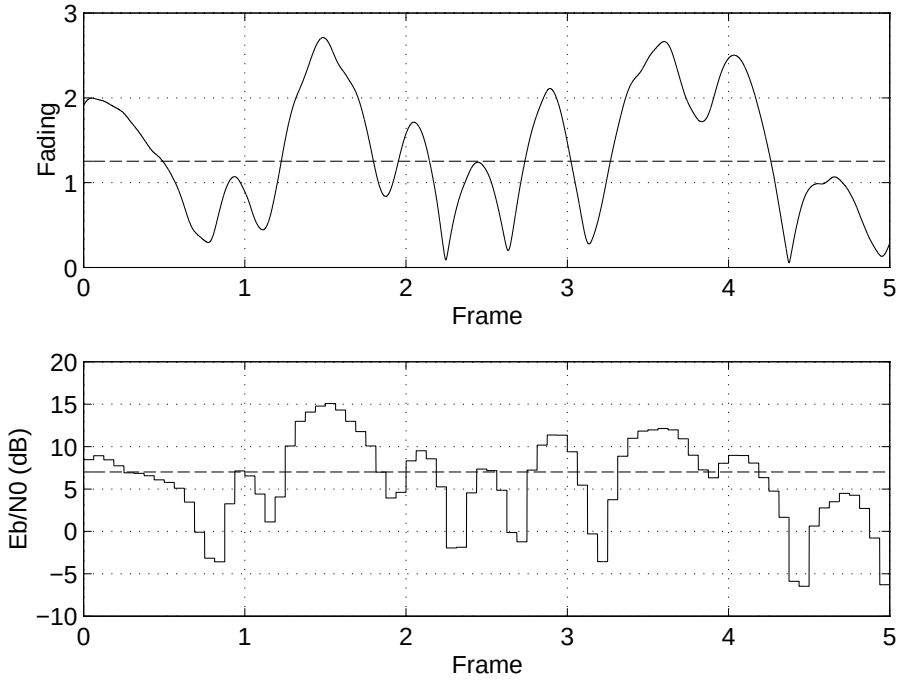

Figure 3.2: Correlated fading and feedback power control at 10 m/s (imperfect power control method A)

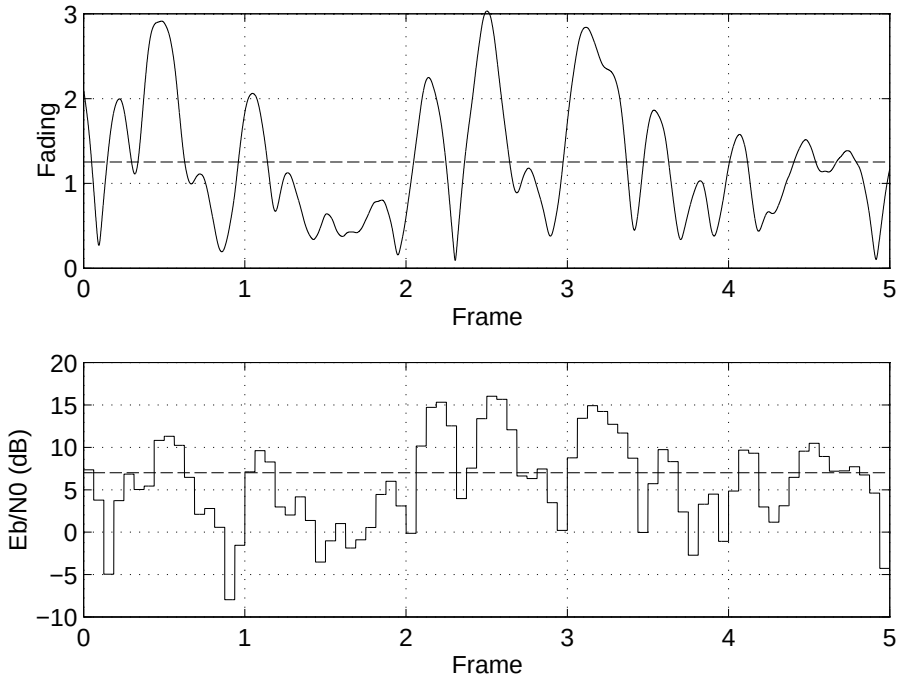

Figure 3.3: Correlated fading and feedback power control at 20 m/s (imperfect power control method A)

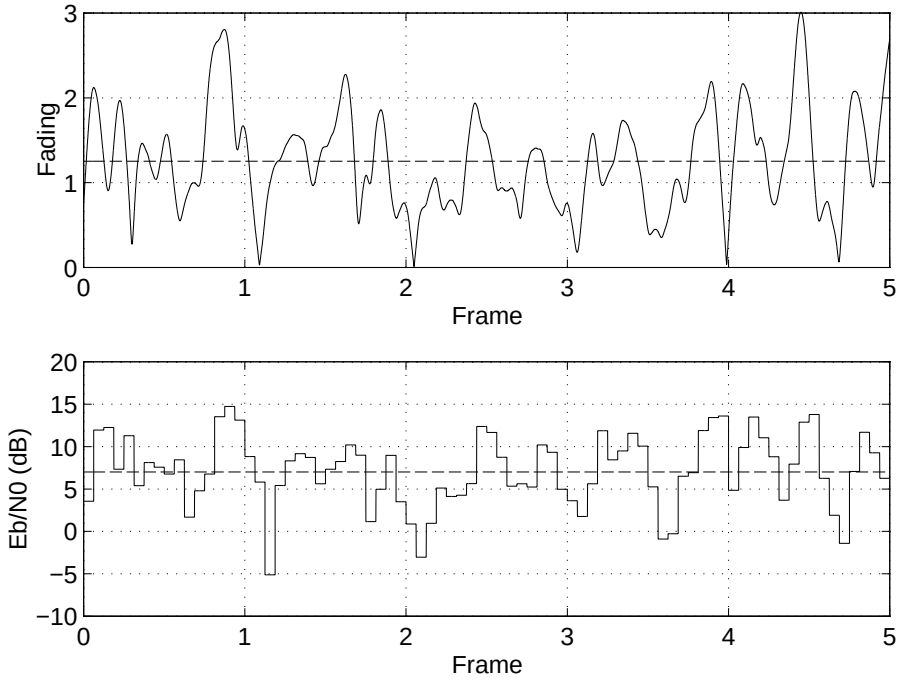

Figure 3.4: Correlated fading and feedback power control at 30 m/s (imperfect power control method A)

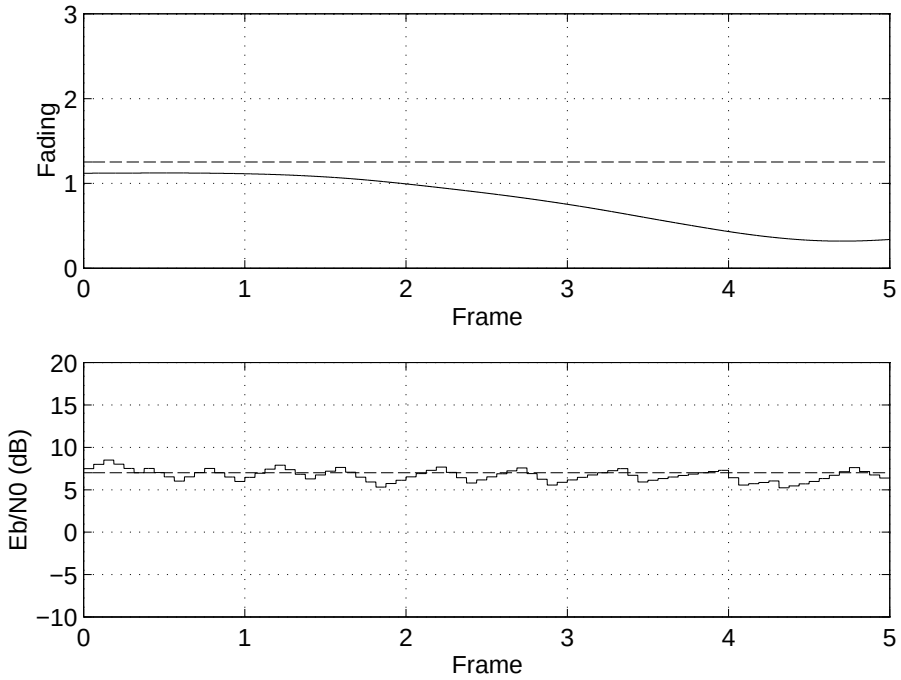

Figure 3.5: Correlated fading and feedback power control at 1 m/s (imperfect power control method B)

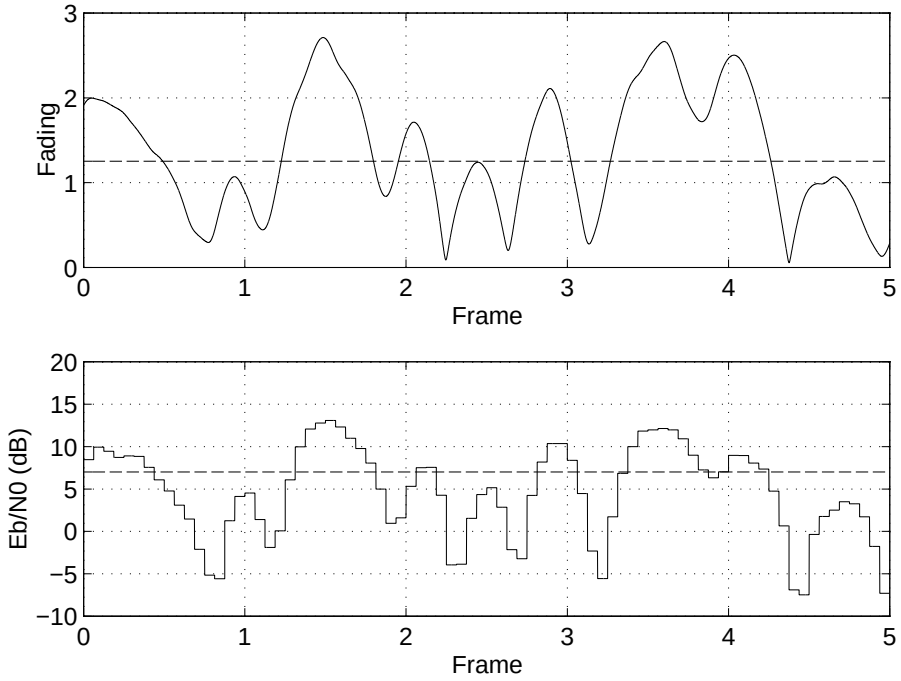

Figure 3.6: Correlated fading and feedback power control at 10 m/s (imperfect power control method B)

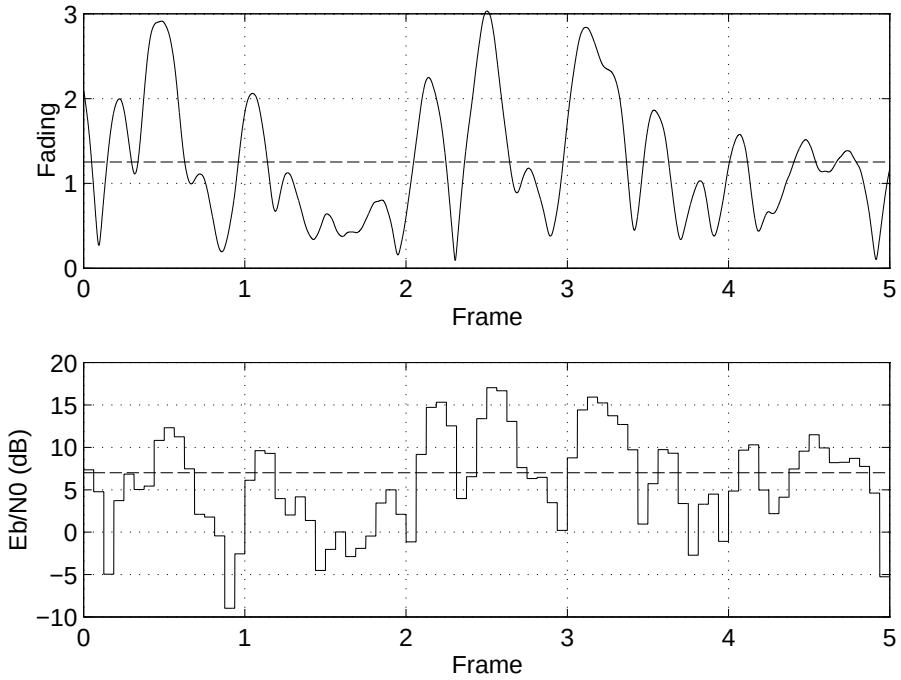

Figure 3.7: Correlated fading and feedback power control at 20 m/s (imperfect power control method B)

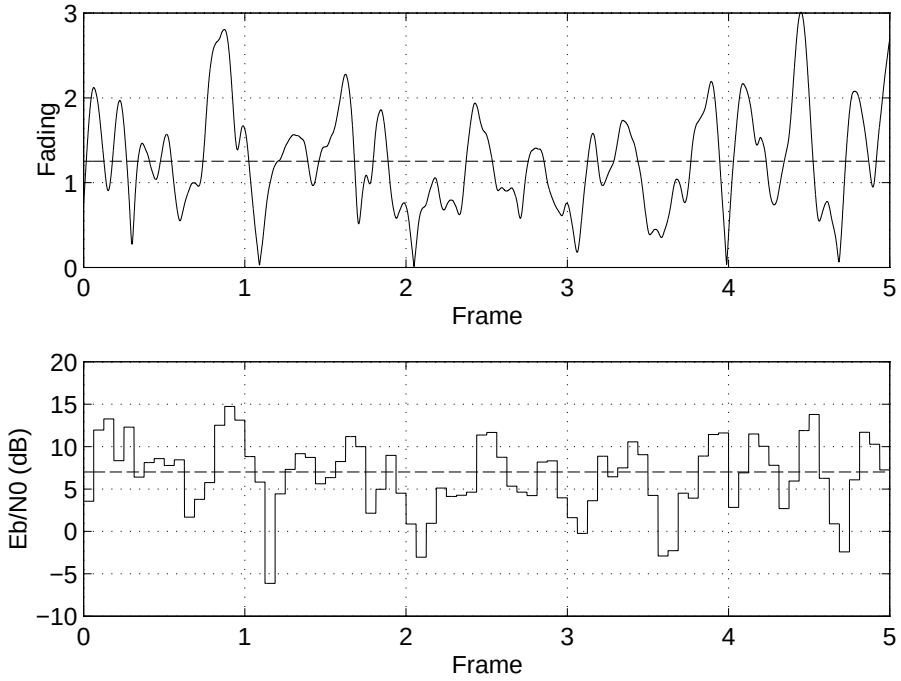

Figure 3.8: Correlated fading and feedback power control at 30 m/s (imperfect power control method B)

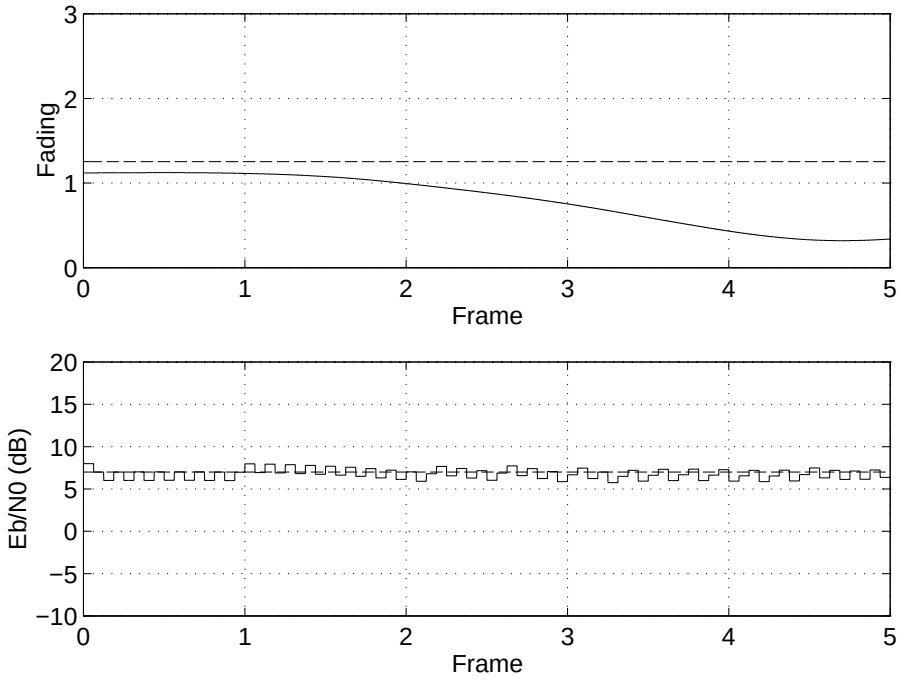

Figure 3.9: Correlated fading and feedback power control at 1 m/s (imperfect power control method C)

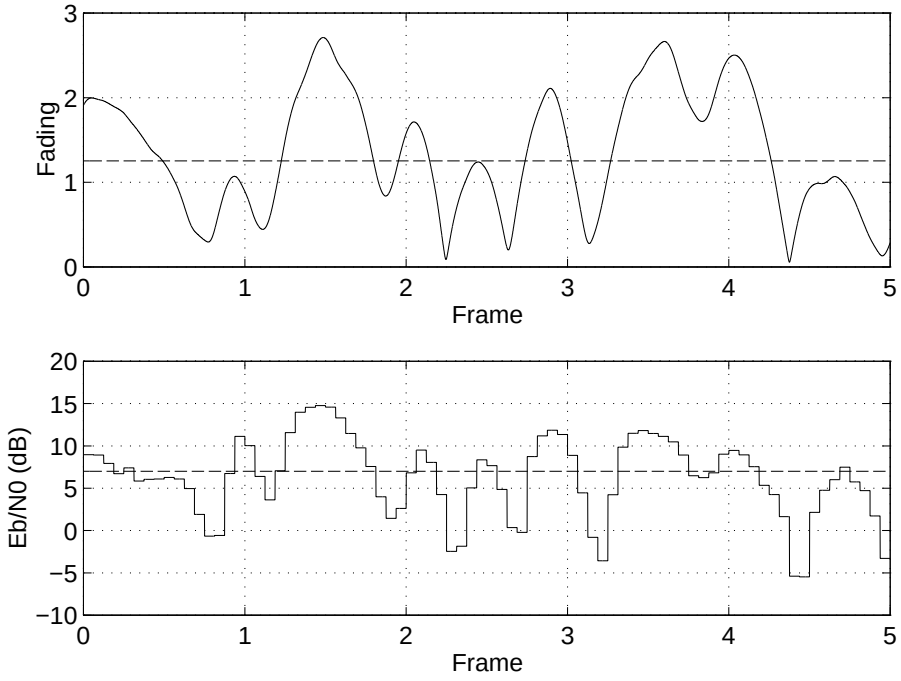

Figure 3.10: Correlated fading and feedback power control at 10 m/s (imperfect power control method C)

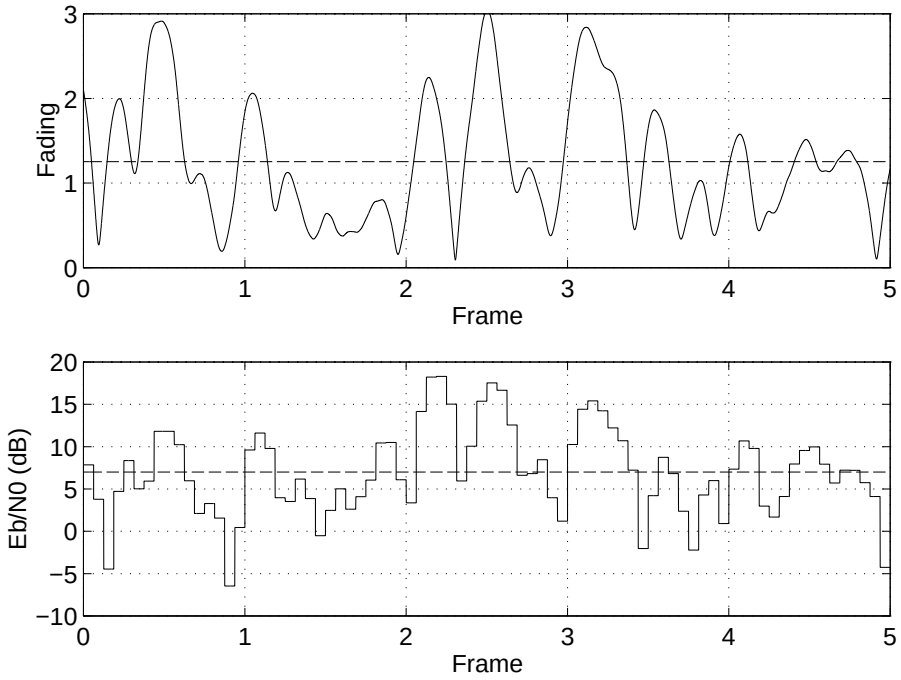

Figure 3.11: Correlated fading and feedback power control at 20 m/s (imperfect power control method C)

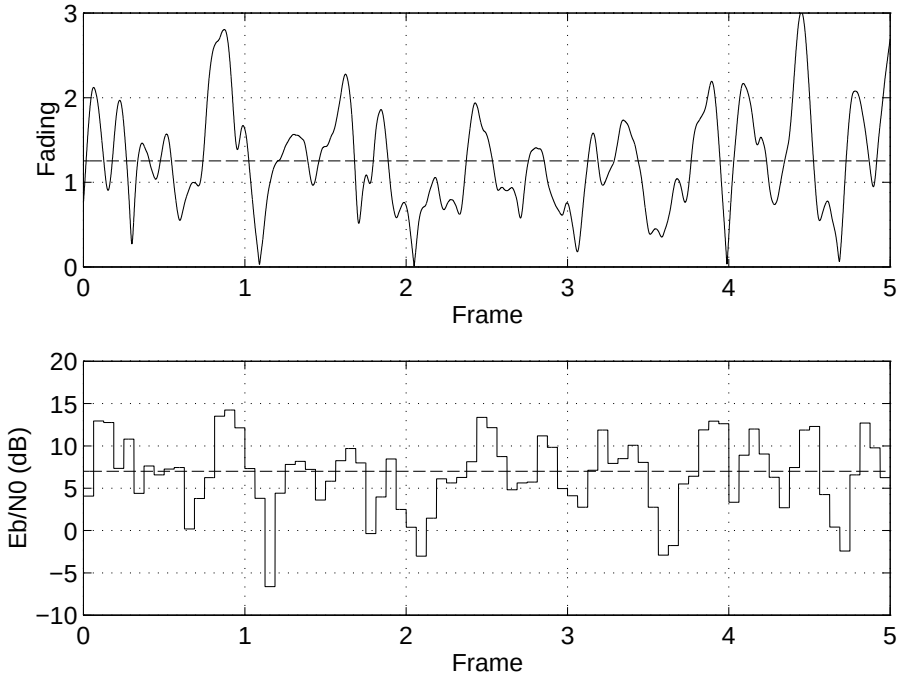

Figure 3.12: Correlated fading and feedback power control at 30 m/s (imperfect power control method C)

remainder of this thesis for experiments involving imperfect power control.

A velocity of 1 m/s corresponds roughly to walking speed, whereas the remaining velocities are primarily for vehicles (note that 10 m/s is 36 km/h). As can be seen from Figures 3.1, 3.5, and 3.9, the closed-loop power control algorithm is rapid enough to follow the slow rate of fading experienced with a mobile velocity of 1 m/s. As vehicle speed increases, however, so does the rate of fading and there are greater fluctuations in the received power levels. This illustrates the importance of encoded bit interleaving, since enough of the redundant information in the signal will still be available for decoding purposes. At high speeds such as 30 m/s, the user does not remain in a particular fade for very long and this actually reduces data loss relative to a slower speed such as 10 m/s as will be demonstrated in Chapter 4.

3.6 Power Levels and Cell Capacity

In CDMA communication systems, the intent of power control is to keep the E_b/N_0 ratio for each mobile at a specified level to guarantee a specific level of performance. When the capacity of the cell has been exceeded, it will prove impossible to accomplish this, as will be shown in Section 7.6. However, the system can still continue to function with additional users by degrading gracefully. That is, if the desired E_b/N_0 value is reduced, a greater number of mobiles can be accommodated at a slightly reduced level of performance before cell capacity is reached. By reducing E_b/N_0 gradually, the corresponding BER will simultaneously gradually increase.

Figures 3.13 through 3.15 show the mean attainable E_b/N_0 ratio from power control simulations for varying numbers of mobiles with desired E_b/N_0 values of 7.0, 6.5 and 6.0 dB, respectively. The solid lines indicate the mean observed values, while the dashed lines represent one standard deviation distance from the mean. The point at which the observed mean begins to decrease represents the maximum capacity of the cell.

If these three graphs are superimposed on top of each other, it will be seen that the three angled lines representing the degraded means will coincide with each other. However, as soon as the capacity of the cell has been attained, the variance of the

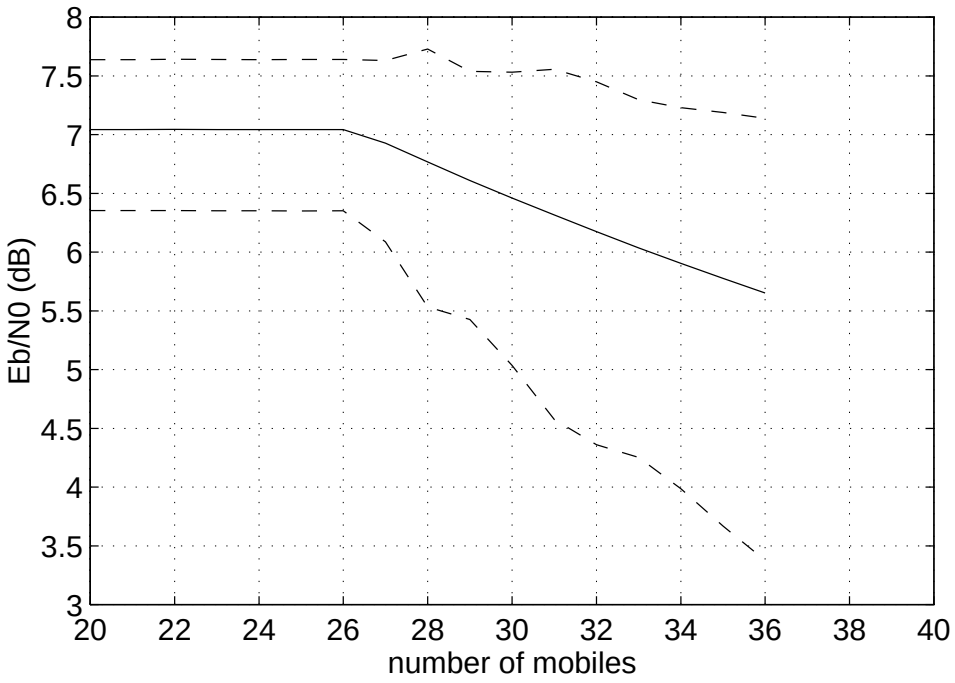

Figure 3.13: Observed power level statistics ($N_A = 1$, $\psi = 1.0$, $E_b/N_0 = 7.0$ dB)

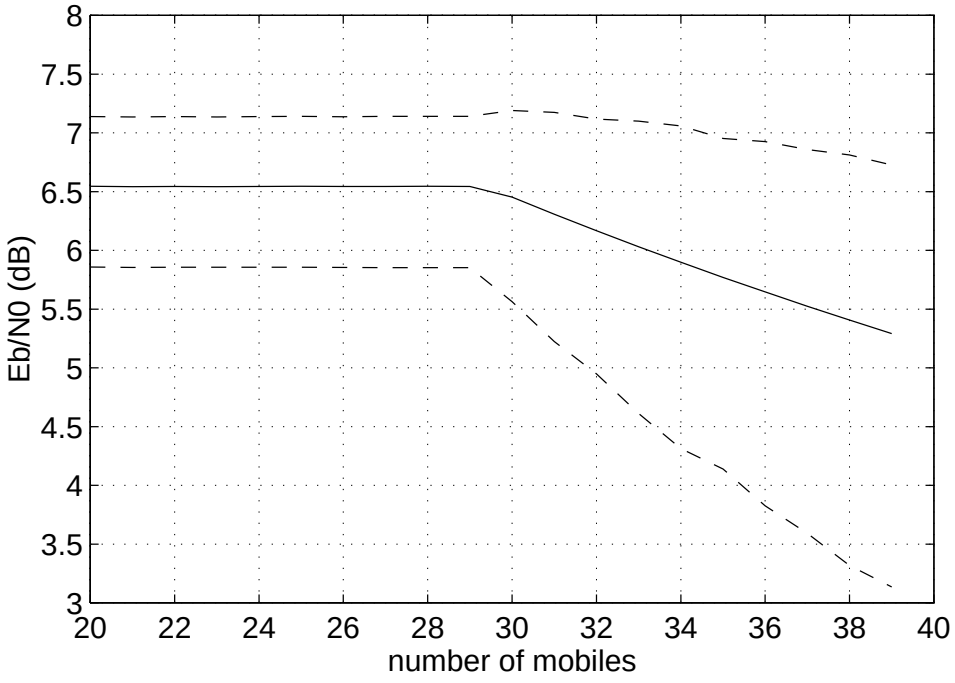

Figure 3.14: Observed power level statistics ($N_A = 1$, $\psi = 1.0$, $E_b/N_0 = 6.5$ dB)

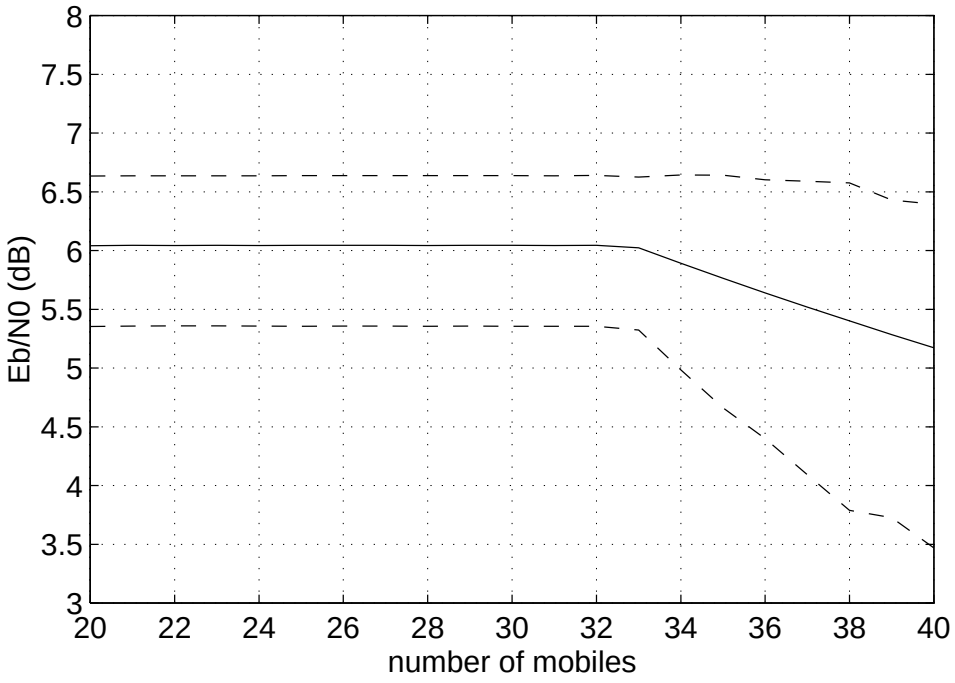

Figure 3.15: Observed power level statistics ($N_A = 1$, $\psi = 1.0$, $E_b/N_0 = 6.0$ dB)

E_b/N_0 values increases significantly, due to the inability of the power control algorithm to maintain each mobile at the desired value. Essentially, the system loses its state of equilibrium. This increased variance results in a significant increase in the observed BER. Consequently, once the cell capacity has been exceeded for $E_b/N_0 = 7.0$ dB, for example, a better level of performance will be obtained by reducing the desired E_b/N_0 to 6.5 dB rather than attempting to maintain $E_b/N_0 = 7.0$ dB for all users. This will degrade system performance slightly, but not to the same extent as would increased variation in the power levels. The alternative, of course, is to refuse to accept new users once the cell has reached capacity. In simulation experiments, mobile calls will be denied if they cannot be initialized with the desired E_b/N_0 ratio due to excessive interference. However, the topic of call admission is not a primary area of focus for this thesis.

3.7 Call Initialization

There are a number of tasks which must be executed whenever a user begins a new call, which include the positioning of the mobile, initialization of transmission paths, selection of the preferred base station, and determination of the mobile's initial transmission power.

The first step is to assign random coordinates to the mobile and ensure that this location physically falls within a valid cell. The nearest base station and its immediately adjacent neighbors (in the event of a multi-cell simulation) are identified and considered as candidates for the base station with which the mobile will communicate.

The length of the call in frames is taken from an exponential probability distribution with a specified mean.

Next, initial path loss and shadowing values are randomly determined for each of the candidate base stations. The path loss depends upon the distances between the mobile and the base stations and is calculated as shown in equation (2.1). The shadowing value is computed from equation (2.2). Based on the path loss and shadowing values, the base station with the least attenuation in the transmission channel is selected as the one with which the mobile will communicate. This may not necessarily

be the nearest one to the mobile due to the variability introduced by the shadowing factor.

The initial transmission power for the mobile is computed. This is accomplished by estimating the total interference and noise power as seen by the base station when synchronized with that particular mobile's signal. This information is then used together with the channel parameters to determine the initial transmission power required to obtain the desired E_b/N_0 ratio. If this power level is above the maximum possible output from the mobile, the call is denied and another attempt must be made to reinitialize it. A count of the number of denied calls is maintained for system performance evaluation purposes.

If P_{M_k} is the power received from the k^{th} mobile and P_{I_k} is the interference power, then the E_b/N_0 ratio is obtained from (3.8) as:

$$\frac{E_b}{N_0} = \frac{P_{M_k}/R_B}{P_{I_k}/B + N_A\sigma_n^2} = \frac{P_{M_k}B}{R_B(P_{I_k} + BN_A\sigma_n^2)} \tag{3.14}$$

Solving (3.14) for P_{M_k} produces:

$$P_{M_k} = \frac{R_B(P_{I_k} + BN_A\sigma_n^2)}{B} \times \frac{E_b}{N_0} \tag{3.15}$$

The average value of the power received from the mobile can be written as:

$$P_{M_k} = E\left[R^2\right]\rho_k\mathcal{S}_k P_{T_k} \tag{3.16}$$

where P_{T_k} is the power of the signal at the transmitter (mobile) and is the quantity to be determined. Note that it is necessary to consider the expected value of the square of R (Rayleigh fading) since it is currently the only quantity which is a random variable during the actual duration of a call.

Equating (3.15) and (3.16) yields:

$$\frac{R_B(P_{I_k} + BN_A\sigma_n^2)}{B} \times \frac{E_b}{N_0} = E\left[R^2\right]\rho_k\mathcal{S}_k P_{T_k} \tag{3.17}$$

Finally, solving (3.17) for P_{T_k} produces:

$$P_{T_k} = \frac{1}{E\left[R^2\right]\rho_k\mathcal{S}_k}\left(\frac{R_B(P_{I_k} + BN_A\sigma_n^2)}{B} \times \frac{E_b}{N_0}\right) \tag{3.18}$$

When simulations are conducted, all of the terms on the right side of (3.18) are known, so the initial signal power can be calculated. The amplitude of the signal envelope at the mobile is the square root of $2P_{T_k}$.

Relative time delays between the signal from the new mobile and signals from existing mobiles are then calculated. This is accomplished by assigning a random absolute time delay for each mobile's signal at each base station whenever a new call is initialized. This time delay is a uniformly distributed random variable in the interval $[0, T_c)$. By comparing the absolute time delay values for the mobiles, it is simple to compute the relative time delays with respect to each mobile.

3.8 Summary

This chapter has described the methodology for performing power estimation and control for the reverse link. To perform accurate power control in a CDMA communication system, it is necessary to estimate the received signal and interference power for each user so that a desired E_b/N_0 ratio can be maintained. Two different power control methods were presented, perfect and imperfect. Perfect power control is useful for simplifying the computational complexity of capacity estimation simulations, as will be shown later, whereas the imperfect algorithm reflects reality more closely. The need for power control to aid in overcoming time-correlated fading was demonstrated with examples showing that fading for slow mobile velocities (*e.g.* 1 m/s) could be tracked with closed-loop power control, whereas faster vehicle speeds resulted in fading situations which relied more upon coding and bit interleaving to protect against data loss. When the system exceeded maximum capacity (in that the desired E_b/N_0 ratio could not be maintained for all mobiles), the feedback power control algorithm was seen to break down with a significant increase in the variance of the mobiles' E_b/N_0 values. Finally, call initialization and the computation of the initial transmission power for a new mobile was discussed.

Chapter 4

Data Decoding

4.1 Introduction

As discussed in Section 2.2, the IS-95 reverse link uses a 32×18 array to block interleave data after convolutional encoding with a rate 1/3 encoder. The resulting bits are then grouped into sets of six that index one of 64 orthogonal Walsh functions, each corresponding to a sequence of 64 Walsh chips.

To decode the received signal, correlation with each of the 64 possible Walsh chip sequences takes place at six-bit intervals. These correlation values may then be used as soft-decision decoding metrics.

Walsh function encoding after block interleaving causes a conventional Viterbi decoder [25] [103] [104] using deinterleaved bit metrics to produce suboptimal results due to suboptimal input metrics. Other techniques for convolutional decoding do exist, such as Fano's sequential decoding algorithm [21], [84, pp. 475] the stack algorithm [40], [84, pp. 477] and feedback decoding [84, pp. 480]. However, these alternative methods are used primarily when dealing with large constraint lengths and are thus not directly applicable to the IS-95 uplink decoding situation.

Chang *et al* [6] compared the performance of two orthogonal coding techniques similar to the Walsh functions of IS-95. For bit interleaving, the soft-decision decoding method outlined in Section 4.2.3 was used. The second method interleaved the Walsh symbols rather than individual bits and was found to outperform the first approach in a personal wireless communications environment, although it did not match the

IS-95 coding standard. However, the combined decoder/deinterleaver proposed here is different from both of these techniques. In addition, Viterbi, Viterbi, and Zehavi [106] investigated a power-controlled CDMA system with orthogonal coding, although this was strictly an analytical study with simplifying assumptions.

In this chapter, Section 4.2 outlines various existing Viterbi-based decoding strategies and then proposes a combined soft-decision deinterleaver/decoder which provides improved performance over conventional Viterbi decoding with deinterleaved soft-decision bit metrics. The expected decoder performance of IS-95 cellular CDMA with no interleaving is then derived in the following section for verification purposes. Simulation results for the various described decoding methods are presented in Section 4.4 and aid in showing the improvement of the new proposed algorithm over previously-used techniques. Details of the combined deinterleaver/decoder have also been proposed in [18].

4.2 Decoding Strategies

This section discusses various options for decoding the received signal data. The case of no interleaving is considered first since it is the simplest and forms the basis for the other methods. Next, the use of deinterleaved hard-decision and soft-decision bit metric values is examined. Finally, a combined deinterleaver/decoder which provides enhanced performance is proposed.

4.2.1 No Interleaving

For noninterleaved data, standard Viterbi decoding [104] may be applied to the Walsh sequences by using the Walsh function correlations as metrics to evaluate surviving paths in the trellis. Each branch between two successive nodes in the decoding trellis has a known Walsh function value associated with it. Thus, the correlation value for a specific Walsh function can be assigned as the metric for any branches which match that particular function value at the given position within the frame. Since each Walsh function represents two data bits, each state transition in the trellis outputs two data bits instead of the usual one. This double state transition eliminates the

need to subdivide the Walsh correlation metrics.

4.2.2 Deinterleaved Hard-Decision Bit Metrics

If a block interleaver is included in the coding process, it is necessary to generate individual metrics for each convolutionally-encoded bit. These bit metrics can then be deinterleaved and summed in groups of six to form deinterleaved Walsh metrics. The result is appropriate for decoding as outlined in Section 4.2.1.

One method to generate such bit metrics is by hard-decision decoding [60, pp. 298]. At each Walsh function boundary, the Walsh function with the highest correlation is selected as being correct. Bit metrics are then assigned based on the Hamming distance from the binary form of the selected Walsh function. That is, bits which match the selected Walsh function value are assigned a bit metric equal to the Walsh correlation value, whereas nonmatching bits are assigned a bit metric of zero.

Table 4.1 illustrates a hard-decision bit metric assignment when three-bit Walsh functions are considered. The maximum value from the upper table occurs for Walsh function 6 (with a binary value of 110), and thus individual hard-decision bit metrics for this particular set of bits within the frame would be set as shown in the lower table.

This technique is suboptimal for two reasons. First, the hard-decision quantization discards useful information. Second, since the Walsh functions are orthogonal, the correlations for incorrect Walsh functions should be zero-mean. However, hard-decision decoding will often cause an incorrect deinterleaved Walsh function to have a nonzero correlation which is closer to that of the correct Walsh function. This will increase the probability of selecting an incorrect path, thus raising the number of decoding errors.

4.2.3 Deinterleaved Soft-Decision Bit Metrics

Soft-decision decoding is more desirable, as it generally outperforms the thresholding of hard-decision decoding [60, pp. 297-302] and can be implemented with almost no additional effort. For this reason, soft-decision Walsh correlation bit metrics have typically been used in recent IS-95 performance studies [6] [37] [69] [71]. For each

Walsh Function	Binary Representation	Correlation Metric
0	000	6
1	001	2
2	010	7
3	011	4
4	100	1
5	101	5
6	**110**	**8**
7	111	3

Bit Position	Bit Value	Bit Metric
0	0	0
	1	8
1	0	0
	1	8
2	0	8
	1	0

Table 4.1: Bit metric calculation example for interleaved hard-decision decoding

Walsh Function	Binary Representation	Correlation Metric
0	000	6
1	001	2
2	010	7
3	011	4
4	100	1
5	101	5
6	110	8
7	111	3

Bit Position	Bit Value	Bit Pattern	Bit Metric
0	0	0−−	7
	1	1−−	8
1	0	−0−	6
	1	−1−	8
2	0	−−0	8
	1	−−1	5

Table 4.2: Bit metric calculation example for interleaved soft-decision decoding

specific bit value and position in the binary representation of a Walsh function, there are 32 Walsh functions which match the given bit value at that bit position. Normally, the largest of these 32 Walsh function correlations is assigned as the soft-decision value for that particular bit position.

Table 4.2 contains a simple example of a bit metric assignment for the case of eight different three-bit Walsh functions. The upper table lists the Walsh function correlations for some position within a frame. The lower table selects the highest correlation from among all Walsh functions which match the specified bit pattern. Thus, individual bit metrics have been assigned for each bit value and position, and the data sequence can be decoded using a method similar to that in Section 4.2.1.

This approach, although representing an improvement over quantized hard decisions, is also suboptimal due to the loss of Walsh function orthogonality as described in Section 4.2.2.

4.2.4 Combined Deinterleaving/Decoding

Observe that the IS-95 interleaved convolutionally-encoded bits appear in the order:

$$b_0 b_{32} b_{64} \ldots b_1 b_{33} b_{65} \ldots b_{543} b_{575} \tag{4.1}$$

where the subscript denotes time. Thus, the correlation value of the first encoded Walsh function will depend on bits $\{b_0, b_{32}, b_{64}, b_{96}, b_{128}, b_{160}\}$. However, for standard Viterbi decoding, the convolutionally-encoded bits must be processed in time-sequential order $(b_0, b_1, b_2, \ldots)$. In the case of interleaving, as a progression is made through the decoding trellis, the six convolutionally-encoded bits corresponding to each pair of data bits will therefore be distributed among six different received Walsh functions in a given frame.

As surviving paths are generated during decoding, a possible received data signal is gradually defined for each path. However, due to the interleaving, not all bits of each received Walsh function will be simultaneously defined during decoding. Clearly, a method of sequentially evaluating a path metric based on the correlations of partially-specified Walsh functions is required. Instead of directly deinterleaving bit metrics, another option is to reevaluate possible path metrics at each stage of the

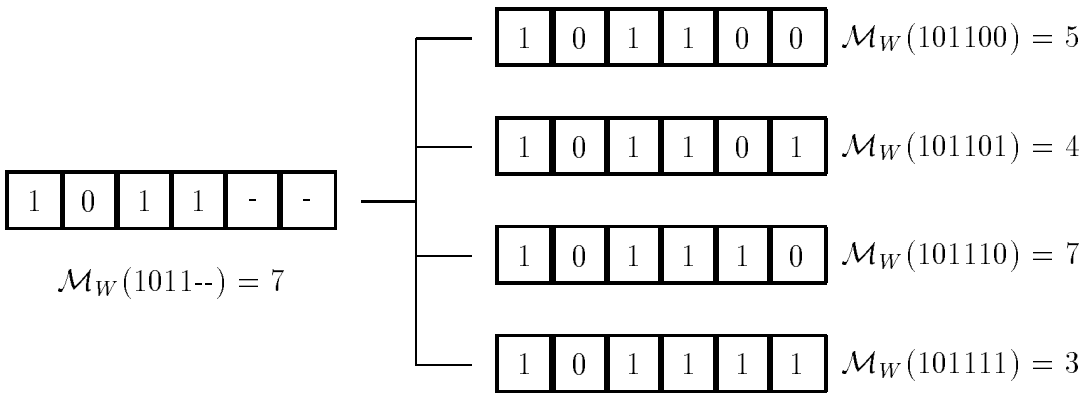

Figure 4.1: Illustration of partially-known Walsh function metric calculation

decoding process, based on available path state information. These calculations can be structured to be efficient in terms of computation time and delay.

There are 2^6 possible metrics for every six bits within a frame. If only the first k of these six bits are known, there are 2^{6-k} different matching Walsh functions. A metric can be formed by taking the maximum Walsh correlation from among these 2^{6-k} partial matches. For example, if the first four bits are 1011, then Walsh functions 44 through 47 are potential matches (see Figure 4.1), and the maximum correlation in this case is $\mathcal{M}_W(1011{-}{-}) = 7$. Another example using three-bit Walsh functions is shown in Table 4.3. The *differential metric* denotes the difference between the metric of the current partially-defined Walsh function and that of the Walsh function with one less bit being defined. These differential metrics are precalculated before decoding each frame for efficient implementation. As can be seen from the tables, these metrics are easily calculated in a progressive manner by selecting the maximum of the two previous matching differential metrics.

A metric value for a partially-specified Walsh function can be defined as:

$$\mathcal{M}_W(\mathcal{P}, i, b_i) \equiv \begin{cases} \max\left[C_F(\mathcal{P}, i, b_i)\right] & b_i > 0 \\ 0 & b_i = 0 \end{cases} \tag{4.2}$$

where b_i bits have been received for the i^{th} Walsh function position in path $\mathcal{P}$. The quantity, $\max\left[C_F(\mathcal{P}, i, b_i)\right]$, represents the maximum correlation for all Walsh functions that share the same first b_i bits in position i of path $\mathcal{P}$.

Binary Form	Metric Value	Differential Metric
000	6	+0
001	2	−4
010	7	+0
011	4	−3
100	1	−4
101	5	+0
110	8	+0
111	3	−5

Binary Form	Metric Value	Differential Metric
00−	6	−1
01−	7	+0
10−	5	−3
11−	8	+0

Binary Form	Metric Value	Differential Metric
0−−	7	+7
1−−	8	+8

Table 4.3: Illustration of computation of partially-known Walsh function metric values

As the bits of a particular Walsh function become defined during decoding, the contribution of that Walsh function to the overall path metric can be adjusted accordingly. The metric value for a surviving path $\mathcal{P}$ can be calculated as:

$$\mathcal{M}_P(\mathcal{P}) = \sum_{i=1}^{96} \mathcal{M}_W(\mathcal{P}, i, b_i) \tag{4.3}$$

Note that only six Walsh functions in each path are modified at each decoding stage. Thus, rather than reevaluating all of the summation terms in (4.3) at every stage, it is only necessary to modify the six $\mathcal{M}_W(\cdot)$ values which have changed. This can be accomplished most efficiently simply by adding the relevant precalculated differential metric values to the current path metric.

In this situation, it is possible that an incorrect path may temporarily have the largest metric value partway through the decoding process. The deinterleaver/decoder should therefore retain multiple surviving paths at each trellis node in order to reduce the possibility of accidentally deleting the optimal path. This differs from the conventional Viterbi decoder where only the best surviving path need be retained since it is known to be optimal.

For further clarification, Figure 4.2 summarizes the basic steps of the proposed decoding process.

4.3 Performance Bound Approximation

It is possible to estimate the BER for uncorrelated Rayleigh fading with no interleaving. This can be used as a performance bound for the case of perfect (infinite) interleaving and also for decoder verification purposes. Holtzman [34] presented a computationally-inexpensive method for evaluating the error probability of a standard spread-spectrum system without the additional coding layer of IS-95. Jalloul and Holtzman [38] conducted a performance analysis of the uplink of a CDMA system with M-ary orthogonal modulation similar to the Walsh functions of IS-95 and derived expressions for the BER, although the convolutional encoding step was not considered. In addition, power control did not appear to be considered which meant that the observed BER increased steadily with the number of users, instead of remaining constant for a given E_b/N_0 value. Consequently, it is necessary to derive the

Let N_S denote the number of surviving paths to be retained.

At each decoding trellis stage and node, do the following:

1. Extend each surviving path P to form four new paths P_i $(1 \leq i \leq 4)$.
2. For each new path, update the appropriate six Walsh functions with the newly-defined bits, and reevaluate the path metric in Equation (4.3) by adding the precalculated differential metrics.
3. Keep the best N_S paths at each trellis node.

Figure 4.2: Summary of the combined deinterleaver/decoder algorithm for the reverse link of IS-95 with interleaving

expected BER for IS-95 from first principles here, due to IS-95's multilevel coding scheme.

The derivation of the Walsh function correlation statistics is postponed until Chapter 6. From Section 6.2, the correct and incorrect Walsh function correlations are Gaussian $N(\mu_F, \sigma_F^2)$ and $N(\mu_{\overline{F}}, \sigma_F^2)$ random variables, respectively, where:

$$\mu_F = 128\sqrt{2\pi}T_c\sqrt{E[P]} \tag{4.4}$$

$$\mu_{\overline{F}} = 0 \tag{4.5}$$

$$\sigma_F^2 = 512\left\{\frac{(N_M-1)T_c^2\{(\nu-1)\psi+1\}E[P]}{3\nu} + \frac{1}{2}T_c\sigma_n^2\right\} \tag{4.6}$$

In (4.4) and (4.6), T_c is the PN chip period, N_M is the number of mobiles, ν is the factor by which transmission power is reduced when no data is being transmitted, ψ is the voice activity factor, and σ_n^2 is the background noise variance. Only the case of a single antenna element is considered here for purposes of simplicity.

The expected received power in (4.4) and (4.6) can be calculated as shown in equations (6.25) or (6.26) for voice activity factors of $\psi = 1.0$ and $\psi < 1.0$, respectively.

4.3.1 Path Metrics

Consider the correct path $\mathcal{P}_1$ and an incorrect path $\mathcal{P}_2$ which differ in d Walsh functions. It is necessary to statistically characterize the Walsh functions which are not common to both paths. Let M_1 and M_2 represent the metric values for the dissimilar portions of the two paths. Since these are simply the summation of Gaussian random variables, M_1 and M_2 will have distributions $N(\mu_1, \sigma_1^2) = N(d\mu_w, d\sigma_w^2)$ and $N(\mu_2, \sigma_2^2) = N(0, d\sigma_w^2)$, respectively. Their difference, $M_3 = M_2 - M_1$, will also be Gaussian with parameters:

$$\mu_3 = \mu_2 - \mu_1 = -d\mu_w \tag{4.7}$$

$$\sigma_3^2 = \sigma_2^2 + \sigma_1^2 = 2d\sigma_w^2 \tag{4.8}$$

The probability of the incorrect path having the higher metric value is:

$$P(M_2 > M_1) = P(M_2 - M_1 > 0) = P(M_3 > 0) \tag{4.9}$$

$$= \frac{1}{2}\,\mathrm{erfc}\left(\frac{0-\mu_3}{\sqrt{2}\sigma_3}\right) = \frac{1}{2}\,\mathrm{erfc}\left(\frac{\mu_w}{2\sigma_F^2}\sqrt{d}\right)$$

4.3.2 Bit Error Rate Evaluation

The above statistics can be propagated through a standard Viterbi decoder to yield an estimated BER. Only the noninterleaved case is considered, since an analytical investigation of the combined deinterleaver/decoder appears intractable.

The approach in [84] [105] for obtaining an upper bound to the BER is refined here in order to obtain an actual approximate expectation. From (4.9) and [84, pp. 459-463]:

$$P_B \approx \frac{1}{2}\sum_{d=d_{\mathrm{free}}}^{\infty} \beta_d\,\mathrm{erfc}\left(\frac{\mu_w}{2\sigma_F}\sqrt{d}\right) \tag{4.10}$$

In (4.10), the minimum free distance is $d_{\mathrm{free}} = 5$ for IS-95, β_d is a weighting coefficient based on the number of paths and output bit errors, and d represents the distance of an incorrect path from the correct path in terms of the number of incorrect Walsh functions. The computation of β_d is described in Appendix A.

It should be noted that (4.10) is only an approximation due to the finite frame length and also to the assumed statistical independence of distinct path metrics, which is not the case in actuality since trellis branches are shared among a number of paths. In practice, usually a maximum of only 25 terms of the summation in (4.10) are required due to the exponential decrease of the erfc$(\cdot)$ term.

4.4 Simulation Results

The combined deinterleaver/decoder algorithm has been evaluated in a chip-level reverse link simulation of IS-95 [15], consisting of a mobile in a circular cell of radius 500 m. The probability distributions for the inputs to the Viterbi decoder in a memoryless channel are derived in Section 6.2 and verified in Section 6.5. It is therefore possible, in this instance, to generate these random values directly without requiring PN chip-level simulation.

Figure 4.3 plots the simulated BER of memoryless Rayleigh fading for deinterleaved hard-decision bit metrics (Sec. 4.2.2), deinterleaved soft-decision bit metrics

(Sec. 4.2.3), and the proposed deinterleaver/decoder (Sec. 4.2.4) with one and two surviving paths being retained, respectively. Simulated noninterleaved results (Sec. 4.2.1) and the analytically calculated BER (Sec. 4.3.2) are also included for comparison. At low E_b/N_0, incorrect path selection reduces interleaving performance, while at high E_b/N_0, the correlated Walsh functions reduce the relative performance of the non-interleaved system. From Figure 4.3, the combined deinterleaver/decoder with one surviving path provides about a 1 dB improvement over soft-decision (Sec. 4.2.3) and a 2 dB improvement over hard-decision (Sec. 4.2.3) at a BER of 10^{-3}. Retaining two surviving paths instead of one yields another 0.5 dB improvement at the cost of additional computational expense.

When comparing the analytical and simulated BER for no interleaving, good agreement is obtained over the E_b/N_0 range from 3.5 to 5.5 dB. An exact correspondence is not expected since there may be significant branch overlap between the longer trellis paths which were assumed to be statistically independent in the analysis. At lower E_b/N_0, longer paths have a nonnegligible contribution to the summation in (4.10), and the assumed statistical independence breaks down.

Time-correlated Rayleigh fading represents a more realistic evaluation environment for interleaving in IS-95. These simulations were conducted at the PN chip-level using correlated shadowed fading [56]. Figures 4.4 through 4.6 show the simulated BER for user velocities ranging from 1 to 30 m/s with soft-decision decoding, and combined deinterleaving/decoding with one and two surviving paths being retained respectively. As expected, lower BERs are observed at higher velocities since the mobile remains in fades for shorter periods of time. At low mobile velocities such as the pedestrian speed of 1 m/s, however, the IS-95 closed-loop power control algorithm is rapid enough to compensate for the slow fading as shown in Section 3.5, and a much lower BER is thus observed. Clearly, as the decoder complexity increases, the corresponding observed BER values simultaneously decrease, and the gains obtained for the proposed decoder with correlated fading appear to be similar to those observed for uncorrelated fading. Figure 4.7 illustrates the improvement in BER through the introduction of interleaving for user velocities of 1 and 20 m/s in correlated fading.

Finally, Figure 4.8 shows the improvement obtained by increasing the number of

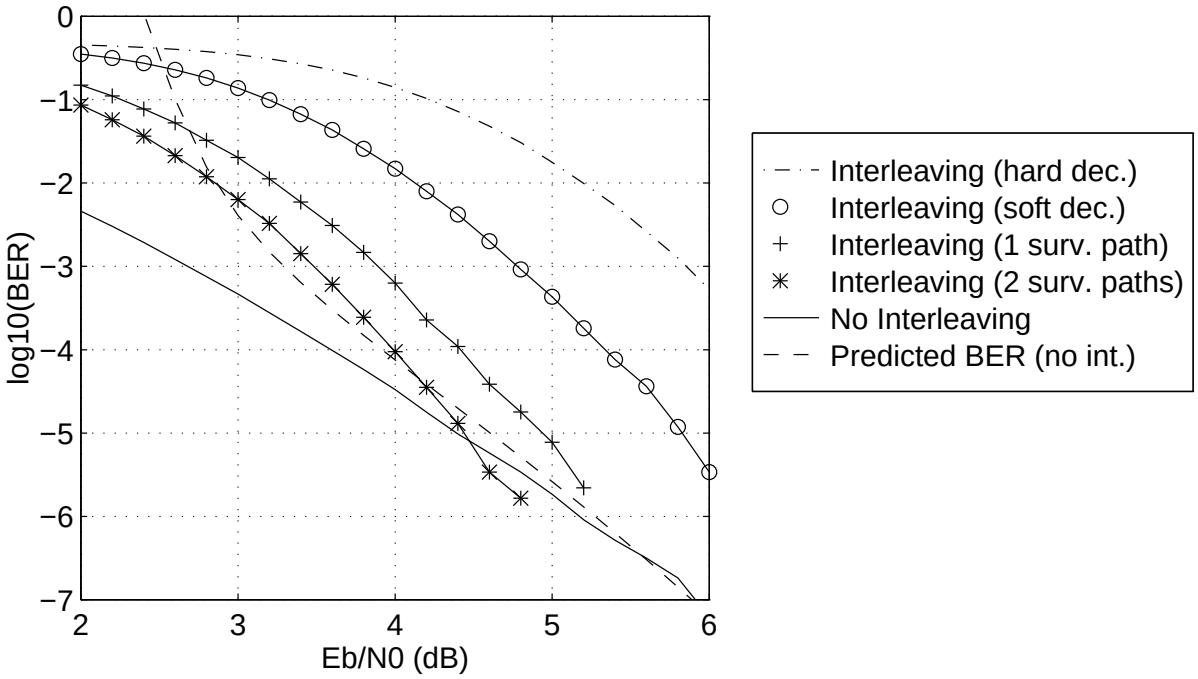

Figure 4.3: BER for 1 mobile with uncorrelated Rayleigh fading

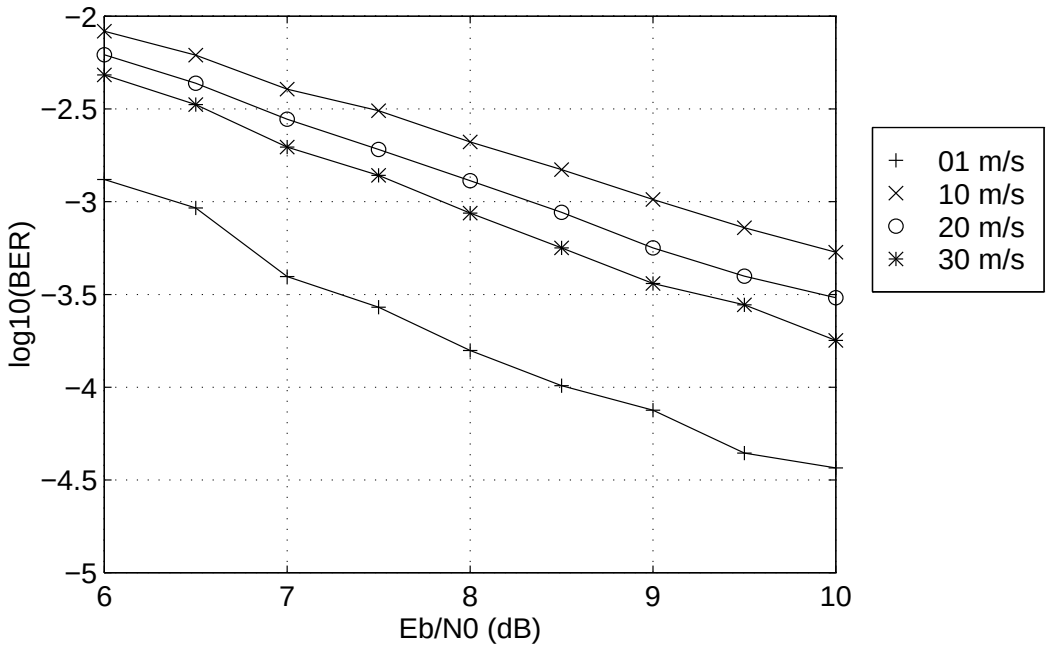

Figure 4.4: BER for 1 mobile with correlated Rayleigh fading and interleaving (deinterleaved soft-decision decoding)

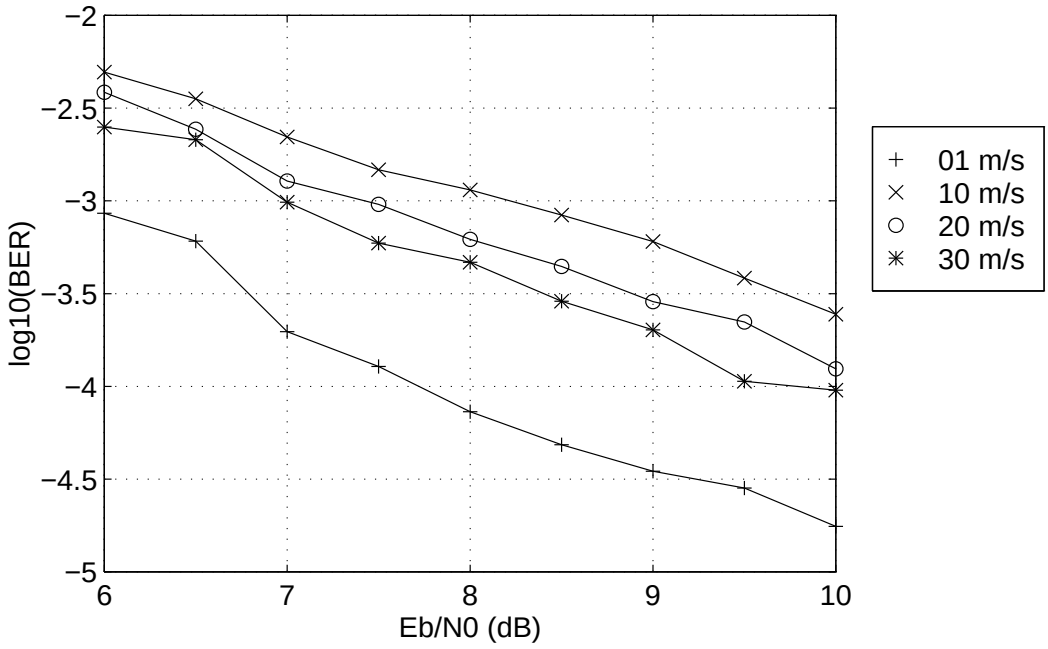

Figure 4.5: BER for 1 mobile with correlated Rayleigh fading and interleaving (combined deinterleaver/decoder with 1 surviving path)

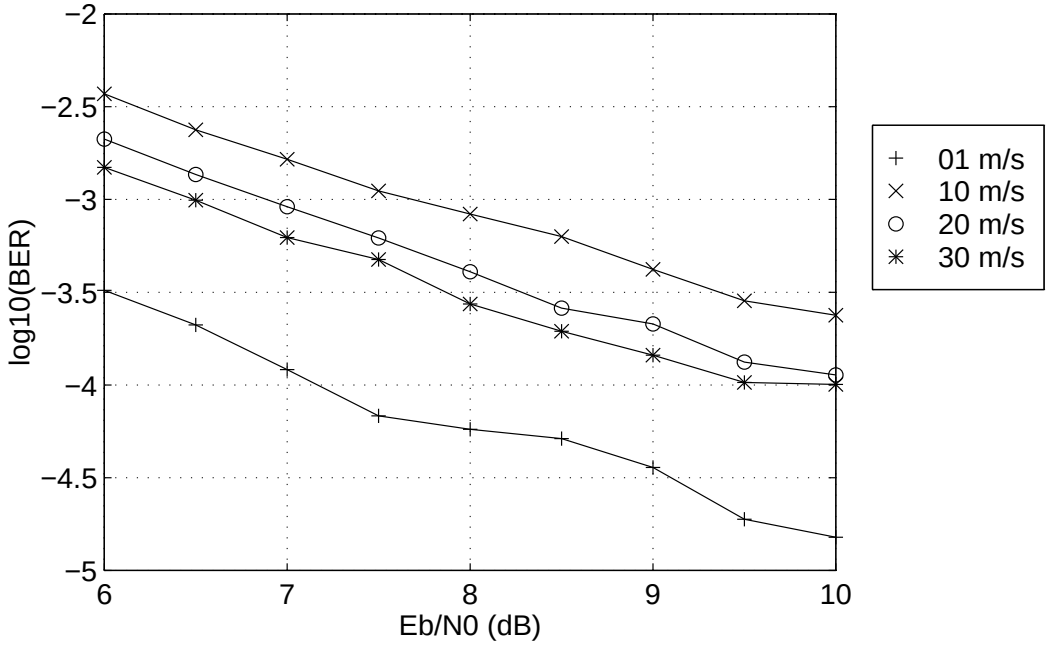

Figure 4.6: BER for 1 mobile with correlated Rayleigh fading and interleaving (combined deinterleaver/decoder with 2 surviving paths)

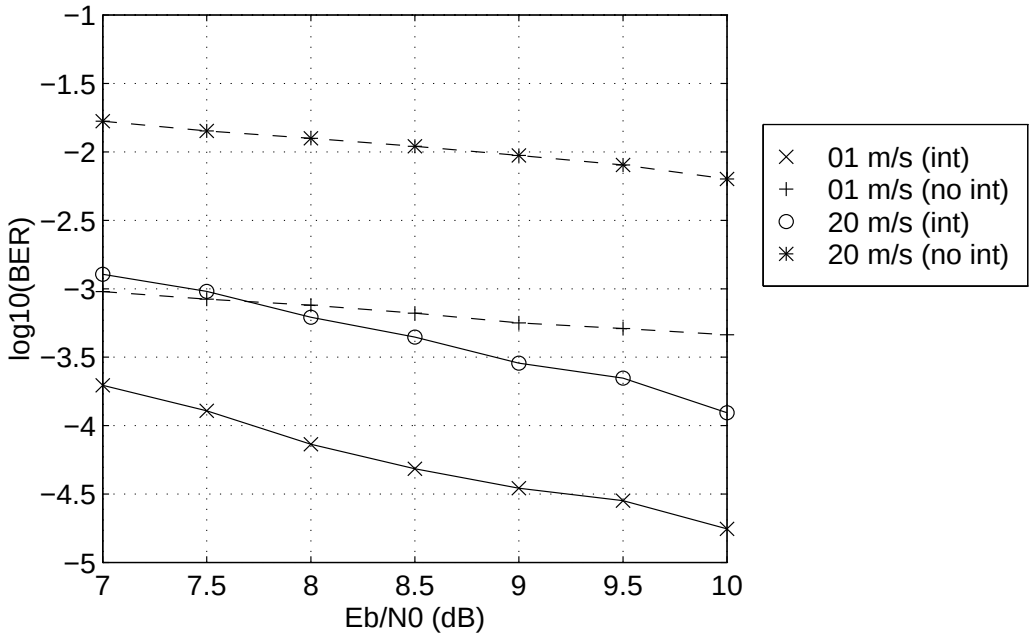

Figure 4.7: BER for 1 mobile with correlated Rayleigh fading (with and without interleaving)

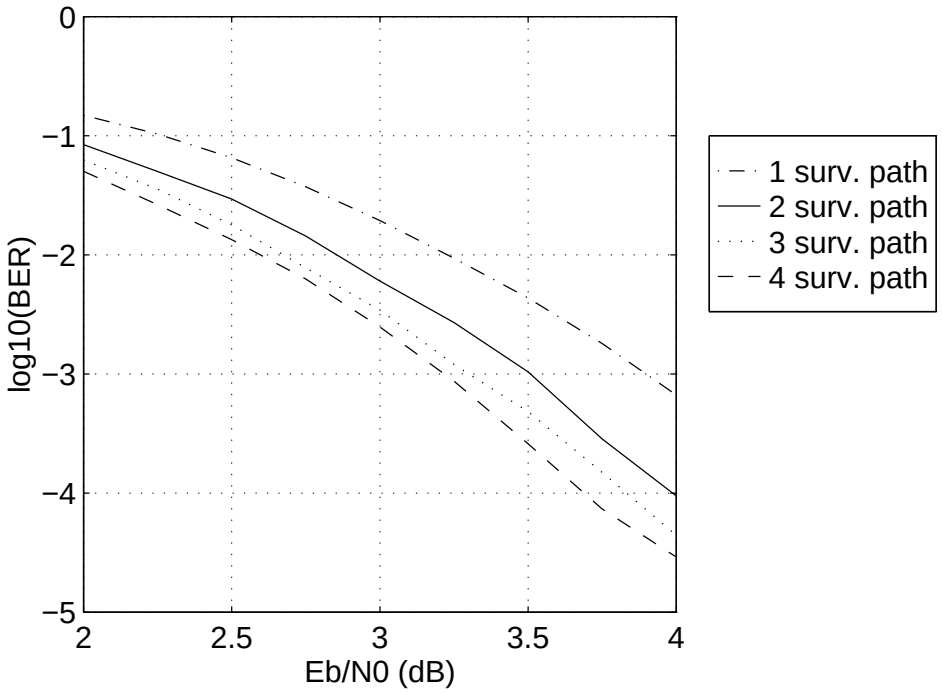

Figure 4.8: BER for 1 mobile with uncorrelated Rayleigh fading (interleaving with combined deinterleaver/decoder)

retained paths in the proposed decoder. However, added path computations trade off against the improved performance. From Figure 4.8, retaining two paths per node seems beneficial, while retaining additional paths provides diminishing returns with increased computational expense.

4.5 Summary

This chapter has discussed the various decoding options previously available for the IS-95 reverse link, including no interleaving, deinterleaved hard-decision bit metrics, and deinterleaved soft-decision bit metrics. The latter choice, deinterleaved soft-decision bit metrics, has typically been the method used in previous research, due to its ease of implementation and improved performance over the hard-decision option. However, a combined deinterleaver/decoder has been proposed here which provides an enhanced level of performance. An expression for the predicted BER for the case of no interleaving was derived for verification purposes. Finally, simulation results demonstrated the extent to which the new proposed algorithm outperforms the traditional existing decoding techniques, and indicated that the modified decoder functions relatively well in correlated fading. In simulation experiments, the proposed decoder with one surviving path being retained at each node provided a gain of 1 dB over soft-decision and 2 dB over hard-decision decoding at the standard acceptable bit error rate of 10^{-3} for voice. Retaining two surviving paths yielded an extra 0.5 dB of gain. As a result, the IS-95 reverse link BER performance can be significantly improved by using the proposed deinterleaver/decoder with no additional decoding delay.

Chapter 5

Digital Beamforming

5.1 Introduction

Digital beamforming can be utilized to increase the capacity of a cell [64] [67] [73] [74]. By using a multi-element antenna array at the base station and a suitable set of beamforming coefficients, it is possible to take a weighted sum of the antenna element outputs which maximizes the ratio of the desired mobile's signal power to the noise and interference power. This is essentially a form of spatial filtering that reduces interference from other mobiles and thus boosts overall cell capacity. Applebaum [1], Swales *et al* [99], and Van Veen and Buckley [101] provide good introductions to beamforming and its effects on increasing the number of users in a communication system. In addition, Krim and Viberg [45] present a comprehensive general overview of parameter estimation methods through the use of sensor array processing, including an extensive set of references. An alternative method of increasing system capacity instead of beamforming is to split individual cells into smaller cells or sectors. However, it can be shown [89] that this increases equipment requirements due to the increased variability of using smaller service areas.

The array response vector $\mathbf{a}_i$ specifies the relative phases of the i^{th} mobile's signal as received at each of the N_A antenna elements. This vector is a function of the signal's direction of arrival and the antenna array geometry, and its derivation for a circular array geometry was shown in Section 2.4.1. If there are a sufficient number of mobiles in the system, the interference will be approximately white [82] and it

will only be necessary to estimate $\mathbf{a}_i$ in order to determine suitable beamforming coefficients since this will maximize the output signal-to-noise-ratio (SNR) [82, pp. 185]. Currently, the received signal data in a frame is used to estimate the required weights for the following frame.

This chapter presents an existing beamforming weight estimation technique and investigates its application to the IS-95 reverse link. An extension to this algorithm is then proposed which yields significantly improved accuracy in the estimation of beamforming coefficients. An error analysis produces expressions for the mean vectors and covariance matrices of the estimators. These derived probability distributions can be used later to simulate imperfect beamforming without the need to resort to computationally expensive chip-level simulations. Finally, predicted and simulated statistical quantities are compared to illustrate the agreement between them.

5.2 Related Research

Beamforming primarily deals with two different types of situations. Assume that there are N_A antenna elements and N_I interferers in the system. In one case, there are only a few strong interferers with $N_I < N_A$. In this situation, it is generally desirable to choose the beamforming weights so that a null is formed in the direction of each of the interferers. Thus, their contribution to the received signal will be suppressed and the interference should ideally not affect the quality of the desired signal. This situation is more likely to arise when dealing with TDMA or FDMA systems when there are fewer users. Often, the goal here is to estimate the direction of arrival (DOA) of one or more signals so that an appropriate steering vector can be computed. Two of the standard algorithms for accomplishing this are MUSIC (MUltiple SIgnal Classification) [92] and ESPRIT (Estimation of Signal Parameters via Rotational Invariance Techniques) [88] which are eigen-based methods that identify the signal subspace from the antenna array output data. MUSIC permits the estimation of such factors as the number of signals and their directions of arrival. ESPRIT is applicable when the sensor array has displacement invariance (*i.e.* the sensors occur in matched symmetrically displaced pairs, as would be the case for a circular antenna array with an even number of

elements) and offers performance and computational advantages over MUSIC. Yuen and Friedlander [120] performed an analysis of three different versions of the ESPRIT algorithm to derive the asymptotic variance of the estimated direction of arrival and verified their results with numerical simulations.

Wang and Cruz [108] managed to use ESPRIT in a CDMA situation by considering the received signal after despreading. In this instance, the data could be treated as consisting of the desired signal and noise (from the multi-user interference) which allowed the use of ESPRIT.

The alternative situation, which is more appropriate for CDMA, is when $N_I > N_A$ and is usually significantly greater. In this case, there are not enough degrees of freedom available to null out all of the other interferers. However, due to the power control facility of the CDMA system, none of the interferers should be significantly stronger than the desired signal. Thus, in this situation, the beamforming weights are selected to optimize some other criterion such as maximizing the signal to interference ratio. This tends to suppress interference from other users, but not totally eliminate it. An advantage of this approach is that it is not necessary to accurately calibrate the antenna array which is required for direction of arrival estimation.

Liberti and Rappaport [55] investigated how capacity could be increased through the use of base station antenna arrays. Their focus was to determine the reduction in BER for a given number of users when antenna array processing was used. This study was analytical in nature and considered five different specific beam patterns, one of which was omnidirectional. Significant BER reductions were observed, especially when sectorization and adaptive antenna techniques were combined.

Lee and Lee [47] considered adaptive array beamforming when errors were present in the steering vector. The task of finding an optimal steering vector was formulated as an optimization problem which used the received signal data and the probabilistic distribution of the steering vector errors. This situation involved fewer interferers than antenna elements.

Yu and Lee [118] investigated the statistical performance of several eigenspace-based adaptive antenna array beamforming algorithms. However, they only considered the case where the number of interferers is less than the number of antenna

elements.

Wax and Anu [109] analyzed the SINR (Signal-to-Interference-plus-Noise-Ratio) at the output of the minimum variance beamformer, although this too was for the case of fewer interferers than antenna elements. The analysis was also extended [110] to consider the effects of steering vector errors.

A projection approach to beamforming designed to reduce beamformer sensitivity to perturbation error and sample covariance error was presented by Feldman and Griffiths [23]. In a following paper [22], Feldman analyzed the expected performance of the projection method beamformer and derived an expression for the SINR when errors were present.

The research presented within this chapter is originally based on work performed at Stanford [64] [67] [73] [74] which is discussed in more detail in Section 5.4. In addition, a recursive method for estimating suitable beamforming coefficients was presented by the same authors in [70].

5.3 Maximum SNR (Perfect) Beamforming

Maximum SNR beamforming (henceforth referred to as perfect beamforming) assumes that the array response vector for the mobile under consideration is known exactly. The beamforming weights for the p^{th} mobile can then be set equal to the entries of the array response vector since this set of weights will be optimum in terms of maximizing the signal to interference and noise ratio when the interference is assumed to be white, which will be the case for a large number of active mobiles [82].

$$\mathbf{w}_p \quad = \quad \mathbf{a}_p \tag{5.1}$$

Although in actual deployment the true array response vector would not be known, this case is useful for test purposes and for verifying error analyses that were performed with simplifying assumptions. In addition, evaluating system performance with perfect beamforming provides an upper bound to the achievable level of service. Conversely, in reality, imperfect beamforming must be used where the beamforming coefficients are estimated from the received signal data.

5.4 Code-Filtering Correlation

The code-filtering correlation technique has received an extensive amount of investigation from Naguib and Paulraj [64] [67] [73] [74]. In the following section, a simple spreading of the data bits via a PN chip sequence is assumed with the actual encoding process of IS-95 being considered immediately after the basic algorithm has been explained.

5.4.1 Basic Algorithm

Let $\mathbf{x}_p(t)$ be the received signal vector and $\mathbf{z}_p[k]$ be the signal vector correlated with the PN sequence of the desired mobile over the time period of the k^{th} Walsh chip. Then, $\mathbf{a}_p$ can be estimated as the principal eigenvector of the matrix $\mathrm{R_{zz}} - \mathrm{R_{xx}}$ where $\mathrm{R_{xx}}$ and $\mathrm{R_{zz}}$ are the correlation matrices of $\mathbf{x}_p(t)$ and $\mathbf{z}_p[k]$ respectively [67]. Since these matrices must be estimated from the observed data, the system performance depends on the accuracy of these estimates. The asymptotic values of $\mathrm{R_{xx}}$ and $\mathrm{R_{zz}}$ for the p^{th} mobile are [67]:

$$\mathrm{R_{xx}} = \beta_p^2 \mathbf{a}_p \mathbf{a}_p^* + \sum_{k \neq p} \beta_k^2 \mathbf{a}_k \mathbf{a}_k^* + \sigma_n^2 \mathrm{I} \tag{5.2}$$

$$\mathrm{R_{zz}} = G_\mathbf{z} \beta_p^2 \mathbf{a}_p \mathbf{a}_p^* + \sum_{k \neq p} \beta_k^2 \mathbf{a}_k \mathbf{a}_k^* + \sigma_n^2 \mathrm{I} \tag{5.3}$$

where $G_\mathbf{z}$ is the gain or spreading factor, β_p^2 represents the received signal power from the p^{th} mobile, and σ_n^2 is the thermal noise power.

If the gain factor $G_\mathbf{z}$ between the Walsh and PN chips is sufficiently large, the array response vector can be approximated simply as the principal eigenvector of $\mathrm{R_{zz}}$ since $G_\mathbf{z} \beta_p^2 \mathbf{a}_p \mathbf{a}_p^*$ will be the dominant component of this matrix. In IS-95, however, $G_\mathbf{z}$ is less than 4 as illustrated in the following section. This gain is too low to accurately estimate $\mathbf{a}_p$ using this approach. Thus, the quality of beamforming coefficients obtained via this technique is poor.

5.4.2 Application to the IS-95 Reverse Link

This section examines the use of the code-filtering beamforming weight estimation technique in the reverse link of IS-95 and then demonstrates why this algorithm does

not work well in this situation.

In the code-filtering correlation method for estimating beamforming coefficients, the received signal vector is correlated over one PN chip to generate a set of $\mathbf{x}$ values. These vectors are in turn further correlated with the desired mobile's PN sequence over the time period of one Walsh chip to yield $\mathbf{z}$ vectors.

Recall that in IS-95, there are both in-phase and quadrature components in the signal. Neglecting the thermal noise component for the time being, the in-phase signal vector for the p^{th} mobile as correlated over one PN chip can be written as:

$$\begin{aligned}
\mathbf{x}_{I_p}[r] &= \frac{1}{2}C_{I_p}[r]\sum_{k=1}^{N_M}\beta_k w_k[r]\Big\{C_{I_k}[r]\exp(-j2\pi f_c\tau_{kp})(T_c-\tau_{kp})\mathbf{a}_k \\
&\qquad + C_{I_k}[r-1]\exp(-j2\pi f_c\tau_{kp})\tau_{kp}\mathbf{a}_k \\
&\qquad + jC_{Q_k}[r]\exp(-j2\pi f_c\tau_{kp})(T_c-\tau_{kp})\mathbf{a}_k \\
&\qquad + jC_{Q_k}[r-1]\exp(-j2\pi f_c\tau_{kp})\tau_{kp}\mathbf{a}_k\Big\} \qquad (5.4) \\
&= \frac{1}{2}C_{I_p}[r]\sum_{k=1}^{N_M}\beta_k w_k[r]\exp(-j2\pi f_c\tau_{kp})\mathbf{a}_k \\
&\qquad \Big\{C_{I_k}[r](T_c-\tau_{kp}) + C_{I_k}[r-1]\tau_{kp} \\
&\qquad + jC_{Q_k}[r](T_c-\tau_{kp}) + jC_{Q_k}[r-1]\tau_{kp}\Big\}
\end{aligned}$$

where C_{I_k} and C_{Q_k} represent the current PN chip value for the k^{th} mobile's in-phase and quadrature components, respectively, β_k is the received signal amplitude, w_k is the current Walsh chip value, τ_{kp} is the relative time delay, and T_c is the period of one PN chip.

Similarly, the corresponding quadrature $\mathbf{x}$ vector will be:

$$\begin{aligned}
\mathbf{x}_{Q_p}[r] &= \frac{1}{2}C_{I_p}[r]\sum_{k=1}^{N_M}\beta_k w_k[r]\exp(-j2\pi f_c\tau_{kp})\mathbf{a}_k \\
&\qquad \Big\{jC_{I_k}[r](T_c-\tau_{kp}) + jC_{I_k}[r-1]\tau_{kp} \qquad (5.5) \\
&\qquad + C_{Q_k}[r](T_c-\tau_{kp}) + C_{Q_k}[r-1]\tau_{kp}\Big\}
\end{aligned}$$

Recall that the Walsh and PN chip values are limited to ± 1 with the assumption of equal probability. Consequently, $\mathbf{x}_{I_p}$ and $\mathbf{x}_{Q_p}$ can easily be seen to be zero-mean.

Let Y_{I_p} and Y_{Q_p} be binary random variables where $Y_{I_p} = \pm 1$ and $Y_{Q_p} = \pm 1$ with

equal probability. Then equation (5.4) can be rewritten as:

$$\begin{aligned}\mathbf{x}_{I_p}[r] &= \frac{1}{2}\beta_p T_c w_p[r]\mathbf{a}_p + j\frac{1}{2}\beta_p T_c Y_{Q_p}[r]\mathbf{a}_p \\ &\quad + \frac{1}{2}\sum_{k\neq p}\beta_k \exp(-j2\pi f_c \tau_{kp})\mathbf{a}_k \\ &\quad \Big\{Y_{I_k}[r](T_c-\tau_{kp}) + Y_{I_k}[r-1]\tau_{kp} \\ &\quad + jY_{Q_k}[r](T_c-\tau_{kp}) + jY_{Q_k}[r-1]\tau_{kp}\Big\}\end{aligned} \tag{5.6}$$

where the relative time delay τ_{pp} has been set to zero with no loss of generality.

The correlation matrix of $\mathbf{x}_{I_p}[r]$ is defined as:

$$\mathrm{R}_{\mathbf{xx}} = E\left[\mathbf{x}_{I_p}[r]\mathbf{x}^*_{I_p}[r]\right] \tag{5.7}$$

When equation (5.6) is substituted into (5.7), any term containing two different Y_{I_k} or Y_{Q_k} random variables will evaluate as zero when the expected value is taken. Similarly, any term containing the square of a Y_{I_k} or Y_{Q_k} random variable will evaluate as one.

$$\begin{aligned}\mathrm{R}_{\mathbf{xx}} &= \frac{1}{4}\beta_p^2 T_c^2 \mathbf{a}_p\mathbf{a}_p^* + \frac{1}{4}\beta_p^2 T_c^2 \mathbf{a}_p\mathbf{a}_p^* \\ &\quad + \frac{1}{4}\sum_{k\neq p}\beta_k^2\mathbf{a}_k\mathbf{a}_k^*\left\{E\left[(T_c-\tau_{kp})\right] + E\left[\tau_{kp}\right] + E\left[(T_c-\tau_{kp})\right] + E\left[\tau_{kp}\right]\right\} \\ &= \frac{1}{2}\beta_p^2 T_c^2 \mathbf{a}_p\mathbf{a}_p^* + \frac{1}{2}\sum_{k\neq p}\beta_k^2\mathbf{a}_k\mathbf{a}_k^*\left\{E\left[(T_c-\tau_{kp})\right] + E\left[\tau_{kp}\right]\right\} \\ &= \frac{1}{2}\beta_p^2 T_c^2 \mathbf{a}_p\mathbf{a}_p^* + \frac{1}{2}\sum_{k\neq p}\beta_k^2\mathbf{a}_k\mathbf{a}_k^*\left\{T_c^2 - 2T_c E\left[\tau_{kp}\right] + 2E\left[\tau_{kp}^2\right]\right\}\end{aligned} \tag{5.8}$$

Note the following expectations for τ_{kp} which has a uniform distribution over the interval $[0, T_c)$.

$$E\left[\tau_{kp}\right] = \frac{1}{2}T_c \tag{5.9}$$

$$E\left[\tau_{kp}^2\right] = \frac{1}{3}T_c^2 \tag{5.10}$$

Substituting (5.9) and (5.10) into (5.8) yields:

$$\begin{aligned}\mathrm{R}_{\mathbf{xx}} &= \frac{1}{2}\beta_p^2 T_c^2 \mathbf{a}_p\mathbf{a}_p^* + \frac{1}{2}\sum_{k\neq p}\beta_k^2\mathbf{a}_k\mathbf{a}_k^*\left\{T_c^2 - T_c^2 + \frac{2}{3}T_c^2\right\} \\ &= \frac{1}{2}T_c^2\beta_p^2\mathbf{a}_p\mathbf{a}_p^* + \frac{1}{3}T_c^2\sum_{k\neq p}\beta_k^2\mathbf{a}_k\mathbf{a}_k^*\end{aligned} \tag{5.11}$$

For the case of a single cell with one antenna element and perfect power control, it is possible to predict $\mathbf{R_{xx}}$ exactly since all of the β_k values will be equal (Section 6.3). When multiple antenna elements are used, an approximation for $\mathbf{R_{xx}}$ can be obtained (Section 6.4).

Now consider the $\mathbf{z}_{I_p}[r]$ vector. Recall that there are $N_W = 4$ PN chips for each Walsh chip. By correlating (5.6) across the period of one Walsh chip, the following expression is obtained.

$$\begin{aligned}\mathbf{z}_{I_p}[r] &= \frac{1}{2}N_W\beta_p T_c w_p[r]\mathbf{a}_p + j\frac{1}{2}\beta_p T_c \mathbf{a}_p \sum_{i=1}^{N_W} Y_{Q_p}[i] \\ &\quad + \frac{1}{2}\sum_{k\neq p}\beta_k \exp(-j2\pi f_c \tau_{kp})\mathbf{a}_k \\ &\quad \sum_{i=1}^{N_W}\Big\{Y_{I_k}[i](T_c-\tau_{kp}) + Y_{I_k}[i-1]\tau_{kp} \\ &\quad + jY_{Q_k}[i](T_c-\tau_{kp}) + jY_{Q_k}[i-1]\tau_{kp}\Big\}\end{aligned} \tag{5.12}$$

The correlation matrix for $\mathbf{z}_{I_p}$ can be derived in a similar fashion as before.

$$\begin{aligned}\mathrm{R_{zz}} &= E\left[\mathbf{z}_{I_p}\mathbf{z}_{I_p}^*\right] \\ &= \frac{1}{4}N_W^2\beta_p^2 T_c^2 \mathbf{a}_p\mathbf{a}_p^* + \frac{1}{4}N_W\beta_p^2 T_c^2\mathbf{a}_p\mathbf{a}_p^* + \frac{1}{4}\sum_{k\neq p}\beta_k^2\mathbf{a}_k\mathbf{a}_k^* \\ &\quad \left(\sum_{i=1}^{N_W}\left\{E\left[(T_c-\tau_{kp})^2\right] + E\left[\tau_{kp}^2\right] + E\left[(T_c-\tau_{kp})^2\right] + E\left[\tau_{kp}^2\right]\right\}\right) \\ &= \frac{1}{4}N_W(N_W+1)\beta_p^2T_c^2\mathbf{a}_p\mathbf{a}_p^* + \frac{1}{4}N_W\sum_{k\neq p}\beta_k^2\mathbf{a}_k\mathbf{a}_k^*\left\{\frac{4}{3}T_c^2\right\} \\ &= \frac{1}{4}N_W(N_W+1)\beta_p^2T_c^2\mathbf{a}_p\mathbf{a}_p^* + \frac{1}{3}N_WT_c^2\sum_{k\neq p}\beta_k^2\mathbf{a}_k\mathbf{a}_k^*\end{aligned} \tag{5.13}$$

Assuming that all of the mobiles have identical received power levels (*i.e.* β_k is constant for all k), the gain for $\mathbf{a}_p$ relative to the array response vectors of the interferers obtained by this correlation method can be easily seen to be:

$$\begin{aligned}G_{\mathbf{z}} &= \left(\frac{1}{4}N_W(N_W+1)\beta_p^2T_c^2\right)\Big/\left(\frac{1}{3}N_WT_c^2\beta_p^2\right) \\ &= \frac{3}{4}(N_W+1) = 3.75\end{aligned} \tag{5.14}$$

The accuracy of this beamforming weight estimation depends on the value of $G_{\mathbf{z}}$. In this application, $G_{\mathbf{z}}$ can be clearly seen to be too low to be of practical use. The

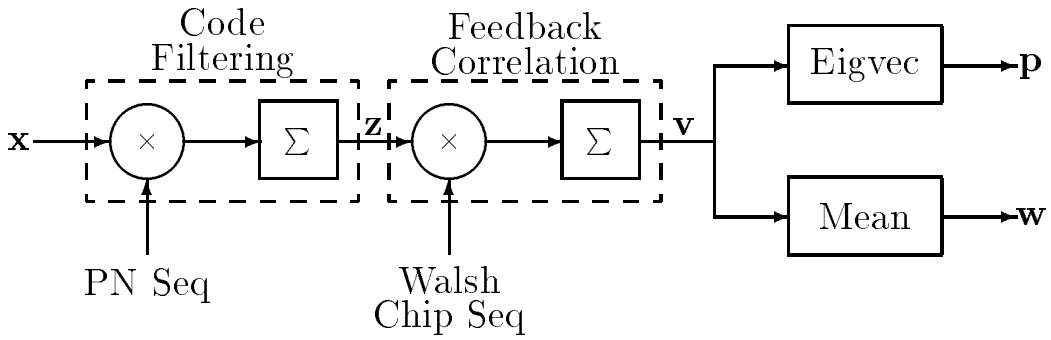

Figure 5.1: Feedback correlation beamforming

noise and interference will cause significant errors in estimates of $\mathbf{R_{zz}}$ obtained from finite sample sizes. A similar result will be obtained if the quadrature signal vectors are correlated. However, only the in-phase case is considered here for reasons of simplicity.

5.5 Walsh Chip Feedback Correlation

As mentioned previously, using a spreading factor of only 4, as is the case for IS-95, yields extremely poor estimates of the array response vectors due to the comparatively significant interference and noise component in $\mathbf{R_{zz}}$. However, an additional correlation step can be performed to yield a much larger enhanced processing gain while not modifying the IS-95 coding process and without introducing any additional processing delay [16].

After the transmitted data bits have been recovered for a given mobile, the data can be reencoded to reconstruct the original Walsh chip sequence, assuming that no errors were made during the decoding process. The $\mathbf{z}_i[k]$ vectors resulting from correlating with the PN chip sequences can then be further correlated with the reconstructed Walsh chip sequence to produce a correlation vector for each Walsh function. This process is illustrated in Figure 5.1. The resulting correlation vectors can be processed in one of two ways to obtain an array response estimate as detailed in the following sections.

Naguib and Paulraj [71] also considered beamforming on the IS-95 reverse link using their code-filtering correlation algorithm. In this case, it was necessary to make a hard decision based on the correlation values prior to Viterbi decoding as to which Walsh function was transmitted so that an appropriate correlation vector could be selected to update the current estimate of the correlation matrix. This approach would likely degrade performance to some extent since there is a certain probability that an incorrect Walsh function and correlation vector would be selected. As a result, a greater amount of variation in the correlation matrix estimate would be expected.

5.5.1 Principal Eigenvector Approach

Let $\mathbf{v}_{I_p}[r]$ be the correlation vector corresponding to the r^{th} Walsh function of the p^{th} mobile. By correlating (5.12) with the correct Walsh function, the following expression can be obtained.

$$\begin{aligned}\mathbf{v}_{I_p}[r] &= \frac{1}{2}N_F N_W \beta_p T_c \mathbf{a}_p + j\frac{1}{2}\beta_p T_c \mathbf{a}_p \sum_{m=1}^{N_F}\sum_{i=1}^{N_W} Y_{Q_p}[m,i] \\ &\quad + \sum_{m=1}^{N_F}\frac{1}{2}\sum_{k\neq p}\beta_k \exp(-j2\pi f_c \tau_{kp})\mathbf{a}_k \\ &\quad \sum_{i=1}^{N_W}\Big\{Y_{I_k}[m,i](T_c-\tau_{kp}) + Y_{I_k}[m,i-1]\tau_{kp} \\ &\quad + jY_{Q_k}[m,i](T_c-\tau_{kp}) + jY_{Q_k}[m,i-1]\tau_{kp}\Big\}\end{aligned} \tag{5.15}$$

where T_c is the time period of one PN chip, $N_W = 4$ specifies the number of PN chips in one Walsh chip, and $N_F = 64$ is the number of Walsh chips in one Walsh function chip sequence. When the expected value of this expression is taken, all of the binary random variables will disappear since they are zero-mean.

$$E\left[\mathbf{v}_{I_p}\right] = \frac{1}{2}N_F N_W \beta_p T_c \mathbf{a}_p \tag{5.16}$$

Note that $\mathbf{v}_{I_p}$, unlike $\mathbf{x}_{I_p}$ and $\mathbf{z}_{I_p}$, is not zero-mean. In a similar manner, it can easily be shown that the correlation matrix of the in-phase $\mathbf{v}_{I_p}[r]$ vectors is:

$$\begin{aligned}\mathrm{R}_{\mathbf{vv}} &= \frac{1}{4}N_W^2 N_F^2 \beta_p^2 T_c^2 \mathbf{a}_p \mathbf{a}_p^* + \frac{1}{4}N_W N_F \beta_p^2 T_c^2 \mathbf{a}_p \mathbf{a}_p^* \\ &\quad + \frac{1}{3}N_W N_F T_c^2 \sum_{k\neq p}\beta_k^2 \mathbf{a}_k \mathbf{a}_k^* + \frac{1}{2}N_W N_F T_c \sigma_n^2 \mathrm{I}\end{aligned} \tag{5.17}$$

The first term in (5.17) comes from the in-phase signal component, the second from the quadrature component, the third represents interference from other mobiles, and the final term originates from the background noise.

The covariance matrix for $\mathbf{v}$ can be easily obtained from equations (5.17) and (5.16).

$$\begin{aligned} \mathrm{C}_{\mathbf{vv}} &= \mathrm{R}_{\mathbf{vv}} - E\left[\mathbf{v}_{I_p}\right] E\left[\mathbf{v}_{I_p}^*\right] \\ &= \frac{1}{4} N_W N_F \beta_p^2 T_c^2 \mathbf{a}_p \mathbf{a}_p^* + \frac{1}{3} N_W N_F T_c^2 \sum_{k \neq p} \beta_k^2 \mathbf{a}_k \mathbf{a}_k^* + \frac{1}{2} N_W N_F T_c \sigma_n^2 \mathrm{I} \end{aligned} \tag{5.18}$$

Assuming that the received powers for each mobile are identical (which is an approximation unless perfect power control and a single antenna element are assumed), the relative gain factor from equation (5.17) can be calculated as:

$$\begin{aligned} G_{\mathbf{v}} &\approx \left(\frac{1}{4} N_W^2 N_F^2 + \frac{1}{4} N_W N_F\right) \Big/ \left(\frac{1}{3} N_W N_F T_c^2\right) \\ &= \frac{3}{4}\left(N_W N_F + 1\right) = \frac{3}{4}\left[(4)(64) + 1\right] = 192.75 \end{aligned} \tag{5.19}$$

A similar result holds for the quadrature signal component.

Simulations have shown that the accuracy of the estimated beamforming weights significantly increases when the principal eigenvector of $\mathrm{R}_{\mathbf{vv}}$ is used to estimate the desired array response vector instead of $\mathrm{R}_{\mathbf{zz}}$, which is as would be expected due to the larger gain factor. Note that it is not necessary to subtract $\mathrm{R}_{\mathbf{zz}}$ from $\mathrm{R}_{\mathbf{vv}}$ in this instance due to the high processing gain which causes the interference and noise terms to become negligible.

5.5.2 Mean Correlation Vector Approach

Due to the large gain observed in (5.19), $\mathrm{R}_{\mathbf{vv}}$ will be a close approximation to a rank-one matrix. Consequently, an alternative to computing the principal eigenvector of $\mathrm{R}_{\mathbf{vv}}$ is to simply take the mean of the $\mathbf{v}_{I_p}$ correlation vectors over a certain period of time (such as one frame). This eliminates the additional computational expense of calculating the principal eigenvector of a matrix, while simultaneously yielding estimates of an equivalent level of accuracy. Wu and Wong [114] independently proposed a similar technique in a cyclic adaptive beamforming algorithm in order to reduce computational complexity.

The expected value of $\mathbf{v}_{I_p}$ is obtained from equation (5.16).

$$E\left[\mathbf{v}_{I_p}\right] = \frac{1}{2}N_F N_W \beta_p T_c \mathbf{a}_p \tag{5.20}$$

Suppose the $\mathbf{v}_{I_p}$ vectors are summed over an entire frame which contains $F_F = 96$ Walsh functions. If this sum is termed $\mathbf{u}_{I_p}$, then (5.20) produces:

$$E\left[\mathbf{u}_{I_p}\right] = \frac{1}{2}F_F N_F N_W \beta_p T_c \mathbf{a}_p \tag{5.21}$$

which is simply a scalar multiple of the desired array response vector so this estimator is unbiased.

It is now necessary to rewrite equation (5.15) so that the correlation is performed across the entire frame.

$$\begin{aligned}\mathbf{u}_{I_p}[r] = {} & \frac{1}{2}F_F N_F N_W \beta_p T_c \mathbf{a}_p + j\frac{1}{2}\beta_p T_c \mathbf{a}_p \sum_{n=1}^{F_F}\sum_{m=1}^{N_F}\sum_{i=1}^{N_W} Y_{Q_p}[n,m,i] \\ & + \sum_{n=1}^{F_F}\sum_{m=1}^{N_F}\frac{1}{2}\sum_{k\neq p}\beta_k \exp(-j2\pi f_c \tau_{kp})\mathbf{a}_k \\ & \sum_{i=1}^{N_W}\Big\{Y_{I_k}[n,m,i](T_c-\tau_{kp}) + Y_{I_k}[n,m,i-1]\tau_{kp} \\ & + jY_{Q_k}[n,m,i](T_c-\tau_{kp}) + jY_{Q_k}[n,m,i-1]\tau_{kp}\Big\}\end{aligned} \tag{5.22}$$

All of the Y_{I_k} and Y_{Q_k} random variables are mutually independent and will thus disappear when the corresponding correlation matrix is calculated.

$$\begin{aligned}\mathrm{R}_{\mathbf{uu}} &= E\left[\mathbf{u}_{I_p}\mathbf{u}_{I_p}^*\right] \\ &= \frac{1}{4}F_F^2 N_W^2 N_F^2 \beta_p^2 T_c^2 \mathbf{a}_p\mathbf{a}_p^* + \frac{1}{4}F_F N_W N_F \beta_p^2 T_c^2 \mathbf{a}_p\mathbf{a}_p^* \\ &\quad + \frac{1}{3}F_F N_W N_F T_c^2 \sum_{k\neq p}\beta_k^2 \mathbf{a}_k\mathbf{a}_k^* + \frac{1}{2}F_F N_W N_F T_c \sigma_n^2 \mathrm{I}\end{aligned} \tag{5.23}$$

From equations (5.21) and (5.23), it is easy to see that the corresponding covariance matrix is:

$$\begin{aligned}\mathrm{C}_{\mathbf{uu}} &= \mathrm{R}_{\mathbf{uu}} - E\left[\mathbf{u}_{I_p}\right]E\left[\mathbf{u}_{I_p}^*\right] \\ &= \frac{1}{4}F_F N_W N_F \beta_p^2 T_c^2 \mathbf{a}_p\mathbf{a}_p^* + \frac{1}{3}F_F N_W N_F T_c^2 \sum_{k\neq p}\beta_k^2 \mathbf{a}_k\mathbf{a}_k^* \\ &\quad + \frac{1}{2}F_F N_W N_F T_c \sigma_n^2 \mathrm{I}\end{aligned} \tag{5.24}$$

Now refer back to equation (5.21). To maintain a constant magnitude, it is necessary to scale $\mathbf{u}_{I_p}$. This step is primarily just important if the correlation process is extended for an arbitrary period of time so that corresponding quantities can be compared with each other. Define the following vector quantity.

$$\mathbf{w}_{I_p} = \frac{1}{F_F N_F N_W T_c}\mathbf{u}_{I_p} \tag{5.25}$$

From (5.21), the mean of the above quantity can be seen to be:

$$E\left[\mathbf{w}_{I_p}\right] = \frac{1}{2}\beta_p \mathbf{a}_p \tag{5.26}$$

and the corresponding covariance matrix is:

$$\begin{aligned} \mathrm{C}_{\mathbf{ww}} &= \frac{1}{4}\frac{1}{F_F N_W N_F}\beta_p^2 \mathbf{a}_p \mathbf{a}_p^* + \frac{1}{3}\frac{1}{F_F N_W N_F}\sum_{k\neq p}\beta_k^2 \mathbf{a}_k \mathbf{a}_k^* \\ &\qquad + \frac{1}{2}\frac{1}{F_F N_W N_F}\frac{1}{T_c}\sigma_n^2 \mathrm{I} \\ &= \frac{1}{F_F N_W N_F}\left(\frac{1}{4}\beta_p^2 \mathbf{a}_p \mathbf{a}_p^* + \frac{1}{3}\sum_{k\neq p}\beta_k^2 \mathbf{a}_k \mathbf{a}_k^* + \frac{1}{2T_c}\sigma_n^2 \mathrm{I}\right) \end{aligned} \tag{5.27}$$

The initial scaling factor in equation (5.27) clearly indicates that as the sample size for estimating the beamforming weight vector increases, the covariance matrix of the estimate will asymptotically approach zero. For example, if the correlation were performed over n frames, a factor of n would appear in the denominator of (5.27). As n was allowed to go to infinity, $\mathrm{C}_{\mathbf{ww}}$ would go to zero.

Equation (5.26) indicates that the $\mathbf{w}_{I_p}$ estimate of the array response vector is unbiased. However, the beamforming weight vector is typically normalized to unit length before being used, and this may introduce a bias into the results as explained in Section 5.5.3.2, although this bias appears to be negligible and has not been observed in simulations.

5.5.3 Normalized Mean Correlation Vector

Since the beamforming weight vector is usually normalized to unit length before being used, it is also possible to derive the expected statistical parameters of the normalized coefficient vector estimate. This provides for a fair comparison with the principal eigenvector approach of Section 5.5.1 which also produces a unit vector estimate.

5.5.3.1 Covariance Matrix

Consider the expression for $\mathbf{w}_{I_p}$ in (5.25) and assume that it has been normalized to unit length. That is, define the following new quantity.

$$\mathbf{q}_{I_p} = \frac{\mathbf{w}_{I_p}}{|\mathbf{w}_{I_p}|} = \frac{\mathbf{u}_{I_p}}{|\mathbf{u}_{I_p}|} \tag{5.28}$$

The quantity in (5.28) represents the actual vector of coefficients used for beamforming purposes. The covariance matrix of this estimator can be approximated by scaling the covariance matrix for $\mathbf{w}_{I_p}$ in (5.27) by the reciprocal of the squared magnitude of the expected value of $\mathbf{w}_{I_p}$. This approximates the effects of the vector normalization process.

$$\mathrm{C}_{\mathbf{qq}} \approx \frac{1}{\left|E\left[\mathbf{w}_{I_p}\right]\right|^2}\mathrm{C}_{\mathbf{ww}} = \frac{4}{\beta_p^2}\mathrm{C}_{\mathbf{ww}} \tag{5.29}$$

When the observed covariance matrix is compared to the above predicted quantity, an exact agreement is not observed. However, since only the direction of the beamforming weight vector is important and the magnitude is always unity, any variation in the same direction as the expected value of the coefficient vector can be ignored. By subtracting off the variation along this direction, an almost exact correspondence between the observed and simulated covariance matrices can be obtained.

Let $\mathrm{C}_{\mathbf{qq}}$ be the predicted covariance matrix as above and $\mu_{\mathbf{q}}$ be the expected value of the normalized estimate. From (5.26), $\mu_{\mathbf{q}}$ can be seen to correspond to the array response vector for the p^{th} mobile.

Note that a Hermitian covariance matrix can be written in terms of its eigenvalues and eigenvectors.

$$\mathrm{C}_{\mathbf{qq}} = \sum_{i=1}^{N_A} \lambda_i \mathbf{v}_i \mathbf{v}_i^* \tag{5.30}$$

For each eigenvector in the above expression, the component which lies along the direction of $\mu_{\mathbf{q}}$ can be subtracted off to yield a new vector.

$$\mathbf{u}_i = \mathbf{v}_i - (\mathbf{v}_i^* \mu_{\mathbf{q}})^* \mu_{\mathbf{q}} \tag{5.31}$$

The modified covariance matrix can now be written in terms of the original eigenvalues and the adjusted eigenvectors from (5.31).

$$\hat{\mathrm{C}}_{\mathbf{qq}} = \sum_{i=1}^{N_A} \lambda_i \mathbf{u}_i \mathbf{u}_i^* \tag{5.32}$$

This process can be repeated using the observed covariance matrix and mean vector from simulations so that equivalent quantities can be compared.

5.5.3.2 Mean Vector

Equation (5.26) showed that the mean correlation vector method of estimating the beamforming weights is unbiased. However, the normalized mean vector from observations will have a magnitude slightly less than unity due to the vector normalization for each observation. The direction of the mean vector remains unbiased though. It will be seen that the difference in magnitude from unity is essentially negligible.

It is not possible to derive an analytical expression for the expected length of the mean observed vector. However, a value can be obtained via numerical integration.

Consider the modified covariance matrix given in equation (5.32) for the p^{th} mobile. One of the eigenvalues of $\hat{\mathrm{C}}_{\mathbf{qq}}$ will be zero and its corresponding eigenvector will be the array response vector $\mathbf{a}_p$, while the remaining eigenvalues will be nonzero.

Assume that the distribution of the intersection of the observed vector estimate with the hyperplane defined by the $N_A - 1$ eigenvectors with nonzero eigenvalues follows a multivariate Gaussian distribution with mean zero and covariance defined by (5.32). In Figure 5.2, the vertical line represents the true mean, whereas the diagonal line represents the current normalized array response vector estimate. The horizontal line represents the distance within the defined hyperplane from the mean point to the current vector estimate. The indicated distances shown in the diagram can be easily derived in terms of known values. The x_i quantities represent the distance along each eigenvector axis that the current vector estimate is from the mean.

It is desired to find d in Figure 5.2 as a function of the other known values. Using similar triangles yields:

$$\frac{d}{1} = \frac{1}{\sqrt{1 + \sum_{i=1}^{N_A - 1} x_i^2}} \tag{5.33}$$

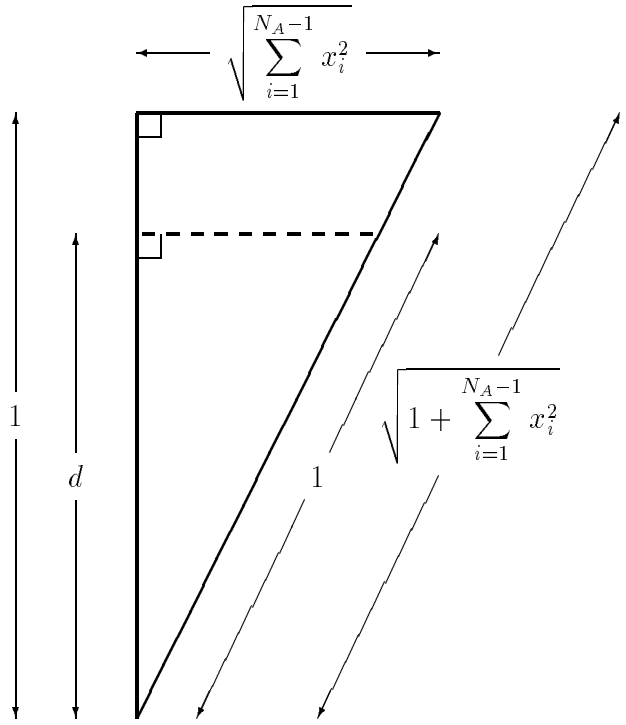

Figure 5.2: Estimation of observed mean vector length

$$d = \left(1 + \sum_{i=1}^{N_A-1} x_i^2\right)^{-\frac{1}{2}} \tag{5.34}$$

The product of this expression and the corresponding pdf can be integrated over the valid range of x_i values to find the expected length of the mean observed vector.

$$E[d] = \int \cdots \int d(x_1, \ldots, x_{N_A-1}) \left[\prod_{i=1}^{N_A-1} \frac{1}{\sqrt{2\pi}\sigma_i} \exp\left(-\frac{x_i^2}{2\sigma_i}\right)\right] dx_{N_A-1} \ldots dx_1 \tag{5.35}$$

Although this integration cannot be performed analytically, a satisfactory result can be obtained quite easily by integrating the above expression numerically.

In practice, the covariance matrix of the normalized mean correlation vector estimator is generally small enough that the mean observed vector has a magnitude only slightly less than unity.

5.5.4 Effect of Rayleigh Fading

For simplicity, the above derivations for mean vectors and covariance matrices assume the absence of Rayleigh fading. However, it is quite simple to introduce fading to the derived expressions. Equations (5.16) and (5.26) should be multiplied by $E[R] = \sqrt{\pi/2}$, and (5.17), (5.18), and (5.27) should be multiplied by $E[R^2] = 2$.

5.5.5 Effect of Decoding Errors

In the code-filtering correlation beamforming weight estimation algorithm, once synchronization with the PN sequence of interest has been acquired, no correlation errors were result. With the feedback correlation method, however, there is the possibility of correlation errors occurring due to a frame's data being decoded incorrectly. At present, no provision against this has been included in the basic algorithm. However, since a mobile's array response vector does not change rapidly from frame to frame, it should be possible to implement some form of filtering to reduce the deleterious effects of any incorrect beamforming coefficient estimates. Another alternative would be to disregard any frame estimates which are significantly different than the current beamforming vector estimate.

In the previous paragraph, an assumption is made that a decoding error will have a catastrophic effect on the beamforming estimate produced by the feedback correlation method. However, it is not clear that this will definitely be true and this assumption may just represent a worst-case scenario. The Walsh chip feedback correlation technique is similar to that used for decision-feedback equalization. Consequently, it may be possible to use the upper bound on error probability decision-feedback equalization derived by Duttweiler, Mazo, and Messerschmitt [12] to obtain a bound on the effects of decoding errors in the feedback correlation algorithm.

5.6 Eigenvector Perturbation Analysis

It is possible to obtain an approximation for the covariance matrix of the principal eigenvector estimator derived in Section 5.5.1. This formulation was originally developed for a similar problem involving the principal eigenvector of a real least-squares

matrix and is described in [13] [14] [17] [19]. An extension to this technique for complex Hermitian matrices is presented here.

It is important to note that this analysis is also applicable to many other least-squares type problems involving complex Hermitian matrices and is not just specific to the beamforming problem.

5.6.1 Statistical Parameters of the Correlation Matrix

It is first necessary to consider the correlation matrix $\hat{\mathrm{R}}_{\mathbf{vv}}$. The expected value of this quantity is given by equation (5.17).

Suppose the columns of $\hat{\mathrm{R}}_{\mathbf{vv}}$ are stacked one above the other to form a vector $\hat{\mathrm{r}}_{\mathbf{vv}}$ of dimension $(N_A)^2$. It is then possible to calculate a covariance matrix for this vector quantity.

$$\mathrm{C}_{\hat{\mathrm{r}}_{\mathbf{vv}}} = E\left[\hat{\mathrm{r}}_{\mathbf{vv}}\hat{\mathrm{r}}^*_{\mathbf{vv}}\right] - E\left[\hat{\mathrm{r}}_{\mathbf{vv}}\right]E\left[\hat{\mathrm{r}}^*_{\mathbf{vv}}\right] \tag{5.36}$$

Consider the $(i,j)^{th}$ entry in the $\mathrm{C}_{\hat{\mathrm{r}}_{\mathbf{vv}}}$ matrix.

$$\hat{\sigma}_{ij} = E\left[(\hat{\mathrm{r}}_{\mathbf{vv}})_i(\hat{\mathrm{r}}^*_{\mathbf{vv}})_j\right] - E\left[(\hat{\mathrm{r}}_{\mathbf{vv}})_i\right]E\left[(\hat{\mathrm{r}}^*_{\mathbf{vv}})_j\right] \tag{5.37}$$

Define the following indices for notational simplicity:

$$\begin{aligned} m &= i \bmod N_A & p &= j \bmod N_A \\ n &= \mathrm{floor}\,(i/N_A) & q &= \mathrm{floor}\,(j/N_A) \end{aligned} \tag{5.38}$$

where floor indicates the largest integer less than or equal to the given quantity. For convenience, it is assumed that $0 \leq i,j < N_A$.

Now consider the first term in equation (5.37). The observed correlation matrix is calculated as:

$$\hat{\mathrm{R}}_{\mathbf{vv}} = \frac{1}{F_F}\sum_{k=1}^{F_F}\hat{\mathbf{v}}_k\hat{\mathbf{v}}_k^* \tag{5.39}$$

where F_F is the number of Walsh functions in one frame, and $\hat{\mathbf{v}}_k$ represents a measured $\mathbf{v}$ vector which includes a zero-mean noise perturbation:

$$\hat{\mathbf{v}}_k = \mathbf{v}_k + \delta\mathbf{v}_k \tag{5.40}$$

Substituting (5.40) into (5.39) yields:

$$\begin{aligned}\hat{\mathrm{R}}_{\mathbf{vv}} &= \frac{1}{F_F}\sum_{k=1}^{F_F}(\mathbf{v}_k+\delta\mathbf{v}_k)(\mathbf{v}_k+\delta\mathbf{v}_k)^* \qquad (5.41)\\ &= \frac{1}{F_F}\sum_{k=1}^{F_F}(\mathbf{v}_k\mathbf{v}_k^*+\mathbf{v}_k\delta\mathbf{v}_k^*+\delta\mathbf{v}_k\mathbf{v}_k^*+\delta\mathbf{v}_k\delta\mathbf{v}_k^*)\end{aligned}$$

By using (5.38) and (5.41), it is possible to write expressions for the two quantities in (5.37).

$$\begin{aligned}(\hat{\mathrm{r}}_{\mathbf{vv}})_i &= \frac{1}{F_F}\sum_{k=1}^{F_F}[(\mathbf{v}_k)_m(\mathbf{v}_k^*)_n+(\mathbf{v}_k)_m(\delta\mathbf{v}_k^*)_n+(\delta\mathbf{v}_k)_m(\mathbf{v}_k^*)_n \qquad (5.42)\\ &\qquad +(\delta\mathbf{v}_k)_m(\delta\mathbf{v}_k^*)_n]\\ (\hat{\mathrm{r}}_{\mathbf{vv}})_j &= \frac{1}{F_F}\sum_{r=1}^{F_F}[(\mathbf{v}_r)_p(\mathbf{v}_r^*)_q+(\mathbf{v}_r)_p(\delta\mathbf{v}_r^*)_q+(\delta\mathbf{v}_r)_p(\mathbf{v}_r^*)_q+(\delta\mathbf{v}_r)_p(\delta\mathbf{v}_r^*)_q] \qquad (5.43)\end{aligned}$$

The second subscript on each vector specifies the individual vector element. Now substitute (5.42) and (5.43) into the first term on the righthand side of (5.37) where (5.43) has been conjugated.

$$\begin{aligned}&E\left[(\hat{\mathrm{r}}_{\mathbf{vv}})_i(\hat{\mathrm{r}}_{\mathbf{vv}}^*)_j\right]\\ &= E\left[\left\{\frac{1}{F_F}\sum_{k=1}^{F_F}[(\mathbf{v}_k)_m(\mathbf{v}_k^*)_n+(\mathbf{v}_k)_m(\delta\mathbf{v}_k^*)_n+(\delta\mathbf{v}_k)_m(\mathbf{v}_k^*)_n+(\delta\mathbf{v}_k)_m(\delta\mathbf{v}_k^*)_n]\right\}\right.\\ &\quad \left.\left\{\frac{1}{F_F}\sum_{r=1}^{F_F}[(\mathbf{v}_r^*)_p(\mathbf{v}_r)_q+(\mathbf{v}_r^*)_p(\delta\mathbf{v}_r)_q+(\delta\mathbf{v}_r^*)_p(\mathbf{v}_r)_q+(\delta\mathbf{v}_r^*)_p(\delta\mathbf{v}_r)_q]\right\}\right]\\ &= \frac{1}{(F_F)^2}\sum_{k=1}^{F_F}\sum_{r=1}^{F_F}E[(\mathbf{v}_k)_m(\mathbf{v}_k^*)_n(\mathbf{v}_r^*)_p(\mathbf{v}_r)_q+(\mathbf{v}_k)_m(\mathbf{v}_k^*)_n(\mathbf{v}_r^*)_p(\delta\mathbf{v}_r)_q \qquad (5.44)\\ &\qquad +(\mathbf{v}_k)_m(\mathbf{v}_k^*)_n(\delta\mathbf{v}_r^*)_p(\mathbf{v}_r)_q+(\mathbf{v}_k)_m(\mathbf{v}_k^*)_n(\delta\mathbf{v}_r^*)_p(\delta\mathbf{v}_r)_q\\ &\qquad +(\mathbf{v}_k)_m(\delta\mathbf{v}_k^*)_n(\mathbf{v}_r^*)_p(\mathbf{v}_r)_q+(\mathbf{v}_k)_m(\delta\mathbf{v}_k^*)_n(\mathbf{v}_r^*)_p(\delta\mathbf{v}_r)_q\\ &\qquad +(\mathbf{v}_k)_m(\delta\mathbf{v}_k^*)_n(\delta\mathbf{v}_r^*)_p(\mathbf{v}_r)_q+(\mathbf{v}_k)_m(\delta\mathbf{v}_k^*)_n(\delta\mathbf{v}_r^*)_p(\delta\mathbf{v}_r)_q \qquad (5.45)\\ &\qquad +(\delta\mathbf{v}_k)_m(\mathbf{v}_k^*)_n(\mathbf{v}_r^*)_p(\mathbf{v}_r)_q+(\delta\mathbf{v}_k)_m(\mathbf{v}_k^*)_n(\mathbf{v}_r^*)_p(\delta\mathbf{v}_r)_q\\ &\qquad +(\delta\mathbf{v}_k)_m(\mathbf{v}_k^*)_n(\delta\mathbf{v}_r^*)_p(\mathbf{v}_r)_q+(\delta\mathbf{v}_k)_m(\mathbf{v}_k^*)_n(\delta\mathbf{v}_r^*)_p(\delta\mathbf{v}_r)_q\\ &\qquad +(\delta\mathbf{v}_k)_m(\delta\mathbf{v}_k^*)_n(\mathbf{v}_r^*)_p(\mathbf{v}_r)_q+(\delta\mathbf{v}_k)_m(\delta\mathbf{v}_k^*)_n(\mathbf{v}_r^*)_p(\delta\mathbf{v}_r)_q\\ &\qquad +(\delta\mathbf{v}_k)_m(\delta\mathbf{v}_k^*)_n(\delta\mathbf{v}_r^*)_p(\mathbf{v}_r)_q+(\delta\mathbf{v}_k)_m(\delta\mathbf{v}_k^*)_n(\delta\mathbf{v}_r^*)_p(\delta\mathbf{v}_r)_q]\end{aligned}$$

The non-δ values are not random variables so they can be factored out of the expectations. In addition, any term in the summation with only one δ component will

disappear when the expectation is taken since $\delta\mathbf{v}$ is zero-mean.

It is reasonable to assume that $\delta\mathbf{v}_k$ and $\delta\mathbf{v}_r$ are independent if $k \neq r$. Thus, any term with three δ's will be zero if $k \neq r$ since it will be possible to factor the expectation of the term into the product of two expectations, one of which will be zero-mean. If $k = r$ and the $\delta\mathbf{v}$ perturbations are assumed to follow a Gaussian distribution, the remaining terms with three δ's will also be zero since all odd moments of a zero-mean Gaussian distribution are zero [59, p. 107].

Eliminating all terms with either one or three δ components from (5.45) produces:

$$\begin{aligned} & E\left[(\hat{\mathrm{r}}_{\mathbf{vv}})_i(\hat{\mathrm{r}}^*_{\mathbf{vv}})_j\right] \\ &= \frac{1}{(F_F)^2}\sum_{k=1}^{F_F}\sum_{r=1}^{F_F} E\left[(\mathbf{v}_k)_m(\mathbf{v}^*_k)_n(\mathbf{v}^*_r)_p(\mathbf{v}_r)_q + (\mathbf{v}_k)_m(\mathbf{v}^*_k)_n(\delta\mathbf{v}^*_r)_p(\delta\mathbf{v}_r)_q\right. \\ &\qquad + (\mathbf{v}_k)_m(\delta\mathbf{v}^*_k)_n(\mathbf{v}^*_r)_p(\delta\mathbf{v}_r)_q + (\mathbf{v}_k)_m(\delta\mathbf{v}^*_k)_n(\delta\mathbf{v}^*_r)_p(\mathbf{v}_r)_q \qquad (5.46) \\ &\qquad + (\delta\mathbf{v}_k)_m(\mathbf{v}^*_k)_n(\mathbf{v}^*_r)_p(\delta\mathbf{v}_r)_q + (\delta\mathbf{v}_k)_m(\mathbf{v}^*_k)_n(\delta\mathbf{v}^*_r)_p(\mathbf{v}_r)_q \\ &\qquad \left. + (\delta\mathbf{v}_k)_m(\delta\mathbf{v}^*_k)_n(\mathbf{v}^*_r)_p(\mathbf{v}_r)_q + (\delta\mathbf{v}_k)_m(\delta\mathbf{v}^*_k)_n(\delta\mathbf{v}^*_r)_p(\delta\mathbf{v}_r)_q\right] \end{aligned}$$

Terms with one $\delta\mathbf{v}_k$ and one $\delta\mathbf{v}_r$ will only be non-zero when $k = r$. Thus, (5.46) can be further simplified to:

$$\begin{aligned} & E\left[(\hat{\mathrm{r}}_{\mathbf{vv}})_i(\hat{\mathrm{r}}^*_{\mathbf{vv}})_j\right] \\ &= \frac{1}{(F_F)^2}\left\{\sum_{k=1}^{F_F}\sum_{r=1}^{F_F} E\left[(\mathbf{v}_k)_m(\mathbf{v}^*_k)_n(\mathbf{v}^*_r)_p(\mathbf{v}_r)_q + (\mathbf{v}_k)_m(\mathbf{v}^*_k)_n(\delta\mathbf{v}^*_r)_p(\delta\mathbf{v}_r)_q\right.\right. \\ &\qquad \left. + (\delta\mathbf{v}_k)_m(\delta\mathbf{v}^*_k)_n(\mathbf{v}^*_r)_p(\mathbf{v}_r)_q + (\delta\mathbf{v}_k)_m(\delta\mathbf{v}^*_k)_n(\delta\mathbf{v}^*_r)_p(\delta\mathbf{v}_r)_q\right] \qquad (5.47) \\ &\quad + \sum_{k=1}^{F_F} E\left[(\mathbf{v}_k)_m(\delta\mathbf{v}^*_k)_n(\mathbf{v}^*_k)_p(\delta\mathbf{v}_k)_q + (\mathbf{v}_k)_m(\delta\mathbf{v}^*_k)_n(\delta\mathbf{v}^*_k)_p(\mathbf{v}_k)_q\right. \\ &\qquad \left.\left. + (\delta\mathbf{v}_k)_m(\mathbf{v}^*_k)_n(\mathbf{v}^*_k)_p(\delta\mathbf{v}_k)_q + (\delta\mathbf{v}_k)_m(\mathbf{v}^*_k)_n(\delta\mathbf{v}^*_k)_p(\mathbf{v}_k)_q\right\}\right. \end{aligned}$$

Terms with two $\delta\mathbf{v}_k$'s or $\delta\mathbf{v}_r$'s can be expressed as the appropriate entry of the covariance matrix $\mathrm{C}_{\mathbf{vv}}$, provided that one of the δ values is conjugated while the other is not.

$$\begin{aligned} E\left[(\hat{\mathrm{r}}_{\mathbf{vv}})_i(\hat{\mathrm{r}}^*_{\mathbf{vv}})_j\right] &= (\mathbf{v})_m(\mathbf{v}^*)_n(\mathbf{v}^*)_p(\mathbf{v})_q + (\mathbf{v})_m(\mathbf{v}^*)_n(\mathrm{C}^*_{\mathbf{vv}})_{pq} \\ &\quad + (\mathrm{C}_{\mathbf{vv}})_{mn}(\mathbf{v}^*)_p(\mathbf{v})_q + \frac{1}{(F_F)^2}\sum_{k=1}^{F_F}\sum_{r=1}^{F_F} E\left[(\delta\mathbf{v}_k)_m(\delta\mathbf{v}^*_k)_n(\delta\mathbf{v}^*_r)_p(\delta\mathbf{v}_r)_q\right] \\ &\quad + \frac{1}{F_F}\left\{(\mathbf{v})_m(\mathbf{v}^*)_p(\mathrm{C}_{\mathbf{vv}})_{qn} + (\mathbf{v})_m(\mathbf{v})_q E\left[(\delta\mathbf{v}^*)_n(\delta\mathbf{v}^*)_p\right]\right. \qquad (5.48) \\ &\quad \left. + (\mathbf{v}^*)_n(\mathbf{v}^*)_p E\left[(\delta\mathbf{v})_m(\delta\mathbf{v})_q\right] + (\mathbf{v}^*)_n(\mathbf{v})_q(\mathrm{C}_{\mathbf{vv}})_{mp}\right\} \end{aligned}$$

The remaining two expectation terms with two $\delta\mathbf{v}$'s will both be zero (see equations (B.18) and (B.19) in Appendix B). Therefore, (5.48) simplifies further to:

$$\begin{aligned} E\left[(\hat{\mathrm{r}}_{\mathbf{vv}})_i(\hat{\mathrm{r}}^*_{\mathbf{vv}})_j\right] &= (\mathbf{v})_m(\mathbf{v}^*)_n(\mathbf{v}^*)_p(\mathbf{v})_q + (\mathbf{v})_m(\mathbf{v}^*)_n(\mathrm{C}^*_{\mathbf{vv}})_{pq} \\ &\quad + (\mathrm{C}_{\mathbf{vv}})_{mn}(\mathbf{v}^*)_p(\mathbf{v})_q \\ &\quad + \frac{1}{(F_F)^2}\sum_{k=1}^{F_F}\sum_{r=1}^{F_F} E\left[(\delta\mathbf{v}_k)_m(\delta\mathbf{v}^*_k)_n(\delta\mathbf{v}^*_r)_p(\delta\mathbf{v}_r)_q\right] \\ &\quad + \frac{1}{F_F}\left\{(\mathbf{v})_m(\mathbf{v}^*)_p(\mathrm{C}_{\mathbf{vv}})_{qn} + (\mathbf{v}^*)_n(\mathbf{v})_q(\mathrm{C}_{\mathbf{vv}})_{mp}\right\} \end{aligned} \tag{5.49}$$

Consider just the fourth term of (5.49) (within the summation). This term with four δ's can be factored when $k \neq r$. When $k = r$, it is necessary to deal with the fourth moment of a complex Gaussian distribution.

$$\begin{aligned} &\frac{1}{(F_F)^2}\sum_{k=1}^{F_F}\sum_{r=1}^{F_F} E\left[(\delta\mathbf{v}_k)_m(\delta\mathbf{v}^*_k)_n(\delta\mathbf{v}^*_r)_p(\delta\mathbf{v}_r)_q\right] \\ &\quad = \frac{1}{(F_F)^2}\sum_{k=1}^{F_F}\left\{E\left[(\delta\mathbf{v}_k)_m(\delta\mathbf{v}^*_k)_n(\delta\mathbf{v}^*_k)_p(\delta\mathbf{v}_k)_q\right] + \sum_{r\neq k}(\mathrm{C}_{\mathbf{vv}})_{mn}(\mathrm{C}^*_{\mathbf{vv}})_{pq}\right\} \end{aligned} \tag{5.50}$$

Now consider the expectation term in (5.50) which represents the fourth moment of a complex Gaussian distribution. As shown in Appendix B (equation (B.40)), this term can be calculated as:

$$\begin{aligned} E\left[(\delta\mathbf{v}_k)_m(\delta\mathbf{v}^*_k)_n(\delta\mathbf{v}^*_k)_p(\delta\mathbf{v}_k)_q\right] &= E\left[(\delta\mathbf{v}_k)_m(\delta\mathbf{v}^*_k)_n\right]E\left[(\delta\mathbf{v}_k)_q(\delta\mathbf{v}^*_k)_p\right] \\ &\quad + E\left[(\delta\mathbf{v}_k)_m(\delta\mathbf{v}^*_k)_p\right]E\left[(\delta\mathbf{v}_k)_q(\delta\mathbf{v}^*_k)_n\right] \\ &\quad + E\left[(\delta\mathbf{v}_k)_m(\delta\mathbf{v}_k)_q\right]E\left[(\delta\mathbf{v}^*_k)_n(\delta\mathbf{v}^*_k)_p\right] \\ &= (\mathrm{C}_{\mathbf{vv}})_{mn}(\mathrm{C}^*_{\mathbf{vv}})_{pq} + (\mathrm{C}_{\mathbf{vv}})_{mp}(\mathrm{C}^*_{\mathbf{vv}})_{nq} \end{aligned} \tag{5.51}$$

Substituting (5.51) into (5.50) and simplifying yields:

$$\begin{aligned} &\frac{1}{(F_F)^2}\sum_{k=1}^{F_F}\sum_{r=1}^{F_F} E\left[(\delta\mathbf{v}_k)_m(\delta\mathbf{v}^*_k)_n(\delta\mathbf{v}^*_r)_p(\delta\mathbf{v}_r)_q\right] \\ &\quad = (\mathrm{C}_{\mathbf{vv}})_{mn}(\mathrm{C}^*_{\mathbf{vv}})_{pq} + \frac{1}{F_F}\left\{(\mathrm{C}_{\mathbf{vv}})_{mp}(\mathrm{C}^*_{\mathbf{vv}})_{nq}\right\} \end{aligned} \tag{5.52}$$

Substituting (5.52) into (5.49) produces:

$$E\left[(\hat{\mathrm{r}}_{\mathbf{vv}})_i(\hat{\mathrm{r}}^*_{\mathbf{vv}})_j\right] = (\mathbf{v})_m(\mathbf{v}^*)_n(\mathbf{v}^*)_p(\mathbf{v})_q + (\mathbf{v})_m(\mathbf{v}^*)_n(\mathrm{C}^*_{\mathbf{vv}})_{pq}$$

$$+ (\mathrm{C}_{\mathbf{vv}})_{mn}(\mathbf{v}^*)_p(\mathbf{v})_q + (\mathrm{C}_{\mathbf{vv}})_{mn}(\mathrm{C}^*_{\mathbf{vv}})_{pq} \tag{5.53}$$
$$+ \frac{1}{F_F}\{(\mathrm{C}_{\mathbf{vv}})_{mp}(\mathrm{C}^*_{\mathbf{vv}})_{nq} + (\mathbf{v})_m(\mathbf{v}^*)_p(\mathrm{C}_{\mathbf{vv}})_{qn} + (\mathbf{v}^*)_n(\mathbf{v})_q(\mathrm{C}_{\mathbf{vv}})_{mp}\}$$

Recalling that $\delta\mathbf{v}$ is zero-mean, the expected values of (5.42) and (5.43) can be found to be (note that (5.43) has been conjugated):

$$E\left[(\hat{\mathrm{r}}_{\mathbf{vv}})_i\right] = (\mathbf{v})_m(\mathbf{v}^*)_n + (\mathrm{C}_{\mathbf{vv}})_{mn} \tag{5.54}$$
$$E\left[(\hat{\mathrm{r}}_{\mathbf{vv}})^*_j\right] = (\mathbf{v}^*)_p(\mathbf{v})_q + (\mathrm{C}^*_{\mathbf{vv}})_{pq} \tag{5.55}$$

Multiplying (5.54) and (5.55) together generates:

$$E\left[(\hat{\mathrm{r}}_{\mathbf{vv}})_i\right]E\left[(\hat{\mathrm{r}}_{\mathbf{vv}})_j\right] = (\mathbf{v})_m(\mathbf{v}^*)_n(\mathbf{v}^*)_p(\mathbf{v})_q + (\mathbf{v})_m(\mathbf{v}^*)_n(\mathrm{C}^*_{\mathbf{vv}})_{pq} + (\mathbf{v}^*)_p(\mathbf{v})_q(\mathrm{C}_{\mathbf{vv}})_{mn} + (\mathrm{C}_{\mathbf{vv}})_{mn}(\mathrm{C}^*_{\mathbf{vv}})_{pq} \tag{5.56}$$

Referring to (5.37), $\hat{\sigma}_{ij}$ may be calculated by subtracting (5.56) from (5.53).

$$\hat{\sigma}_{ij} = \frac{1}{F_F}\{(\mathrm{C}_{\mathbf{vv}})_{mp}(\mathrm{C}^*_{\mathbf{vv}})_{nq} + (\mathbf{v})_m(\mathbf{v}^*)_p(\mathrm{C}_{\mathbf{vv}})_{qn} + (\mathbf{v}^*)_n(\mathbf{v})_q(\mathrm{C}_{\mathbf{vv}})_{mp}\} \tag{5.57}$$

Thus, entries of the covariance matrix of $\hat{\mathrm{r}}_{\mathbf{vv}}$ can now be expressed in terms of known quantities.

5.6.2 Eigenvalue and Eigenvector Covariance

Using equation (5.57), it is possible to approximate the covariance matrices for the actual eigenvalues and eigenvectors of $\hat{\mathrm{R}}_{\mathbf{vv}}$ using matrix perturbation theory [112]. This component of the derivation was also originally performed for a real symmetric matrix [13] [14] [17] [19], but can be adapted directly to Hermitian matrices.

Based on Weng's [111] first-order Taylor series expansion for the real case, the first-order perturbation terms for the eigenvalues and eigenvectors of a Hermitian matrix may be derived as:

$$\Delta\lambda_i \approx \delta\lambda_i = \mathbf{v}_i^*\Delta_{\mathrm{R}_{\mathbf{vv}}}\mathbf{v}_i \tag{5.58}$$
$$\Delta\mathbf{v}_i \approx \delta\mathbf{v}_i = \mathrm{V}\Delta_i\mathrm{V}^*\Delta_{\mathrm{R}_{\mathbf{vv}}}\mathbf{v}_i \tag{5.59}$$

where the columns of V are the eigenvectors of the true (predicted) $\mathrm{R}_{\mathbf{vv}}$, $\Delta_{\mathrm{R}_{\mathbf{vv}}}$ represents the perturbation in the $\hat{\mathrm{R}}_{\mathbf{vv}}$ matrix, and Δ_1 is defined as (Δ_i is defined similarly, but $i = 1$ can be assumed for the principal eigenvector without loss of generality):

$$\Delta_1 \equiv \begin{bmatrix} 0 & 0 & \dots & 0 \\ 0 & \frac{1}{\lambda_1 - \lambda_2} & \dots & 0 \\ \vdots & \vdots & \ddots & \vdots \\ 0 & 0 & \dots & \frac{1}{\lambda_1 - \lambda_{N_A}} \end{bmatrix} \tag{5.60}$$

It is assumed that the second and higher order terms in the Taylor series expansion will be negligible.

Note that $\Delta_{\mathrm{R}_{\mathbf{vv}}}\mathbf{v}_i$ may be rewritten as:

$$\Delta_{\mathrm{R}_{\mathbf{vv}}}\mathbf{v}_i = \begin{bmatrix} (v_1)_i \mathrm{I}_{N_A} & \dots & (v_{N_A})_i \mathrm{I}_{N_A} \end{bmatrix} \Delta_{\mathrm{R}_{\mathbf{vv}}} = \mathrm{U}_i \Delta_{\mathrm{R}_{\mathbf{vv}}} \tag{5.61}$$

The first-order eigenvalue and eigenvector perturbations are both zero-mean. The covariance matrix for $\mathbf{v}_i$ may therefore be approximated as:

$$\begin{aligned} \Sigma &= E\left[\Delta\mathbf{v}_i \Delta\mathbf{v}_i^*\right] \\ &\approx E\left[\left(\mathrm{V}\Delta_i\mathrm{V}^*\mathrm{U}_i\Delta_{\mathrm{R}_{\mathbf{vv}}}\right)\left(\Delta_{\mathrm{R}_{\mathbf{vv}}}^*\mathrm{U}_i^*\mathrm{V}\Delta_i\mathrm{V}^*\right)\right] \\ &= \mathrm{V}\Delta_i\mathrm{V}^*\mathrm{U}_i E\left[\Delta_{\mathrm{R}_{\mathbf{vv}}}\Delta_{\mathrm{R}_{\mathbf{vv}}}^*\right]\mathrm{U}_i^*\mathrm{V}\Delta_i\mathrm{V}^* \\ &= \mathrm{V}\Delta_i\mathrm{V}^*\mathrm{U}_i\mathrm{C}_{\hat{\mathbf{r}}\mathbf{vv}}\mathrm{U}_i^*\mathrm{V}\Delta_i\mathrm{V}^* \end{aligned} \tag{5.62}$$

Equation (5.63) is used in Section 5.8 to predict covariance matrices for the eigenvector estimators which may then be compared to the observed covariance matrices from simulations.

The (i, j) entry of the $N_A \times N_A$ eigenvalue covariance matrix may be approximated as:

$$\begin{aligned} (\Sigma)_{i,j} &= E\left[\Delta\lambda_i \Delta\lambda_j^*\right] \\ &\approx E\left[\left(\mathbf{v}_i^*\Delta_{\mathrm{R}_{\mathbf{vv}}}\mathbf{v}_i\right)\left(\mathbf{v}_j^*\Delta_{\mathrm{R}_{\mathbf{vv}}}\mathbf{v}_j\right)^*\right] \\ &\approx E\left[\left(\mathbf{v}_i^*\mathrm{U}_i\Delta_{\mathrm{R}_{\mathbf{vv}}}\right)\left(\Delta_{\mathrm{R}_{\mathbf{vv}}}^*\mathrm{U}_j^*\mathbf{v}_j\right)\right] \\ &= \mathbf{v}_i^*\mathrm{U}_i E\left[\Delta_{\mathrm{R}_{\mathbf{vv}}}\Delta_{\mathrm{R}_{\mathbf{vv}}}^*\right]\mathrm{U}_j^*\mathbf{v}_j \\ &= \mathbf{v}_i^*\mathrm{U}_i\mathrm{C}_{\hat{\mathbf{r}}\mathbf{vv}}\mathrm{U}_j^*\mathbf{v}_j \end{aligned} \tag{5.63}$$

The above expression for the covariance matrix of the eigenvalues can be used, if so desired, to determine the probability that the principal eigenvector of a matrix is incorrectly identified due to variation in the eigenvalues.

5.7 Cramér-Rao Lower Bound

There are two important quantities to consider when evaluating the performance of a given estimator. The mean indicates whether or not the estimator is biased, and the covariance matrix quantifies the reliability of the estimator. A smaller covariance matrix is more desirable since any individual estimate will be more likely to be closer to the mean. The *Cramér-Rao lower bound* (CRLB) represents the minimum possible covariance matrix for any estimator. This implies that the difference between any estimator's covariance matrix and the CRLB will be a positive semi-definite matrix (*i.e.* the eigenvalues will be non-negative).

In this situation, the observations correspond directly to the parameter which is to be estimated (*i.e.* the array response vector). Consequently, the CRLB actually corresponds to the covariance matrix of the estimator. Formally, the CRLB is the inverse of the Fisher information matrix J [30] which is defined as:

$$\mathrm{J} \equiv \mathrm{C}_{\mathbf{qq}}^{-1} \tag{5.64}$$

However, $\mathbf{q}$ is constrained to have unit magnitude so the above bound is not quite correct. Gorman and Hero [30] [31] developed the necessary modifications for constrained situations with real parameters, although the analysis can also be applied directly to complex situations. With an unbiased estimator, as is the case here, the constrained lower bound $\mathrm{B_C}$ is:

$$\mathrm{B_C} = \mathrm{Q}_{\mathbf{q}}\mathrm{J}^{-1} \tag{5.65}$$

$$\mathrm{Q}_{\mathbf{q}} \equiv \mathrm{I}_{N_M} - \mathrm{J}^{-1}[\nabla \mathrm{G}_{\mathbf{q}}]^* \left\{ [\nabla \mathrm{G}_{\mathbf{q}}]\mathrm{J}^{-1}[\nabla \mathrm{G}_{\mathbf{q}}]^* \right\}^{\dagger} [\nabla \mathrm{G}_{\mathbf{q}}] \tag{5.66}$$

where the $\dagger$ operator represents the Moore-Penrose pseudo-inverse. In this case, the quantity within parentheses is a scalar so it is only necessary to take its reciprocal.

$\nabla \mathrm{G}_{\mathbf{q}}$ is the gradient matrix of the equality constraint which applies in this problem.

$$\mathrm{G}_{\mathbf{q}} = \mathbf{q}^{*}\mathbf{q} - 1 = \left(\sum_{i=1}^{N_A} \mathbf{q}_i^{*} \mathbf{q}_i \right) - 1 = 0 \tag{5.67}$$

$$\nabla \mathrm{G}_{\mathbf{q}} = \left[\begin{array}{ccc} 2\mathbf{q}_1 & \ldots & 2\mathbf{q}_{N_A} \end{array} \right] = 2\mathbf{a}^{*} \tag{5.68}$$

where $\mathbf{a}$ is the true array response vector.

Substituting (5.64) and (5.68) into (5.66) produces:

$$\begin{aligned} \mathrm{Q}_{\mathbf{q}} &= \mathrm{I}_{N_M} - \mathrm{C}_{\mathbf{qq}}(2\mathbf{a}) \left\{ (2\mathbf{a}^{*}) \mathrm{C}_{\mathbf{qq}}(2\mathbf{a}) \right\}^{\dagger} (2\mathbf{a}^{*}) \\ &= \mathrm{I}_{N_M} - \frac{1}{\mathbf{a}^{*}\mathrm{C}_{\mathbf{qq}}\mathbf{a}} \mathrm{C}_{\mathbf{qq}}\mathbf{a}\mathbf{a}^{*} \end{aligned} \tag{5.69}$$

Substituting (5.69) and (5.64) into (5.66) yields:

$$\mathrm{B}_{\mathrm{C}} = \left(\mathrm{I}_{N_M} - \frac{1}{\mathbf{a}^{*}\mathrm{C}_{\mathbf{qq}}\mathbf{a}} \mathrm{C}_{\mathbf{qq}}\mathbf{a}\mathbf{a}^{*} \right) \mathrm{C}_{\mathbf{qq}} \tag{5.70}$$

As will be seen in the following section, the above expression gives a result that is similar, but not quite identical to equation (5.32). This is due to $\mathrm{C}_{\mathbf{qq}}$ having an eigenvector which is close to, but not exactly equal to, $\mathbf{a}_p$.

To show the approximate equivalence of these two covariance matrix predictions, assume that $\mathbf{v}_1$ is an eigenvector of $\mathrm{C}_{\mathbf{qq}}$ which is equal to $\mathbf{a}_p$. Note that this is an approximation. In this situation, the constrained bound in (5.70) evaluates as:

$$\begin{aligned} \mathrm{B}_{\mathrm{C}} &= \left(\mathrm{I}_{N_M} - \frac{1}{\mathbf{v}_1^{*}\mathrm{C}_{\mathbf{qq}}\mathbf{v}_1} \mathrm{C}_{\mathbf{qq}}\mathbf{v}_1\mathbf{v}_1^{*} \right) \mathrm{C}_{\mathbf{qq}} \\ &= \mathrm{C}_{\mathbf{qq}} - \frac{1}{\lambda_1} (\lambda_1 \mathbf{v}_1)(\lambda_1 \mathbf{v}_1^{*}) \\ &= \mathrm{C}_{\mathbf{qq}} - \lambda_1 \mathbf{v}_1 \mathbf{v}_1^{*} \end{aligned} \tag{5.71}$$

If $\mu_{\mathbf{q}} = \mathbf{a}_p$ is assumed to be an eigenvector of $\mathrm{C}_{\mathbf{qq}}$ in (5.31), then it can be seen that equations (5.32) and (5.71) are equivalent.

5.8 Simulation Results and Predictions

Tables 5.1 through 5.4 contain sample results obtained from PN chip-level simulations along with the predicted values calculated as shown earlier in this chapter. The

desired received E_b/N_0 was 5 dB in this instance, and perfect power control was used. Each simulation was executed for 10000 frames in order to obtain a suitable sample size, and the statistics were recorded for one of the mobiles. During the course of each simulation, all of the users remained stationary so that the true array response vectors did not vary. However, the transmitted data and background noise did vary from frame to frame. The beamforming coefficient vector for the desired mobile was estimated from the data received during each frame. A transmission activity factor of $\psi = 1.0$ was used for all of these experiments.

The statistics in Tables 5.1 through 5.3 were obtained from the following combinations of numbers of antenna elements and mobiles: (2,30), (3,40), and (4,50). Fading was not initially considered. As can be seen from the sample data, there is generally consistent agreement between the simulation observations (indicated by O) and predictions (indicated by P). The sole exception appears to be the covariance matrix of the normalized mean vector ($\mathbf{C_{qq}}$) which is due to the normalization process as discussed in Section 5.5.3.1. This can be compensated for by using the modified covariance matrix from equation (5.32) or the constrained CRLB from equation (5.70), as shown in the tables.

Table 5.4 contains observed and predicted statistics for 3 antenna elements and 40 mobiles when uncorrelated Rayleigh fading is introduced. The mobile positions and transmission channel parameters are identical to those of Table 5.2, so that the results can be compared directly. As expected, larger covariance matrices for the estimators are obtained in the presence of fading. In addition, the mean vector approach appears to perform slightly better than the principal eigenvector estimator when fading is considered. This is evident from the presence of a possible bias in the observed array response vector estimate from the eigenvector method ($E[\mathbf{p}]$) and the smaller covariance matrix of the mean vector estimator.

Tables 5.5 and 5.6 contain the observed and predicted statistics when half and double the number of correlation vector samples are used to estimate the array response vector, respectively. As before, the mobile positions and transmission channel parameters are identical to those of Table 5.2. For Table 5.5, a half-size frame contained 88 data bits and 8 tail bits with 100 frames per second. Conversely, for Table

Quantity	O/P	Value
$\mathrm{R}_{\mathbf{vv}}$	O	$\begin{bmatrix} 1.5590 & 0.6983 + j0.6563 \\ 0.6983 - j0.6563 & 1.5602 \end{bmatrix} \times 10^{-24}$
	P	$\begin{bmatrix} 1.5615 & 0.6996 + j0.6572 \\ 0.6996 - j0.6572 & 1.5615 \end{bmatrix} \times 10^{-24}$
$E[\mathbf{p}]$	O	$\begin{bmatrix} 6.5579 + j2.5968 & 6.5618 - j2.5984 \end{bmatrix} \times 10^{-1}$
	P	$\begin{bmatrix} 6.5953 + j2.5499 & 6.5953 - j2.5499 \end{bmatrix} \times 10^{-1}$
$\mathrm{C}_{\mathbf{pp}}$	O	$\begin{bmatrix} 2.2072 & -1.6155 - j1.4972 \\ -1.6155 + j1.4972 & 2.2080 \end{bmatrix} \times 10^{-3}$
	P	$\begin{bmatrix} 2.1434 & -1.5622 - j1.4676 \\ -1.5622 + j1.4676 & 2.1434 \end{bmatrix} \times 10^{-3}$
$\hat{\mathrm{C}}_{\mathbf{pp}}$	O	$\begin{bmatrix} 2.2064 & -1.6073 - j1.5096 \\ -1.6073 + j1.5096 & 2.2037 \end{bmatrix} \times 10^{-3}$
	P	$\begin{bmatrix} 2.1433 & -1.5859 - j1.4418 \\ -1.5859 + j1.4418 & 2.1433 \end{bmatrix} \times 10^{-3}$

Table 5.1: Sample observed and predicted feedback correlation beamforming statistics with 2 antenna elements and 30 users ($\psi = 1.0$)

Quantity	O/P	Value
$E[\mathbf{w}]$	O	$\begin{bmatrix} 4.4319 + j1.7134 & 4.4319 - j1.7134 \end{bmatrix} \times 10^{-9}$
	P	$\begin{bmatrix} 4.4319 + j1.7134 & 4.4319 - j1.7134 \end{bmatrix} \times 10^{-9}$
$E[\mathbf{q}]$	O	$\begin{bmatrix} 6.5857 + j2.5206 & 6.5721 - j2.5703 \end{bmatrix} \times 10^{-1}$
	P	$\begin{bmatrix} 6.5953 + j2.5499 & 6.5953 - j2.5499 \end{bmatrix} \times 10^{-1}$
$\mathrm{C}_{\mathbf{ww}}$	O	$\begin{bmatrix} 1.4152 & -0.0803 - j0.0222 \\ -0.0803 + j0.0222 & 1.4064 \end{bmatrix} \times 10^{-19}$
	P	$\begin{bmatrix} 1.3959 & -0.0611 - j0.0047 \\ -0.0611 + j0.0047 & 1.3959 \end{bmatrix} \times 10^{-19}$
$\mathrm{C}_{\mathbf{qq}}$	O	$\begin{bmatrix} 2.3795 & -0.6813 - j0.0583 \\ -0.6813 + j0.0583 & 2.3841 \end{bmatrix} \times 10^{-3}$
	P	$\begin{bmatrix} 3.0913 & -0.1354 - j0.0103 \\ -0.1354 + j0.0103 & 3.0913 \end{bmatrix} \times 10^{-3}$
$\hat{\mathrm{C}}_{\mathbf{qq}}$	O	$\begin{bmatrix} 1.6403 & -1.2123 - j1.1032 \\ -1.2123 + j1.1032 & 1.6379 \end{bmatrix} \times 10^{-3}$
	P	$\begin{bmatrix} 1.5992 & -1.1833 - j1.0758 \\ -1.1833 + j1.0758 & 1.5992 \end{bmatrix} \times 10^{-3}$
CRLB	P	$\begin{bmatrix} 1.5981 & -1.1824 - j1.0750 \\ -1.1824 + j1.0750 & 1.5981 \end{bmatrix} \times 10^{-3}$

Table 5.1: (continued)

Quantity	O/P	Value
$\mathbf{R_{vv}}$	O	$\begin{bmatrix} 1.2405 & -0.4059 - j0.5260 & 0.3766 + j0.4904 \\ -0.4059 + j0.5260 & 1.2409 & -0.7217 + j0.0708 \\ 0.3766 - j0.4904 & -0.7217 - j0.0708 & 1.2410 \end{bmatrix} \times 10^{-24}$
	P	$\begin{bmatrix} 1.2417 & -0.4068 - j0.5267 & 0.3776 + j0.4905 \\ -0.4068 + j0.5267 & 1.2417 & -0.7225 + j0.0703 \\ 0.3776 - j0.4905 & -0.7225 - j0.0703 & 1.2417 \end{bmatrix} \times 10^{-24}$
$E[\mathbf{p}]$	O	$\begin{bmatrix} 5.0591 - j2.3728 & -1.0858 + j5.7918 & 1.4485 - j5.5848 \end{bmatrix} \times 10^{-1}$
	P	$\begin{bmatrix} 5.1722 - j2.5654 & -1.0266 + j5.6815 & 1.6048 - j5.5460 \end{bmatrix} \times 10^{-1}$
$\mathbf{C_{pp}}$	O	$\begin{bmatrix} 2.9412 & 0.5577 + j1.1790 & -1.2373 - j1.0419 \\ 0.5577 - j1.1790 & 2.1716 & 0.9406 + j0.1614 \\ -1.2373 + j1.0419 & 0.9406 - j0.1614 & 2.5195 \end{bmatrix} \times 10^{-3}$
	P	$\begin{bmatrix} 3.0308 & 0.5709 + j1.1894 & -1.2096 - j1.0864 \\ 0.5709 - j1.1894 & 2.1473 & 0.9495 + j0.1614 \\ -1.2096 + j1.0864 & 0.9495 - j0.1614 & 2.5145 \end{bmatrix} \times 10^{-3}$
$\hat{\mathbf{C}}_{\mathbf{pp}}$	O	$\begin{bmatrix} 2.9788 & 0.5423 + j1.1830 & -1.2063 - j1.0533 \\ 0.5424 - j1.1830 & 2.1419 & 0.9652 + j0.1774 \\ -1.2063 + j1.0533 & 0.9652 - j0.1774 & 2.5021 \end{bmatrix} \times 10^{-3}$
	P	$\begin{bmatrix} 2.9536 & 0.6019 + j1.1823 & -1.2761 - j1.0627 \\ 0.6019 - j1.1823 & 2.1989 & 0.9091 + j0.1295 \\ -1.2761 + j1.0627 & 0.9091 - j0.1295 & 2.5367 \end{bmatrix} \times 10^{-3}$

Table 5.2: Sample observed and predicted feedback correlation beamforming statistics with 3 antenna elements and 40 users ($\psi = 1.0$)

Quantity	O/P	Value
$E[\mathbf{w}]$	O	$\begin{bmatrix} 3.5129 - j1.7588 & -0.6849 + j3.8685 & 1.0762 - j3.7797 \end{bmatrix} \times 10^{-9}$
	P	$\begin{bmatrix} 3.5184 - j1.7451 & -0.6984 + j3.8649 & 1.0917 - j3.7727 \end{bmatrix} \times 10^{-9}$
$E[\mathbf{q}]$	O	$\begin{bmatrix} 5.1435 - j2.5759 & -1.0023 + j5.6629 & 1.5767 - j5.5333 \end{bmatrix} \times 10^{-1}$
	P	$\begin{bmatrix} 5.1722 - j2.5654 & -1.0266 + j5.6815 & 1.6048 - j5.5460 \end{bmatrix} \times 10^{-1}$
$\mathrm{C}_{\mathbf{ww}}$	O	$\begin{bmatrix} 1.3585 & -0.0170 + j0.0251 & -0.1893 + j0.0064 \\ -0.0170 - j0.0251 & 1.3652 & -0.1389 - j0.0062 \\ -0.1893 - j0.0064 & -0.1389 + j0.0062 & 1.3629 \end{bmatrix} \times 10^{-19}$
	P	$\begin{bmatrix} 1.3732 & -0.0178 + j0.0256 & -0.1796 - j0.0070 \\ -0.0178 - j0.0256 & 1.3732 & -0.1357 + j0.0036 \\ -0.1796 + j0.0070 & -0.1357 - j0.0036 & 1.3732 \end{bmatrix} \times 10^{-19}$
$\mathrm{C}_{\mathbf{qq}}$	O	$\begin{bmatrix} 2.5245 & 0.2302 + j0.4474 & -0.6230 - j0.3759 \\ 0.2302 - j0.4474 & 2.3650 & 0.2351 + j0.0098 \\ -0.6230 + j0.3759 & 0.2351 - j0.0098 & 2.4399 \end{bmatrix} \times 10^{-3}$
	P	$\begin{bmatrix} 2.9676 & -0.0386 + j0.0552 & -0.3882 - j0.0150 \\ -0.0386 - j0.0552 & 2.9676 & -0.2932 + j0.0079 \\ -0.3882 + j0.0150 & -0.2932 - j0.0079 & 2.9676 \end{bmatrix} \times 10^{-3}$
$\hat{\mathrm{C}}_{\mathbf{qq}}$	O	$\begin{bmatrix} 2.1350 & 0.5034 + j0.8564 & -0.8542 - j0.7735 \\ 0.5034 - j0.8564 & 1.7721 & 0.7907 + j0.0264 \\ -0.8542 + j0.7735 & 0.7907 - j0.0264 & 1.9307 \end{bmatrix} \times 10^{-3}$
	P	$\begin{bmatrix} 2.1744 & 0.5135 + j0.8682 & -0.8696 - j0.7917 \\ 0.5135 - j0.8682 & 1.7971 & 0.8007 + j0.0237 \\ -0.8696 + j0.7917 & 0.8007 - j0.0237 & 1.9652 \end{bmatrix} \times 10^{-3}$
CRLB	P	$\begin{bmatrix} 2.1597 & 0.5019 + j0.8683 & -0.8712 - j0.7797 \\ 0.5019 - j0.8683 & 1.7879 & 0.7994 + j0.0332 \\ -0.8712 + j0.7797 & 0.7994 - j0.0332 & 1.9552 \end{bmatrix} \times 10^{-3}$

Table 5.2: (continued)

Qnty	O/P	Value
$\mathrm{R}_{\mathbf{vv}}$	O	$\begin{bmatrix} 1.085 & 0.113-j0.496 & -0.332+j0.447 & -0.528-j0.148 \\ 0.113+j0.496 & 1.085 & -0.528-j0.149 & -0.104-j0.513 \\ -0.332-j0.447 & -0.528+j0.149 & 1.087 & 0.112+j0.496 \\ -0.528+j0.148 & -0.104+j0.513 & 0.112-j0.496 & 1.084 \end{bmatrix} \times 10^{-24}$
	P	$\begin{bmatrix} 1.086 & 0.113-j0.496 & -0.331+j0.447 & -0.530-j0.148 \\ 0.113+j0.496 & 1.086 & -0.530-j0.148 & -0.105-j0.514 \\ -0.331-j0.447 & -0.530+j0.148 & 1.086 & 0.113+j0.496 \\ -0.530+j0.148 & -0.105+j0.514 & 0.113-j0.496 & 1.086 \end{bmatrix} \times 10^{-24}$
$E[\mathbf{p}]$	O	$\begin{bmatrix} -2.399-j4.404 & 3.355-j3.613 & -2.402+j4.409 & 3.354+j3.611 \end{bmatrix} \times 10^{-1}$
	P	$\begin{bmatrix} -2.370-j4.403 & 3.411-j3.656 & -2.370+j4.403 & 3.411+j3.656 \end{bmatrix} \times 10^{-1}$
$\mathrm{C}_{\mathbf{pp}}$	O	$\begin{bmatrix} 2.546 & -0.798+j0.905 & 0.140-j0.758 & 0.740+j0.017 \\ -0.798-j0.905 & 2.707 & 0.715+j0.020 & -0.567+j0.918 \\ 0.140+j0.758 & 0.715-j0.020 & 2.467 & -0.772-j0.863 \\ 0.740-j0.017 & -0.567-j0.918 & -0.772+j0.863 & 2.682 \end{bmatrix} \times 10^{-3}$
	P	$\begin{bmatrix} 2.517 & -0.789+j0.889 & 0.127-j0.785 & 0.735+j0.039 \\ -0.789-j0.889 & 2.727 & 0.735+j0.039 & -0.547+j0.927 \\ 0.127+j0.785 & 0.735-j0.039 & 2.517 & -0.789-j0.889 \\ 0.735-j0.039 & -0.547-j0.927 & -0.789+j0.889 & 2.727 \end{bmatrix} \times 10^{-3}$
$\hat{\mathrm{C}}_{\mathbf{pp}}$	O	$\begin{bmatrix} 2.533 & -0.797+j0.908 & 0.145-j0.769 & 0.743+j0.018 \\ -0.797-j0.908 & 2.724 & 0.717+j0.021 & -0.569+j0.911 \\ 0.145+j0.769 & 0.717-j0.021 & 2.456 & -0.771-j0.865 \\ 0.743-j0.018 & -0.569-j0.911 & -0.771+j0.865 & 2.689 \end{bmatrix} \times 10^{-3}$
	P	$\begin{bmatrix} 2.529 & -0.792+j0.888 & 0.126-j0.772 & 0.734+j0.043 \\ -0.792-j0.888 & 2.715 & 0.734+j0.043 & -0.547+j0.939 \\ 0.126+j0.772 & 0.734-j0.043 & 2.529 & -0.792-j0.888 \\ 0.734-j0.043 & -0.547-j0.939 & -0.792+j0.888 & 2.715 \end{bmatrix} \times 10^{-3}$

Table 5.3: Sample observed and predicted feedback correlation beamforming statistics with 4 antenna elements and 50 users ($\psi = 1.0$)

Qnty	O/P	Value
$E[\mathbf{w}]$	O	$\begin{bmatrix} -1.653 - j3.052 & 2.358 - j2.543 & -1.636 + j3.066 & 2.378 + j2.524 \end{bmatrix} \times 10^{-9}$
	P	$\begin{bmatrix} -1.645 - j3.056 & 2.368 - j2.538 & -1.645 + j3.056 & 2.368 + j2.538 \end{bmatrix} \times 10^{-9}$
$E[\mathbf{q}]$	O	$\begin{bmatrix} -2.370 - j4.376 & 3.381 - j3.646 & -2.345 + j4.396 & 3.410 + j3.618 \end{bmatrix} \times 10^{-1}$
	P	$\begin{bmatrix} -2.370 - j4.403 & 3.411 - j3.656 & -2.370 + j4.403 & 3.411 + j3.656 \end{bmatrix} \times 10^{-1}$
$\mathrm{C}_{\mathbf{ww}}$	O	$\begin{bmatrix} 1.359 & -0.129 - j0.001 & -0.098 + j0.010 & -0.045 - j0.033 \\ -0.129 + j0.001 & 1.342 & -0.060 - j0.047 & -0.174 + j0.010 \\ -0.098 - j0.010 & -0.060 + j0.047 & 1.336 & -0.128 - j0.004 \\ -0.045 + j0.033 & -0.174 - j0.010 & -0.128 + j0.004 & 1.332 \end{bmatrix} \times 10^{-19}$
	P	$\begin{bmatrix} 1.352 & -0.130 - j0.002 & -0.102 + j0.026 & -0.059 - j0.036 \\ -0.130 + j0.002 & 1.352 & -0.059 - j0.036 & -0.165 + j0.017 \\ -0.102 - j0.026 & -0.059 + j0.036 & 1.352 & -0.130 + j0.002 \\ -0.059 + j0.036 & -0.165 - j0.017 & -0.130 - j0.002 & 1.352 \end{bmatrix} \times 10^{-19}$
$\mathrm{C}_{\mathbf{qq}}$	O	$\begin{bmatrix} 2.425 & -0.378 + j0.338 & -0.005 - j0.297 & 0.247 + j0.003 \\ -0.378 - j0.338 & 2.424 & 0.226 - j0.018 & -0.318 + j0.353 \\ -0.005 + j0.297 & 0.226 + j0.018 & 2.379 & -0.378 - j0.338 \\ 0.247 - j0.003 & -0.318 - j0.353 & -0.378 + j0.338 & 2.412 \end{bmatrix} \times 10^{-3}$
	P	$\begin{bmatrix} 2.806 & -0.269 - j0.005 & -0.212 + j0.053 & -0.123 - j0.075 \\ -0.269 + j0.005 & 2.806 & -0.123 - j0.075 & -0.343 + j0.036 \\ -0.212 - j0.053 & -0.123 + j0.075 & 2.806 & -0.269 + j0.005 \\ -0.123 + j0.075 & -0.343 - j0.036 & -0.269 - j0.005 & 2.806 \end{bmatrix} \times 10^{-3}$
$\hat{\mathrm{C}}_{\mathbf{qq}}$	O	$\begin{bmatrix} 2.039 & -0.496 + j0.689 & 0.200 - j0.620 & 0.599 + j0.084 \\ -0.496 - j0.689 & 2.069 & 0.582 + j0.070 & -0.283 + j0.697 \\ 0.200 + j0.620 & 0.582 - j0.070 & 2.001 & -0.497 - j0.674 \\ 0.599 - j0.084 & -0.283 - j0.697 & -0.497 + j0.674 & 2.077 \end{bmatrix} \times 10^{-3}$
	P	$\begin{bmatrix} 2.029 & -0.500 + j0.692 & 0.188 - j0.615 & 0.595 + j0.084 \\ -0.500 - j0.692 & 2.115 & 0.595 + j0.084 & -0.272 + j0.723 \\ 0.188 + j0.615 & 0.595 - j0.084 & 2.029 & -0.500 - j0.692 \\ 0.595 - j0.084 & -0.272 - j0.723 & -0.500 + j0.692 & 2.115 \end{bmatrix} \times 10^{-3}$
CRLB	P	$\begin{bmatrix} 2.028 & -0.500 + j0.692 & 0.187 - j0.615 & 0.594 + j0.084 \\ -0.500 - j0.692 & 2.115 & 0.594 + j0.084 & -0.272 + j0.724 \\ 0.187 + j0.615 & 0.594 - j0.084 & 2.028 & -0.500 - j0.692 \\ 0.594 - j0.084 & -0.272 - j0.724 & -0.500 + j0.692 & 2.115 \end{bmatrix} \times 10^{-3}$

Table 5.3: (continued)

Quantity	O/P	Value
$\mathbf{R_{vv}}$	O	$\begin{bmatrix} 1.0977 & -0.3196 - j0.4124 & 0.2790 + j0.3851 \\ -0.3196 + j0.4124 & 1.0979 & -0.5793 + j0.0560 \\ 0.2790 - j0.3851 & -0.5793 - j0.0560 & 1.0976 \end{bmatrix} \times 10^{-24}$
	P	$\begin{bmatrix} 1.0657 & -0.3195 - j0.4136 & 0.2966 + j0.3853 \\ -0.3195 + j0.4136 & 1.0657 & -0.5674 + j0.0552 \\ 0.2966 - j0.3853 & -0.5674 - j0.0552 & 1.0657 \end{bmatrix} \times 10^{-24}$
$E[\mathbf{p}]$	O	$\begin{bmatrix} 5.0306 - j2.3105 & -1.0944 + j5.8204 & 1.4021 - j5.5918 \end{bmatrix} \times 10^{-1}$
	P	$\begin{bmatrix} 5.1722 - j2.5654 & -1.0266 + j5.6815 & 1.6048 - j5.5460 \end{bmatrix} \times 10^{-1}$
$\mathbf{C_{pp}}$	O	$\begin{bmatrix} 4.1231 & 0.7845 + j1.5874 & -1.7035 - j1.5161 \\ 0.7845 - j1.5874 & 2.8858 & 1.2157 + j0.1958 \\ -1.7035 + j1.5161 & 1.2157 - j0.1958 & 3.4460 \end{bmatrix} \times 10^{-3}$
	P	$\begin{bmatrix} 3.7478 & 0.7393 + j1.4706 & -1.4617 - j1.3458 \\ 0.7393 - j1.4706 & 2.7390 & 1.2389 + j0.1688 \\ -1.4617 + j1.3458 & 1.2389 - j0.1688 & 3.1582 \end{bmatrix} \times 10^{-3}$
$\hat{\mathbf{C}}_{\mathbf{pp}}$	O	$\begin{bmatrix} 4.1843 & 0.7523 + j1.5994 & -1.6450 - j1.5399 \\ 0.7523 - j1.5994 & 2.8348 & 1.2571 + j0.2236 \\ -1.6450 + j1.5399 & 1.2571 - j0.2236 & 3.4172 \end{bmatrix} \times 10^{-3}$
	P	$\begin{bmatrix} 3.6514 & 0.7764 + j1.4618 & -1.5454 - j1.3169 \\ 0.7764 - j1.4618 & 2.8053 & 1.1883 + j0.1276 \\ -1.5454 + j1.3169 & 1.1883 - j0.1276 & 3.1840 \end{bmatrix} \times 10^{-3}$

Table 5.4: Sample observed and predicted feedback correlation beamforming statistics with 3 antenna elements and 40 users ($\psi = 1.0$) (uncorrelated fading)

Quantity	O/P	Value
$E[\mathbf{w}]$	O	$\begin{bmatrix} 3.1142 - j1.5559 & -0.6010 + j3.4292 & 0.9505 - j3.3498 \end{bmatrix} \times 10^{-9}$
	P	$\begin{bmatrix} 3.1181 - j1.5466 & -0.6189 + j3.4252 & 0.9675 - j3.3435 \end{bmatrix} \times 10^{-9}$
$E[\mathbf{q}]$	O	$\begin{bmatrix} 5.1401 - j2.5688 & -0.9916 + j5.6590 & 1.5699 - j5.5280 \end{bmatrix} \times 10^{-1}$
	P	$\begin{bmatrix} 5.1722 - j2.5654 & -1.0266 + j5.6815 & 1.6048 - j5.5460 \end{bmatrix} \times 10^{-1}$
$\mathrm{C}_{\mathbf{ww}}$	O	$\begin{bmatrix} 1.3913 & -0.0056 + j0.0289 & -0.1798 - j0.0200 \\ -0.0056 - j0.0289 & 1.3660 & -0.1340 - j0.0011 \\ -0.1798 + j0.0200 & -0.1340 + j0.0011 & 1.3972 \end{bmatrix} \times 10^{-19}$
	P	$\begin{bmatrix} 1.3732 & -0.0178 + j0.0256 & -0.1796 - j0.0070 \\ -0.0178 - j0.0256 & 1.3732 & -0.1357 + j0.0036 \\ -0.1796 + j0.0070 & -0.1357 - j0.0036 & 1.3732 \end{bmatrix} \times 10^{-19}$
$\mathrm{C}_{\mathbf{qq}}$	O	$\begin{bmatrix} 3.3346 & -1.9601 - j2.6483 & 2.2189 + j2.4327 \\ -1.9601 + j2.6483 & 3.3312 & -3.2810 + j0.3404 \\ 2.2189 - j2.4327 & -3.2810 - j0.3404 & 3.3342 \end{bmatrix} \times 10^{-3}$
	P	$\begin{bmatrix} 3.7785 & -0.0491 + j0.0703 & -0.4943 - j0.0191 \\ -0.0491 - j0.0703 & 3.7785 & -0.3733 + j0.0100 \\ -0.4943 + j0.0191 & -0.3733 - j0.0100 & 3.7785 \end{bmatrix} \times 10^{-3}$
$\hat{\mathrm{C}}_{\mathbf{qq}}$	O	$\begin{bmatrix} 2.7931 & 0.6673 + j1.0946 & -1.1071 - j1.0424 \\ 0.6673 - j1.0946 & 2.2862 & 1.0153 + j0.0099 \\ -1.1071 + j1.0424 & 1.0153 - j0.0099 & 2.5248 \end{bmatrix} \times 10^{-3}$
	P	$\begin{bmatrix} 2.7685 & 0.6538 + j1.1055 & -1.1072 - j1.0080 \\ 0.6538 - j1.1055 & 2.2882 & 1.0194 + j0.0302 \\ -1.1072 + j1.0080 & 1.0194 - j0.0302 & 2.5022 \end{bmatrix} \times 10^{-3}$
CRLB	P	$\begin{bmatrix} 2.7498 & 0.6390 + j1.1055 & -1.1093 - j0.9927 \\ 0.6390 - j1.1055 & 2.2765 & 1.0178 + j0.0423 \\ -1.1093 + j0.9927 & 1.0178 - j0.0423 & 2.4894 \end{bmatrix} \times 10^{-3}$

Table 5.4: (continued)

Quantity	O/P	Value
$\mathbf{R_{vv}}$	O	$\begin{bmatrix} 1.2417 & -0.4040 - j0.5266 & 0.3766 + j0.4886 \\ -0.4040 + j0.5266 & 1.2374 & -0.7191 + j0.0710 \\ 0.3766 - j0.4886 & -0.7191 - j0.0710 & 1.2372 \end{bmatrix} \times 10^{-24}$
	P	$\begin{bmatrix} 1.2417 & -0.4068 - j0.5267 & 0.3776 + j0.4905 \\ -0.4068 + j0.5267 & 1.2417 & -0.7225 + j0.0703 \\ 0.3776 - j0.4905 & -0.7225 - j0.0703 & 1.2417 \end{bmatrix} \times 10^{-24}$
$E[\mathbf{p}]$	O	$\begin{bmatrix} 5.0524 - j2.3686 & -1.0745 + j5.7652 & 1.4457 - j5.5549 \end{bmatrix} \times 10^{-1}$
	P	$\begin{bmatrix} 5.1722 - j2.5654 & -1.0266 + j5.6815 & 1.6048 - j5.5460 \end{bmatrix} \times 10^{-1}$
$\mathbf{C_{pp}}$	O	$\begin{bmatrix} 5.9246 & 1.1309 + j2.3396 & -2.4881 - j2.1165 \\ 1.1309 - j2.3396 & 4.2985 & 1.8134 + j0.3043 \\ -2.4881 + j2.1165 & 1.8134 - j0.3043 & 5.0090 \end{bmatrix} \times 10^{-3}$
	P	$\begin{bmatrix} 6.0617 & 1.1417 + j2.3787 & -2.4192 - j2.1727 \\ 1.1417 - j2.3787 & 4.2947 & 1.8991 + j0.3228 \\ -2.4192 + j2.1727 & 1.8991 - j0.3228 & 5.0290 \end{bmatrix} \times 10^{-3}$
$\hat{\mathbf{C}}_{\mathbf{pp}}$	O	$\begin{bmatrix} 5.9833 & 1.1026 + j2.3613 & -2.4227 - j2.1475 \\ 1.1026 - j2.3613 & 4.2313 & 1.8616 + j0.3380 \\ -2.4227 + j2.1475 & 1.8616 - j0.3380 & 4.9838 \end{bmatrix} \times 10^{-3}$
	P	$\begin{bmatrix} 5.9072 & 1.2038 + j2.3645 & -2.5521 - j2.1255 \\ 1.2038 - j2.3645 & 4.3979 & 1.8183 + j0.2591 \\ -2.5521 + j2.1255 & 1.8183 - j0.2591 & 5.0735 \end{bmatrix} \times 10^{-3}$

Table 5.5: Sample observed and predicted feedback correlation beamforming statistics with 3 antenna elements and 40 users ($\psi = 1.0$) (half frame length)

Quantity	O/P	Value
$E[\mathbf{w}]$	O	$\begin{bmatrix} 3.5134 - j1.7607 & -0.6835 + j3.8635 & 1.0763 - j3.7677 \end{bmatrix} \times 10^{-9}$
	P	$\begin{bmatrix} 3.5184 - j1.7451 & -0.6984 + j3.8649 & 1.0917 - j3.7727 \end{bmatrix} \times 10^{-9}$
$E[\mathbf{q}]$	O	$\begin{bmatrix} 5.1325 - j2.5731 & -0.9980 + j5.6415 & 1.5733 - j5.5022 \end{bmatrix} \times 10^{-1}$
	P	$\begin{bmatrix} 5.1722 - j2.5654 & -1.0266 + j5.6815 & 1.6048 - j5.5460 \end{bmatrix} \times 10^{-1}$
$\mathrm{C}_{\mathbf{ww}}$	O	$\begin{bmatrix} 2.7448 & -0.0059 + j0.0640 & -0.3719 - j0.0497 \\ -0.0059 - j0.0640 & 2.6917 & -0.2417 + j0.0280 \\ -0.3719 + j0.0497 & -0.2417 - j0.0280 & 2.7291 \end{bmatrix} \times 10^{-19}$
	P	$\begin{bmatrix} 2.7465 & -0.0357 + j0.0511 & -0.3593 - j0.0139 \\ -0.0357 - j0.0511 & 2.7465 & -0.2713 + j0.0073 \\ -0.3593 + j0.0139 & -0.2713 - j0.0073 & 2.7465 \end{bmatrix} \times 10^{-19}$
$\mathrm{C}_{\mathbf{qq}}$	O	$\begin{bmatrix} 5.1071 & 0.4931 + j0.8984 & -1.2729 - j0.8360 \\ 0.4931 - j0.8984 & 4.6686 & 0.5099 + j0.0465 \\ -1.2729 + j0.8360 & 0.5099 - j0.0465 & 4.8753 \end{bmatrix} \times 10^{-3}$
	P	$\begin{bmatrix} 5.9352 & -0.0771 + j0.1104 & -0.7764 - j0.0301 \\ -0.07712 - j0.1104 & 5.9352 & -0.5864 + j0.0157 \\ -0.7764 + j0.0301 & -0.5864 - j0.0157 & 5.9352 \end{bmatrix} \times 10^{-3}$
$\hat{\mathrm{C}}_{\mathbf{qq}}$	O	$\begin{bmatrix} 4.3186 & 1.0178 + j1.7082 & -1.7417 - j1.5943 \\ 1.0178 - j1.7082 & 3.5321 & 1.5643 + j0.0428 \\ -1.7417 + j1.5943 & 1.5643 - j0.0428 & 3.9133 \end{bmatrix} \times 10^{-3}$
	P	$\begin{bmatrix} 4.3488 & 1.0270 + j1.7365 & -1.7392 - j1.5834 \\ 1.0270 - j1.7365 & 3.5943 & 1.6013 + j0.0475 \\ -1.7392 + j1.5834 & 1.6013 - j0.0475 & 3.9304 \end{bmatrix} \times 10^{-3}$
CRLB	P	$\begin{bmatrix} 4.3193 & 1.0037 + j1.7365 & -1.7424 - j1.5593 \\ 1.0037 - j1.7365 & 3.5759 & 1.5987 + j0.0665 \\ -1.7424 + j1.5593 & 1.5987 - j0.0665 & 3.9103 \end{bmatrix} \times 10^{-3}$

Table 5.5: (continued)

Quantity	O/P	Value
$\mathbf{R_{vv}}$	O	$\begin{bmatrix} 1.2405 & -0.4053 - j0.5266 & 0.3767 + j0.4893 \\ -0.4053 + j0.5266 & 1.2410 & -0.7216 + j0.0711 \\ 0.3767 - j0.4893 & -0.7216 - j0.0711 & 1.2397 \end{bmatrix} \times 10^{-25}$
	P	$\begin{bmatrix} 1.2417 & -0.4068 - j0.5267 & 0.3776 + j0.4905 \\ -0.4068 + j0.5267 & 1.2417 & -0.7225 + j0.0703 \\ 0.3776 - j0.4905 & -0.7225 - j0.0703 & 1.2417 \end{bmatrix} \times 10^{-24}$
$E[\mathbf{p}]$	O	$\begin{bmatrix} 5.0685 - j2.3765 & -1.0858 + j5.8071 & 1.4526 - j5.5918 \end{bmatrix} \times 10^{-1}$
	P	$\begin{bmatrix} 5.1722 - j2.5654 & -1.0266 + j5.6815 & 1.6048 - j5.5460 \end{bmatrix} \times 10^{-1}$
$\mathbf{C_{pp}}$	O	$\begin{bmatrix} 1.4915 & 0.2983 + j0.5878 & -0.6141 - j0.5388 \\ 0.2983 - j0.5878 & 1.0840 & 0.4597 + j0.0644 \\ -0.6141 + j0.5388 & 0.4597 - j0.0644 & 1.2577 \end{bmatrix} \times 10^{-3}$
	P	$\begin{bmatrix} 1.5154 & 0.2854 + j0.5947 & -0.6048 - j0.5432 \\ 0.2854 - j0.5947 & 1.0737 & 0.4748 + j0.0807 \\ -0.6048 + j0.5432 & 0.4748 - j0.0807 & 1.2573 \end{bmatrix} \times 10^{-3}$
$\hat{\mathbf{C}}_{\mathbf{pp}}$	O	$\begin{bmatrix} 1.5104 & 0.2900 + j0.5902 & -0.5969 - j0.5448 \\ 0.2900 - j0.5902 & 1.0691 & 0.4711 + j0.0732 \\ -0.5969 + j0.5448 & 0.4711 - j0.0732 & 1.2509 \end{bmatrix} \times 10^{-3}$
	P	$\begin{bmatrix} 1.4768 & 0.3009 + j0.5911 & -0.6380 - j0.5314 \\ 0.3009 - j0.5911 & 1.0995 & 0.4546 + j0.0648 \\ -0.6380 + j0.5314 & 0.4546 - j0.0648 & 1.2684 \end{bmatrix} \times 10^{-3}$

Table 5.6: Sample observed and predicted feedback correlation beamforming statistics with 3 antenna elements and 40 users ($\psi = 1.0$) (double frame length)

Quantity	O/P	Value
$E[\mathbf{w}]$	O	$\begin{bmatrix} 3.5121 - j1.7590 & -0.6842 + j3.8693 & 1.0771 - j3.7761 \end{bmatrix} \times 10^{-9}$
	P	$\begin{bmatrix} 3.5184 - j1.7451 & -0.6984 + j3.8649 & 1.0917 - j3.7727 \end{bmatrix} \times 10^{-9}$
$E[\mathbf{q}]$	O	$\begin{bmatrix} 5.1529 - j2.5811 & -1.0038 + j5.6763 & 1.5807 - j5.5399 \end{bmatrix} \times 10^{-1}$
	P	$\begin{bmatrix} 5.1722 - j2.5654 & -1.0266 + j5.6815 & 1.6048 - j5.5460 \end{bmatrix} \times 10^{-1}$
$\mathrm{C}_{\mathbf{ww}}$	O	$\begin{bmatrix} 6.8709 & -0.0894 + j0.1486 & -0.8859 - 0.0867 \\ -0.0894 - j0.1486 & 6.8506 & -0.6122 + j0.0643 \\ -0.8859 + j0.0867 & -0.6122 - j0.0643 & 6.8099 \end{bmatrix} \times 10^{-20}$
	P	$\begin{bmatrix} 6.8662 & -0.0892 + j0.1278 & -0.8982 - j0.0348 \\ -0.0892 - j0.1278 & 6.8662 & -0.6783 + j0.0182 \\ -0.8982 + j0.0348 & -0.6783 - j0.0182 & 6.8662 \end{bmatrix} \times 10^{-20}$
$\mathrm{C}_{\mathbf{qq}}$	O	$\begin{bmatrix} 1.2803 & 0.1155 + j0.2368 & -0.3108 - j0.2080 \\ 0.1155 - j0.2368 & 1.1857 & 0.1362 + j0.0125 \\ -0.3108 + j0.2080 & 0.1362 - j0.0125 & 1.2225 \end{bmatrix} \times 10^{-3}$
	P	$\begin{bmatrix} 1.4838 & -0.0193 + j0.0276 & -0.1941 - j0.0075 \\ -0.0193 - j0.0276 & 1.4838 & -0.1466 + j0.0039 \\ -0.1941 + j0.0075 & -0.1466 - j0.0039 & 1.4838 \end{bmatrix} \times 10^{-3}$
$\hat{\mathrm{C}}_{\mathbf{qq}}$	O	$\begin{bmatrix} 1.0833 & 0.2552 + j0.4344 & -0.4339 - j0.3924 \\ 0.2552 - j0.4344 & 0.8988 & 0.4018 + j0.0133 \\ -0.4339 + j0.3924 & 0.4018 - j0.0133 & 0.9812 \end{bmatrix} \times 10^{-3}$
	P	$\begin{bmatrix} 1.0872 & 0.2567 + j0.4341 & -0.4348 - j0.3959 \\ 0.2567 - j0.4341 & 0.8986 & 0.4003 + j0.0119 \\ -0.4348 + j0.3959 & 0.4003 - j0.0119 & 0.9826 \end{bmatrix} \times 10^{-3}$
CRLB	P	$\begin{bmatrix} 1.0798 & 0.2509 + j0.4341 & -0.4356 - j0.3898 \\ 0.2509 - j0.4341 & 0.8940 & 0.3997 + j0.0166 \\ -0.4356 + j0.3898 & 0.3997 - j0.0166 & 0.9776 \end{bmatrix} \times 10^{-3}$

Table 5.6: (continued)

5.6, a double-length frame consisted of 376 data bits and 8 tail bits with 25 frames per second. These two tables relate back to equation (5.27) which indicates that the estimator covariance matrices should become smaller as more samples are used to estimate the beamforming weight vector. This can be seen by comparing the corresponding covariance matrices from Tables 5.2 (normal frame length), 5.5 (half frame length), and 5.6 (double frame length). As can be seen, the covariance matrix entries are doubled in size when a half-length frame is used and halved for double-length frames, which is as expected.

5.9 Summary

This chapter has shown how the code-filtering correlation method of estimating beamforming weights can be applied to the reverse link of IS-95, including the derivation of expressions for the correlation matrices of the correlation vectors. However, the IS-95 coding scheme is such that the accuracy of this technique is extremely limited due to a low PN spreading gain (~ 4). A new algorithm involving feedback correlation of the reencoded data and a much higher processing gain (~ 200) was proposed and shown to outperform code-filtering correlation. The use of the mean correlation vector rather than the principal eigenvector of the correlation matrix as the array response vector estimate provided equally accurate values with less computational cost. An error analysis derived the mean vectors and covariance matrices of the various estimators in terms of known quantities within a simulation environment. This allows the quality of the obtained estimates to be evaluated and the different estimators to be compared with each other. In addition, the derived probability distributions may be used to simulate imperfect beamforming by generating random weight samples without the need for computationally expensive chip-level simulations. An eigenvector perturbation analysis derived the covariance matrices for the eigenvectors and eigenvalues of a Hermitian correlation matrix generated from noisy measurements. An expression for the constrained Cramér-Rao Lower Bound on the covariance matrices of the different estimators was obtained. Finally, simulation results were compared with predicted values to show the close agreement between them. This provides justification for using

the predicted mean vectors and covariance matrices to generate random beamforming coefficient vectors from the derived distributions instead of using chip-level data to obtain these estimates.

Chapter 6

Error Analysis and System Validation

6.1 Introduction

An error analysis of the IS-95 simulator system will now be described. This allows the statistical properties of key correlation quantities to be predicted and compared with the corresponding values from simulations. A reasonable agreement between the predictions and observations tends to support the acceptability of the simulation results and thus the validity of the simulator. In addition, the equations derived here are useful for predicting system performance as shown in the following chapter.

6.2 Statistical Parameters of Correlation Values

Equation (2.35) contains the correlated in-phase signal component for the p^{th} mobile. Neglecting the thermal noise term for the moment, this equation is:

$$\begin{aligned} U_{I_p}[r] \;=\; & \frac{1}{2} C_{I_p}[r] \sum_{k=1}^{N_M} \beta_k w_k(t) \sum_{i=1}^{N_A} \Big\{ C_{I_k}[r] \cos(\phi_{pi} - \alpha_{ki} - 2\pi f_c \tau_{kp})(T_c - \tau_{kp}) \\ & + C_{I_k}[r-1] \cos(\phi_{pi} - \alpha_{ki} - 2\pi f_c \tau_{kp}) \tau_{kp} \\ & + C_{Q_k}[r] \sin(\phi_{pi} - \alpha_{ki} - 2\pi f_c \tau_{kp})(T_c - \tau_{kp}) \\ & + C_{Q_k}[r-1] \sin(\phi_{pi} - \alpha_{ki} - 2\pi f_c \tau_{kp}) \tau_{kp} \Big\} \end{aligned} \tag{6.1}$$

Assume that the τ_{kp} time delay values are uniformly distributed between 0 and T_c and that $\tau_{pp} = 0$. Therefore, the quadrature components of mobile p will disappear since the sin terms will evaluate as zero. Multiplying the other $w_k C_{I_k}$ and $w_k C_{Q_k}$

terms by $C_{I_p}[r]$ will result in binary random variables with the values ± 1 (Y_{I_k} and Y_{Q_k}). Also, $\Phi_{pki} = \phi_{pi} - \alpha_{ki} - 2\pi f_c \tau_{kp}$ can be assumed to be a uniformly distributed random variable in $[0, 2\pi)$. If the in-phase PN chip correlation value is treated as a random variable, it can be written as:

$$\begin{aligned} U_{I_p}[r] &= \frac{1}{2} N_A \beta_p T_c w_p(t) + \frac{1}{2} \sum_{k \neq p} \beta_k \sum_{i=1}^{N_A} \\ &\quad \Big\{ Y_{I_k}[r] \cos(\Phi_{pki})(T_c - \tau_{kp}) + Y_{I_k}[r-1] \cos(\Phi_{pki}) \tau_{kp} \\ &\quad + Y_{Q_k}[r] \sin(\Phi_{pki})(T_c - \tau_{kp}) + Y_{Q_k}[r-1] \sin(\Phi_{pki}) \tau_{kp} \Big\} \end{aligned} \tag{6.2}$$

Let I_p be a random variable equal to the summation term in (6.2) which represents interference from other mobiles and which can be modelled as being Gaussian via the Central Limit Theorem. It is now desirable to determine the mean and variance of this distribution.

Y_{I_k}, Y_{Q_k}, Φ_{pki}, and τ_{pk} can all be assumed to be independent. Although Φ_{pki} is a function of τ_{pk}, the fact that its value also depends on ϕ_{pi} and α_{ki} lessens the dependence on τ_{pk}. Thus, when taking the expected value of I_p, the individual terms in the summation can be factored into the products of the expectations. Since Y_{I_k} and Y_{Q_k} are both zero-mean, the mean of I_p will also be zero.

$$E[I_p] = 0 \tag{6.3}$$

The expected value of I_p^2 (which will equal the variance since I_p is zero-mean) is therefore:

$$\begin{aligned} E\left[I_p^2\right] &= \frac{1}{4} E \Bigg[\Bigg(\sum_{k \neq p} \beta_k \sum_{i=1}^{N_A} \Big\{ Y_{I_k}[r] \cos(\Phi_{pki})(T_c - \tau_{kp}) + Y_{I_k}[r-1] \cos(\Phi_{pki}) \tau_{kp} \\ &\quad + Y_{Q_k}[r] \sin(\Phi_{pki})(T_c - \tau_{kp}) + Y_{Q_k}[r-1] \sin(\Phi_{pki}) \tau_{kp} \Big\} \Bigg) \\ &\quad \Bigg(\sum_{m \neq p} \beta_m \sum_{n=1}^{N_A} \Big\{ Y_{I_m}[r] \cos(\Phi_{pmn})(T_c - \tau_{mp}) + Y_{I_m}[r-1] \cos(\Phi_{pmn}) \tau_{mp} \\ &\quad + Y_{Q_m}[r] \sin(\Phi_{pmn})(T_c - \tau_{mp}) + Y_{Q_m}[r-1] \sin(\Phi_{pmn}) \tau_{mp} \Big\} \Bigg) \Bigg] \\ &= \frac{1}{4} E \Bigg[\sum_{k \neq p} \beta_k \sum_{m \neq p} \beta_m \sum_{i=1}^{N_A} \sum_{n=1}^{N_A} \\ &\quad \Big\{ Y_{I_k}[r] \cos(\Phi_{pki})(T_c - \tau_{kp}) + Y_{I_k}[r-1] \cos(\Phi_{pki}) \tau_{kp} \end{aligned} \tag{6.4}$$

$$+ Y_{Q_k}[r]\sin(\Phi_{pki})(T_c - \tau_{kp}) + Y_{Q_k}[r-1]\sin(\Phi_{pki})\tau_{kp}\Big\}$$
$$\Big\{Y_{I_m}[r]\cos(\Phi_{pmn})(T_c - \tau_{mp}) + Y_{I_m}[r-1]\cos(\Phi_{pmn})\tau_{mp}$$
$$+ Y_{Q_m}[r]\sin(\Phi_{pmn})(T_c - \tau_{mp}) + Y_{Q_m}[r-1]\sin(\Phi_{pmn})\tau_{mp}\Big\}\Bigg]$$

The cos and sin terms are all zero-mean. Since Φ_{pki} and Φ_{pmn} are assumed to be independent unless $k = m$ and $i = n$, all of the expectations in (6.4) with $k \neq m$ and/or $i \neq n$ can be factored and will consequently evaluate as zero. Thus, (6.4) can be immediately simplified to:

$$E\left[I_p^2\right] = \frac{1}{4}E\left[\sum_{k\neq p}\beta_k^2\sum_{i=1}^{N_A}\Big\{Y_{I_k}[r]\cos(\Phi_{pki})(T_c - \tau_{kp}) + Y_{I_k}[r-1]\cos(\Phi_{pki})\tau_{kp}\right. \quad (6.5)$$
$$\left. + Y_{Q_k}[r]\sin(\Phi_{pki})(T_c - \tau_{kp}) + Y_{Q_k}[r-1]\sin(\Phi_{pki})\tau_{kp}\Big\}^2\right]$$

Similarly, $Y_{I_k}[r]$, $Y_{I_k}[r-1]$, $Y_{Q_k}[r]$, and $Y_{Q_k}[r-1]$ are all independent zero-mean random variables, so product terms in (6.5) which do not include a squared random variable can be factored and will have an expected value of zero. Therefore, (6.5) can be further reduced to:

$$E\left[I_p^2\right] = \frac{1}{4}E\left[\sum_{k\neq p}\beta_k^2\sum_{i=1}^{N_A}\Big(\{Y_{I_k}[r]\cos(\Phi_{pki})(T_c - \tau_{kp})\}^2\right.$$
$$+ \{Y_{I_k}[r-1]\cos(\Phi_{pki})\tau_{kp}\}^2 \quad (6.6)$$
$$+ \{Y_{Q_k}[r]\sin(\Phi_{pki})(T_c - \tau_{kp})\}^2$$
$$\left. + \{Y_{Q_k}[r-1]\sin(\Phi_{pki})\tau_{kp}\}^2\Big)\right]$$

The expected values of $(Y_{I_k}[r])^2$, $(Y_{I_k}[r-1])^2$, $(Y_{Q_k}[r])^2$, and $(Y_{Q_k}[r-1])^2$ will all be $+1$. Thus:

$$E\left[I_p^2\right] = \frac{1}{4}E\left[\sum_{k\neq p}\beta_k^2\sum_{i=1}^{N_A}\Big(\{\cos(\Phi_{pki})(T_c - \tau_{kp})\}^2 + \{\cos(\Phi_{pki})\tau_{kp}\}^2\right. \quad (6.7)$$
$$\left. + \{\sin(\Phi_{pki})(T_c - \tau_{kp})\}^2 + \{\sin(\Phi_{pki})\tau_{kp}\}^2\Big)\right]$$
$$= \frac{1}{4}N_A E\left[\sum_{k\neq p}\beta_k^2\left\{(T_c - \tau_{kp})^2 + \tau_{kp}^2\right\}\right] \quad (6.8)$$

β_k and τ_{kp} are the only two remaining random variables. Since they are independent, the expected value can be factored and evaluated as follows:

$$E\left[I_p^2\right] = \frac{1}{4}N_A\sum_{k\neq p}E\left[\beta_k^2\right]\left\{T_c^2 - 2T_cE\left[\tau_{kp}\right] + 2E\left[\tau_{kp}^2\right]\right\} \quad (6.9)$$

where τ_{kp} has a uniform distribution between 0 and T_c. Therefore, its first two moments are:

$$E\left[\tau_{kp}\right] = \frac{1}{2}T_c \tag{6.10}$$

$$E\left[\tau_{kp}^2\right] = \frac{1}{3}T_c^2 \tag{6.11}$$

Substituting (6.10) and (6.11) into (6.9) yields:

$$E\left[I_p^2\right] = \frac{1}{6}N_A T_c^2 \sum_{k \neq p} E\left[\beta_k^2\right] \tag{6.12}$$

The power received from the k^{th} mobile is given by $N_A\beta_k^2/2$. Let P represent the power received from a mobile with active speech. Assuming perfect power control and the voice activity situation described in Section 3.3.3, the expected value of β_k^2 will be:

$$E\left[\beta_k^2\right] = \frac{2}{N_A}E\left[\psi P + (1-\psi)\frac{P}{\nu}\right] = \frac{2}{N_A}\left(\frac{(\nu-1)\psi+1}{\nu}\right)E\left[P\right] \tag{6.13}$$

where ψ is the voice activity factor and ν is the factor by which a mobile's transmission power is reduced when speech is not active.

Substituting (6.13) into (6.12) and eliminating the summation produces:

$$E\left[I_p^2\right] = \frac{(N_M-1)T_c^2\{(\nu-1)\psi+1\}E\left[P\right]}{3\nu} \tag{6.14}$$

The calculation of $E\left[P\right]$ is shown in Sections 6.3 and 6.4 for single and multiple antenna elements, respectively.

Therefore, $U_{I_p}[r]$ will have a Gaussian distribution with the following parameters.

$$\mu_c = \frac{1}{2}N_A w_k(t) T_c E[R]\sqrt{\frac{2E[P]}{E[R^2]}} = \frac{\sqrt{2\pi}}{4}N_A w_k(t) T_c \sqrt{E[P]} \tag{6.15}$$

$$\sigma_c^2 = \frac{(N_M-1)T_c^2\{(\nu-1)\psi+1\}E[P]}{3\nu} + \frac{1}{2}N_A T_c \sigma_n^2 \tag{6.16}$$

$E[R] = \sqrt{\pi/2}$ and $E[R^2] = 2$ are included in (6.15) to account for Rayleigh fading, and the second term in (6.16) is due to thermal noise as obtained from Section 2.5.2.1. Similarly, $U_{Q_p}[r]$ should have the same Gaussian distribution.

Based on the above, the sum of the $N_W = 4$ in-phase and quadrature PN chip correlations over one Walsh chip will be a Gaussian random variable with the following parameters.

$$\mu_w = 2N_W\mu_c \tag{6.17}$$

$$\sigma_w^2 = 2N_W\sigma_c^2 \tag{6.18}$$

Correlating with the Walsh functions over $N_F = 64$ Walsh chips will also produce a Gaussian random variable due to linearity. If the signal is correlated with the correct Walsh function chip sequence (*i.e.* the one which was actually transmitted), the mean should be:

$$\mu_F = N_F\mu_w = 2N_FN_W\mu_c \tag{6.19}$$

If the signal is correlated with any of the other Walsh function chip sequences which do not match the transmitted sequence and are therefore incorrect, the result will be zero-mean since the Walsh function chip sequences are all mutually orthogonal.

$$\mu_{\overline{F}} = 0 \tag{6.20}$$

In both of these cases, the variance of the Walsh function correlation values will be the same.

$$\sigma_F^2 = N_F\sigma_w^2 = 2N_FN_W\sigma_c^2 \tag{6.21}$$

As a result, equations (6.15) through (6.21) specify the expected statistical parameters of correlation quantities which are generated during the decoding process.

6.3 Single Element Power Value Calculation

If P is the power level received from a mobile with active speech and perfect power control is being used so that the same power is received from each user, then the interference power seen by that mobile will be:

$$\begin{aligned} I &= N_IP + (N_M - N_I - 1)\frac{P}{\nu} \\ &= \left(N_I + \frac{N_M - N_I - 1}{\nu}\right)P \end{aligned} \tag{6.22}$$

where N_I is the number of interfering mobiles with active speech.

Using these two power values, the E_b/N_0 ratio is defined as:

$$\frac{E_b}{N_0} = \frac{P/R_B}{I/B + \sigma_n^2} \tag{6.23}$$

Substituting (6.22) into (6.23) and solving for P yields:

$$P = \left(\frac{E_b}{N_0}\right)\sigma_n^2\left\{\frac{1}{R_B} - \frac{1}{B}\left(\frac{E_b}{N_0}\right)\left(N_I + \frac{N_M - N_I - 1}{\nu}\right)\right\}^{-1} \tag{6.24}$$

For the case of $\psi = 1.0$, $N_I = N_M - 1$ and the expectation of both sides of (6.24) can be taken directly.

$$E[P] = \left(\frac{E_b}{N_0}\right)\sigma_n^2\left\{\frac{1}{R_B} - \frac{N_M - 1}{B}\left(\frac{E_b}{N_0}\right)\right\}^{-1} \tag{6.25}$$

When the voice activity factor is less than 1, the number of interferers with active speech becomes a random variable and the expectation of (6.24) must be taken as a weighted sum.

$$E[P] = \left(\frac{E_b}{N_0}\right)\sigma_n^2\sum_{n_I=0}^{N_M-1}\left\{\frac{1}{R_B} - \frac{1}{B}\left(\frac{E_b}{N_0}\right)\left(n_I + \frac{N_M - n_I - 1}{\nu}\right)\right\}^{-1} P(N_I = n_I) \tag{6.26}$$

The probability term in the above equation is governed by a binomial distribution.

$$P(N_I = n_I) = \left(\begin{array}{c} N_M - 1 \\ n_I \end{array}\right)\psi^{n_I}(1-\psi)^{N_M - 1 - n_I} \tag{6.27}$$

For reasonable values of N_M (*e.g.* $N_M > 20$) and a voice activity factor of $\psi = 0.5$, this can be well-approximated by a Gaussian random variable with the following parameters [42, pp. 245].

$$\mu = (N_M - 1)\psi \tag{6.28}$$

$$\sigma^2 = (N_M - 1)\psi(1-\psi) \tag{6.29}$$

Thus, the probability expression of (6.27) may be approximated as:

$$P(N_I = n_I) \approx \frac{1}{2}\left\{\mathrm{erf}\left(\frac{(n_I + 0.5) - \mu}{\sqrt{2}\sigma}\right) - \mathrm{erf}\left(\frac{(n_I - 0.5) - \mu}{\sqrt{2}\sigma}\right)\right\} \tag{6.30}$$

Depending upon the voice/transmission activity factor, either equation (6.25) or (6.26) can now be used in (6.15) and (6.16) to determine μ_c and σ_c^2.

Finally, for $\psi = 1$, the expected interference power can be obtained from (6.25).

$$E[I] = (N_M - 1)\left(\frac{E_b}{N_0}\right)\sigma_n^2\left\{\frac{1}{R_B} - \frac{N_M - 1}{B}\left(\frac{E_b}{N_0}\right)\right\}^{-1} \tag{6.31}$$

For a non-unity voice activity factor, equations (6.22) and (6.26) can be combined to yield:

$$E[I] = \left(\frac{E_b}{N_0}\right)\sigma_n^2\sum_{n_I=0}^{N_M-1}\left\{\frac{1}{R_B} - \frac{1}{B}\left(\frac{E_b}{N_0}\right)\left(n_I + \frac{N_M - n_I - 1}{\nu}\right)\right\}^{-1} \left(n_I + \frac{N_M - n_I - 1}{\nu}\right)P(N_I = n_I) \tag{6.32}$$

Consequently, it is also possible to predict the expected received interference power from known quantities.

6.4 Multi-Element Power Value Calculation

The results from Section 6.3 may now be generalized to cover the case of base station antenna arrays. Consider the sums of sin and cos from (3.5).

$$S_{pk} = \sum_{i=1}^{N_A}\sin(\phi_{pi} - \alpha_{ki} - 2\pi f_c\tau_{kp}) = \sum_{i=1}^{N_A}\sin(\Phi_{pki}) \tag{6.33}$$

$$C_{pk} = \sum_{i=1}^{N_A}\cos(\phi_{pi} - \alpha_{ki} - 2\pi f_c\tau_{kp}) = \sum_{i=1}^{N_A}\cos(\Phi_{pki}) \tag{6.34}$$

where the phase angles of the sin and cos expressions are assumed to be uniformly distributed random variables in the interval $[0, 2\pi)$. By the Central Limit Theorem, both S_{pk} and C_{pk} can be approximated by a Gaussian distribution. From simulations, it has been verified that a close to Gaussian approximation is obtained even when N_A is as small as 4 or 5.

Since sin and cos are zero-mean, S_{pk} and C_{pk} will also both be zero-mean.

$$\mu_S = \mu_C = 0 \tag{6.35}$$

The variances of $\sin(\Phi)$ and $\cos(\Phi)$, where Φ has a uniform distribution, are:

$$\begin{aligned}\mathrm{var}[\sin(\Phi)] = \mathrm{var}[\cos(\Phi)] &= \int_0^{2\pi}\frac{1}{2\pi}\{\cos(\Phi)\}^2\,d\Phi \\ &= \frac{1}{2\pi}(\pi) = \frac{1}{2}\end{aligned} \tag{6.36}$$

Thus, the variances of S_{pk} and C_{pk} are:

$$\sigma_S^2 \;=\; \sigma_C^2 \;=\; N_A \times \mathrm{var}\left[\sin(\Phi)\right] \;=\; \frac{1}{2}N_A \tag{6.37}$$

Combining equations (3.5), (6.33), and (6.34) yields:

$$\Upsilon_{pk} \;=\; \frac{1}{2}\left(S_{pk}^2 + C_{pk}^2\right) \tag{6.38}$$

Since both S_{pk} and C_{pk} can be approximated by the same Gaussian distribution, Υ_{pk} will have a central χ^2 distribution with two degrees of freedom and parameters [84, pp. 26]:

$$\mu_\Upsilon \;=\; 2\left(\frac{1}{2}\sigma_S^2\right) \;=\; \frac{1}{2}N_A \tag{6.39}$$

$$\sigma_\Upsilon^2 \;=\; 4\left(\frac{1}{2}\sigma_S^2\right)^2 \;=\; \frac{1}{4}\left(N_A\right)^2 \tag{6.40}$$

Now consider the interference power expression given in equation (3.7).

$$P_{I_p} \;=\; \sum_{k\neq p}\Upsilon_{pk}\beta_k^2 \;=\; \beta^2\sum_{k\neq p}\Upsilon_{pk} \tag{6.41}$$

It has been assumed that β_k^2 is a constant over all k due to perfect power control. Since β_k will actually be a random variable in the multiple antenna situation, this is not a completely valid assumption as will be illustrated shortly, but is required in order to make the analysis tractable.

Let V be the summation in (6.41) of $N_M - 1$ independent χ^2 random variables which can be approximated as Gaussian via the Central Limit Theorem. Equation (6.41) actually assumes a voice activity factor of $\psi = 1.0$, but can easily be generalized by assuming that there are N_I mobiles with active speech. Thus, the parameters of the Gaussian random variable will be:

$$\mu_V \;=\; \left(N_I + \frac{N_M - 1 - N_I}{\nu}\right)\mu_\Upsilon \;=\; \frac{1}{2}\left(N_I + \frac{N_M - 1 - N_I}{\nu}\right)N_A \tag{6.42}$$

$$\sigma_V^2 \;=\; \left(N_I + \frac{N_M - 1 - N_I}{\nu^2}\right)\sigma_\Upsilon^2 \;=\; \frac{1}{4}\left(N_I + \frac{N_M - 1 - N_I}{\nu^2}\right)\left(N_A\right)^2 \tag{6.43}$$

Consequently, equation (6.41) can be approximated as:

$$P_{I_p} \;\approx\; \beta^2 V \tag{6.44}$$

If perfect beamforming is assumed, then $\phi_{pi} = \alpha_{pi}$ in (6.33) and (6.34) and the received power from the desired mobile will be:

$$P_{M_p} = \frac{1}{2}(N_A)^2 \beta^2 \tag{6.45}$$

Now consider finding the required received power levels for the desired E_b/N_0 ratio.

$$\frac{E_b}{N_0} = \frac{P_{M_p}/R_B}{P_{I_p}/B + N_A\sigma_n^2} \tag{6.46}$$

Note that background noise is received at each antenna element, which accounts for the $N_A\sigma_n^2$ term in the denominator of the above expression. Substituting for P_{M_p} and P_{I_p} from (6.45) and (6.44), respectively, and solving for β^2 yields:

$$\beta^2 = \left(\frac{E_b}{N_0}\right) N_A\sigma_n^2 \left\{ \frac{(N_A)^2}{2R_B} - \frac{1}{B}\left(\frac{E_b}{N_0}\right) V \right\}^{-1} \tag{6.47}$$

Substituting (6.47) into (6.45) produces:

$$P = \frac{1}{2}(N_A)^3 \left(\frac{E_b}{N_0}\right) \sigma_n^2 \left\{ \frac{(N_A)^2}{2R_B} - \frac{1}{B}\left(\frac{E_b}{N_0}\right) V \right\}^{-1} \tag{6.48}$$

If the transmission activity factor is 1, then $N_I = N_M - 1$ and the expectation of (6.48) can be taken directly.

$$E[P] = \frac{1}{2}(N_A)^3 \left(\frac{E_b}{N_0}\right) \sigma_n^2 E\left[\left\{ \frac{(N_A)^2}{2R_B} - \frac{1}{B}\left(\frac{E_b}{N_0}\right) V \right\}^{-1} \right] \tag{6.49}$$

Alternatively, for a non-unity voice activity factor, the expected received power must be calculated as a weighted sum.

$$E[P] = \frac{1}{2}(N_A)^3 \left(\frac{E_b}{N_0}\right) \sigma_n^2 \sum_{N_I=0}^{N_M-1} P(N_I = n_I) E\left[\left\{ \frac{(N_A)^2}{2R_B} - \frac{1}{B}\left(\frac{E_b}{N_0}\right) V \right\}^{-1} \right] \tag{6.50}$$

$P(N_I = n_I)$ may be calculated as shown in (6.30). Recall also that V is a function of N_I.

As a consistency check, it can easily be seen that if N_A is set to 1 and V is set equal to μ_V (since σ_V^2 will be zero for the case of one antenna element and perfect power control), equations (6.48) and (6.50) reduce to (6.25) and (6.26), respectively, which is as expected.

Since the random variable V is in the denominator of a fraction together with other terms, the expressions in (6.48) and (6.50) cannot be simplified further. However, the probability distribution of V is known, so the desired expected value can be found via numerical integration.

Equation (6.44) implies that P_{I_p} will be Gaussian since V can be approximated by a Gaussian distribution. However, the assumption that β was equal for all mobiles in the multi-element scenario is incorrect. For a single antenna element with perfect power control, all of the mobiles will have the same received power at the base station. When an antenna array is used, the interference will be slightly different for each user, so the corresponding received powers from each mobile will also vary, even though all of the users have the same E_b/N_0 ratio.

To illustrate this point, Figures 6.1 and 6.2 show frequency histograms of the interference power (P_{I_p}) from simulations for 50 mobiles and 3 and 7 antenna elements, respectively. The distribution tails are definitely stretched out more on the right than on the left, and thus a Gaussian distribution does not provide a completely accurate model of the true situation, although it is a suitable first approximation.

6.5 System Validation Results

Tables 6.1 through 6.5 compare observed and predicted values (based on the derivations in Sections 6.2, 6.3, and 6.4) for the correlation quantities prior to Viterbi decoding. Note that correct Viterbi decoder operation is easily verified separately as discussed in Chapter 4. These values were generated over 100 frames, with 20 mobiles and 1 antenna element (Tables 6.1 and 6.2), 30 mobiles and 3 elements (Table 6.3), 30 mobiles and 5 elements, (Table 6.4), and 40 mobiles and 5 elements (Table 6.5). As can be seen from Tables 6.1 and 6.2 for a single antenna element, there is generally excellent agreement between the two columns which supports the validity of the simulation program implementation. The observed and predicted values in Tables 6.3 through 6.5 are for multiple element antenna arrays and agree to a lesser extent due to the reasons discussed at the end of Section 6.4. However, they are still useful for system analysis and verification purposes.

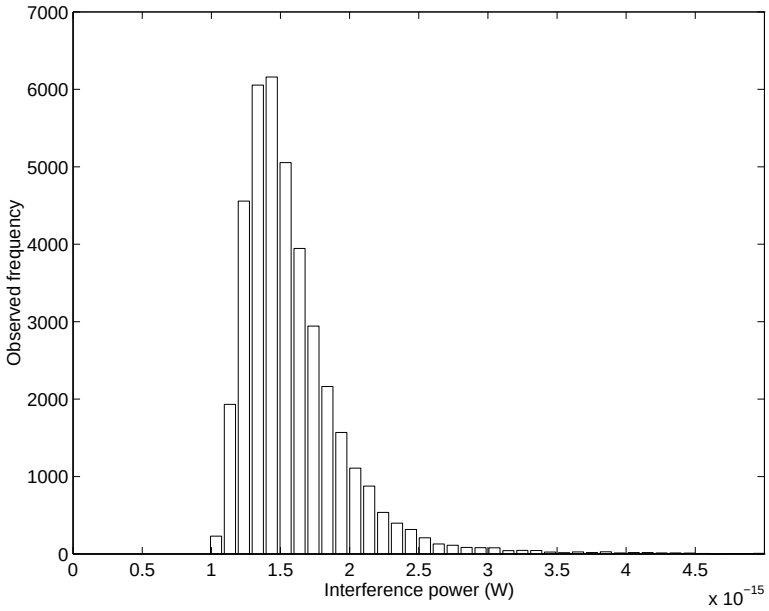

Figure 6.1: Interference power distribution for 3 antenna elements and 50 mobiles

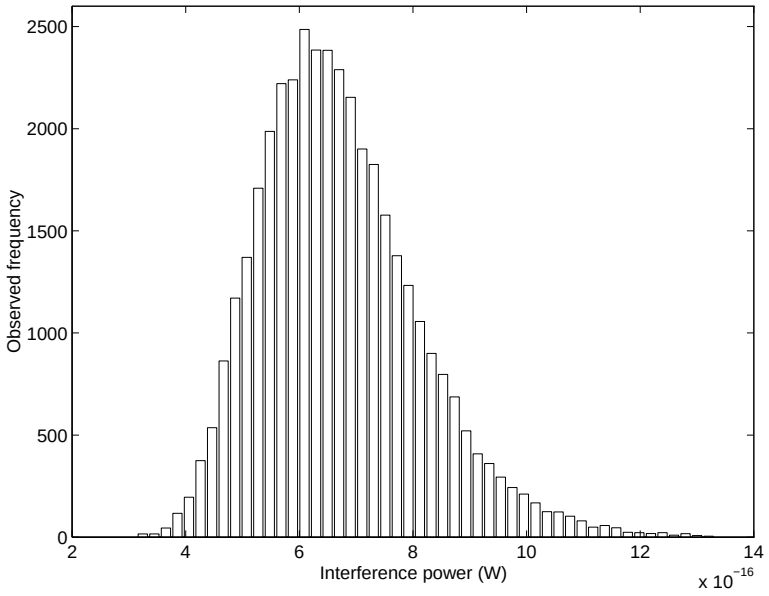

Figure 6.2: Interference power distribution for 7 antenna elements and 50 mobiles

Quantity	Observed Value	Predicted Value	Ref. Eqn.
Mean mobile power	3.8041×10^{-16}	3.8051×10^{-16}	(6.25)
Mean interference power	7.2275×10^{-15}	7.2298×10^{-15}	(6.31)
Mean interference and noise	9.7158×10^{-15}	9.7181×10^{-15}	
Mean PN chip correlation	9.9442×10^{-15}	9.9480×10^{-15}	(6.15)
Variance PN chip correlation	2.4510×10^{-27}	2.4200×10^{-27}	(6.16)
Mean Walsh chip correlation	7.9554×10^{-14}	7.9584×10^{-14}	(6.17)
Variance Walsh chip correlation	2.1124×10^{-26}	1.9360×10^{-26}	(6.18)
Mean Walsh func. corr. (correct)	5.0914×10^{-12}	5.0934×10^{-12}	(6.19)
Mean Walsh func. corr. (incorr.)	7.8604×10^{-17}	0.0000	(6.20)
Variance Walsh func. correlation	1.3467×10^{-24}	1.2390×10^{-24}	(6.21)

Table 6.1: Observed and predicted statistical parameters of correlation values for 1 antenna element, 20 mobiles, and $\psi = 1.0$

Quantity	Observed Value	Predicted Value	Ref. Eqn.
Mean mobile power	1.7013×10^{-16}	1.7051×10^{-16}	(6.26)
Mean interference power	1.8566×10^{-15}	1.8663×10^{-15}	(6.32)
Mean interference and noise	4.3450×10^{-15}	4.3547×10^{-15}	
Mean PN chip correlation	6.6386×10^{-15}	6.6592×10^{-15}	(6.15)
Variance PN chip correlation	1.2478×10^{-27}	1.2263×10^{-27}	(6.16)
Mean Walsh chip correlation	5.3109×10^{-14}	5.3273×10^{-14}	(6.17)
Variance Walsh chip correlation	1.0669×10^{-26}	9.8101×10^{-27}	(6.18)
Mean Walsh func. corr. (correct)	3.3990×10^{-12}	3.4095×10^{-12}	(6.19)
Mean Walsh func. corr. (incorr.)	1.2870×10^{-16}	0.0000	(6.20)
Variance Walsh func. correlation	6.7973×10^{-25}	6.2785×10^{-25}	(6.21)

Table 6.2: Observed and predicted statistical parameters of correlation values for 1 antenna element, 20 mobiles, and $\psi = 0.5$

Quantity	Observed Value	Predicted Value	Ref. Eqn.
Mean mobile power	5.4193×10^{-16}	4.7656×10^{-16}	(6.48)
Mean interference power	6.3758×10^{-15}	4.6068×10^{-15}	(6.44)
Mean interference and noise	1.3841×10^{-14}	1.2072×10^{-14}	
Mean PN chip correlation	1.1845×10^{-14}	1.1133×10^{-14}	(6.15)
Variance PN chip correlation	3.9172×10^{-27}	2.8109×10^{-27}	(6.16)
Mean Walsh chip correlation	9.4756×10^{-14}	8.9063×10^{-14}	(6.17)
Variance Walsh chip correlation	3.3506×10^{-26}	2.2487×10^{-26}	(6.18)
Mean Walsh func. corr. (correct)	6.0644×10^{-12}	5.7001×10^{-12}	(6.19)
Mean Walsh func. corr. (incorr.)	2.6601×10^{-16}	0.0000	(6.20)
Variance Walsh func. correlation	2.1354×10^{-24}	1.4392×10^{-24}	(6.21)

Table 6.3: Observed and predicted statistical parameters of correlation values for 3 antenna elements, 30 mobiles, and $\psi = 1.0$

Quantity	Observed Value	Predicted Value	Ref. Eqn.
Mean mobile power	6.7858×10^{-16}	6.3219×10^{-16}	(6.48)
Mean interference power	4.8870×10^{-15}	3.6667×10^{-15}	(6.44)
Mean interference and noise	1.7328×10^{-14}	1.6108×10^{-14}	
Mean PN chip correlation	1.3282×10^{-14}	1.2822×10^{-14}	(6.15)
Variance PN chip correlation	5.2498×10^{-27}	4.2818×10^{-27}	(6.16)
Mean Walsh chip correlation	1.0625×10^{-13}	1.0258×10^{-13}	(6.17)
Variance Walsh chip correlation	4.4697×10^{-26}	3.4254×10^{-26}	(6.18)
Mean Walsh func. corr. (correct)	6.8002×10^{-12}	6.5651×10^{-12}	(6.19)
Mean Walsh func. corr. (incorr.)	4.8667×10^{-16}	0.0000	(6.20)
Variance Walsh func. correlation	2.8507×10^{-24}	2.1923×10^{-24}	(6.21)

Table 6.4: Observed and predicted statistical parameters of correlation values for 5 antenna elements, 30 mobiles, and $\psi = 1.0$

Quantity	Observed Value	Predicted Value	Ref. Eqn.
Mean mobile power	7.8537×10^{-16}	7.0489×10^{-16}	(6.48)
Mean interference power	7.6094×10^{-15}	5.4981×10^{-15}	(6.44)
Mean interference and noise	2.0051×10^{-14}	1.7940×10^{-14}	
Mean PN chip correlation	1.4287×10^{-14}	1.3540×10^{-14}	(6.15)
Variance PN chip correlation	5.8569×10^{-27}	4.3626×10^{-27}	(6.16)
Mean Walsh chip correlation	1.1430×10^{-13}	1.0832×10^{-13}	(6.17)
Variance Walsh chip correlation	4.9986×10^{-26}	3.4901×10^{-26}	(6.18)
Mean Walsh func. corr. (correct)	7.3151×10^{-12}	6.9323×10^{-12}	(6.19)
Mean Walsh func. corr. (incorr.)	1.3464×10^{-16}	0.0000	(6.20)
Variance Walsh func. correlation	3.1873×10^{-24}	2.2337×10^{-24}	(6.21)

Table 6.5: Observed and predicted statistical parameters of correlation values for 5 antenna elements, 40 mobiles, and $\psi = 1.0$

6.6 Summary

This chapter has presented a derivation of the statistical parameters of the various correlation quantities obtained from the received signals, including PN chip, Walsh chip, and Walsh function correlation values. In addition, expressions for the estimated received power for single and multiple antenna element configurations were obtained. These values can be used both for system validation purposes and also to reduce the complexity of simulations. For example, input values for testing the data decoding algorithms in Chapter 4 can be generated directly from the derived probability distributions without the need for PN chip-level simulations. In addition, the expected received power equations may be used to predict cell capacity as will be shown in the next chapter. Sample results showed the agreement between predicted and simulated values for various numbers of antenna elements, mobiles, and voice activity factors. Close agreement was observed for the case of a single antenna element, whereas the correspondence between predictions and simulations for multiple elements was less exact due to the inexact approximation used for estimating the expected received power. In particular, the predicted power appears to be underestimated when antenna arrays are considered.

Chapter 7

Cell Capacity Estimation

7.1 Introduction

A critical area of investigation in cellular communications is cell capacity improvement techniques that have minimal additional expense. Overall system capacity can be increased in two different ways. Splitting existing cells into smaller subcells is one option that may not be desirable for PCS (Personal Communication Systems) since it requires additional base station hardware and increases the complexity of performing hand-offs between different base stations. However, if individual cell capacity can be increased through a method such as digital beamforming as discussed in Chapter 5, then system capacity will also increase with potentially less impact on the base station costs.

In order to obtain a prediction of how well a given system will perform, it is necessary to employ both analyses and simulations. This relatively low-cost evaluation methodology is useful for testing various system designs before a potentially expensive prototype is constructed.

This chapter concerns itself with how cell capacity can be estimated in a cellular CDMA communication system. Two different capacity estimation techniques for use in a simulation environment are described in Section 7.3, while the following section describes how beamforming can be integrated with these two techniques. Confidence intervals for the simulation results are discussed in Section 7.5. Predicted values for cell capacity are then derived before actual simulation results for single and multi-cell

configurations are presented in Sections 7.7 and 7.8, respectively. Finally, Section 7.9 presents simulation results for a system which provides multi-service access (*i.e.* both data and voice).

7.2 Related Research

Gilhousen *et al* [29] produced one of the earlier definitive papers on CDMA cellular capacity and derived expressions for estimating cell capacity for both the forward and reverse links. However, direct comparison to [29] is difficult due to the assumptions which were made. For example, [29] assumes an optimistic value of 0.375 for the voice activity factor, as compared to the value of 0.5 used within this thesis. More importantly though, was their assumption that speech-inactive mobiles would not be transmitting, which is unrealistic since it is necessary to maintain the link, albeit at a reduced data rate and interference power level. In addition, [29] also assumes that each cell is split into three triangular sectors with directional antennas being used at the base station for each sector. Although, this corresponds to the formal IS-95 standard, it is a configuration which does not lend itself as easily to beamforming which is the subject of this thesis.

The work performed by a group of researchers at Stanford is the most similar to the work presented in this thesis. Approximate expressions for the outage probability (defined in this instance as the probability of the BER exceeding 10^{-3}) as a function of beamwidth and number of users were originally derived in [72] for both the uplink and downlink. The uplink performance of a cellular CDMA network with an antenna array at the base station and multipath propagation was considered in [66], whereas the corresponding downlink analysis can be found in [74]. A longer analysis of the uplink performance with base-station antenna arrays is contained in [67]. The earlier work by Naguib and Paulraj is essentially summarized in [73] which considers base station antenna arrays for both the forward and reverse links. The performance enhancement due to linear antenna arrays in a sectorized system with 120° sectors was investigated in [68]. The effects of the resulting gain in E_b/N_0 on system capacity, area of coverage, and mobile transmitter power were also examined. A similar sectorized system was

also the focus of [69] which included M-ary orthogonal modulation (matching the IS-95 standard) on the uplink. In [71], the performance of an IS-95 system with a sectorized uniform linear antenna array and beam-steered Rake architecture was analyzed by extending the results in [38]. Diversity combining was used to exploit delay spread, and the estimation of the array response of multiple paths per mobile was required. Due to the delay spread arising from statistical variation of unresolvable paths, the multiple access interference was approximated by white noise. Errors in closed-loop power control were modeled by an equivalent Doppler shift. Finally, the use of directional antennas for the reverse link of a fixed wireless CDMA system was investigated in [20]. It should be noted that most of the work described in this paragraph focussed on analyzing system performance via probabilistic equations that were derived using simplifying assumptions. Simulations were used only to estimate probability distributions for random variables when these distributions could not be derived analytically. In contrast, the work presented in this thesis is based on a significantly more comprehensive chip-level simulation methodology.

Jalali and Mermelstein investigated the effects of diversity, power control, and bandwidth on CDMA system capacity in [37]. Both the forward and reverse links were considered, with system bandwidths of 1.25 and 10 MHz, and the encoding scheme used for transmission complied with IS-95. The path loss exponent was found to significantly affect cell capacity since it determined the amount of intercell interference. In addition, the wideband system was more bandwidth efficient due to the larger number of users that could be accommodated which reduced the variance of the multiple access interference.

Stüber and Kchao considered both single cell [43] and multi-cell [98] CDMA systems. Analytical expressions were derived to give the expected BER as a function of the number of users per cell for both the uplink and downlink. The presence or absence of power control was also a factor.

Milstein, Rappaport, and Barghouti [61] derived expressions for the expected BER in terms of the number of users for different path loss exponents. Both the forward and reverse links were considered, together with the effects of imperfect power control.

Recently, Foschini [26] investigated a fixed wireless system with equal numbers

of antenna elements at both the transmitter and receiver. In a non-mobile system, sufficient processing power is available at both ends of the communications link to permit this. An architecture for layering signals in both space and time was developed for increasing data rate capacity.

The above papers considered cell capacity to be defined as the maximum number of users which can be simultaneously supported by the system. Conversely, Viterbi and Viterbi [107] investigated the Erlang capacity of the reverse link of a power-controlled cellular CDMA system. This type of capacity is defined as the average number of mobiles requesting service which results in a specified blocking probability. The blocking probability is the probability that a user attempting to initiate a call will be denied access due to the system already being at peak load for the specified level of service, and typically might have a value of 1%. In this particular research, blocking was deemed to have occurred when the interference-to-noise ratio (INR) had reached a certain level. In a power-controlled situation, the INR should be proportional to the SINR (signal-to-interference-plus-noise-ratio) which is another measure of system quality. The CDMA system considered by this paper was found to have an Erlang capacity about 20 times that of the existing AMPS system.

7.3 Cell Capacity Estimation Methods

Cell capacity can be defined as the maximum number of users per cell that can be supported with a given level of performance. For voice, this implies a BER (Bit Error Rate) of 10^{-3} or less. Consequently, a simple way of measuring cell capacity is to gradually add more users until the observed BER exceeds the desired value. The proposed simulation technique is capable of estimating cell capacity using either a detailed PN chip-level approach or a less computationally expensive power control method.

7.3.1 Chip-Level Capacity Estimation

This thesis proposes the use of PN chip-level capacity simulations to investigate situations involving imperfect power control and/or imperfect beamforming. These

simulations are computationally expensive and so must be limited to a small number of antenna elements (*e.g.* $N_A \leq 3$). However, the ability to obtain data at the PN chip level is extremely important since it serves to validate simplifying assumptions that will allow faster simulations to be performed.

Since data is actually being transmitted through the system, BER estimation is easily performed provided that a sufficient number of data frames are processed to ensure a tight enough confidence interval as discussed in Section 7.5.

7.3.2 Power-Level Capacity Estimation

It is well-accepted that a specified E_b/N_0 ratio corresponds roughly to a given BER. For example, an E_b/N_0 of 7 dB is typically used for voice situations which require a maximum BER of 10^{-3}. This approximate correspondence can be seen from Figures 4.4 through 4.6. If perfect power control is used so that this E_b/N_0 value is maintained for all mobiles, the observed BER should not be greater than the desired limit. This eliminates the need to encode and decode data bits via the chip-level technique. Consequently, it is possible to generate capacity estimates over longer time periods and for more antenna elements.

To obtain a capacity estimate for a given number of antenna elements, power-level simulations are performed for successively increasing numbers of mobiles. A large number of frames is required for accuracy since the interference power for multiple antenna elements depends on the spatial distribution of the users which must continually be randomly changed in order to ensure a uniform distribution (as assumed in Section 6.4) over a period of time. If the percentage of frames where the desired E_b/N_0 ratio could not be achieved for all mobiles exceeds a certain threshold (*e.g.* 1%), the capacity of the cell is deemed to have been reached. This percentage is termed the *outage probability*.

7.3.3 Execution Time Comparison

Table 7.1 gives a comparison of sample execution times on a Sun UltraSparc 1 for both the chip-level and power-level capacity estimation methods. These simulations were

# of Users	Capacity Estimation Method		Savings Factor
	Chip-Level	Power-Level	
10	1091.85	4.21	259
15	2006.54	6.90	291
20	3989.55	9.81	407
25	5623.97	13.40	420
30	7632.78	17.95	425
35	9384.77	23.73	395

Table 7.1: Execution time comparison between the capacity estimation methods (in seconds)

for three antenna elements over a time period of 100 frames and with a transmission activity factor of 1.0 corresponding to full loading of the system.

The power-level capacity estimation method clearly provides a computational savings of more than two orders of magnitude over the chip-level simulations. This serves to motivate the development of the power-level capacity estimation technique, since larger-scale simulations may now be performed with only modest computational requirements. Note also that the large CPU time requirements for the PN chip-level simulations explain why these simulations were limited in terms of antenna elements, simulation length, and intercell interference.

7.4 Capacity Estimation with Beamforming

When beamforming is used to increase the capacity of a cell, it is possible to consider a variety of different simulation alternatives. Results have been generated for all of the various combinations of options so that the similarities between the different simulation methods may be compared.

7.4.1 Perfect Beamforming

For perfect beamforming, it is assumed that the correct array response vector for each mobile is known exactly. The array response values are used to form the beamforming weight vector directly so it is not necessary to estimate these coefficients from the received signal data. Consequently, perfect beamforming can be easily used with either the chip-level or power-level capacity estimation methods described in the previous section.

7.4.2 Imperfect Beamforming

In imperfect beamforming, the beamforming coefficients are estimated from the received data and are therefore corrupted by measurement noise and interference. Imperfect beamforming in both types of simulation environments, chip-level and power-level, has been considered as described below.

7.4.2.1 Imperfect Beamforming – Chip-Level Simulations

With PN chip-level simulations, the beamforming weights can be estimated directly from the received signal data for each mobile as detailed in Section 5.5. Currently, the data from one frame is used to estimate the beamforming coefficients for the following frame. Since the mobiles do not move a significant distance within the time period of one frame (1/50 of a second), the array response vectors do not change significantly between frames under the assumed channel model.

Ideally, it would be preferable to track the array response vectors over time which would reduce the effects of noise and interference on the weight estimates. Since the coefficients do not change significantly between frames, a significant amount of information is discarded after each frame. The computational requirements of estimating the beamforming coefficients could be reduced with a lower-complexity updating method such as the computationally-efficient algorithm for tracking array response vectors given in [93].

7.4.2.2 Imperfect Beamforming – Power-Level Simulations

When the more computationally-efficient power-level capacity simulations are conducted, it is not possible to estimate suitable beamforming data from the received signals since chip-level data is required for this purpose. However, it is possible to use the statistical development in Sections 5.5 and 5.6 to generate random estimates of the current array response vector for each frame. This is a significant accomplishment since it allows the effects of imperfect beamforming on cell capacity to be investigated without having to resort to chip-level simulations which are computationally intractable except for small numbers of antenna elements.

7.5 Confidence Intervals

When performing simulations, it is important to quantify the accuracy of the observed results. This can be accomplished by determining confidence intervals for the observed parameter estimates. By specifying the desired width of each interval, the necessary simulation length can be calculated. The following sections describe various confidence intervals for the parameters which are investigated later in this chapter. The purpose of these confidence intervals is to ensure that sufficient simulations have been performed in order to justify the conclusions which are made from the observed results.

7.5.1 Bit Error Rate

When performing chip-level simulations, it is necessary to ensure that a sufficient number of data bits have been processed through the system in order to obtain an accurate estimate of the actual BER for the current parameter configuration.

If B_E and $\hat{B}_E$ represent the true and observed BER values and N_B the total number of data bits processed in the simulation, then an approximate $q\%$ confidence interval for B_E can be calculated from the observed value as [11, pp. 564]:

$$\hat{B}_E - Q\sqrt{\frac{\hat{B}_E(1-\hat{B}_E)}{N_B}} \;\leq\; B_E \;\leq\; \hat{B}_E + Q\sqrt{\frac{\hat{B}_E(1-\hat{B}_E)}{N_B}} \tag{7.1}$$

q	90%	95%	99%
Q	1.65	1.96	2.58

Table 7.2: Standard deviation multipliers for various confidence intervals

where the value of Q depends on q as shown in Table 7.2. A Gaussian distribution for $\hat{B}_E$ is assumed here.

By choosing a sufficiently large value for N_B, the width of the confidence interval given by (7.1) can be made as narrow as desired for a given level of accuracy.

If W is the desired width of the confidence interval, then (7.1) yields:

$$W = 2Q\sqrt{\frac{\hat{B}_E(1-\hat{B}_E)}{N_B}} \tag{7.2}$$

Solving for N_B in terms of the other parameters produces:

$$N_B = \frac{4\hat{B}_E(1-\hat{B}_E)Q^2}{W^2} \tag{7.3}$$

This expression gives the number of bits required to obtain the desired confidence interval width.

7.5.2 Number of Frames – Outage Probability

The power control outage probability is defined as the probability that perfect power control will fail for a given number of users. Suppose that an estimate $\hat{P}$ of this quantity is desired. Equation (7.2) can be used to obtain the following expression for the confidence interval width as a function of the number of frames:

$$W = 2Q\sqrt{\frac{\hat{P}(1-\hat{P})}{F}} \tag{7.4}$$

where F is the number of frames tested in a simulation run. This expression gives an indication of the accuracy of a given outage probability estimate, which is important in estimating cell capacity using the power-level method.

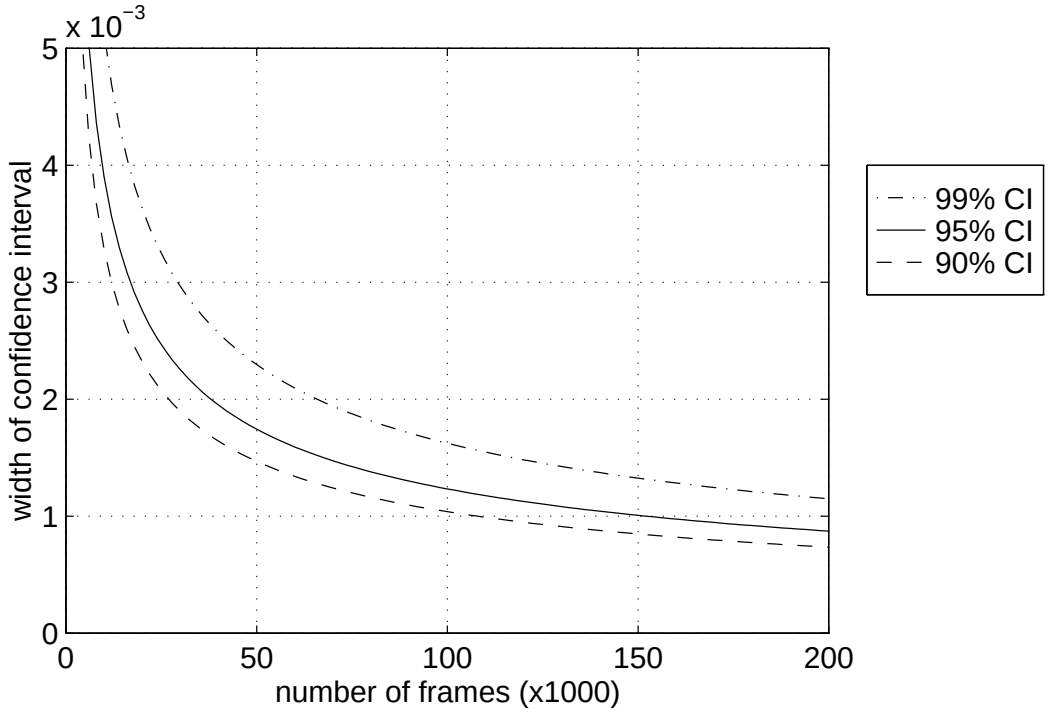

Figure 7.1: Confidence interval width for a power control outage probability estimate of 1% as a function of number of frames

Figure 7.1 shows the confidence interval width as a function of the number of frames for 90%, 95%, and 99% confidence intervals. A power control outage probability of 1% was assumed as discussed in Section 7.3.2. For example, if the observed $\hat{P}$ is 0.01 and 150000 frames have been simulated, then the 95% confidence interval for the true power outage probability will be $[0.0095, 0.0105]$.

7.5.3 Number of Frames – Voice Activity Factor

In a simulation with N_M mobiles and a non-unity voice activity factor ψ, it is important to ensure that a sufficient number of frames have been processed in order to ensure that a suitable distribution of the number of speech active mobiles has been attained. This is especially important in the case of the more computationally expensive chip-level simulations where a much smaller number of frames can be processed as compared to the power-level capacity estimation simulations.

In a voice communications system, setting ψ to 0.5 is typical. Let N_s be a random

variable representing the number of mobiles with active speech for a particular frame. This quantity will have the following binomial probability distribution:

$$P\left(N_s = n_s\right) = \left(\begin{array}{c} N_M \\ n_s \end{array} \right) \psi^{n_s} (1-\psi)^{n_s} \tag{7.5}$$

For a reasonable number of mobiles (*e.g.* $N_M \geq 20$) and the given voice activity factor ($\psi = 0.5$), the above distribution can be accurately approximated by a Gaussian distribution with the following parameters [42, pp. 245].

$$\mu_s = N_M \psi \tag{7.6}$$

$$\sigma_s^2 = N_M \psi (1-\psi) \tag{7.7}$$

Thus, equation (7.5) can be approximated as:

$$\begin{aligned} p(n_s) \equiv P\left(N_s = n_s\right) &\approx P\left(n_s - 0.5 < N_s \leq n_s + 0.5\right) \\ &= \left\{ \frac{1}{2} + \frac{1}{2} \operatorname{erf}\left(\frac{(n_s + 0.5) - \mu_s}{\sqrt{2}\sigma_s} \right) \right\} \\ &\qquad - \left\{ \frac{1}{2} + \frac{1}{2} \operatorname{erf}\left(\frac{(n_s - 0.5) - \mu_s}{\sqrt{2}\sigma_s} \right) \right\} \\ &= \frac{1}{2} \left\{ \operatorname{erf}\left(\frac{(n_s + 0.5) - \mu_s}{\sqrt{2}\sigma_s} \right) - \operatorname{erf}\left(\frac{(n_s - 0.5) - \mu_s}{\sqrt{2}\sigma_s} \right) \right\} \end{aligned} \tag{7.8}$$

Now consider a simulation which is run for F frames and assume that successive frames are independent. The quantity of interest is now the number of frames which have exactly n_s active speech mobiles. Let $N_f(n_s)$ be a random variable representing this quantity. Its probability distribution can be approximated as binomial:

$$P\left(N_f(n_s) = n_f\right) \approx \left(\begin{array}{c} F \\ n_f \end{array} \right) p(n_s)^{n_f} (1 - p(n_s))^{n_f} \tag{7.9}$$

where $p(n_s)$ is given by (7.8). Once again, the distribution in (7.9) can be approximated as Gaussian with parameters:

$$\mu_f = F p(n_s) \tag{7.10}$$

$$\sigma_f^2 = F p(n_s)(1 - p(n_s)) \tag{7.11}$$

Suppose it is desired to estimate $p(n_s)$ from observations as:

$$\hat{p}(n_s) = \frac{n_f}{F} \tag{7.12}$$

where n_f is the number of frames with n_s mobiles having active speech. The mean and variance for $\hat{p}(n_s)$ can be obtained from (7.10) and (7.11).

$$\mu_{p(n_s)} = \frac{\mu_f}{F} = p(n_s) \tag{7.13}$$

$$\sigma^2_{p(n_s)} = \frac{\sigma^2_f}{F^2} = \frac{p(n_s)(1-p(n_s))}{F} \tag{7.14}$$

Since the true value of $p(n_s)$ can be predicted, a sum of squared error terms between the observed values of $\hat{p}(n_s)$ and the true values of $p(n_s)$ can be defined as:

$$E_T \equiv \sum_{n_s=0}^{N_M} [\hat{p}(n_s) - p(n_s)]^2 \tag{7.15}$$

It can be easily seen that this represents a summation of squared zero-mean Gaussian random variables each with variance given by (7.14). Equation (7.14) will be maximized when $p(n_s)$ is as near as possible to 0.5 which will occur for:

$$n_{max} = \begin{cases} N_M/2 & N_M \text{ even} \\ (N_M-1)/2 & N_M \text{ odd} \end{cases} \tag{7.16}$$

Thus, (7.15) can be upper-bounded by the summation of $N_M + 1$ independent and identically distributed zero-mean Gaussian random variables with variance given by substituting (7.16) into (7.14). This corresponds to a χ^2 distribution with $N_M + 1$ degrees of freedom and variance:

$$\sigma^2_\chi = 2(N_M+1)\left(\sigma^2_{p(n_s)}\right)^2 \tag{7.17}$$

Let E_{max} represent the maximum desired squared error given by expression (7.15). The following equality can then be derived.

$$E_{max} = \left(\sigma^2_{p(n_s)}\right)^2 \chi^{-1}(N_M+1, q) \tag{7.18}$$

where χ^{-1} is the inverse standard χ^2 cdf with $N_M + 1$ degrees of freedom and a cdf value of q (0.90, 0.95, or 0.99).

Finally, combining (7.18), (7.16), and (7.14) allows a value for F to be calculated.

$$E_{max} = \frac{p(n_{max})(1-p(n_{max}))}{F}\chi^{-1}(N_M+1, q) \tag{7.19}$$

$$F = \frac{p(n_{max})(1-p(n_{max}))}{E_{max}}\chi^{-1}(N_M+1, q) \tag{7.20}$$

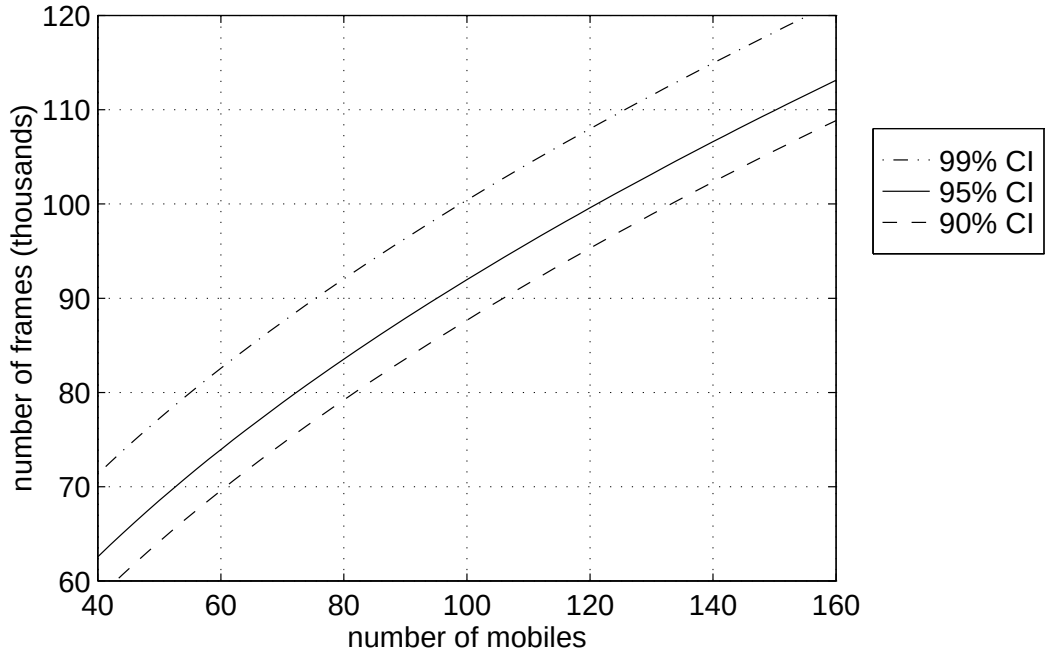

Figure 7.2: Number of frames required for $E_{max} = 10^{-4}$ with confidences of 99%, 95%, and 90% when $\psi = 0.5$

Although the expression in (7.20) is only an upper bound, it gives an indication as to the number of frames required for a given confidence.

As an example, Figure 7.2 shows the required number of frames to achieve $E_{max} = 10^{-4}$ with confidences of 99%, 95%, and 90%.

7.6 Predicting Single Cell Capacities

By using the equations from Sections 6.3 and 6.4, it is possible to generate approximate predictions for the capacity of a single cell with a given number of antenna elements. These predictions are obtained by considering the expected received power values.

7.6.1 Single Antenna Element

Consider equations (6.25) and (6.26) which give the expected received power for a specified number of mobiles and voice activity factors of $\psi = 1.0$ and $\psi < 1.0$,

respectively, when only a single antenna element is considered.

$$E[P] = \left(\frac{E_b}{N_0}\right)\sigma_n^2\left\{\frac{1}{R_B} - \frac{N_M - 1}{B}\left(\frac{E_b}{N_0}\right)\right\}^{-1} \tag{7.21}$$

$$E[P] = \left(\frac{E_b}{N_0}\right)\sigma_n^2\sum_{n_I=0}^{N_M-1}\left\{\frac{1}{R_B} - \frac{1}{B}\left(\frac{E_b}{N_0}\right)\left(n_I + \frac{N_M - n_I - 1}{\nu}\right)\right\}^{-1} P(N_I = n_I) \tag{7.22}$$

Clearly, as N_M increases, the above quantities will increase in size and then eventually become negative. Consequently, a simple method of predicting cell capacity in this situation is to simply increase N_M until the expected power becomes negative. At that point, the predicted capacity of the cell has been exceeded. Equation (7.21) can be rearranged to yield a closed-form solution when $\psi = 1.0$ with $E[P]$ being set to zero to indicate the boundary between positive and negative expected received power values.

$$N_M = \text{floor}\left(B\left[\frac{1}{R_B(E_b/N_0)} - \sigma_n^2\right] + 1\right) \tag{7.23}$$

However, the summation in (7.22) with a variable number of active speech interferers makes it impossible to obtain a closed-form solution for $\psi < 1.0$. Thus, it is necessary to use an incremental search technique in this situation to predict cell capacity.

7.6.2 Multiple Antenna Elements

Equations (6.49) and (6.50) specify the expected received power for the multi-element case with $\psi = 1$ and $\psi \leq 1$, respectively, as:

$$E[P] = \frac{1}{2}(N_A)^3\left(\frac{E_b}{N_0}\right)\sigma_n^2 E\left[\left\{\frac{(N_A)^2}{2R_B} - \frac{1}{B}\left(\frac{E_b}{N_0}\right)V\right\}^{-1}\right] \tag{7.24}$$

$$E[P] = \frac{1}{2}(N_A)^3\left(\frac{E_b}{N_0}\right)\sigma_n^2\sum_{N_I=0}^{N_M-1}P(N_I = n_I)E\left[\left\{\frac{(N_A)^2}{2R_B} - \frac{1}{B}\left(\frac{E_b}{N_0}\right)V\right\}^{-1}\right] \tag{7.25}$$

where N_I is the number of interferers with active speech, $P(N_I = n_I)$ is calculated from (6.30), and V is a Gaussian random variable with the following parameters.

$$\mu_V = \frac{1}{2}\left(N_I + \frac{N_M - 1 - N_I}{\nu}\right)N_A \tag{7.26}$$

$$\sigma_V^2 = \frac{1}{4}\left(N_I + \frac{N_M - 1 - N_I}{\nu^2}\right)(N_A)^2 \tag{7.27}$$

N_I can be set to $N_M - 1$ when the voice activity factor is $\psi = 1.0$.

Unlike (7.21), both of the above expressions must be numerically integrated in order to obtain an estimate of the received power. For large values of V, the quantities inside the expectations will have a negative value which implies that the cell capacity has been exceeded in that particular situation.

Consequently, a method for estimating cell capacity with equation (7.24) or (7.25) is to evaluate the area under the pdf curve of V for which the received power expression in the numerical integration evaluates as a negative number. This value will increase as the number of mobiles is increased. Once this probability value exceeds a certain threshold (such as the outage probability of 1% mentioned in Section 7.3.2), the capacity of the cell can be deemed to have been exceeded.

7.6.3 Predicted Cell Capacities

Tables 7.3 and 7.4 show predicted capacity values for single cells with voice activity factors of 1.0 and 0.5, respectively. In Table 7.4, it is interesting to note that the capacity relative to that for a single antenna element increases by more than 100% for each additional element, beginning with the transition from 2 to 3 elements. This is due to the reduction in the relative variance of the number of speech active mobiles as the number of mobiles in the cell increases. That is, as the total number of mobiles increases with $\psi = 0.5$, the magnitude of the standard deviation of the binomial distribution governing N_I (the number of interferers with active speech) relative to the mean will decrease.

7.7 Single Cell Capacity

This section contains a variety of capacity results for a single cell as estimated from simulations. Sample results for the computationally more expensive multi-cell simulations are contained in Section 7.8.

A number of parameters remain constant for all of the simulations. In the case of multiple antenna elements, the spacing between the elements was equal to half the wavelength of the carrier frequency (2 GHz). Rayleigh fading was assumed, which is

Antenna Elements	Capacity	% of 1 Element Cap.
1	26	100%
2	37	142%
3	59	227%
4	82	315%
5	104	400%
6	128	492%

Table 7.3: Capacity predictions for a single cell ($\psi = 1.0$)

Antenna Elements	Capacity	% of 1 Element Cap.
1	35	100%
2	62	177%
3	100	286%
4	139	397%
5	179	511%
6	220	629%

Table 7.4: Capacity predictions for a single cell ($\psi = 0.5$)

a worst-case scenario, and the fading gains were changed at least every 48 PN chips (roughly corresponding to the time of one data bit). The desired E_b/N_0 ratio was set at 7 dB, and the power control step size was 0.5 dB. Power transmitted by a mobile was reduced by a factor of 8 (corresponding to a data rate of 1200 bps) when speech was inactive. All simulations in this section are for a hexagonal cell with a radius of 500 m.

When imperfect power control was used, three different control methods were defined. Method A had no feedback delay and zero probability of feedback error for the power control bits. Method B represents a more realistic situation and delayed the power control bits by one power control period (1536 PN chips) with a probability of feedback error of 10%. Method C is the same as A, although with a power adjustment step size of 1 dB as compared to the 0.5 dB step size used for methods A and B.

7.7.1 Single Cell Capacity with Perfect Beamforming

Figures 7.3 through 7.7 show the observed BER values from PN chip-level simulations with perfect beamforming. Various combinations of interleaving, power control methods, and voice activity factors were considered. The legends indicate the power control method and whether or not interleaving was used. Since no interleaving with uncorrelated Rayleigh fading is essentially the same as infinite interleaving, not all combinations of input parameters were considered for multiple antenna elements, due to the required computational expense. Sufficient simulations were performed in order to produce relatively smooth BER curves, although these results really only represent approximations to the true cell capacity. Capacity results from the BER plots are summarized in Tables 7.5 and 7.6 for the two voice activity factors.

Power control method B appears to reduce capacity slightly as compared to method A. In addition, interleaving does not appear to have much effect when uncorrelated Rayleigh fading is used, although interleaving is essential for dealing with correlated fading. This is as expected, since uncorrelated fading is essentially the same as infinite interleaving. A 50% increase in capacity for 2 elements and 130% for 3 elements were observed for $\psi = 1.0$. For $\psi = 0.5$, the capacity increase from 1 to 2 elements was approximately 65%.

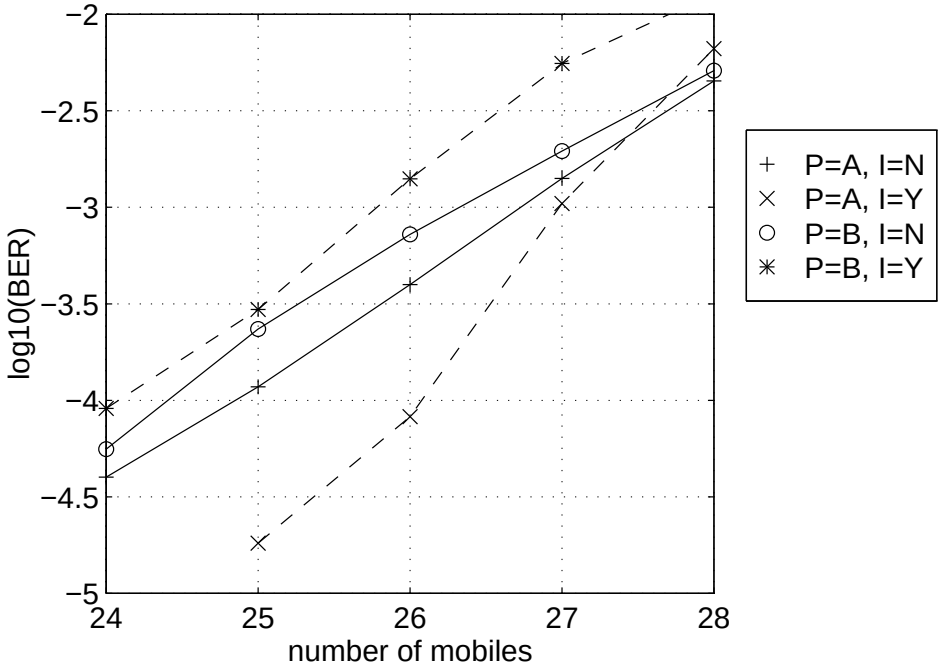

Figure 7.3: Observed BER curves for PN chip-level capacity estimation with perfect beamforming ($N_A = 1$, $\psi = 1.0$)

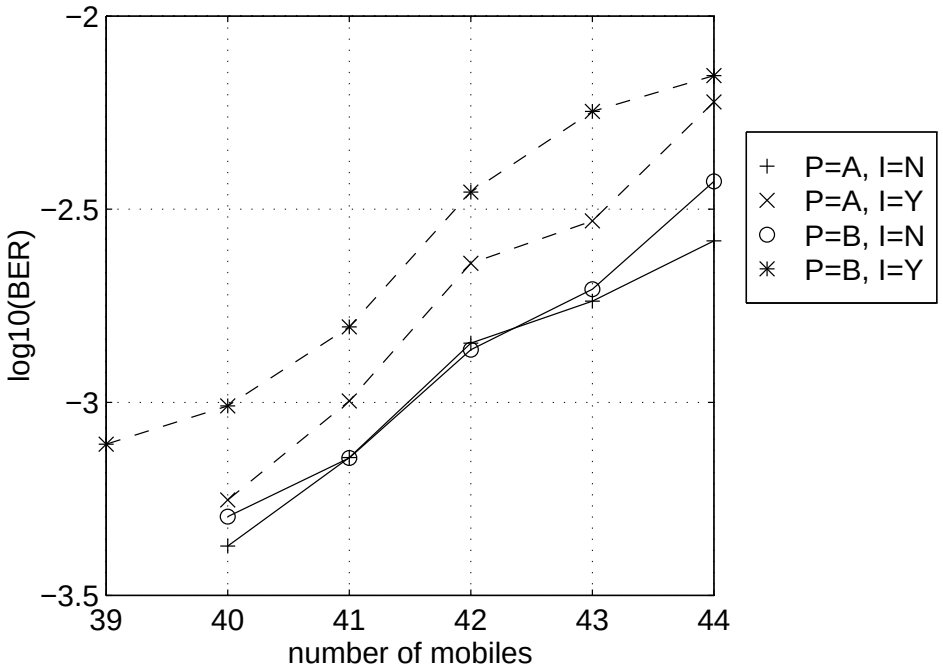

Figure 7.4: Observed BER curves for PN chip-level capacity estimation with perfect beamforming ($N_A = 1$, $\psi = 0.5$)

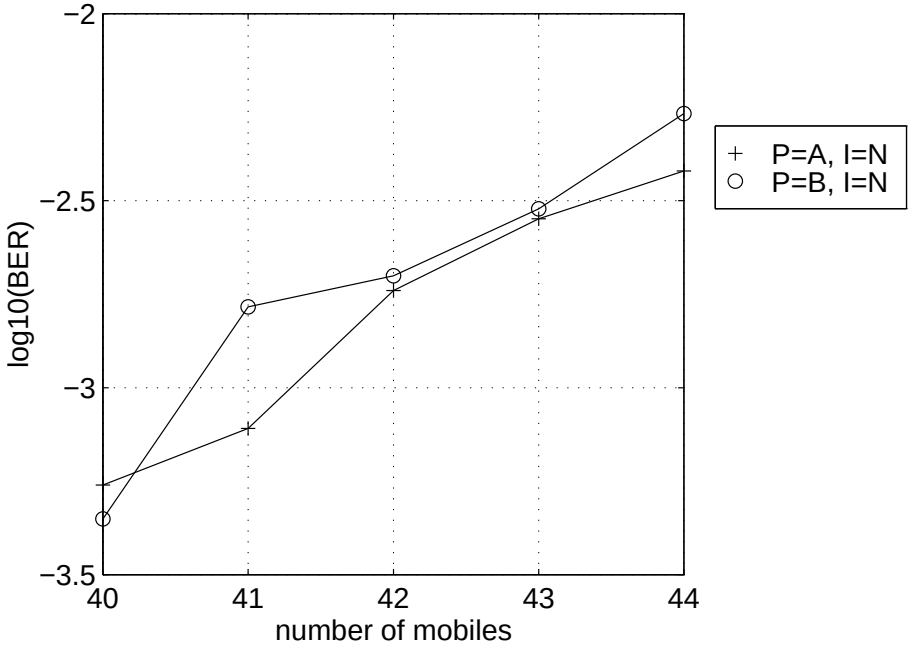

Figure 7.5: Observed BER curves for PN chip-level capacity estimation with perfect beamforming ($N_A = 2$, $\psi = 1.0$)

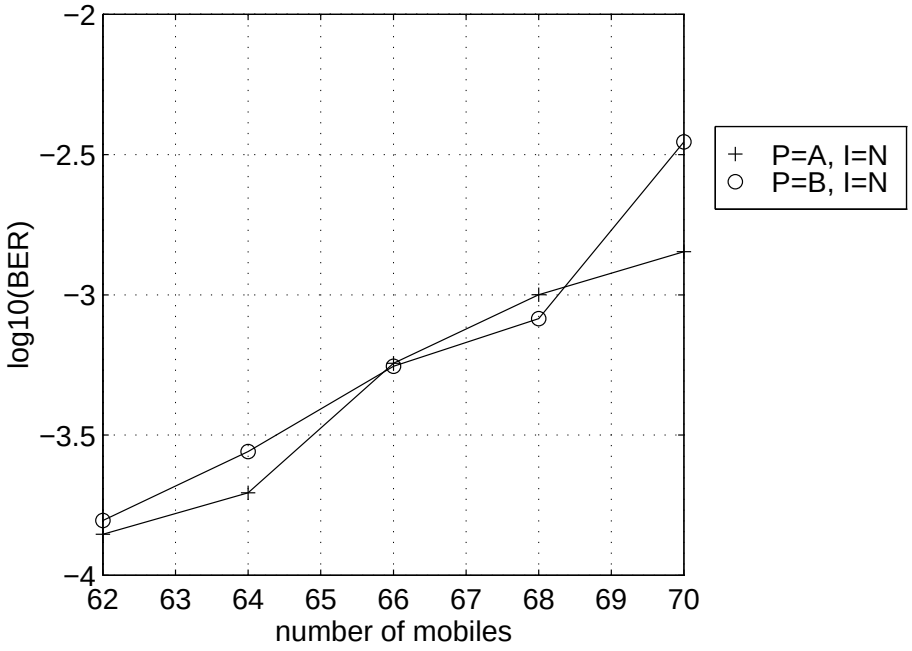

Figure 7.6: Observed BER curves for PN chip-level capacity estimation with perfect beamforming ($N_A = 2$, $\psi = 0.5$)

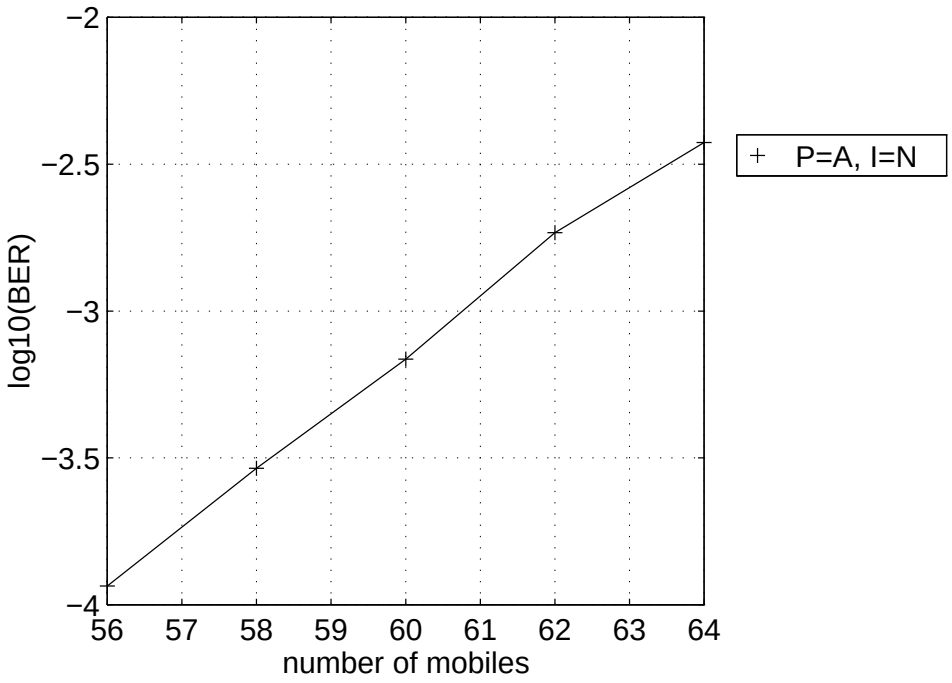

Figure 7.7: Observed BER curve for PN chip-level capacity estimation with perfect beamforming ($N_A = 3$, $\psi = 1.0$)

Antenna Elements	Power Control Method	Interleaving	Cell Capacity
1	A	N	26
		Y	27
	B	N	26
		Y	25
2	A	N	41
	B	N	40
3	A	N	60

Table 7.5: Estimated cell capacities from chip-level simulations with perfect beamforming and uncorrelated fading ($\psi = 1.0$)

Antenna Elements	Power Control Method	Interleaving	Cell Capacity
1	A	N	41
		Y	41
	B	N	41
		Y	40
2	A	N	68
	B	N	68

Table 7.6: Estimated cell capacities from chip-level simulations with perfect beamforming and uncorrelated fading ($\psi = 0.5$)

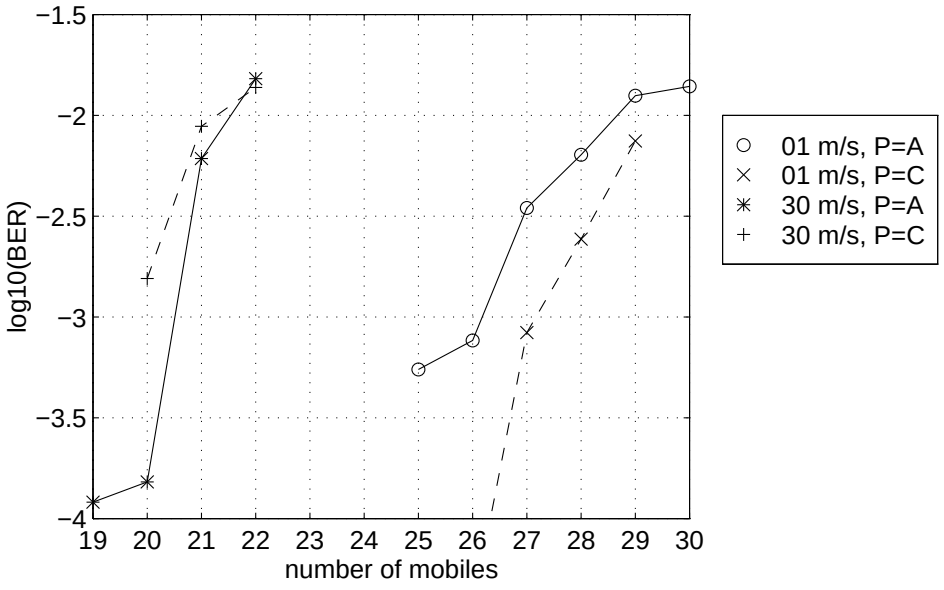

Figure 7.8: Observed BER for PN chip-level capacity estimation with perfect beamforming, correlated fading, interleaving, and 1 antenna element ($\psi = 1.0$)

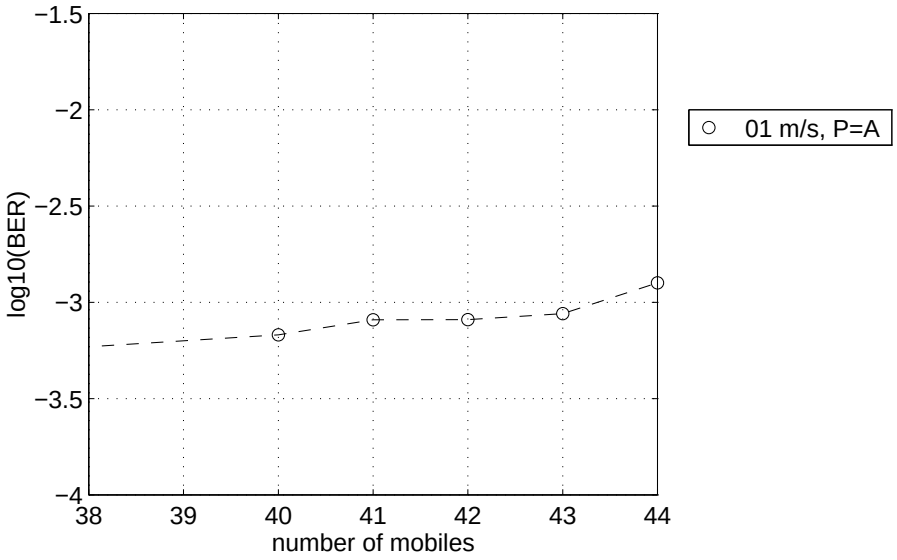

Figure 7.9: Observed BER for PN chip-level capacity estimation with perfect beamforming, correlated fading, interleaving, power control method A, and 2 antenna elements ($\psi = 1.0$)

Antenna Elements	Mobile Velocity	Power Control	Cell Capacity
1	1 m/s	A	26
		C	27
	30 m/s	A	20
		C	19
2	1 m/s	A	43

Table 7.7: Estimated cell capacities from chip-level simulations with perfect beamforming, correlated fading, and interleaving ($\psi = 1.0$)

Figures 7.8 and 7.9 and Table 7.7 show the observed BER curves and corresponding cell capacities when correlated fading is used with chip-level simulations. Power control methods A and C were tested here to determine the effect of the size of the power adjustment step on fading compensation. As can be seen, when all of the mobiles moved at 1 m/s (suitable for pedestrians), the power control algorithm could operate quickly enough to compensate for the fading and the cell capacity was not reduced as compared to the uncorrelated fading results in Table 7.5. In addition, a larger power step size appeared to improve performance slightly by allowing the fading to be tracked more accurately. Conversely, for faster mobile speeds such as 30 m/s, the fading had a greater effect on cell capacity due to the inability of the power control scheme to compensate for the fades as shown in Figure 3.4.

Tables 7.8 and 7.9 show the estimated cell capacities using the power-level capacity estimation method with perfect beamforming for voice activity factors of 1.0 and 0.5, respectively. In order to estimate cell capacity in this instance, 200000 frames were processed for each antenna element and voice activity factor pair. This yielded a sufficiently narrow confidence interval width for the observed outage probability as described in Section 7.5.2. The observed power outage probabilities (the percentage of frames where a transmission power solution could not be found via perfect power control) are shown in Figures 7.10 and 7.11. The point at which each curve crosses the 0.01 horizontal line determines the estimated capacity of the cell. The curves are occasionally less smooth further away from this line since fewer than 200000 frames were processed for those numbers of mobiles during the initial determination of the interval containing the desired capacity.

There is reasonable agreement between the chip-level and power-level capacity estimates contained in Tables 7.5 and 7.6, and Tables 7.8 and 7.9, respectively. The chip-level simulations likely yielded higher capacity values since a BER of 10^{-3} can be maintained at less than $E_b/N_0 = 7$ dB in the presence of uncorrelated fading as shown by Figure 4.3. Many of the bit errors are likely due to the increased variation in the power control when the system becomes overloaded (as discussed in Section 3.6 and observed by other researchers [4] [39] [75]).

Antenna Elements	Capacity	% of 1 Element Cap.
1	26	100%
2	36	138%
3	58	223%
4	67	258%
5	96	369%
6	107	412%

Table 7.8: Power-level capacity estimates for a single hexagonal cell with perfect beamforming ($\psi = 1.0$)

Antenna Elements	Capacity	% of 1 Element Cap.
1	36	100%
2	57	158%
3	95	264%
4	112	311%
5	158	439%

Table 7.9: Power-level capacity estimates for a single hexagonal cell with perfect beamforming ($\psi = 0.5$)

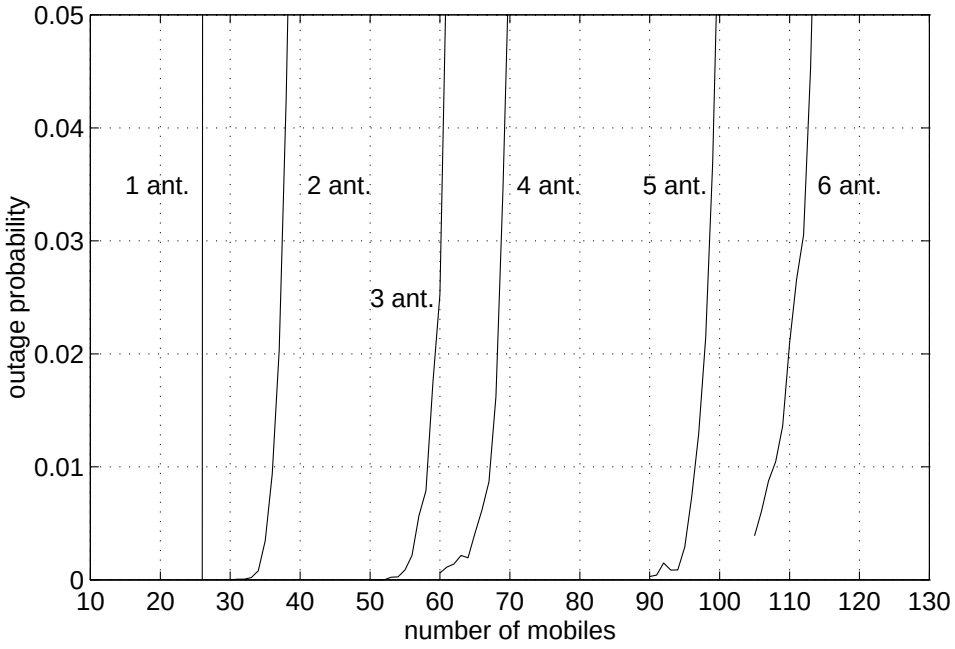

Figure 7.10: Outage probabilities for power-level capacity estimation with perfect beamforming ($\psi = 1.0$)

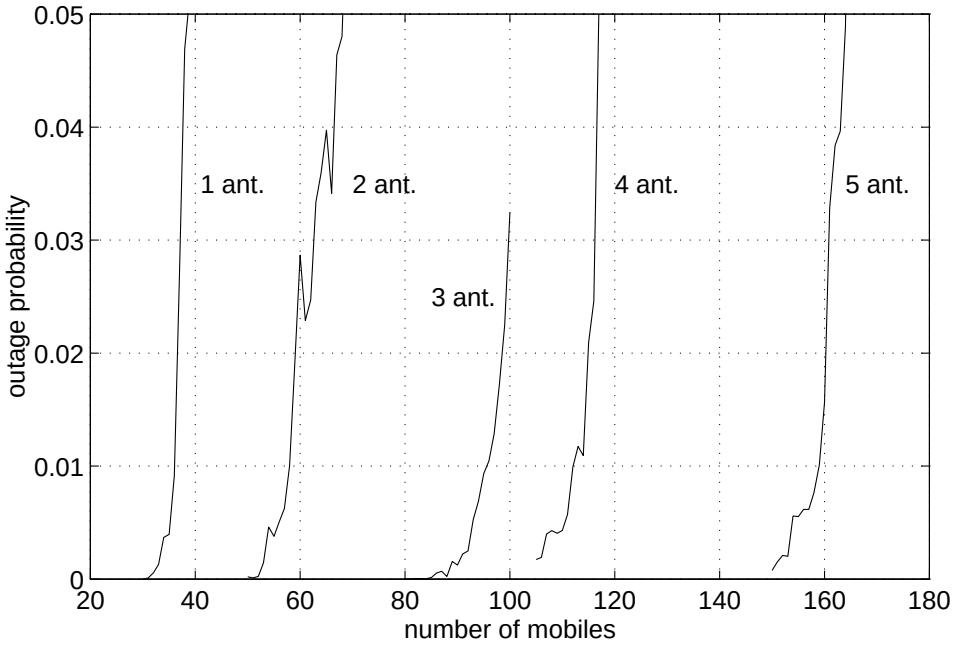

Figure 7.11: Outage probabilities for power-level capacity estimation with perfect beamforming ($\psi = 0.5$)

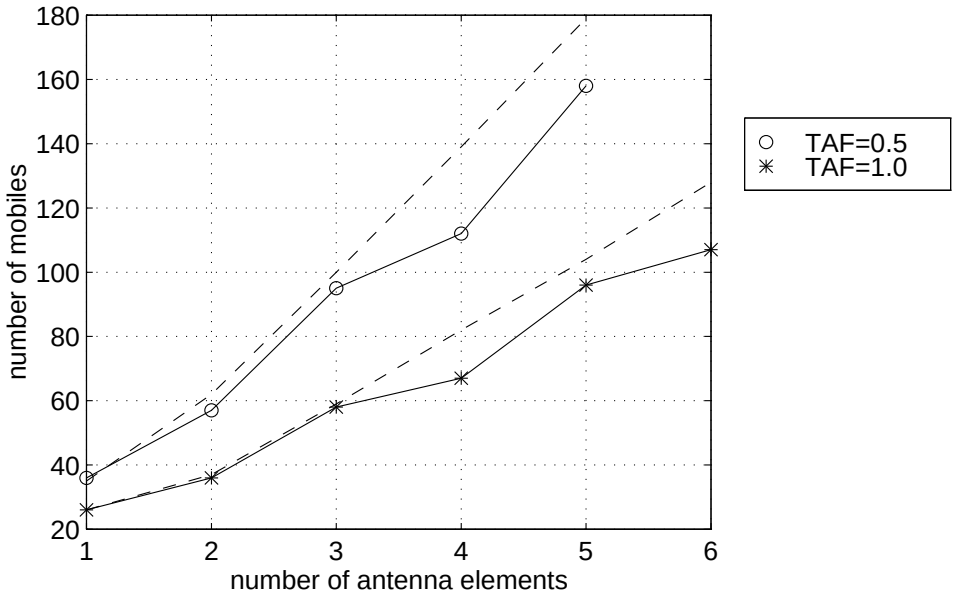

Figure 7.12: Observed and predicted cell capacity values from power-level simulations with perfect beamforming

Finally, Figure 7.12 summarizes the observed cell capacities from power-level simulations with perfect beamforming for voice activity factors of $\psi = 1.0$ and $\psi = 0.5$. In addition, the predicted cell capacities from Tables 7.3 and 7.4 have been included to represent an upper bound on cell capacity. As can be seen, agreement between the predicted and observed values is quite good, especially for 3 or fewer antenna elements. This latter observation may be a little surprising, given that the interference modelling assumption in Section 6.4 was assumed to improve as the number of antenna elements increased, rather than decreased. As observed from Tables 6.3 through 6.5, the expected received power is underestimated as compared to the values obtained from simulations. Since this value forms the basis for the predicted cell capacities, it is not surprising that the predicted values in Figure 7.12 are slightly greater than the estimates obtained from simulations.

7.7.2 Single Cell Capacity with Imperfect Beamforming

Table 7.10 contains chip-level simulation results for imperfect (feedback correlation) beamforming with two antenna elements and a voice activity factor of $\psi = 1.0$. Note

Antenna Elements	Power Control Method	Interleaving	Cell Capacity
1	A	N	26
		Y	27
	B	N	26
		Y	25
2	A	N	45

Table 7.10: Estimated cell capacities from chip-level simulations with feedback correlation beamforming and uncorrelated fading ($\psi = 1.0$)

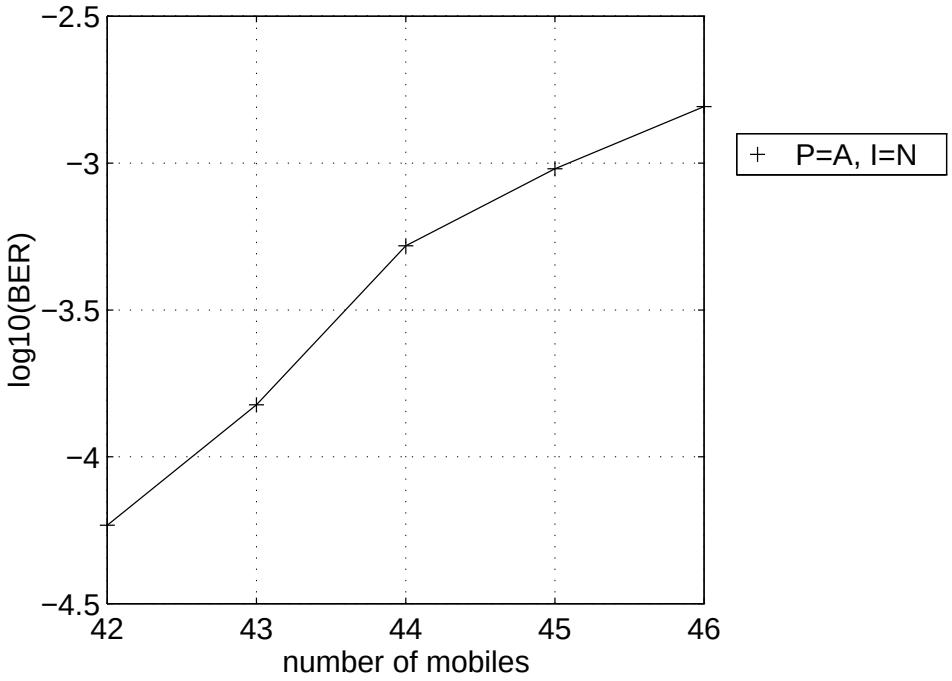

Figure 7.13: Observed BER for PN chip-level capacity estimation with imperfect beamforming ($N_A = 2$, $\psi = 1.0$)

that the single element capacity values are the same as in Table 7.5 since no beamforming is performed for a single antenna element. Figure 7.13 shows the observed BER curve from chip-level simulations with imperfect beamforming for two antenna elements. It is interesting to note that when Figures 7.13 (imperfect beamforming) and 7.3 (perfect beamforming) are compared, it actually appears as though imperfect beamforming yields a higher capacity than does the theoretically optimum perfect beamforming. One possible explanation is that an insufficient number of trials were conducted to obtain fully accurate BER curves due to the computational expense involved. Another potential cause of this effect would be an incorrect implementation of the PN chip level imperfect beamforming algorithm, although significant precautions were taken to guard against the likelihood of this event occurring.

Tables 7.11 and 7.12 show the estimated cell capacities for a single hexagonal cell with voice activity factors of 1.0 and 0.5, respectively. These estimates were obtained using the power-level capacity estimation method with simulated feedback correlation beamforming. Only 100000 frames were processed for each case here, due to the additional computational expense of producing the random beamforming weight estimates. Figures 7.14 and 7.15 show the observed power outage probabilities which were used to determine the cell capacities. By comparing Tables 7.8 and 7.9 to Tables 7.11 and 7.12, it can be seen that the feedback correlation method of estimating beamforming weights performs almost as well as the upper bound of perfect beamforming. The cases where imperfect beamforming appeared to slightly outperform the perfect method were likely due to a requirement for additional simulation frames in order to obtain a more exact capacity estimate.

Finally, Figure 7.16 compares the observed cell capacity estimates for imperfect beamforming from power-level simulations with the predicted values.

7.7.3 Comparison to Other Researchers' Results

As mentioned previously, the work presented within this thesis most closely resembles that performed by Naguib and Paulraj at Stanford University. Of course, there are differences in assumed system parameters and configurations between their work and that contained within this document. However, it is still possible to perform

Antenna Elements	Capacity	% of 1 Element Cap.
1	26	100%
2	36	138%
3	59	227%
4	66	254%
5	95	365%
6	106	408%

Table 7.11: Power-level capacity estimates for a single hexagonal cell with simulated feedback correlation beamforming ($\psi = 1.0$)

Antenna Elements	Capacity	% of 1 Element Cap.
1	36	100%
2	61	169%
3	95	264%
4	113	314%
5	156	433%

Table 7.12: Power-level capacity estimates for a single hexagonal cell with simulated feedback correlation beamforming ($\psi = 0.5$)

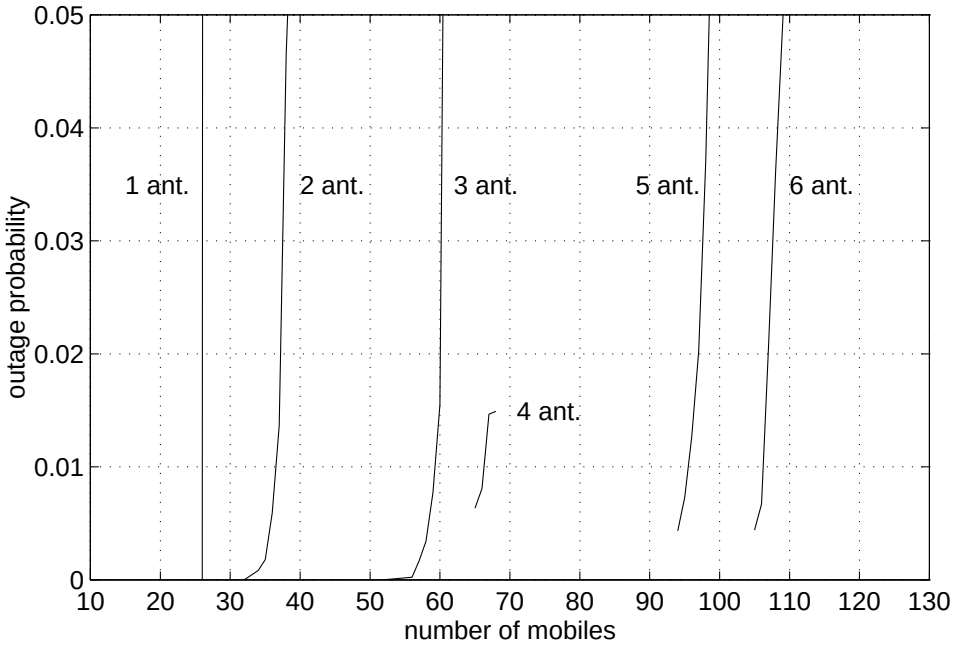

Figure 7.14: Outage probabilities for power-level capacity estimation with simulated feedback correlation beamforming ($\psi = 1.0$)

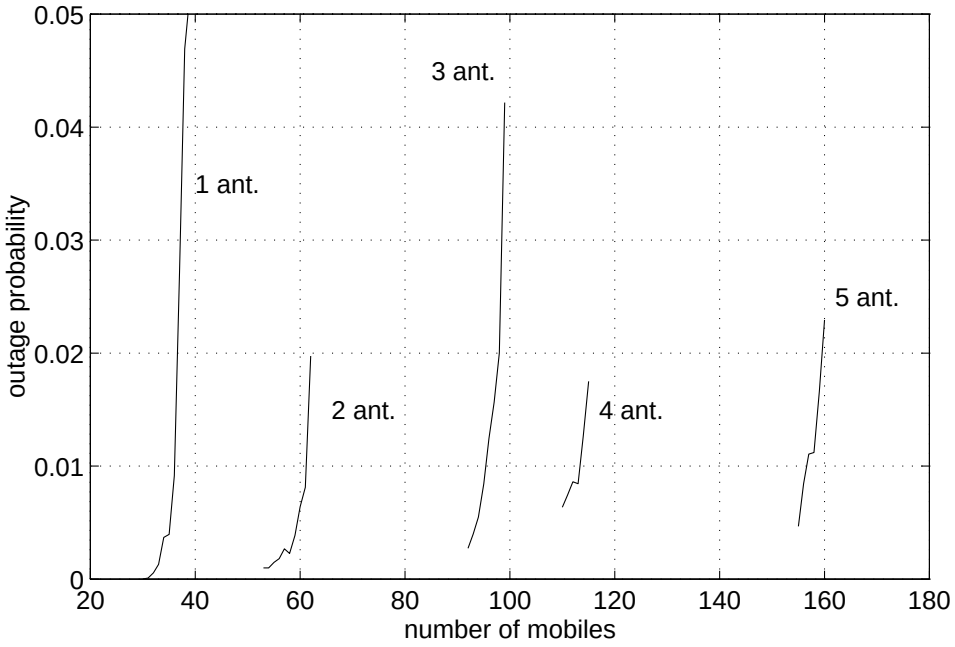

Figure 7.15: Outage probabilities for power-level capacity estimation with simulated feedback correlation beamforming ($\psi = 0.5$)

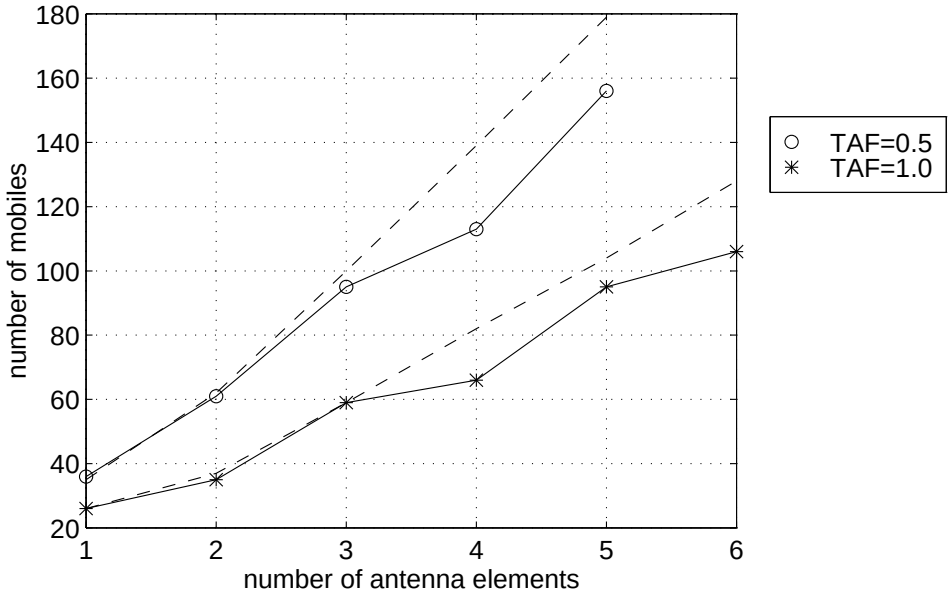

Figure 7.16: Observed and predicted cell capacity values from power-level simulations with simulated feedback correlation beamforming

a comparison of the observed relative capacity improvements due to beamforming with multiple antenna elements in order to ensure that reasonable results have been obtained.

A hexagonal cell with two surrounding tiers of interfering cells and circular antenna arrays was analyzed in [67] and [66] where a 1-D and 2-D RAKE receiver were included in the base station design, respectively. Cell capacity was measured in terms of the system outage probability. Their sample results showed that a 5 element array yielded a cell capacity which was approximately 440% to 450% of the single antenna capacity value, depending upon the actual RAKE receiver being utilized.

A three-sector cell with linear antenna arrays, an equivalent coding scheme to IS-95, and a voice activity factor of 0.375 was considered in [69] [71]. This investigation consisted primarily of an analytical study of expected system performance. For 3 and 5 elements, Naguib and Paulraj predicted improvements of approximately 295% and 495% relative to the single element case.

The corresponding relative capacity improvements from Table 7.9 for a voice activity factor of 0.5 are roughly 260% and 440% for 3 and 5 antenna elements, respectively. These are quite comparable to the values given above and aid to support the validity of the results presented here. An exact correspondence between the observed improvements would not be expected due to differences in the parameter values used (such as the voice activity factor).

7.7.4 Effects of Antenna Array Topology on Capacity

It is interesting to note that in the observed cell capacity results, an exact linear relationship between the number of antenna elements and corresponding cell capacity is not obtained. Instead, when an even number of array elements are used, the capacity increase over the previous number of odd elements is less than expected. This is clearly visible in Figures 7.12 and 7.16 which exhibit a slight staircase-type effect for the observed results. One possible explanation for this phenomenon lies with the antenna array geometry and the corresponding beam patterns that are produced.

Figures 7.17 through 7.21 show sample beamforming patterns for the indicated directions of arrival for 2 to 6 antenna elements, respectively. One antenna element is

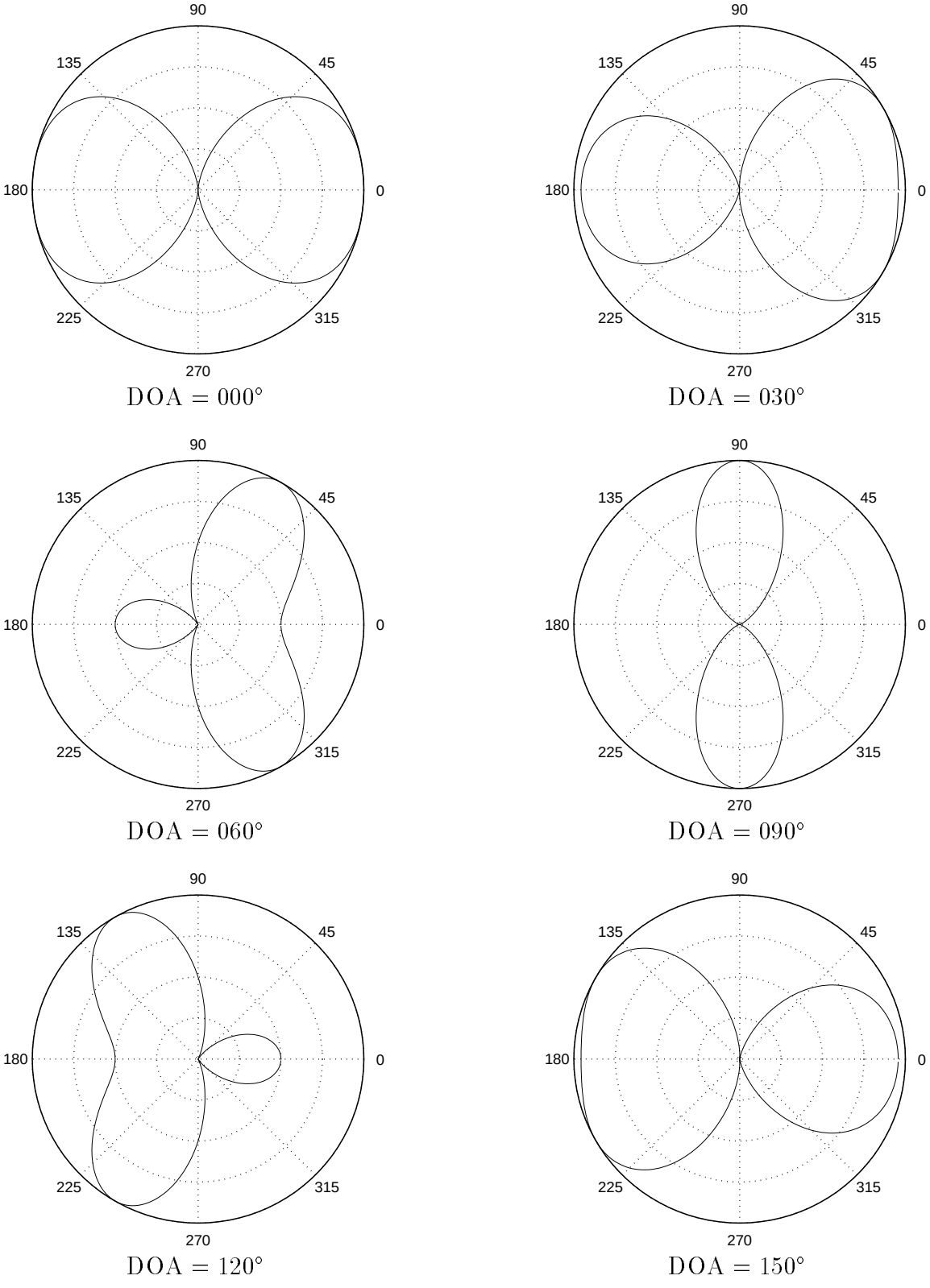

Figure 7.17: Beamforming patterns for 2 antenna elements (circular array)

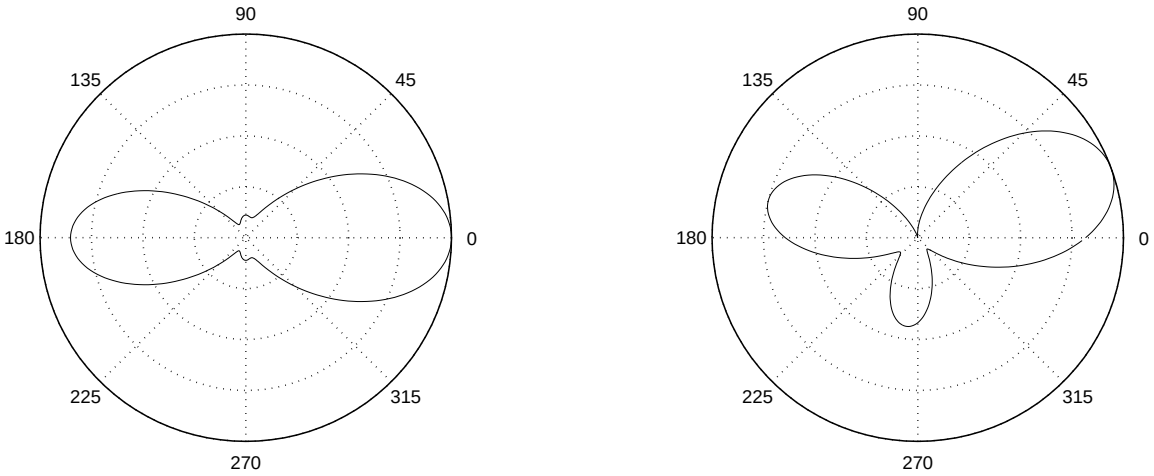

DOA = 000°

DOA = 020°

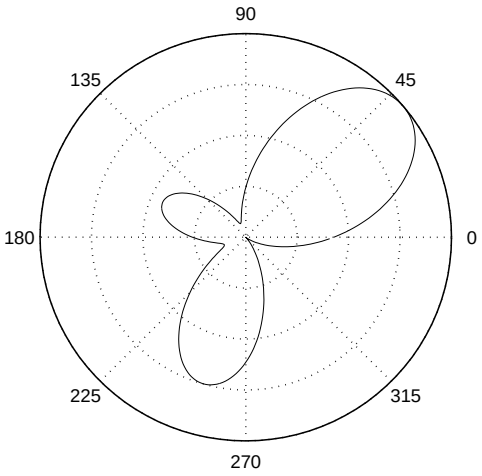

DOA = 040°

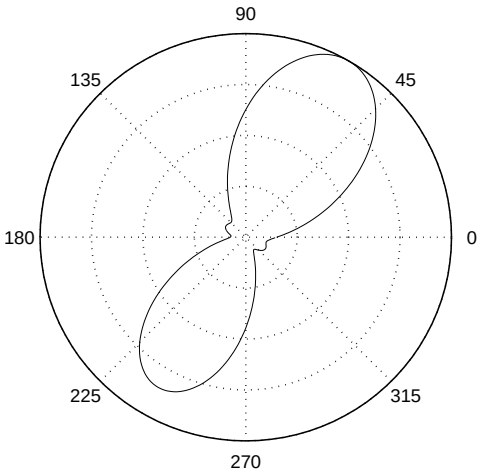

DOA = 060°

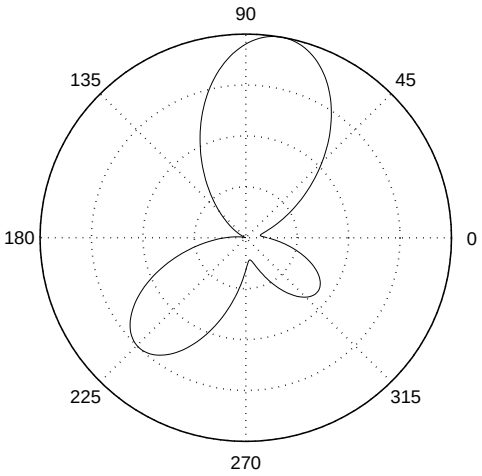

DOA = 080°

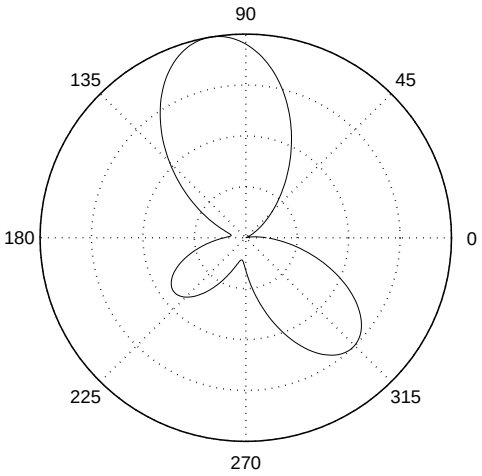

DOA = 100°

Figure 7.18: Beamforming patterns for 3 antenna elements (circular array)

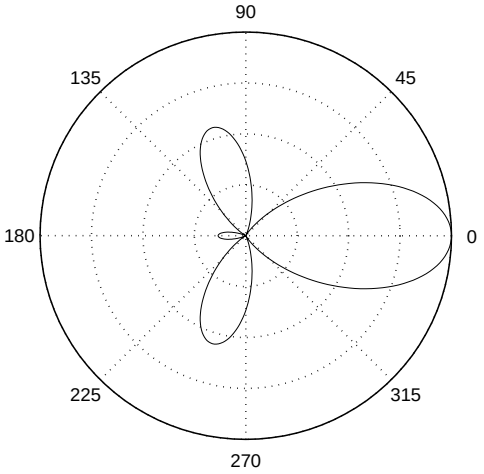

DOA = 000°

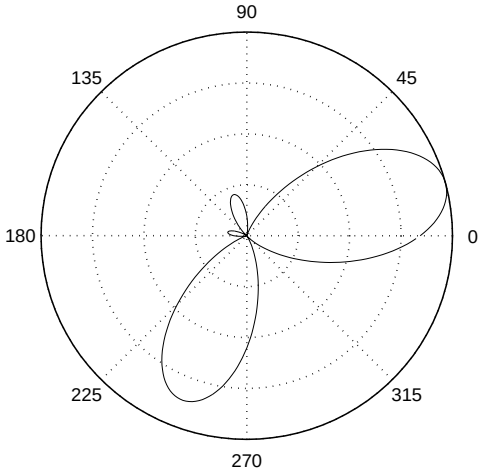

DOA = 015°

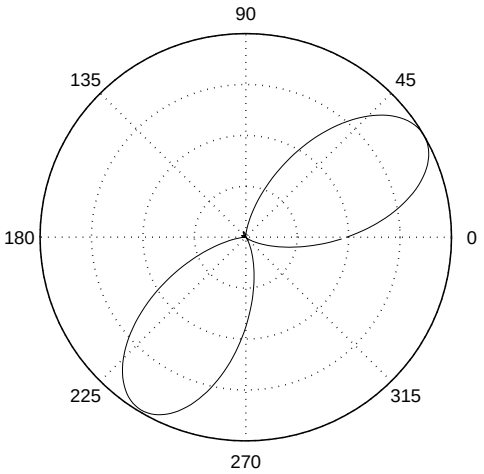

DOA = 030°

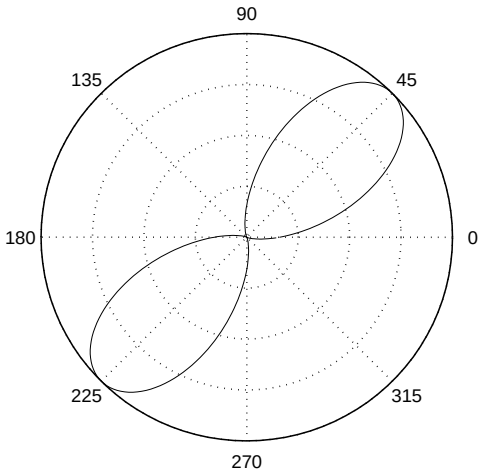

DOA = 045°

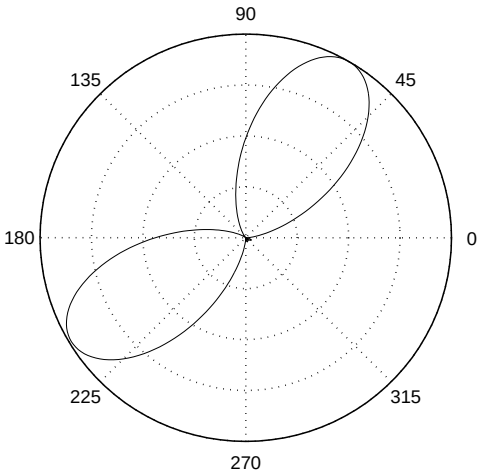

DOA = 060°

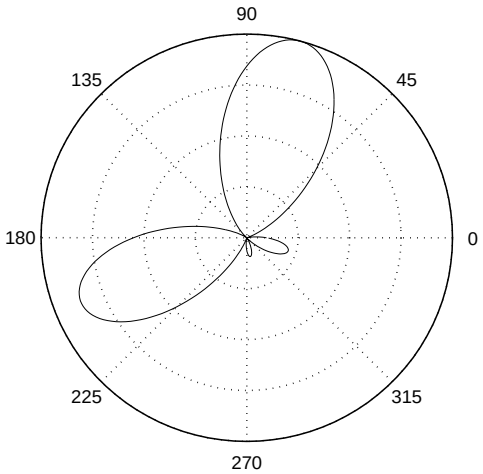

DOA = 075°

Figure 7.19: Beamforming patterns for 4 antenna elements (circular array)

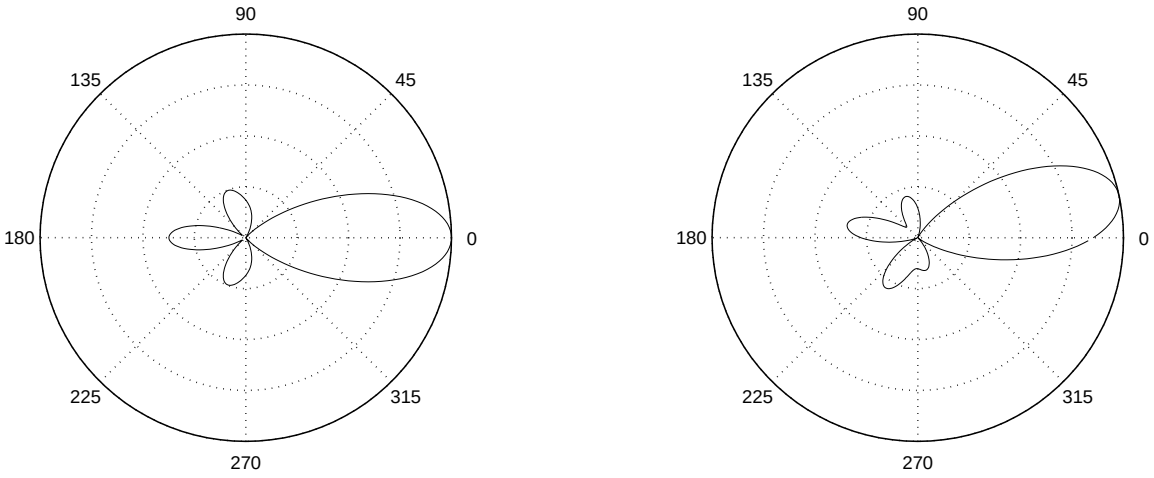

DOA = 000°

DOA = 012°

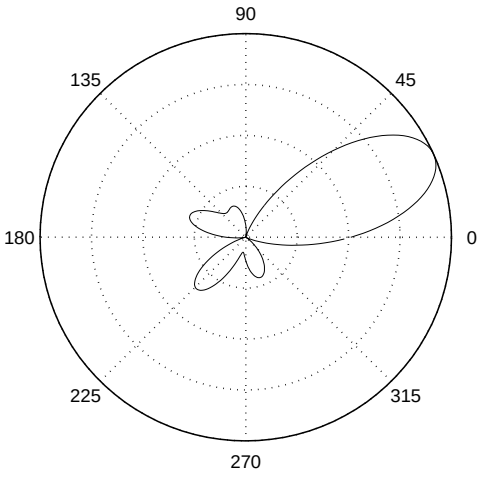

DOA = 024°

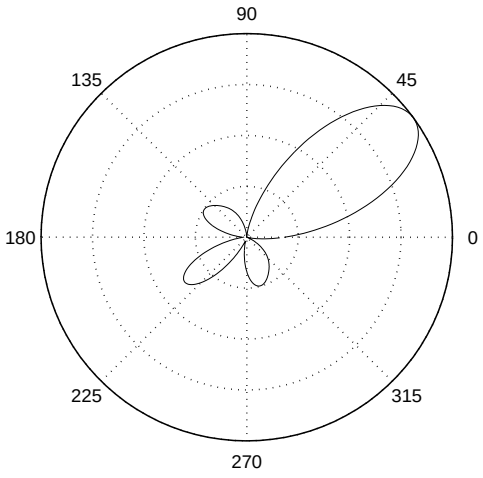

DOA = 036°

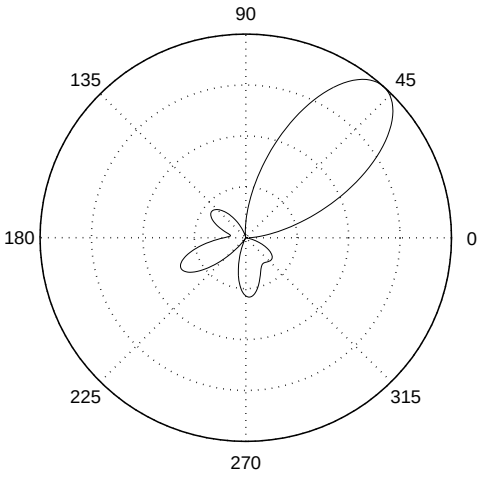

DOA = 048°

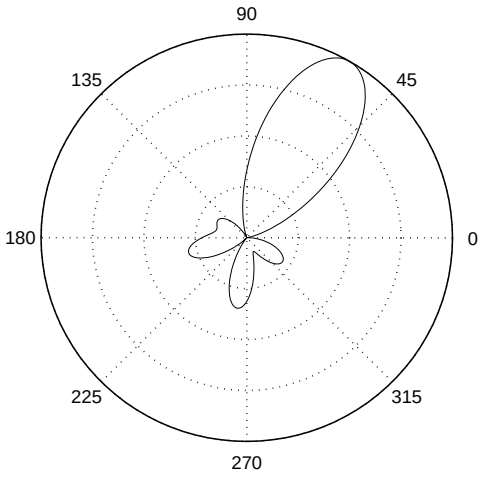

DOA = 060°

Figure 7.20: Beamforming patterns for 5 antenna elements (circular array)

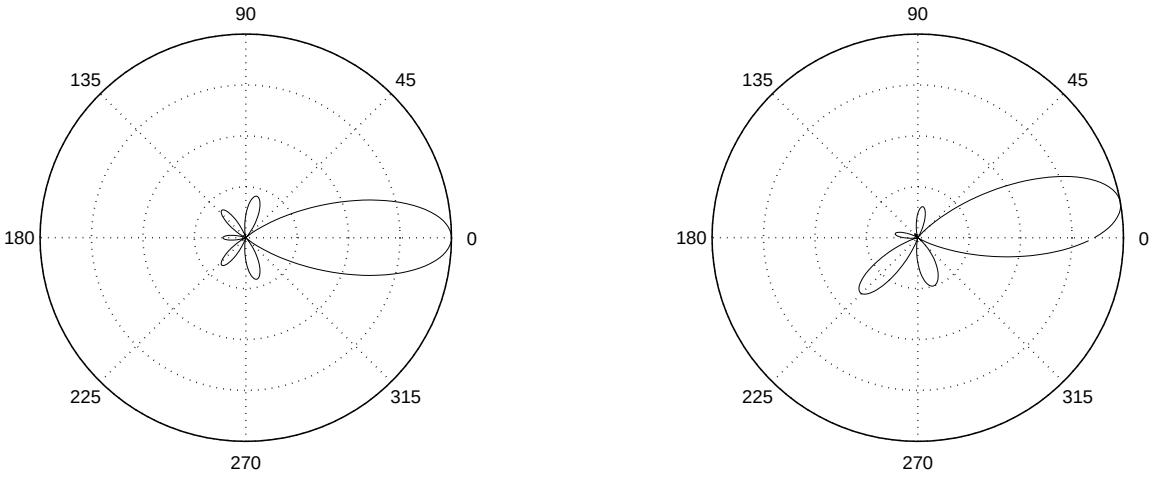

DOA = 000°

DOA = 010°

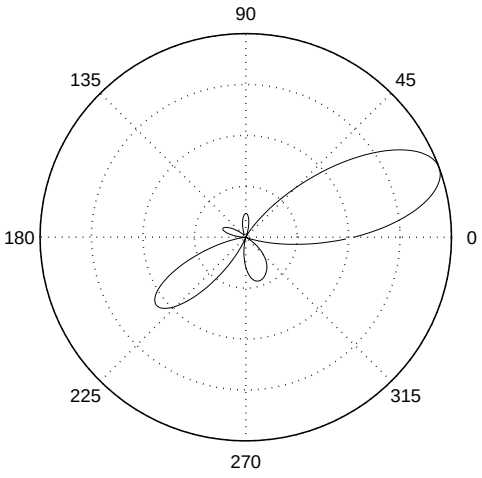

DOA = 020°

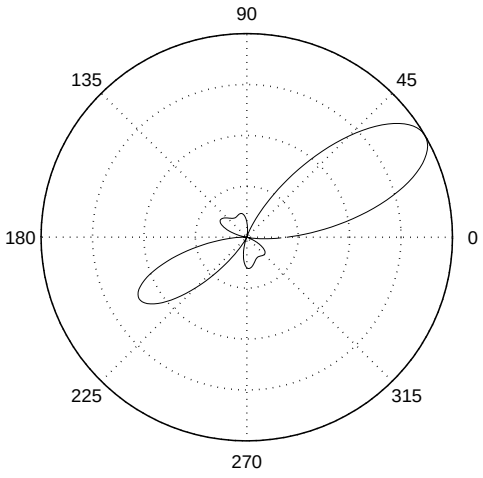

DOA = 030°

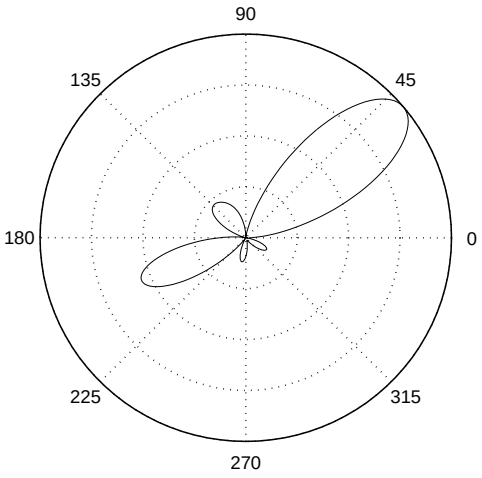

DOA = 040°

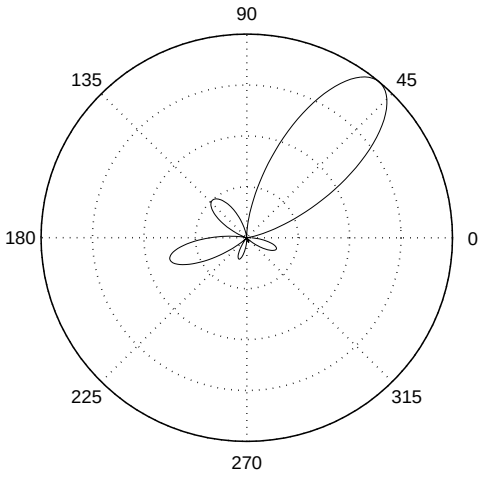

DOA = 050°

Figure 7.21: Beamforming patterns for 6 antenna elements (circular array)

always located at 0° on the circle, with the remaining elements being spaced evenly at $\lambda_c/2$ intervals to produce a circle. The direction of arrival (DOA) indicates the direction from which the desired signal propagates, and the beamforming weights are assumed to correspond to the array response vector (*i.e.* perfect beamforming). The beam patterns represent the attenuation due to beamforming of an interferer's power whose signal arrives from another direction relative to the received power from the desired mobile. For example, in Figure 7.17 with a DOA of 0°, signals arriving from either 0° or 180° are not suppressed at all. Conversely, signals arriving from 90° and 270° will be completely suppressed. Interfering signals arriving from 45°, 135°, 225°, and 315° will retain approximately 80% of their power (*i.e.* 20% attenuation). The sample directions of arrival only cover a range of $360/N_A$ degrees, since the beamforming patterns will repeat after that range due to the symmetry of the circular antenna array.

One interesting effect observed by comparing DOA = 090° and DOA = 045° in Figures 7.17 and 7.19, respectively, is that the 4 element array can reduce to an equivalent of a 2 element array. In addition, by comparing the secondary lobes for 4 elements (DOA = 045°) versus 3 (DOA = 060°), and 6 elements (DOA = 030°) versus 5 (DOA = 036°), it can be seen that the antenna arrays with even numbers of elements have larger secondary lobes for certain directions of arrival. Thus, interference power from certain directions will be less attenuated, and this may account for the less-than-expected increase in cell capacity for the antenna arrays with even numbers of elements.

7.8 Multi-Cell Capacity

Although the single cell simulations give a good indication as to the type of capacity increases that can be obtained through the use of beamforming, a multi-cell environment with interference occurring between adjacent cells is clearly more realistic in nature. Consequently, sample multi-cell simulations have been performed to explore the difference between the single cell and multi-cell cases. However, it should be remembered that these simulations are computationally expensive due to the large

numbers of mobiles, so their scope is restricted to some illustrative examples.

One advantage of CDMA is that adjacent cells are able to use the same frequency bandwidth allocations since undesired signals are treated as interference. Consequently, it is possible to increase capacity in a given area by splitting a given cell into smaller cells. Kajiwara [41], for example, investigated the effects of cell size (and indirectly the number of cells) on total capacity in a CDMA system using directional antennas. This study was accomplished via computer simulations, although exact details of the nature of the simulations do not seem to be provided. With directional antennas, capacity increases were found to be roughly proportional to the number of cells.

In this multi-cell investigation, a square area measuring 1200 m on each side was considered, and the power-level capacity estimation method with perfect beamforming was used to obtain results. The tested cell configurations were one square cell with a radius of 600 m, a 3×3 grid of square cells each with radius 200 m, and a 5×5 grid of cells each with radius 120 m. It would be expected that per cell capacity would decrease as the number of cells increases due to increased intercell interference. However, the total capacity for the same area of land should increase as the number of base stations increases. With more base stations, mobiles will be able to interact with a base that is less distant. Therefore, a lower transmission power will be required and the interference to other users will decrease. Although the cell sizes vary in this experiment, depending on the number of cells being considered, this simply affects a scaling factor by which all of the transmission power values would be multiplied. Consequently, modifying the sizes of the cells would not affect the observed capacity values, and this example serves as a valid multi-cell scenario.

Table 7.13 contains the total system and per cell capacity values, and Figures 7.22 through 7.24 show the corresponding outage curves from which the capacity estimates were obtained. By comparing the single cell capacities (1×1 grid) for a square cell with those for a hexagonal cell in Table 7.8, it can be seen that almost exact agreement is obtained, so it is more likely that the staircase capacity effect discussed in Section 7.7.4 is due to the antenna array topology rather than being an artifact of the assumed cell geometry. In Table 7.13, cell capacity is clearly reduced

Antennas	Cell Grid	System Capacity	Per Cell Capacity	% Increase
1	1×1	26	26.0	100%
	3×3	129	14.3	496%
	5×5	309	12.4	1188%
2	1×1	36	36.0	100%
	3×3	217	24.1	603%
3	1×1	59	59.0	100%
	3×3	339	37.7	575%

Table 7.13: Capacity estimates for varying numbers of cells for a given area ($\psi = 1.0$)

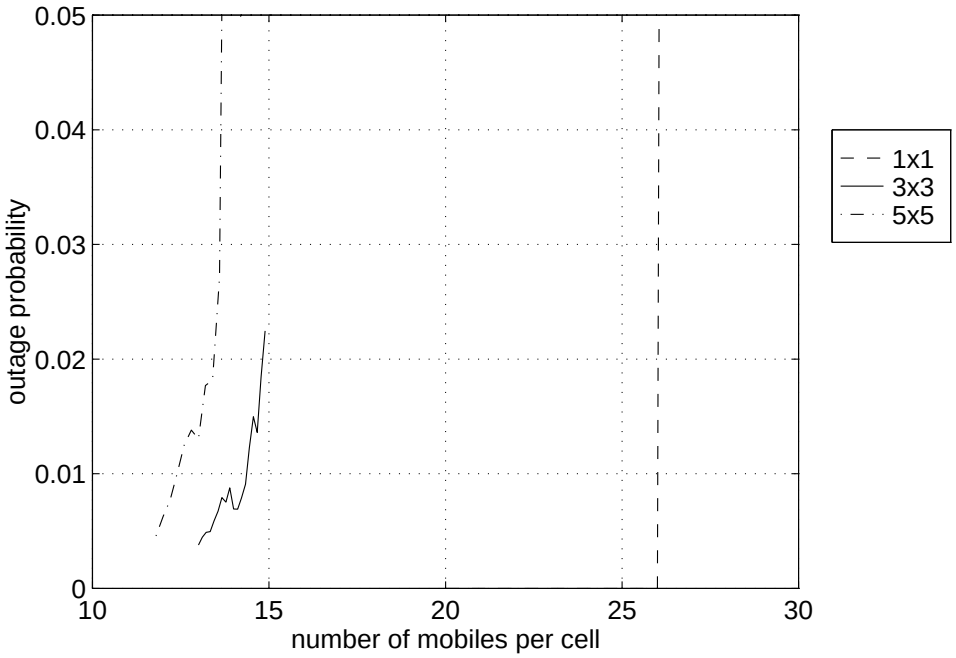

Figure 7.22: Outage probabilities for power-level capacity estimation in multi-cell simulations with perfect beamforming ($N_A = 1$, $\psi = 1.0$)

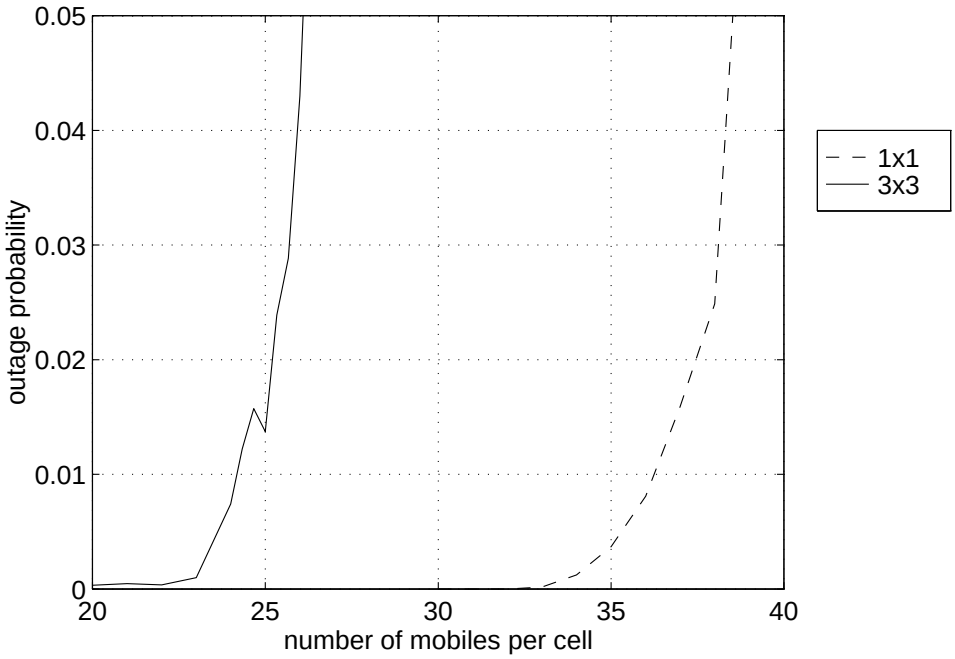

Figure 7.23: Outage probabilities for power-level capacity estimation in multi-cell simulations with perfect beamforming ($N_A = 2$, $\psi = 1.0$)

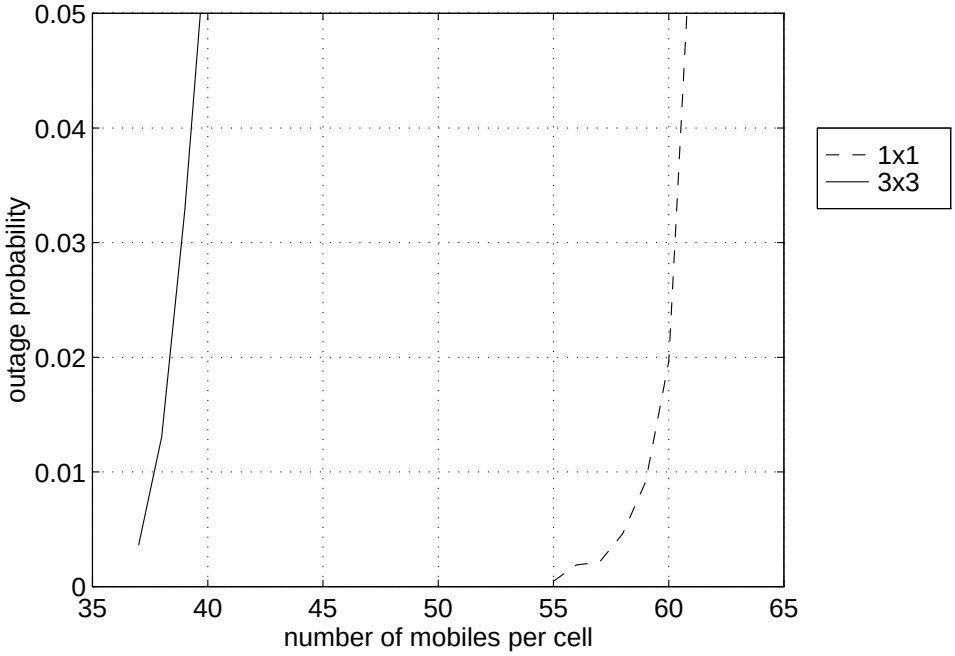

Figure 7.24: Outage probabilities for power-level capacity estimation in multi-cell simulations with perfect beamforming ($N_A = 3$, $\psi = 1.0$)

as the number of cells is increased due to increasing intercell interference. This effect appears to be most pronounced when going from a 1×1 grid to a 3×3 configuration. The 5×5 grid considered for a single antenna element indicates that per cell capacity is further reduced by additional intercell interference, but not to as great an extent. Consequently, 5×5 cell grids were not considered for the cases of two and three antenna elements due to computational expense.

Even though the per cell capacity was dramatically reduced by the introduction of intercell interference, the total system capacity for a multi-cell configuration was found to increase significantly. The final column in Table 7.13 lists the relative increase in system capacity as compared to the single cell case with the same number of antenna elements. It appears as though total capacity can be increased by a factor of between 5 and 6 when a 3×3 grid of cells is used as compared to a single cell. It should be noted, however, that in a true large-scale system, the observed increase should be larger since the 1×1 cell grid would also be subject to intercell interference which was not the case in this particular simulation study.

Note that as the number of cells increases and cell size decreases, it is likely that an increased number of hand-offs between cells will be required as mobiles move around. This is a significant research area in itself and has not been considered within the context of this thesis.

7.9 Multi-Service Cell Capacity

7.9.1 Introduction

In future wireless communication networks, there will be a demand for services other than voice. For example, video and data file transfers will be equally as important in a multimedia environment. These services, of course, will require a higher bandwidth than does voice and are also more likely to be continuously operating (*i.e.* a transmission activity factor of $\psi = 1.0$).

It is possible to emulate a mixed voice and data environment fairly easily with the existing simulation program. As before, voice is assumed to be transmitted at 9600 bits per second, while data is sent at 64 kilobits per second. Thus, a data mobile

can be easily simulated by positioning seven voice mobiles at the same location and synchronizing them in time. Each group of seven mobiles has the same path loss, shadowing, and Rayleigh fading values, and also responds to the closed-loop power control identically. Recalling that voice actually has 9200 data bits per second (the remaining 400 represent coding overhead), it can be seen that this corresponds to a data rate of 64400 bits per second. In addition, voice mobiles are assumed to have an activity factor of $\psi = 0.5$, whereas data mobiles have a transmission activity factor of $\psi = 1.0$.

The above method for modelling data mobiles is very similar to that proposed for the MC-CDMA (multicode CDMA) system described in [35]. This is a packet-based wireless system which can accommodate multimedia traffic. MC-CDMA preserves the existing physical layer of IS-95 by allocating multiple streams for a single user when a higher bit rate than the base rate is required. The LIDA (Load- and Interference-Based Demand Assignment) network is also discussed in this paper. This network design protects voice users in a communications system from the bursty demand of high-bandwidth data users. Sourour and Nakagawa [97] also investigated the performance of an orthogonal multicarrier CDMA system which converted a high data rate bit stream into a set of parallel lower rate streams.

A circular cell of radius 500 m was used for simulation purposes with a desired E_b/N_0 of 7 dB and Rayleigh fading. It should be noted that in reality, a BER of 10^{-3} is acceptable for voice, but a lower BER would be required for other types of communication such as video. Thus, the capacity values presented here represent an upper bound since the data mobiles should really have a higher E_b/N_0 than 7 dB. Wu and Kohno [113] developed methods for the optimum allocation of transmission power in a multimedia wireless CDMA system where the different media have different acceptable BER values and priorities. Their algorithms used channel measurement information such as traffic amounts and patterns to determine the optimum power allocation.

Cell capacity was determined in this instance by using the power-level capacity estimation method with perfect power control and perfect beamforming. For a given number of data mobiles, a binary search was performed to determine the number of

voice mobiles which produced an observed outage probability of 1%. The number of frames processed for each search point varied depending on computational expense, but sufficient frames were used to ensure a reasonable sampling of the distribution of speech-active voice mobiles.

7.9.2 Multi-Service Capacity Predictions

7.9.2.1 Single Antenna Element

For the case of a single antenna element, it is possible to easily predict the approximate expected cell capacity for a multi-service situation. This is accomplished by modifying equation (7.21) as shown below.

$$E[P] = \left(\frac{E_b}{N_0}\right)\sigma_n^2 \sum_{n_I=0}^{N_V-1} P(N_I = n_I) \left\{\frac{1}{R_B} - \frac{1}{B}\left(\frac{E_b}{N_0}\right)\left(7N_D + n_I + \frac{N_V - n_I - 1}{\nu}\right)\right\}^{-1} \tag{7.28}$$

N_D represents the number of data mobiles, and N_V the number of voice mobiles.

To predict cell capacity for a given number of data mobiles, N_D is fixed at the desired value and then N_V is increased until a negative power value is obtained, at which point the predicted capacity of the cell has been exceeded.

7.9.2.2 Multiple Antenna Elements

When multiple antenna elements are utilized, it is necessary to reconsider part of the multi-element power value calculation originally presented in Section 6.4. The sin/cos term defined in (6.38) for a voice mobile can be approximated by a central χ^2 distribution with parameters:

$$(\mu_\Upsilon)_V = 2\left(\frac{1}{2}\sigma_S^2\right) = \frac{1}{2}N_A \tag{7.29}$$

$$(\sigma_\Upsilon^2)_V = 4\left(\frac{1}{2}\sigma_S^2\right)^2 = \frac{1}{4}(N_A)^2 \tag{7.30}$$

Note that equation (6.38) is simply multiplied by 7 (the number of voice mobiles which represent one data mobile) when a data mobile interferer is being considered.

Thus, for a data mobile, the χ^2 distribution parameters are:

$$(\mu_\Upsilon)_D = 7(\mu_\Upsilon)_V = \frac{7}{2}N_A \tag{7.31}$$

$$(\sigma^2_\Upsilon)_D = (7)^2(\sigma^2_\Upsilon)_V = \frac{49}{4}(N_A)^2 \tag{7.32}$$

When N_D data mobiles and N_V voice mobiles (N_I of which have active speech) are considered, the summation of the above interference random variables can still be approximated as Gaussian via the Central Limit Theorem with the following parameters.

$$\begin{aligned}\mu_V &= N_D(\mu_\Upsilon)_D + \left(N_I + \frac{N_V - 1 - N_I}{\nu}\right)(\mu_\Upsilon)_V \qquad (7.33)\\ &= \frac{1}{2}N_A\left[7N_D + \left(N_I + \frac{N_V - 1 - N_I}{\nu}\right)\right]\\ \sigma^2_V &= N_D(\sigma^2_\Upsilon)_D + \left(N_I + \frac{N_V - 1 - N_I}{\nu^2}\right)(\sigma^2_\Upsilon)_V \qquad (7.34)\\ &= \frac{1}{4}(N_A)^2\left[49N_D + \left(N_I + \frac{N_V - 1 - N_I}{\nu^2}\right)\right]\end{aligned}$$

Similarly to (6.50), the expected received power can be calculated as a weighted sum.

$$E[P] = \frac{1}{2}(N_A)^3\left(\frac{E_b}{N_0}\right)\sigma_n^2 \sum_{N_I=0}^{N_V-1} P(N_I = n_I)E\left[\left\{\frac{(N_A)^2}{2R_B} - \frac{1}{B}\left(\frac{E_b}{N_0}\right)V\right\}^{-1}\right] \tag{7.35}$$

Note that in (7.35), V is a function of the current value of N_I.

It is now simply necessary to fix the value of N_D in (7.33) and (7.34), and then to increase N_V until the probability of obtaining a negative power value during the numerical integration of (7.35) exceeds the chosen threshold of 1%.

7.9.3 Multi-Service Results

Figure 7.25 shows the observed voice/data cell capacity from simulations for 1, 2, 3, and 4 antenna elements, using the standard IS-95 bandwidth of 1.2288 MHz. The corresponding predicted values are contained in Figure 7.26. Obviously, as the number of active data mobiles within the cell increases, the allowable number of voice mobiles simultaneously decreases.

Figure 7.27 shows the total observed throughput of the cell for a given number of antenna elements and data mobiles at 1.2288 MHz, and Figure 7.28 contains the corresponding predictions. Throughput is measured in terms of equivalent full-time voice

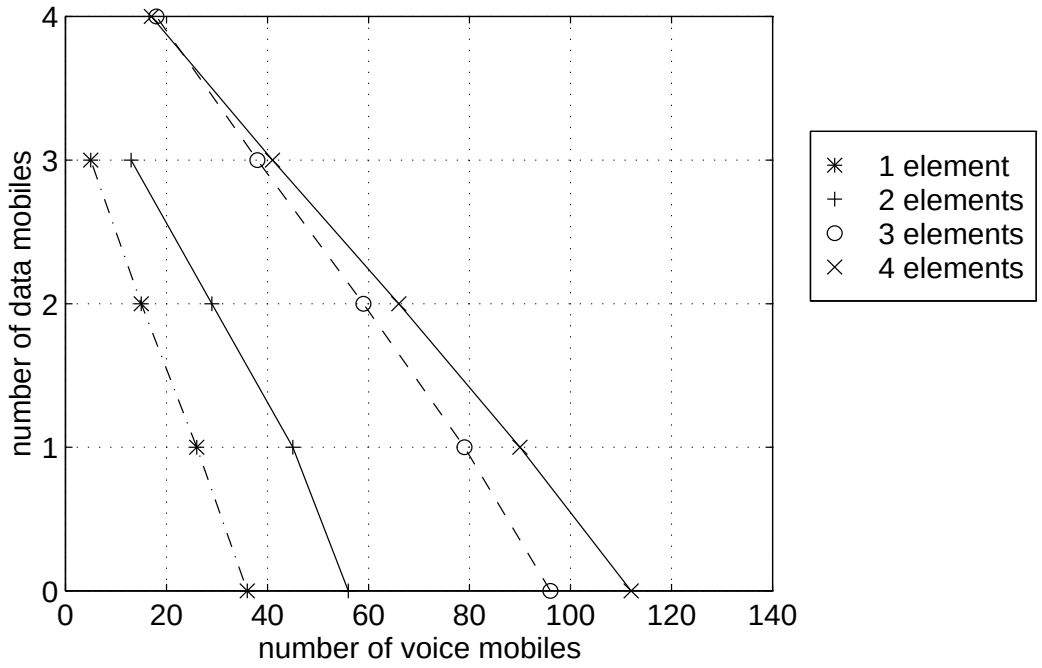

Figure 7.25: Observed multi-service voice and data user capacity for 1.2288 MHz

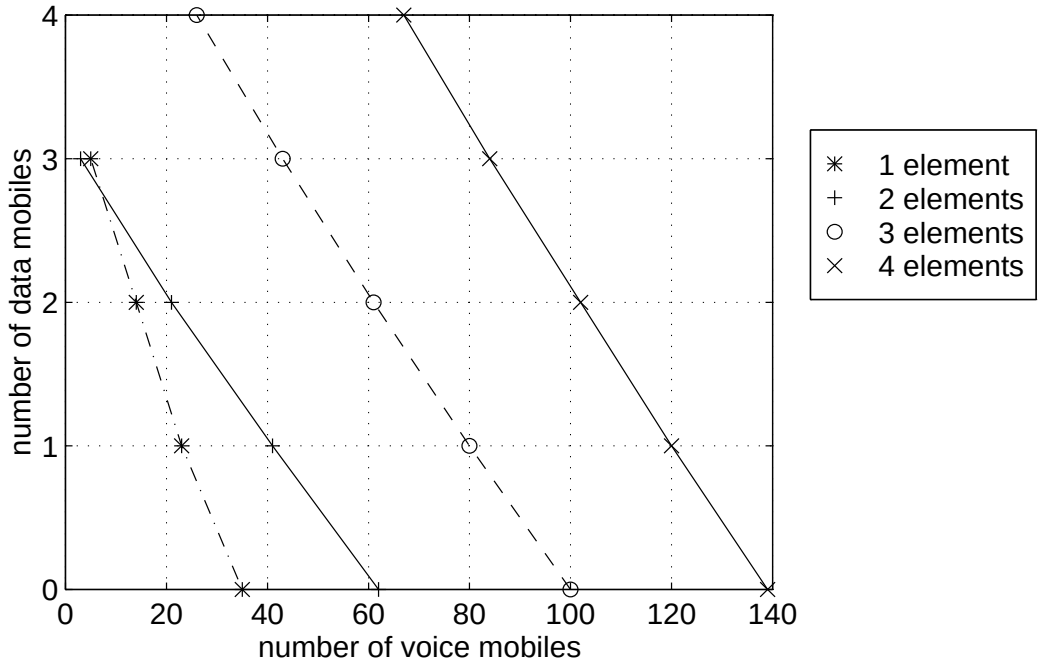

Figure 7.26: Predicted multi-service voice and data user capacity for 1.2288 MHz

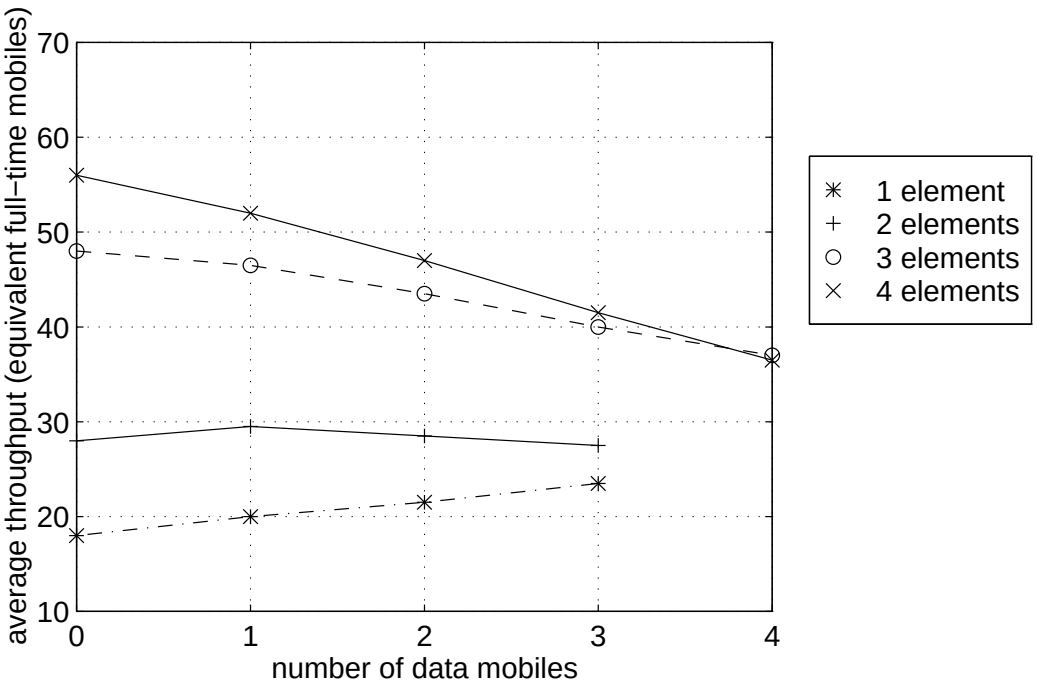

Figure 7.27: Observed multi-service total cell throughput for 1.2288 MHz

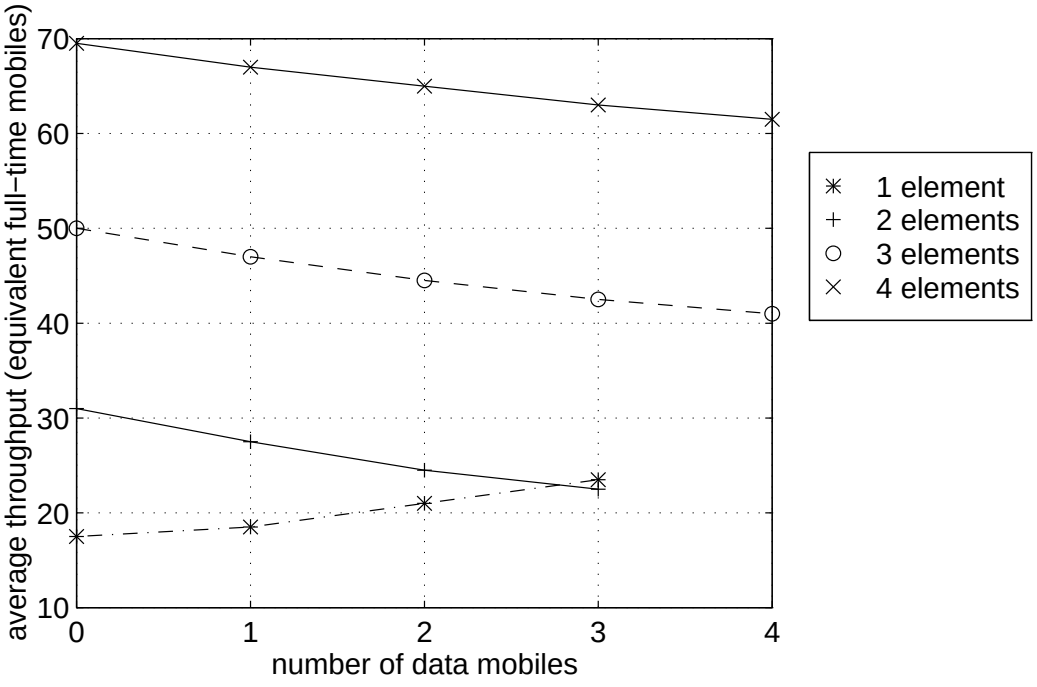

Figure 7.28: Predicted multi-service total cell throughput for 1.2288 MHz

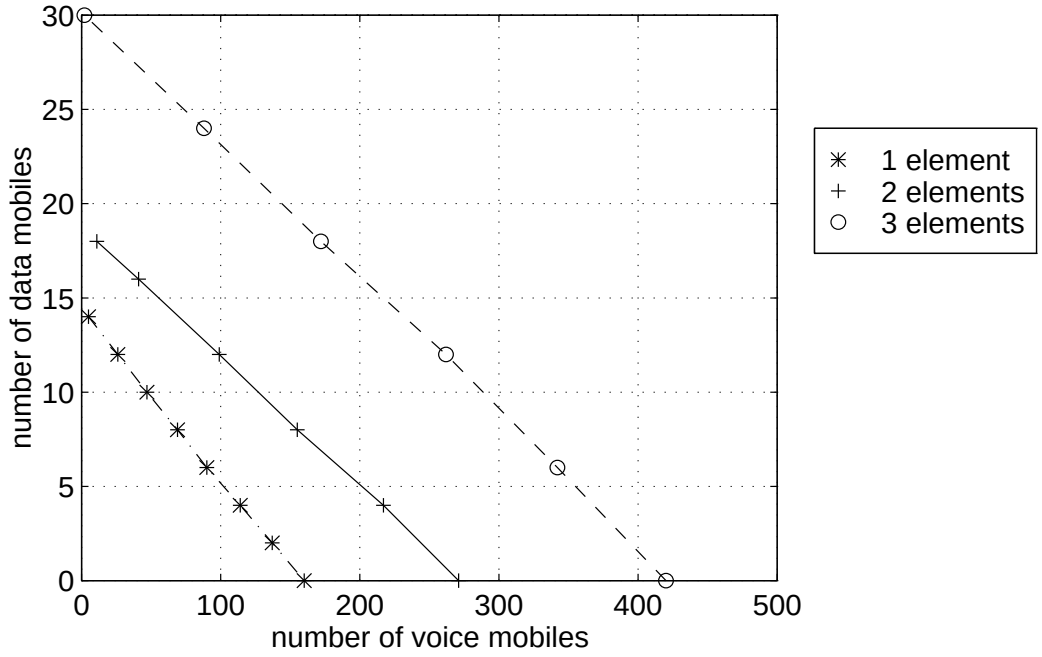

Figure 7.29: Observed multi-service voice and data user capacity for 4.9152 MHz

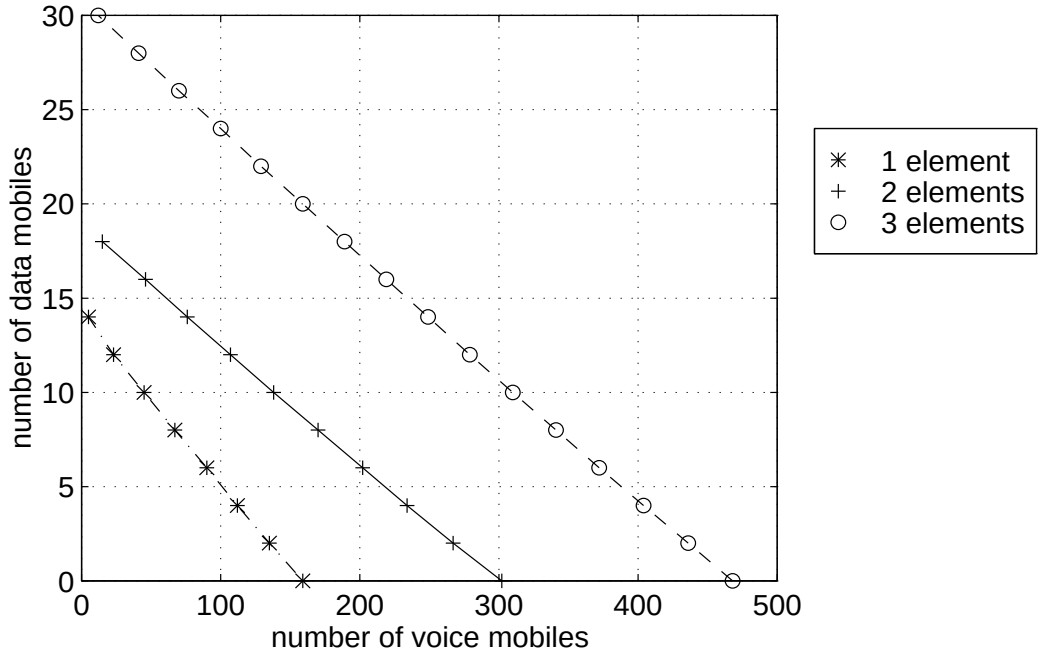

Figure 7.30: Predicted multi-service voice and data user capacity for 4.9152 MHz

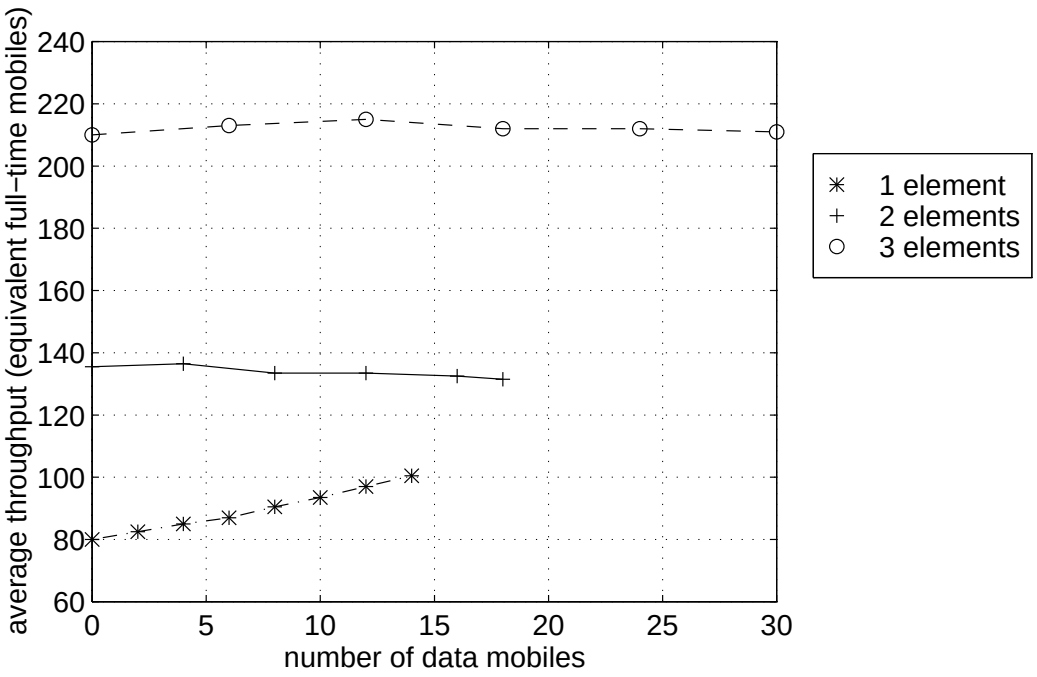

Figure 7.31: Observed multi-service total cell throughput for 4.9152 MHz

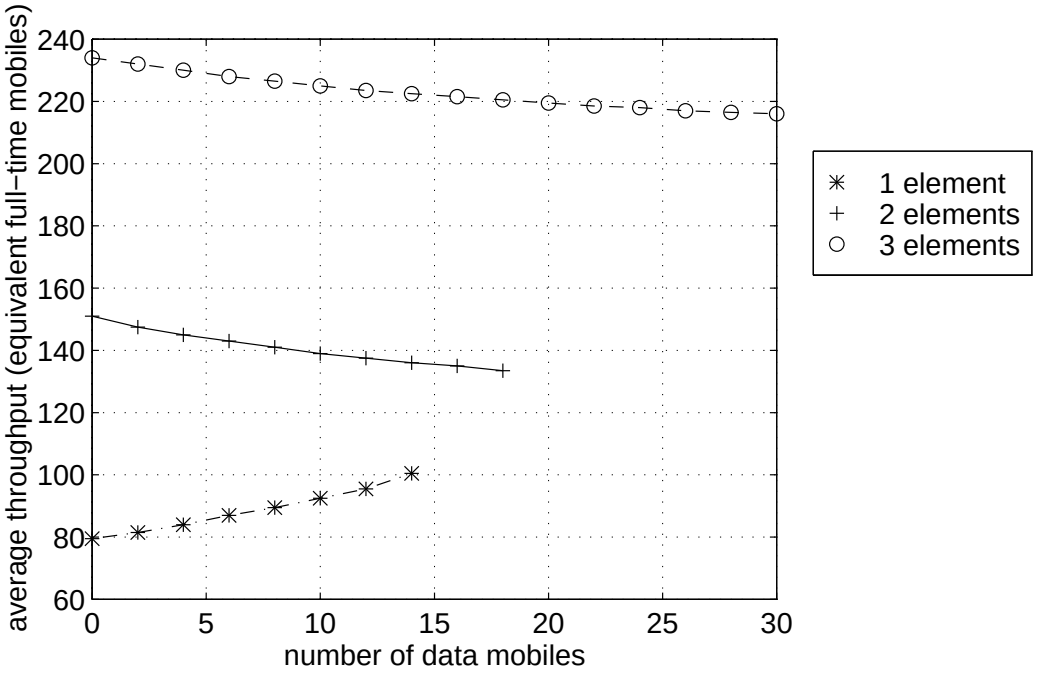

Figure 7.32: Predicted multi-service total cell throughput for 4.9152 MHz

mobiles. Therefore, each data mobile corresponds to seven full-time voice mobiles, and each regular voice mobile to one-half.

As can be seen, the relatively narrow bandwidth of standard IS-95 is not particularly suitable for multimedia services. A maximum of only 3 or 4 data mobiles can be accommodated within the cell. In addition, very little improvement is observed when going from 3 to 4 antenna elements. The clustering effect of the data mobiles significantly reduces the validity of the white interference and noise assumption, thereby reducing capacity. In this instance, it may be more advantageous to select beamforming coefficients such that nulls are steered towards any interfering data mobiles. When beamforming is used, the overall throughput decreases as the number of data mobiles goes up. The observations and predictions for 1 and 3 antenna elements agree quite well, with reasonable agreement for 2 elements, and poor correlation for 4 elements. This latter situation is likely due to a combination of the antenna array geometry and corresponding beam patterns as discussed in Section 7.7.4 and the small number of data mobiles that can actually be accommodated in the cell.

To increase cell capacity, despite the higher volumes of data which must be transmitted in this situation, a higher spreading factor and a bandwidth of approximately 5 MHz can be used. Since no definitive coding standard yet exists for this type of multimedia network, the IS-95 coding method was retained with an increase in the PN spreading factor from 4 to 16, thereby resulting in a bandwidth of 4.9152 MHz.

Figure 7.29 shows the observed voice/data cell capacity from simulations for 1, 2, and 3 antenna elements, with Figure 7.30 containing the corresponding predicted values. Clearly, capacity in terms of the total number of data mobiles which can be accommodated has increased significantly over the 1.2288 MHz system. In addition, there is quite good correspondence between the observed and predicted results.

Figure 7.31 shows the total observed throughput of the cell for a given number of antenna elements and data mobiles, and Figure 7.32 contains the corresponding predicted total throughput. As can be seen, throughput for a single antenna element actually increases as the number of data mobiles increases. This is likely due to the voice activity factor of the voice mobiles being less than unity. The number of voice

mobiles which currently have active speech is a random variable which follows a binomial distribution. This quantity will vary over time within a reasonable range of values. Consequently, in order to ensure that a power control outage does not occur if significantly more than half of the voice mobiles have active speech, it is necessary to reserve a certain amount of the cell throughput which will not be utilized all of the time (*i.e.* when fewer voice mobiles have active speech). In addition, voice mobiles which are not currently transmitting speech do not contribute towards the cell throughput, but they still produce a certain amount of interference, albeit at reduced power. However, the data mobiles transmit continuously with constant throughput. In effect, the data mobiles can utilize cell throughput more efficiently than can the voice mobiles. Thus, when the number of data mobiles is increased and the number of voice mobiles is decreased, the cell throughput can be utilized more efficiently. Conversely, the cell throughput for multiple antenna elements appears to stay relatively constant regardless of the number of data mobiles. In a beamforming situation, it would be expected that the data mobiles would degrade system performance to some extent by reducing the uniformity of the spatial distribution of the users. However, it would appear that this is offset by the voice activity factor effect which was observed for a single base station antenna.

7.10 Summary

This chapter has presented an investigation into estimating cell capacity in a CDMA system, both through theoretical analyses and simulations. Two simulation methods were utilized: a PN chip-level approach and a more computationally efficient power-level method. Sample execution times demonstrated the computational savings offered by the latter technique. In simulation experiments, reasonable agreement was obtained between these capacity estimation methods, as well as with the predicted capacity values obtained by considering the expected received power values. These latter predictions tended to be slightly optimistic when multiple antenna elements were considered due to the underestimation of the expected received power value which was used to predict cell capacity.

In addition, two types of beamforming were tested: perfect beamforming (where the true array response vector is used as the beamforming weight vector), and imperfect beamforming (where the beamforming coefficients are estimated from the received data). Due to the excellent performance of the feedback correlation beamforming weight estimation method as described in Chapter 5, simulated capacity estimates for both perfect and imperfect beamforming agreed quite well. Confidence intervals were also calculated to determine the number of frames to be tested in each simulation run.

Capacity results for both single and multiple cells demonstrated that significant increases in capacity could be obtained through the use of multi-element antenna arrays. For example, in a single cell with a transmission activity factor of $\psi = 1.0$, capacity can be approximately quadrupled with the use of six elements, and with $\psi = 0.5$, capacity can be approximately tripled by using a four element array. Multi-cell simulations demonstrated that individual cell capacity went down dramatically due to intercell interference. However, similar improvements in cell capacity were observed when antenna arrays were applied in a multi-cell situation. It was also observed that even numbers of antenna elements did not provide as great a capacity increase as did odd numbers, and this appeared to be due to the antenna array geometry.

Finally, an investigation into multimedia service and its effects on cell capacity was included. The relatively narrow bandwidth of IS-95 was found to be unsuitable for satisfactorily accommodating data mobiles, and beamforming did not appear to provide much assistance in increasing capacity when data mobiles were present in the system, due to the loss of a uniform spatial distribution of interferers. However, by expanding the system bandwidth from 1.2288 MHz to 4.9152 MHz, system performance was found to improve since sufficient data mobiles could be active within the system that the interfering signals were still uniformly distributed in space. Agreement between predicted and observed capacity values was fair at a bandwidth of 1.2288 MHz and quite good at 4.9152 MHz. In the latter case, total system throughput appeared to remain relatively constant as the number of data mobiles was varied.

Chapter 8

Summary and Conclusions

8.1 Introduction

This thesis opened with a brief description of the motivation behind the specific research problems investigated here. The reverse link of the IS-95 cellular CDMA standard was then examined in detail, including separate chapters for power control and data decoding. The use of beamforming to increase cell capacity by reducing the effects of multi-user interference was analyzed, which was itself followed by an error analysis of the IS-95 reverse link. Finally, an investigation into estimating cell capacity and the improvements that can be achieved through base station beamforming was included.

This chapter first summarizes the most significant research contributions contained in this thesis. Section 8.3 then presents the conclusions which may be drawn from the research results. Finally, the last section describes a number of ways in which this thesis work may be further extended.

8.2 Summary of Contributions

One of the major achievements accomplished during the course of this thesis research was the development of a comprehensive simulation platform for the IS-95 reverse link. This detailed program allowed for the verification of various analyses and assisted in the development and testing of new algorithms while this research was being

conducted. In addition, the simulator is easily usable and expandable by other individuals for performing further research in this area.

In the IS-95 reverse link, the block-interleaving followed by orthogonal Walsh function encoding after the convolutional encoder causes a standard Viterbi decoder with deinterleaved soft-decision bit metrics to produce suboptimal results. To overcome this problem, a combined deinterleaver/decoder was proposed in Section 4.2.4, and simulation results demonstrated superior performance to the traditional approach of using soft-decision bit metric values.

The potential increase in cell capacity through the use of beamforming to reduce multi-user interference was a primary concern of this thesis. The code-filtering correlation algorithm [64] [67] [73] [74] has provided promising results in the past, but was not directly applicable to IS-95 due to the low actual spreading factor of 4. However, Section 5.5 presented a new feedback correlation algorithm for estimating suitable beamforming weights for the IS-95 reverse link. By using the decoded data to provide a second layer of correlation with the received signal data, it was possible to improve the effective spreading factor to almost 200 which greatly increased the accuracy of the beamforming coefficient estimation process. In addition, a detailed error analysis of the proposed algorithm was included and verified with simulation results.

The error analysis of the IS-95 reverse link performed in Chapter 6 served two useful purposes. First, it allowed the operation of the simulation program to be validated by comparing predicted values with simulated results. In addition, the expected received power equations which were derived were useful in obtaining approximate predictions for cell capacity which also aided in verifying the simulation results contained in the following chapter.

The power-level capacity estimation approach described in Section 7.3.2 is a much more computationally-efficient technique for performing cell capacity estimation than are chip-level simulations. Without this method, it would not have been possible to obtain accurate capacity estimates for higher numbers of antenna elements.

The error analysis of the feedback correlation beamforming algorithm allowed this technique to be used with the power-level capacity estimation method, which

resulted in significant computational savings. Rather than having to perform PN chip-level simulations in order to obtain the required signal data for beamforming weight estimation purposes, it was simply necessary to use the derived probability distribution for the beamforming coefficient vector to produce a random estimate for each frame. This allowed the realistic imperfect beamforming method to be tested in a feasible and efficient manner with several antenna elements and with multiple cells.

Finally, an investigation into the area of multi-service operation was performed. This combined data mobiles (with a higher bit rate) and voice mobiles in the same cell. When a larger bandwidth was available for communication, the use of data mobiles did not seem to affect the total cell throughput when beamforming was used to increase cell capacity.

8.3 Conclusions

Based on the analyses and simulations presented within this document, the following conclusions may be drawn.

Accurate power control is required within a cellular CDMA system in order to minimize multi-access interference and thereby maximize system capacity. The closed-loop control algorithm considered here appears to be capable of fully compensating for correlated Rayleigh fading at low mobile velocities, but less so at higher velocities. When the system capacity has been exceeded, the variance of the received E_b/N_0 values increases significantly unless the desired target ratio is reduced.

System performance on the IS-95 reverse link can be increased through the use of a combined deinterleaver/decoder rather than the more traditional Viterbi decoder with deinterleaved soft-decision bit metric inputs. At a voice-quality BER of 10^{-3}, the proposed decoder offered gains of 1.0 or 1.5 dB over soft-decision decoding with both uncorrelated and correlated fading, depending on whether one or two surviving paths were retained, respectively. Further gains can be obtained by retaining additional surviving paths, although the additional computational expense does not appear to make this worthwhile.

The proposed feedback correlation method of estimating beamforming weight vectors is much more suited to the IS-95 reverse link due to its significantly higher processing gain (~ 200 as compared to ~ 4). Analytical and simulation results demonstrated that using the mean correlation vector as the array response vector estimate was equally accurate as taking the principal eigenvector of the appropriate correlation matrix, with reduced computational expense. The mean vectors and covariance matrices of the various estimators can be predicted with high accuracy and then used to simplify simulation complexity by generating random beamforming vectors from the derived distributions instead of using chip-level data to obtain these estimates.

The statistical parameters of key correlation quantities prior to decoding can be accurately predicted for single antenna systems and reasonably approximated for multi-element arrays. A more exact approximation for the expected received power from an antenna array would be useful for predicting the correlation quantities with greater accuracy in this situation. The derived probability distributions may be utilized for purposes such as reducing simulation complexity or predicting cell capacity.

System capacity on the reverse link can be significantly improved through the use of antenna arrays and beamforming at the base station. Sample capacity improvements for the case of a single cell can be seen in Tables 7.8 and 7.9. Incorporating intercell interference into the system through consideration of multi-cell environments demonstrated that this factor dramatically reduces per cell capacity, although beamforming still provided a similar capacity improvement as before. When a multimedia-type environment was considered, it was found that a wider system bandwidth was required in order for data mobiles to be accommodated within the cell without violating the assumption of a uniform spatial distribution of interferers. In all instances, cell capacity values could be predicted with a reasonable level of accuracy.

8.4 Future Directions

There are, of course, a significant number of issues remaining to be explored with respect to the research results presented in this thesis. This section discusses a number of these issues and illustrates how the work which has already been performed can be

extended. Some of these proposals could be implemented with little additional effort, but would require more time for simulations to be run and the results to be analyzed.

Most of the results presented in this document are for a single cell, primarily due to computational limitations. The capacity values do give a reasonable indication of the gains that can be made through the use of digital beamforming. However, a multi-cell situation would provide a more realistic scenario and would also take into consideration the interference between adjacent cells. This facility is already contained in the simulation program, although a more efficient method of modelling multi-cell interference would aid greatly in reducing the required computation time. It should not be difficult to incorporate an effective multi-access interference model since its statistics can be tested against those of the existing simulation system. One factor which has not been considered is that of performing hand-offs as mobiles move from one cell to another. It would likely be relatively simple to incorporate this into the simulation program, although it would be necessary to have some method for determining when a hand-off should occur.

The user motion model in the current simulation program is relatively simplistic, in that mobiles move in a random direction with a constant velocity and then change both direction and speed according to a certain specified probability. An interesting area of exploration could be to implement a motion model with specified constraints. For example, a cell could represent part of an urban environment where the mobiles are constrained to move along a grid of city streets. Another possible scenario would involve using a building's internal floorplan to model users walking around while communicating. This constraint could easily reduce the assumed uniformity of the spatial distribution of the users, and thereby have a negative effect on system capacity. Rudokas [89] used measured data to show that call traffic is not uniform across geography (or time of day), for example, unlike the assumptions made earlier.

Different array geometries could easily be tested, simply by deriving the appropriate array response vectors in a manner similar to that of Section 2.4.1. Linear arrays have also received a significant amount of study. This geometry tends to be more directional in nature than is a circular array, although this may actually be advantageous depending upon the actual topography of the cell being considered. In

addition, rectangular arrays might represent another candidate geometry, although the computational expense of computing the beamforming weights increases with the number of antenna elements being considered. Yu and Lee [119] proposed a partially adaptive beamforming technique for dealing with a 2-D rectangular array which required less computational complexity than fully adaptive algorithms for the same situation.

The current shadowing model simply assigns a shadowing value at the beginning of each call and then does not modify this value during the duration of the call. To be more realistic, the shadowing parameter should be varied at a regular interval to simulate slow fading, even though fast fading is more likely to have a significant effect on the mobile's signal.

In equations (2.25) and (2.27), it has been assumed that the demodulation has been performed with perfect synchronization. To model imperfect synchronization, the cos and sin terms in (2.24) and (2.26), respectively, can be perturbed by a random phase shift. It would be expected that this would have a negative effect on system capacity due to the increased effects of multi-user interference relative to the desired signal. In addition, a random phase term due to either imperfect synchronization or fading would likely affect the quality of the beamforming weight estimates to some extent.

It is presently assumed that the same signal, subject to a phase shift, is received at each element of an antenna array. That is, the correlation between all of the signal components from the array is assumed to be 1.0. However, there will be some degree of independent fading due to multipath propagation in a real-life scenario. A more realistic correlation value for adjacent elements would lie in the range from 0.5 to 0.8 [90] [91]. In addition, the incorporation of an alternative correlated fading model such as the ARMA model proposed by Colman, Blostein and Beaulieu [9] into the system simulation component may be useful. Fast fading in a multi-antenna communication system suitable for adaptive beamforming was also investigated in [87].

Some type of robust algorithm should be implemented for tracking array response vector estimates for each mobile over time. Currently, the estimate obtained from the previous frame is used to generate the beamforming weights for the current frame.

However, there are problems with this approach. One problem is that a significant amount of useful information is discarded by not utilizing the array response estimates from previous frames. This implies that the estimation process could be made more computationally efficient. For example, Shiu and Blostein [93] presented a low-complexity method for updating beamforming weights via a noniterative rank-one signal subspace eigenstructure update algorithm [10]. Secondly, the feedback correlation method of increasing the gain for improved estimation accuracy assumes that the data for the current frame has been correctly decoded. This, of course, is not always the case, particularly in an environment with high interference and noise levels. Consequently, some kind of smoothing technique such as a Kalman filter would significantly reduce the effects of incorrect data decoding within a single frame. If the beamforming weights are generated from incorrect data, they will affect the quality of the decoded data for the next frame and there could be a catastrophic cascade effect before the system recovers.

Although both uncorrelated and correlated Rayleigh fading due to multipath propagation have been considered, the signal from each mobile has been assumed to have only one resolvable path. This may be suitable for modelling a narrowband CDMA system such as IS-95. However, a wideband system should consider additional resolvable paths due to the propagation environment. Consequently, implementing a RAKE receiver [84, pp. 732] at the base station together with multipath propagation would certainly be a useful area to explore. Kchao and Stüber [43] analyzed a single-cell spread-spectrum system and considered three different types of receivers: multipath rejection, RAKE with predetection selective diversity combining, and RAKE with postdetection equal gain combining. The RAKE receivers resulted in a significant performance improvement when the channel contained multiple faded paths. Naguib and Paulraj [66] [69] [71] also considered using a RAKE receiver in a cellular CDMA uplink system. In addition, only amplitude fading is considered at the moment. If the fading value were maintained as a complex quantity, a phase component would be introduced as well. The basis for conducting such an analysis might be to include a random phase term due to fading in the demodulation and correlation equations contained in Section 2.5.

The current matched filter model for the receiver which considers users other than the desired one to be interference may not be optimal. It is suitable for a reasonable number of mobiles with effective power control. However, with fading and shadowing, the power control algorithm is not always able to adjust the transmitted power fast enough to keep up. This results in a near-far problem where some users have much larger power values than do others. An alternative is to simultaneously decode all of the signals using a multi-user detection algorithm rather than the more traditional single user approach, although algorithm complexity can increase exponentially with the number of users. Tsatsanis and Giannakis [100] derived linear decorrelating receivers to address this problem and based their work on earlier research by Lupas and Verdú [57] [58]. In particular, Verdú [102] proposed a multiuser detector that has formed the basis for work by many other researchers. Also, an overview of multi-user detection algorithms in CDMA communication systems (which includes an extensive bibliography) was prepared by Moshavi [63]. This area of investigation may promise a BER reduction through the use of potentially superior receivers.

Finally, it may be possible to apply importance sampling (IS) to certain aspects of the simulation process in order to significantly reduce the computational requirements. Importance sampling reduces the variance of the estimator being evaluated by choosing a distribution of random input values which emphasizes their impact on the parameter being estimated. The biased outputs can then be weighted in such a way to ensure that the IS estimator is unbiased. Thus, a desired precision in the estimated outputs can be obtained with fewer simulation runs. Smith, Shafi, and Gao [96] provide an introduction to importance sampling and review its use in various aspects of simulating communication systems. Particular examples of the use of importance sampling in relevant situations can be found in [51] which outlines how BER values for a BPSK CDMA system can be efficiently evaluated, and [52] which details the simulation and determination of error-rate performance of wireless CDMA over multiple Rayleigh fading paths.

Appendix A

Calculation of β_d

This appendix outlines the numerical calculation of the β_d coefficients used in the expression for the approximate predicted BER for IS-95 with no interleaving as given by equation (4.10).

It is first necessary to obtain the transfer function [84, pp. 451-454], $T(D,N)$, for IS-95 encoding without interleaving, where the exponent of D is the distance of the current path from the correct path in terms of incorrect Walsh functions, and the exponent of N is the number of output bit errors. $T(D,N)$ can be obtained by deriving a system of equations from the encoding trellis, which can then be solved using symbolic computation software.

An infinite series representation of the transfer function is:

$$T(D,N) = \sum_{d=d_{\text{free}}}^{\infty} a_d D^d N^{f(d)} \tag{A.1}$$

where a_d is the number of paths of distance d from the correct path with the specified number of output bit errors. From (A.1):

$$\left.\frac{dT(D,N)}{dN}\right|_{N=1} = \sum_{d=d_{\text{free}}}^{\infty} f(d) a_d D^d = \sum_{d=d_{\text{free}}}^{\infty} \beta_d D^d \tag{A.2}$$

where β_d is a weighting term which combines the number of paths and the number of output bit errors for the current probability term.

Since Equation (A.2) specifies the β_d coefficients in (4.9), the approximate BER in (4.10) can be obtained. For numerical purposes, (A.2) can also be expressed as the ratio of two polynomials which, for the case of IS-95 encoding with no interleaving,

can be derived as:

$$\begin{aligned} G \;=\;& d^{51} - 16d^{50} + 118d^{49} - 532d^{48} + 1664d^{47} - 4003d^{46} + 8338d^{45} - 16528d^{44} \\ & + 30644d^{43} - 47518d^{42} + 52593d^{41} - 24631d^{40} - 43887d^{39} + 125350d^{38} \\ & - 161892d^{37} + 108602d^{36} + 17501d^{35} - 139070d^{34} + 178294d^{33} - 117113d^{32} \\ & + 6252d^{31} + 76146d^{30} - 83526d^{29} + 34115d^{28} + 14432d^{27} - 27526d^{26} \\ & + 19847d^{25} - 15612d^{24} + 11283d^{23} + 3658d^{22} - 18527d^{21} + 18427d^{20} \\ & - 7280d^{19} - 1594d^{18} + 2691d^{17} - 169d^{16} - 667d^{15} - 386d^{14} + 1214d^{13} \\ & - 847d^{12} - 43d^{11} + 168d^{10} + 42d^{9} + 17d^{8} - 41d^{7} + 11d^{6} + 4d^{5} \end{aligned} \tag{A.3}$$

$$\begin{aligned} H \;=\;& 4d^{50} - 52d^{49} + 289d^{48} - 864d^{47} + 1350d^{46} - 436d^{45} - 2491d^{44} + 5576d^{43} \\ & - 6912d^{42} + 7382d^{41} - 5944d^{40} - 3360d^{39} + 20574d^{38} - 33378d^{37} + 30938d^{36} \\ & - 14968d^{35} - 6965d^{34} + 28584d^{33} - 44096d^{32} + 45376d^{31} - 25127d^{30} \\ & - 11006d^{29} + 41533d^{28} - 45134d^{27} + 19584d^{26} + 12746d^{25} - 25958d^{24} \\ & + 17018d^{23} - 174d^{22} - 10366d^{21} + 8565d^{20} - 1402d^{19} - 2548d^{18} + 2762d^{17} \\ & - 850d^{16} - 314d^{15} - 29d^{14} - 26d^{13} - 22d^{12} + 110d^{11} + 297d^{10} - 24d^{9} \\ & - 132d^{8} - 54d^{7} - 21d^{6} + 22d^{5} + 54d^{4} + 14d^{3} + d^{2} - 6d + 1 \end{aligned} \tag{A.4}$$

The values of β_d in (A.2) can then be calculated by dividing H into G until a sufficient number of nonnegligible summation terms have been determined.

Appendix B

Complex Gaussian Moments

This appendix derives expressions for certain moments of complex Gaussian random vectors that are required for the beamforming error analysis performed in Chapter 5. Note that the moments considered here are not the typical first and second moments of complex vectors.

B.1 Complex Eigenvector Phase Shifts

Let A be a Hermitian matrix which will thus have real eigenvalues and orthogonal eigenvectors. Let λ and $\mathbf{v}$ be an eigenvalue/eigenvector pair of A.

$$\mathrm{A}\mathbf{v} = \lambda\mathbf{v} \tag{B.1}$$

Now multiply both sides of equation (B.1) by $\exp(-j\theta)$ where θ is an arbitrary angle.

$$\exp(-j\theta)\{\mathrm{A}\mathbf{v}\} = \exp(-j\theta)\{\lambda\mathbf{v}\} \tag{B.2}$$

$$\mathrm{A}\{\exp(-j\theta)\mathbf{v}\} = \lambda\{\exp(-j\theta)\mathbf{v}\} \tag{B.3}$$

Clearly, $\exp(-j\theta)\mathbf{v}$ is also an eigenvector of A. Consequently, it is possible to induce an arbitrary phase shift of θ into all of the elements of an eigenvector of a complex matrix without affecting its eigenvector properties.

B.2 Complex Second Moments

Let $\mathbf{x}$ be a zero-mean complex Gaussian random vector with covariance matrix P. P will be a Hermitian matrix and, as a result, will have real eigenvalues and orthogonal eigenvectors. Thus, P can be factored into a product of these components.

$$\mathrm{P} = \mathrm{U}\Lambda\mathrm{U}^* \tag{B.4}$$

The columns of U are the eigenvectors of P, and Λ is a real diagonal matrix containing the eigenvalues of P.

Now define a new random vector $\mathbf{w}$ where:

$$\mathbf{w} = \mathrm{U}^*\mathbf{x} \tag{B.5}$$

$\mathbf{w}$ will also be zero-mean with the following covariance matrix.

$$\begin{aligned} \mathrm{C}_{\mathbf{ww}} &= E[\mathbf{w}\mathbf{w}^*] = E[(\mathrm{U}^*\mathbf{x})(\mathrm{U}^*\mathbf{x})^*] \\ &= E[\mathrm{U}^*\mathbf{x}\mathbf{x}^*\mathrm{U}] = \mathrm{U}^*E[\mathbf{x}\mathbf{x}^*]\mathrm{U} \\ &= \mathrm{U}^*\mathrm{P}\mathrm{U} \end{aligned} \tag{B.6}$$

Substituting (B.4) into (B.6) produces:

$$\mathrm{C}_{\mathbf{ww}} = \mathrm{U}^*(\mathrm{U}\Lambda\mathrm{U}^*)\mathrm{U} = \Lambda \tag{B.7}$$

Recalling that $\mathrm{U}^{-1} = \mathrm{U}^*$, (B.2) can be rewritten as:

$$\mathbf{x} = \mathrm{U}\mathbf{w} \tag{B.8}$$

Note that $\mathbf{w}$ will be a complex vector, even though it has a strictly real covariance matrix.

Consider (B.5), but define another new random vector as:

$$\mathbf{y} = \Theta\mathrm{U}^*\mathbf{x} \tag{B.9}$$

where Θ is defined as:

$$\Theta = \begin{bmatrix} \exp(-j\theta_1) & 0 & \dots & 0 \\ 0 & \exp(-j\theta_2) & \dots & 0 \\ \vdots & \vdots & \ddots & \vdots \\ 0 & 0 & \dots & \exp(-j\theta_n) \end{bmatrix} \tag{B.10}$$

The θ_i values are chosen to give an appropriate phase shift to the corresponding eigenvector so that $\mathbf{y}$ will be a strictly real vector with the same covariance matrix as $\mathbf{w}$.

$$\mathrm{C}_{\mathbf{yy}} = \Lambda \tag{B.11}$$

Clearly, a different Θ must be selected for each specific random sample of $\mathbf{x}$ in order to satisfy the condition that $\mathbf{y}$ is real. The θ_i values will therefore be uniformly distributed in the interval $[0, 2\pi)$.

Inverting (B.9) yields:

$$\mathbf{x} = \mathrm{U}\Theta^*\mathbf{y} \tag{B.12}$$

Consider only the m^{th} entry of $\mathbf{x}$ in the above equation which can be written as:

$$\mathbf{x}_m = \mathrm{U}_m\Theta^*\mathbf{y} \tag{B.13}$$

where U_m is the m^{th} row of U. Since the columns of U are the eigenvectors of P, note that U_m is not an eigenvector of P.

Now consider the following second moment of $\mathbf{x}$.

$$E\left[\mathbf{x}_m\mathbf{x}_n\right] = E\left[\left\{\mathrm{U}_m\Theta^*\mathbf{y}\right\}\left\{\mathrm{U}_n\Theta^*\mathbf{y}\right\}\right] \tag{B.14}$$

Unlike the typical second moment of a complex quantity, this does not correspond directly to an entry of the P matrix since neither of the terms is conjugated. Since (B.13) represents a scalar quantity, (B.14) can be rewritten as:

$$E\left[\mathbf{x}_m\mathbf{x}_n\right] = E\left[\left\{\mathrm{U}_m\Theta^*\mathbf{y}\right\}\left\{\mathbf{y}^T\Theta^*\mathrm{U}_n^T\right\}\right] \tag{B.15}$$

Noting that U_m and U_n are not random quantities and that $\mathbf{y}$ is independent of the other quantities in the expression, (B.15) can be written as:

$$\begin{aligned} E\left[\mathbf{x}_m\mathbf{x}_n\right] &= \mathrm{U}_m E\left[\Theta^*\mathbf{y}\mathbf{y}^T\Theta^*\right]\mathrm{U}_n^T \\ &= \mathrm{U}_m E\left[\Theta^* E\left[\mathbf{y}\mathbf{y}^T\right]\Theta^*\right]\mathrm{U}_n^T \\ &= \mathrm{U}_m E\left[\Theta^*\Lambda\Theta^*\right]\mathrm{U}_n^T \end{aligned} \tag{B.16}$$

The expectation is now of the product of three diagonal matrices and will thus also be a diagonal matrix. Consider the i^{th} element of this expectation and recall that θ_i has a uniform distribution on $[0, 2\pi)$.

$$\begin{aligned} E\left[\exp(j\theta_i)\lambda_i \exp(j\theta_i)\right] &= \lambda_i E\left[\exp(j2\theta_i)\right] \\ &= \lambda_i \left\{E\left[\cos(2\theta_i)\right] + jE\left[\sin(2\theta_i)\right]\right\} \\ &= \frac{1}{2\pi}\lambda_i \left\{\int_0^{2\pi} \cos(2\theta_i)d\theta + j\int_0^{2\pi} \sin(2\theta_i)d\theta\right\} \\ &= \frac{1}{4\pi}\lambda_i \left\{\sin(2\theta_i)|_0^{2\pi} - \cos(2\theta_i)|_0^{2\pi}\right\} \\ &= \frac{1}{4\pi}\lambda_i \left\{(0-0) - (1-1)\right\} \\ &= 0 \end{aligned} \tag{B.17}$$

By substituting (B.16) into (B.17), it can be seen that:

$$E\left[\mathbf{x}_m \mathbf{x}_n\right] = 0 \tag{B.18}$$

Similarly, by conjugating the above expression:

$$E\left[\mathbf{x}_m^* \mathbf{x}_n^*\right] = 0 \tag{B.19}$$

Thus, these particular complex second moments have been shown to be zero. This corresponds to the assumption of circularity for a complex random vector [77] which also implies that these moments would be zero. Circularity has been assumed within this thesis. Additional information on second-order complex Gaussian random vectors which are not subject to the circularity assumption may be found in [78] and [79].

B.3 Complex Fourth Moments

As before, let $\mathbf{x}$ be a zero-mean complex Gaussian random vector of size d with covariance matrix P. This vector can be written as the sum of a real and imaginary vector.

$$\mathbf{x} = \mathbf{y} + j\mathbf{z} \tag{B.20}$$

Now define a new real vector as:

$$\mathbf{v} \equiv \begin{bmatrix} \mathbf{y} \\ \mathbf{z} \end{bmatrix} \tag{B.21}$$

$\mathbf{v}$ will also be zero-mean since $\mathbf{y}$ and $\mathbf{z}$ are both zero-mean. Let Q represent the covariance matrix of $\mathbf{v}$. Q can be calculated as:

$$\mathrm{Q} = E\left[\mathbf{v}\mathbf{v}^T\right] = E\left\{\begin{bmatrix}\mathbf{y}\\ \mathbf{z}\end{bmatrix}\begin{bmatrix}\mathbf{y}^T & \mathbf{z}^T\end{bmatrix}\right\} = E\left\{\begin{bmatrix}\mathbf{y}\mathbf{y}^T & \mathbf{y}\mathbf{z}^T\\ \mathbf{z}\mathbf{y}^T & \mathbf{z}\mathbf{z}^T\end{bmatrix}\right\} \quad \text{(B.22)}$$

where each of the blocks in the resulting matrix is a $d \times d$ submatrix. It can be shown (see Section B.4) that Q can also be written as:

$$\mathrm{Q} = \frac{1}{2}\begin{bmatrix}\mathrm{R} & \mathrm{S}^T\\ \mathrm{S} & \mathrm{R}\end{bmatrix} \quad \text{(B.23)}$$

where the submatrices are the real (symmetric) and imaginary (skew-symmetric) components of the complex covariance matrix.

$$\mathrm{P} = \mathrm{R} + j\mathrm{S} \quad \text{(B.24)}$$

Consider the following fourth moment of the complex Gaussian random vector.

$$\begin{aligned}
E\left[\mathbf{x}_m\mathbf{x}_n^*\mathbf{x}_p^*\mathbf{x}_q\right] &= E\left[(\mathbf{y}_m + j\mathbf{z}_m)(\mathbf{y}_n - j\mathbf{z}_n)(\mathbf{y}_p - j\mathbf{z}_p)(\mathbf{y}_q + j\mathbf{z}_q)\right]\\
&= E\left[\{(\mathbf{y}_m\mathbf{y}_n + \mathbf{z}_m\mathbf{z}_n) + j(\mathbf{z}_m\mathbf{y}_n - \mathbf{y}_m\mathbf{z}_n)\}\right.\\
&\qquad \left.\{(\mathbf{y}_p\mathbf{y}_q + \mathbf{z}_p\mathbf{z}_q) + j(\mathbf{y}_p\mathbf{z}_q - \mathbf{z}_p\mathbf{y}_q)\}\right]\\
&= E\left[\{(\mathbf{y}_m\mathbf{y}_n + \mathbf{z}_m\mathbf{z}_n)(\mathbf{y}_p\mathbf{y}_q + \mathbf{z}_p\mathbf{z}_q)\right.\\
&\qquad \left. - (\mathbf{z}_m\mathbf{y}_n - \mathbf{y}_m\mathbf{z}_n)(\mathbf{y}_p\mathbf{z}_q - \mathbf{z}_p\mathbf{y}_q)\}\right.\\
&\qquad + j\left\{(\mathbf{y}_m\mathbf{y}_n + \mathbf{z}_m\mathbf{z}_n)(\mathbf{y}_p\mathbf{z}_q - \mathbf{z}_p\mathbf{y}_q)\right.\\
&\qquad \left.\left. + (\mathbf{z}_m\mathbf{y}_n - \mathbf{y}_m\mathbf{z}_n)(\mathbf{y}_p\mathbf{y}_q + \mathbf{z}_p\mathbf{z}_q)\}\right]\right.\\
&= E\left[\{\mathbf{y}_m\mathbf{y}_n\mathbf{y}_p\mathbf{y}_q + \mathbf{y}_m\mathbf{y}_n\mathbf{z}_p\mathbf{z}_q + \mathbf{z}_m\mathbf{z}_n\mathbf{y}_p\mathbf{y}_q + \mathbf{z}_m\mathbf{z}_n\mathbf{z}_p\mathbf{z}_q\right.\\
&\quad - \mathbf{z}_m\mathbf{y}_n\mathbf{y}_p\mathbf{z}_q + \mathbf{z}_m\mathbf{y}_n\mathbf{z}_p\mathbf{y}_q + \mathbf{y}_m\mathbf{z}_n\mathbf{y}_p\mathbf{z}_q - \mathbf{y}_m\mathbf{z}_n\mathbf{z}_p\mathbf{y}_q\}\\
&\quad + j\left\{\mathbf{y}_m\mathbf{y}_n\mathbf{y}_p\mathbf{z}_q - \mathbf{y}_m\mathbf{y}_n\mathbf{z}_p\mathbf{y}_q + \mathbf{z}_m\mathbf{z}_n\mathbf{y}_p\mathbf{z}_q - \mathbf{z}_m\mathbf{z}_n\mathbf{z}_p\mathbf{y}_q\right.\\
&\quad \left.\left. + \mathbf{z}_m\mathbf{y}_n\mathbf{y}_p\mathbf{y}_q + \mathbf{z}_m\mathbf{y}_n\mathbf{z}_p\mathbf{z}_q - \mathbf{y}_m\mathbf{z}_n\mathbf{y}_p\mathbf{y}_q - \mathbf{y}_m\mathbf{z}_n\mathbf{z}_p\mathbf{z}_q\right\}\right]
\end{aligned} \quad \text{(B.25)}$$

The complex fourth moment has now been written entirely in terms of real fourth moments. As an illustrative example, the fourth moment of a real Gaussian vector can be written as the following [59, p. 107].

$$E\left[\mathbf{y}_m\mathbf{z}_n\mathbf{z}_p\mathbf{y}_q\right] = E\left[\mathbf{y}_m\mathbf{z}_n\right]E\left[\mathbf{z}_p\mathbf{y}_q\right] + E\left[\mathbf{y}_m\mathbf{z}_p\right]E\left[\mathbf{z}_n\mathbf{y}_q\right]$$

$$+ E\left[\mathbf{y}_m \mathbf{y}_q\right] E\left[\mathbf{z}_n \mathbf{z}_p\right] \qquad \text{(B.26)}$$

$$= \quad \mathrm{Q}_{m,d+n}\mathrm{Q}_{d+p,q} + \mathrm{Q}_{m,d+p}\mathrm{Q}_{d+n,q} + \mathrm{Q}_{mq}\mathrm{Q}_{d+n,d+p}$$

where the Q terms are the specified entries from the Q covariance matrix defined in (B.22). Essentially, d is added to the subscript of Q corresponding to each term that is a $\mathbf{z}$ instead of a $\mathbf{y}$.

Thus, equation (B.25) can be written in terms of entries from the Q covariance matrix.

$$\begin{aligned}
E\left[\mathbf{x}_m \mathbf{x}_n^* \mathbf{x}_p^* \mathbf{x}_q\right] \quad = \quad & \{(\mathrm{Q}_{mn}\mathrm{Q}_{pq} + \mathrm{Q}_{mp}\mathrm{Q}_{nq} + \mathrm{Q}_{mq}\mathrm{Q}_{np}) \\
& + (\mathrm{Q}_{mn}\mathrm{Q}_{d+p,d+q} + \mathrm{Q}_{m,d+p}\mathrm{Q}_{n,d+q} + \mathrm{Q}_{m,d+q}\mathrm{Q}_{n,d+p}) \\
& + (\mathrm{Q}_{d+m,d+n}\mathrm{Q}_{pq} + \mathrm{Q}_{d+m,p}\mathrm{Q}_{d+n,q} + \mathrm{Q}_{d+m,q}\mathrm{Q}_{d+n,p}) \\
& + (\mathrm{Q}_{d+m,d+n}\mathrm{Q}_{d+p,d+q} + \mathrm{Q}_{d+m,d+p}\mathrm{Q}_{d+n,d+q} + \mathrm{Q}_{d+m,d+q}\mathrm{Q}_{d+n,d+p}) \\
& - (\mathrm{Q}_{d+m,n}\mathrm{Q}_{p,d+q} + \mathrm{Q}_{d+m,p}\mathrm{Q}_{n,d+q} + \mathrm{Q}_{d+m,d+q}\mathrm{Q}_{np}) \\
& + (\mathrm{Q}_{d+m,n}\mathrm{Q}_{d+p,q} + \mathrm{Q}_{d+m,d+p}\mathrm{Q}_{nq} + \mathrm{Q}_{d+m,q}\mathrm{Q}_{n,d+p}) \\
& + (\mathrm{Q}_{m,d+n}\mathrm{Q}_{p,d+q} + \mathrm{Q}_{mp}\mathrm{Q}_{d+n,d+q} + \mathrm{Q}_{m,d+q}\mathrm{Q}_{d+n,p})\} \\
& - (\mathrm{Q}_{m,d+n}\mathrm{Q}_{d+p,q} + \mathrm{Q}_{m,d+p}\mathrm{Q}_{d+n,q} + \mathrm{Q}_{mq}\mathrm{Q}_{d+n,d+p}) \qquad \text{(B.27)} \\
& + j\,\{(\mathrm{Q}_{mn}\mathrm{Q}_{p,d+q} + \mathrm{Q}_{mp}\mathrm{Q}_{n,d+q} + \mathrm{Q}_{m,d+q}\mathrm{Q}_{np}) \\
& - (\mathrm{Q}_{mn}\mathrm{Q}_{d+p,q} + \mathrm{Q}_{m,d+p}\mathrm{Q}_{nq} + \mathrm{Q}_{mq}\mathrm{Q}_{n,d+p}) \\
& + (\mathrm{Q}_{d+m,d+n}\mathrm{Q}_{p,d+q} + \mathrm{Q}_{d+m,p}\mathrm{Q}_{d+n,d+q} + \mathrm{Q}_{d+m,d+q}\mathrm{Q}_{d+n,p}) \\
& - (\mathrm{Q}_{d+m,d+n}\mathrm{Q}_{d+p,q} + \mathrm{Q}_{d+m,d+p}\mathrm{Q}_{d+n,q} + \mathrm{Q}_{d+m,q}\mathrm{Q}_{d+n,d+p}) \\
& + (\mathrm{Q}_{d+m,n}\mathrm{Q}_{pq} + \mathrm{Q}_{d+m,p}\mathrm{Q}_{nq} + \mathrm{Q}_{d+m,q}\mathrm{Q}_{np}) \\
& + (\mathrm{Q}_{d+m,n}\mathrm{Q}_{d+p,d+q} + \mathrm{Q}_{d+m,d+p}\mathrm{Q}_{n,d+q} + \mathrm{Q}_{d+m,d+q}\mathrm{Q}_{n,d+p}) \\
& - (\mathrm{Q}_{m,d+n}\mathrm{Q}_{pq} + \mathrm{Q}_{mp}\mathrm{Q}_{d+n,q} + \mathrm{Q}_{mq}\mathrm{Q}_{d+n,p}) \\
& - (\mathrm{Q}_{m,d+n}\mathrm{Q}_{d+p,d+q} + \mathrm{Q}_{m,d+p}\mathrm{Q}_{d+n,d+q} + \mathrm{Q}_{m,d+q}\mathrm{Q}_{d+n,d+p})\}
\end{aligned}$$

Rearranging terms produces the following.

$$\begin{aligned}
E\left[\mathbf{x}_m \mathbf{x}_n^* \mathbf{x}_p^* \mathbf{x}_q\right] \quad = \quad & \{(\mathrm{Q}_{mn}\mathrm{Q}_{pq} + \mathrm{Q}_{mn}\mathrm{Q}_{d+p,d+q} + \mathrm{Q}_{d+m,d+n}\mathrm{Q}_{pq} \\
& + \mathrm{Q}_{d+m,d+n}\mathrm{Q}_{d+p,d+q} - \mathrm{Q}_{d+m,n}\mathrm{Q}_{p,d+q} + \mathrm{Q}_{d+m,n}\mathrm{Q}_{d+p,q} \\
& + \mathrm{Q}_{m,d+n}\mathrm{Q}_{p,d+q} - \mathrm{Q}_{m,d+n}\mathrm{Q}_{d+p,q})
\end{aligned}$$

$$
\begin{aligned}
&+ j\,(\mathrm{Q}_{mn}\mathrm{Q}_{p,d+q} - \mathrm{Q}_{mn}\mathrm{Q}_{d+p,q} + \mathrm{Q}_{d+m,d+n}\mathrm{Q}_{p,d+q} \\
&\quad - \mathrm{Q}_{d+m,d+n}\mathrm{Q}_{d+p,q} + \mathrm{Q}_{d+m,n}\mathrm{Q}_{pq} + \mathrm{Q}_{d+m,n}\mathrm{Q}_{d+p,d+q} \\
&\quad - \mathrm{Q}_{m,d+n}\mathrm{Q}_{pq} - \mathrm{Q}_{m,d+n}\mathrm{Q}_{d+p,d+q})\} \\
&+ \{(\mathrm{Q}_{mp}\mathrm{Q}_{nq} + \mathrm{Q}_{mp}\mathrm{Q}_{d+n,d+q} + \mathrm{Q}_{d+m,d+p}\mathrm{Q}_{nq} \\
&\quad + \mathrm{Q}_{d+m,d+p}\mathrm{Q}_{d+n,d+q} - \mathrm{Q}_{d+m,p}\mathrm{Q}_{n,d+q} + \mathrm{Q}_{d+m,p}\mathrm{Q}_{d+n,q} \\
&\quad + \mathrm{Q}_{m,d+p}\mathrm{Q}_{n,d+q} - \mathrm{Q}_{m,d+p}\mathrm{Q}_{d+n,q}) \qquad \text{(B.28)} \\
&+ j\,(\mathrm{Q}_{mp}\mathrm{Q}_{n,d+q} - \mathrm{Q}_{mp}\mathrm{Q}_{d+n,q} + \mathrm{Q}_{d+m,d+p}\mathrm{Q}_{n,d+q} \\
&\quad - \mathrm{Q}_{d+m,d+p}\mathrm{Q}_{d+n,q} + \mathrm{Q}_{d+m,p}\mathrm{Q}_{nq} + \mathrm{Q}_{d+m,p}\mathrm{Q}_{d+n,d+q} \\
&\quad - \mathrm{Q}_{m,d+p}\mathrm{Q}_{nq} - \mathrm{Q}_{m,d+p}\mathrm{Q}_{d+n,d+q})\} \\
&+ \{(\mathrm{Q}_{mq}\mathrm{Q}_{np} - \mathrm{Q}_{mq}\mathrm{Q}_{d+n,d+p} - \mathrm{Q}_{d+m,d+q}\mathrm{Q}_{np} \\
&\quad + \mathrm{Q}_{d+m,d+q}\mathrm{Q}_{d+n,d+p} + \mathrm{Q}_{d+m,q}\mathrm{Q}_{n,d+p} + \mathrm{Q}_{d+m,q}\mathrm{Q}_{d+n,p} \\
&\quad + \mathrm{Q}_{m,d+q}\mathrm{Q}_{n,d+p} + \mathrm{Q}_{m,d+q}\mathrm{Q}_{d+n,p}) \\
&+ j\,(-\mathrm{Q}_{mq}\mathrm{Q}_{n,d+p} - \mathrm{Q}_{mq}\mathrm{Q}_{d+n,p} + \mathrm{Q}_{d+m,d+q}\mathrm{Q}_{n,d+p} \\
&\quad + \mathrm{Q}_{d+m,d+q}\mathrm{Q}_{d+n,p} + \mathrm{Q}_{d+m,q}\mathrm{Q}_{np} - \mathrm{Q}_{d+m,q}\mathrm{Q}_{d+n,d+p} \\
&\quad + \mathrm{Q}_{m,d+q}\mathrm{Q}_{np} - \mathrm{Q}_{m,d+q}\mathrm{Q}_{d+n,d+p})\}
\end{aligned}
$$

Substituting for the Q terms from (B.23) yields:

$$
\begin{aligned}
E\left[\mathbf{x}_m\mathbf{x}_n^*\mathbf{x}_p^*\mathbf{x}_q\right] \;=\; & \frac{1}{4}\{(\mathrm{R}_{mn}\mathrm{R}_{pq} + \mathrm{R}_{mn}\mathrm{R}_{pq} + \mathrm{R}_{mn}\mathrm{R}_{pq} + \mathrm{R}_{mn}\mathrm{R}_{pq} \\
& \quad - \mathrm{S}_{mn}\mathrm{S}_{qp} + \mathrm{S}_{mn}\mathrm{S}_{pq} + \mathrm{S}_{nm}\mathrm{S}_{qp} - \mathrm{S}_{nm}\mathrm{S}_{pq}) \\
& + j\,(\mathrm{R}_{mn}\mathrm{S}_{qp} - \mathrm{R}_{mn}\mathrm{S}_{pq} + \mathrm{R}_{mn}\mathrm{S}_{qp} - \mathrm{R}_{mn}\mathrm{S}_{pq} \\
& \quad + \mathrm{S}_{mn}\mathrm{R}_{pq} + \mathrm{S}_{mn}\mathrm{R}_{pq} - \mathrm{S}_{nm}\mathrm{R}_{pq} - \mathrm{S}_{nm}\mathrm{R}_{pq})\} \\
& + \frac{1}{4}\{(\mathrm{R}_{mp}\mathrm{R}_{nq} + \mathrm{R}_{mp}\mathrm{R}_{nq} + \mathrm{R}_{mp}\mathrm{R}_{nq} + \mathrm{R}_{mp}\mathrm{R}_{nq} \\
& \quad - \mathrm{S}_{mp}\mathrm{S}_{qn} + \mathrm{S}_{mp}\mathrm{S}_{nq} + \mathrm{S}_{pm}\mathrm{S}_{qn} - \mathrm{S}_{pm}\mathrm{S}_{nq}) \qquad \text{(B.29)} \\
& + j\,(\mathrm{R}_{mp}\mathrm{S}_{qn} - \mathrm{R}_{mp}\mathrm{S}_{nq} + \mathrm{R}_{mp}\mathrm{S}_{qn} - \mathrm{R}_{mp}\mathrm{S}_{nq} \\
& \quad + \mathrm{S}_{mp}\mathrm{R}_{nq} + \mathrm{S}_{mp}\mathrm{R}_{nq} - \mathrm{S}_{pm}\mathrm{R}_{nq} - \mathrm{S}_{pm}\mathrm{R}_{nq})\} \\
& + \frac{1}{4}\{(\mathrm{R}_{mq}\mathrm{R}_{np} - \mathrm{R}_{mq}\mathrm{R}_{np} - \mathrm{R}_{mq}\mathrm{R}_{np} + \mathrm{R}_{mq}\mathrm{R}_{np} \\
& \quad + \mathrm{S}_{mq}\mathrm{S}_{pn} + \mathrm{S}_{mq}\mathrm{S}_{np} + \mathrm{S}_{qm}\mathrm{S}_{pn} + \mathrm{S}_{qm}\mathrm{S}_{np}) \\
& + j\,(-\mathrm{R}_{mq}\mathrm{S}_{pn} - \mathrm{R}_{mq}\mathrm{S}_{np} + \mathrm{R}_{mq}\mathrm{S}_{pn} + \mathrm{R}_{mq}\mathrm{S}_{np}
\end{aligned}
$$

$$+ \mathrm{S}_{mq}\mathrm{R}_{np} - \mathrm{S}_{mq}\mathrm{R}_{np} + \mathrm{S}_{qm}\mathrm{R}_{np} - \mathrm{S}_{qm}\mathrm{R}_{np})\}$$

Note that S is a skew-symmetric matrix. Simplifying the above expression produces: yields:

$$\begin{aligned}
E\left[\mathbf{x}_m\mathbf{x}_n^*\mathbf{x}_p^*\mathbf{x}_q\right] &= \frac{1}{4}\{(\mathrm{R}_{mn}\mathrm{R}_{pq} + \mathrm{R}_{mn}\mathrm{R}_{pq} + \mathrm{R}_{mn}\mathrm{R}_{pq} + \mathrm{R}_{mn}\mathrm{R}_{pq} \\
&\quad + \mathrm{S}_{mn}\mathrm{S}_{pq} + \mathrm{S}_{mn}\mathrm{S}_{pq} + \mathrm{S}_{mn}\mathrm{S}_{pq} + \mathrm{S}_{mn}\mathrm{S}_{pq}) \\
&\quad + j\,(-\mathrm{R}_{mn}\mathrm{S}_{pq} - \mathrm{R}_{mn}\mathrm{S}_{pq} - \mathrm{R}_{mn}\mathrm{S}_{pq} - \mathrm{R}_{mn}\mathrm{S}_{pq} \\
&\quad + \mathrm{S}_{mn}\mathrm{R}_{pq} + \mathrm{S}_{mn}\mathrm{R}_{pq} + \mathrm{S}_{mn}\mathrm{R}_{pq} + \mathrm{S}_{mn}\mathrm{R}_{pq})\} \\
&\quad + \frac{1}{4}\{(\mathrm{R}_{mp}\mathrm{R}_{nq} + \mathrm{R}_{mp}\mathrm{R}_{nq} + \mathrm{R}_{mp}\mathrm{R}_{nq} + \mathrm{R}_{mp}\mathrm{R}_{nq} \\
&\quad + \mathrm{S}_{mp}\mathrm{S}_{nq} + \mathrm{S}_{mp}\mathrm{S}_{nq} + \mathrm{S}_{mp}\mathrm{S}_{nq} + \mathrm{S}_{mp}\mathrm{S}_{nq}) \\
&\quad + j\,(-\mathrm{R}_{mp}\mathrm{S}_{nq} - \mathrm{R}_{mp}\mathrm{S}_{nq} - \mathrm{R}_{mp}\mathrm{S}_{nq} - \mathrm{R}_{mp}\mathrm{S}_{nq} \qquad \text{(B.30)} \\
&\quad + \mathrm{S}_{mp}\mathrm{R}_{nq} + \mathrm{S}_{mp}\mathrm{R}_{nq} + \mathrm{S}_{mp}\mathrm{R}_{nq} + \mathrm{S}_{mp}\mathrm{R}_{nq})\} \\
&\quad + \frac{1}{4}\{(\mathrm{R}_{mq}\mathrm{R}_{np} - \mathrm{R}_{mq}\mathrm{R}_{np} - \mathrm{R}_{mq}\mathrm{R}_{np} + \mathrm{R}_{mq}\mathrm{R}_{np} \\
&\quad - \mathrm{S}_{mq}\mathrm{S}_{pn} + \mathrm{S}_{mq}\mathrm{S}_{np} + \mathrm{S}_{mq}\mathrm{S}_{np} - \mathrm{S}_{mq}\mathrm{S}_{np}) \\
&\quad + j\,(\mathrm{R}_{mq}\mathrm{S}_{np} - \mathrm{R}_{mq}\mathrm{S}_{np} - \mathrm{R}_{mq}\mathrm{S}_{np} + \mathrm{R}_{mq}\mathrm{S}_{np} \\
&\quad + \mathrm{S}_{mq}\mathrm{R}_{np} - \mathrm{S}_{mq}\mathrm{R}_{np} - \mathrm{S}_{mq}\mathrm{R}_{np} + \mathrm{S}_{mq}\mathrm{R}_{np})\} \\
&= \{(\mathrm{R}_{mn}\mathrm{R}_{pq} + \mathrm{S}_{mn}\mathrm{S}_{pq}) + j\,(-\mathrm{R}_{mn}\mathrm{S}_{pq} + \mathrm{S}_{mn}\mathrm{R}_{pq})\} \\
&\quad + \{(\mathrm{R}_{mp}\mathrm{R}_{nq} + \mathrm{S}_{mp}\mathrm{S}_{nq}) + j\,(-\mathrm{R}_{mp}\mathrm{S}_{nq} + \mathrm{S}_{mp}\mathrm{R}_{nq})\}
\end{aligned}$$

Referring to equations (B.22) and (B.23), it is possible to write entries from the complex covariance matrix P in terms of R and S as shown below.

$$\mathrm{P}_{mn} = \mathrm{R}_{mn} + j\mathrm{S}_{mn} \qquad \text{(B.31)}$$

$$\mathrm{P}_{pq}^* = \mathrm{R}_{pq} - j\mathrm{S}_{pq} \qquad \text{(B.32)}$$

$$\mathrm{P}_{mp} = \mathrm{R}_{mp} + j\mathrm{S}_{mp} \qquad \text{(B.33)}$$

$$\mathrm{P}_{nq}^* = \mathrm{R}_{nq} - j\mathrm{S}_{nq} \qquad \text{(B.34)}$$

From (B.18) and (B.19), respectively, the following equalities are known.

$$E\left[\mathbf{x}_m\mathbf{x}_q\right] = 0 \qquad \text{(B.35)}$$

$$E\left[\mathbf{x}_n^*\mathbf{x}_p^*\right] = 0 \qquad \text{(B.36)}$$

Multiplying equations (B.31) and (B.32) together yields:

$$\begin{aligned} \mathrm{P}_{mn}\mathrm{P}^*_{pq} &= (\mathrm{R}_{mn} + j\mathrm{S}_{mn})(\mathrm{R}_{pq} + j\mathrm{S}_{pq}) \\ &= (\mathrm{R}_{mn}\mathrm{R}_{pq} + \mathrm{S}_{mn}\mathrm{S}_{pq}) + j(-\mathrm{R}_{mn}\mathrm{S}_{pq} + \mathrm{S}_{mn}\mathrm{R}_{pq}) \end{aligned} \tag{B.37}$$

Similarly, multiplying equations (B.33) and (B.34) together yields:

$$\begin{aligned} \mathrm{P}_{mp}\mathrm{P}^*_{nq} &= (\mathrm{R}_{mp} + j\mathrm{S}_{mp})(\mathrm{R}_{nq} + j\mathrm{S}_{nq}) \\ &= (\mathrm{R}_{mp}\mathrm{R}_{nq} + \mathrm{S}_{mp}\mathrm{S}_{nq}) + j(-\mathrm{R}_{mp}\mathrm{S}_{nq} + \mathrm{S}_{mp}\mathrm{R}_{nq}) \end{aligned} \tag{B.38}$$

Finally, multiplying equations (B.35) and (B.36) together yields:

$$E[\mathbf{x}_m\mathbf{x}_q]\,E\left[\mathbf{x}^*_n\mathbf{x}^*_p\right] = 0 \tag{B.39}$$

By comparing equations (B.30), (B.37), (B.38), and (B.39), it can be seen that (B.30) can be written as:

$$\begin{aligned} E\left[\mathbf{x}_m\mathbf{x}^*_n\mathbf{x}^*_p\mathbf{x}_q\right] &= \mathrm{P}_{mn}\mathrm{P}^*_{pq} + \mathrm{P}_{mp}\mathrm{P}^*_{nq} + E[\mathbf{x}_m\mathbf{x}_q]\,E\left[\mathbf{x}^*_n\mathbf{x}^*_p\right] \\ &= \mathrm{P}_{mn}\mathrm{P}^*_{pq} + \mathrm{P}_{mp}\mathrm{P}^*_{nq} \end{aligned} \tag{B.40}$$

B.4 Covariance Matrix Expansion

Equation (B.23) claims that the covariance matrix of the expanded real vector $\mathbf{v}$ can be written as:

$$\mathrm{Q} = \frac{1}{2}\begin{bmatrix} \mathrm{R} & \mathrm{S}^T \\ \mathrm{S} & \mathrm{R} \end{bmatrix} \tag{B.41}$$

where the submatrices are the real (symmetric) and imaginary (skew-symmetric) components of the complex covariance matrix of $\mathbf{x}$.

$$\mathrm{P} = \mathrm{R} + j\mathrm{S} \tag{B.42}$$

The covariance matrix of $\mathbf{x} = \mathbf{y} + j\mathbf{z}$ can be written as:

$$\begin{aligned} \mathrm{P} &= E[\mathbf{x}\mathbf{x}^*] = E\left[(\mathbf{y} + j\mathbf{z})\left(\mathbf{y}^T - j\mathbf{z}^T\right)\right] \\ &= E\left[\left(\mathbf{y}\mathbf{y}^T + \mathbf{z}\mathbf{z}^T\right) + j\left(\mathbf{z}\mathbf{y}^T - \mathbf{y}\mathbf{z}^T\right)\right] \end{aligned} \tag{B.43}$$

By equating the real and imaginary terms in (B.42) and (B.43), it can be seen that:

$$\mathrm{R} = E\left[\mathbf{y}\mathbf{y}^T + \mathbf{z}\mathbf{z}^T\right] = E\left[\mathbf{y}\mathbf{y}^T\right] + E\left[\mathbf{z}\mathbf{z}^T\right] \tag{B.44}$$

$$\mathrm{S} = E\left[\mathbf{z}\mathbf{y}^T - \mathbf{y}\mathbf{z}^T\right] = E\left[\mathbf{z}\mathbf{y}^T\right] - E\left[\mathbf{y}\mathbf{z}^T\right] \tag{B.45}$$

Since $\mathbf{y}$ and $\mathbf{z}$ should have identical distributions, their covariance matrices are constrained to be equal and equation (B.44) gives:

$$E\left[\mathbf{y}\mathbf{y}^T\right] = E\left[\mathbf{z}\mathbf{z}^T\right] = \frac{1}{2}\mathrm{R} \tag{B.46}$$

It can easily be seen that the general solution to (B.45) can be written in the form:

$$\mathrm{V} = \mathrm{W} + \frac{1}{2}\mathrm{S} \tag{B.47}$$

where W is an arbitrary symmetric matrix and:

$$E\left[\mathbf{z}\mathbf{y}^T\right] = \mathrm{V} = \mathrm{W} + \frac{1}{2}\mathrm{S} \tag{B.48}$$

$$E\left[\mathbf{y}\mathbf{z}^T\right] = \mathrm{V}^T = \mathrm{W} - \frac{1}{2}\mathrm{S} \tag{B.49}$$

Subtracting (B.49) from (B.48) yields:

$$E\left[\mathbf{z}\mathbf{y}^T\right] - E\left[\mathbf{y}\mathbf{z}^T\right] = \left(\mathrm{W} + \frac{1}{2}\mathrm{S}\right) - \left(\mathrm{W} - \frac{1}{2}\mathrm{S}\right) = \mathrm{S} \tag{B.50}$$

Consequently, equation (B.45) is satisfied and it now only remains to show that W must be zero.

Recall that $\mathbf{y}$ and $\mathbf{z}$ represent the real and imaginary parts of $\mathbf{x}$, respectively. They should also be identically distributed. Therefore, V should be either a symmetric or skew-symmetric matrix. By performing a 90° rotation of the axes which maps $\mathbf{y}$ to $\mathbf{z}$ and $\mathbf{z}$ to $-\mathbf{y}$, and consulting equations (B.48) and (B.49), it can be seen that V must necessarily be a skew-symmetric matrix. Thus, W must be zero and it has now been shown that equation (B.41) holds.

Bibliography

[1] Sidney P. Applebaum. "Adaptive arrays". *IEEE Transactions on Antennas and Propagation*, 24(5):585–598, 1976.

[2] Sirikiat Ariyavisitakul. "Signal and interference statistics of a CDMA system with feedback power control – Part II". *IEEE Transactions on Communications*, 42(2/3/4):597–605, 1994.

[3] Sirikiat Ariyavisitakul and Li Fung Chang. "Signal and interference statistics of a CDMA system with feedback power control". *IEEE Transactions on Communications*, 41(11):1626–1634, 1993.

[4] Rick Cameron and Brian Woerner. "Performance analysis of CDMA with imperfect power control". *IEEE Transactions on Communications*, 44(7):777–781, 1996.

[5] L.F. Chang and S. Ariyavisitakul. "Performance of power control method for CDMA radio communications system". *Electronics Letters*, 27(11):920–922, 1991.

[6] Li Fung Chang, Fuyun Ling, David D. Falconer, and Nelson R. Sollenberger. "Comparison of two convolutional orthogonal coding techniques for CDMA radio communications systems". *IEEE Transactions on Communications*, 43(6):2028–2037, 1995.

[7] A. Chockalingam and Laurence B. Milstein. "Performance of DS-CDMA networks on Rician fading channels with open-loop power control". In *28th Asilomar Conference on Signals, Systems and Computers*, pages 837–841, 1994.

[8] A. Chockalingam and Laurence B. Milstein. "Capacity of DS-CDMA networks on frequency selective fading channels with open-loop power control". In *1995 International Conference on Communications*, pages 703–707, 1995.

[9] Geoffrey W.K. Colman, Steven D. Blostein, and Norman C. Beaulieu. "An ARMA multipath fading simulator". In *The 7th Annual Virginia Tech Symposium on Wireless Personal Communications*, 1997.

[10] Ronald D. DeGroat. "Noniterative subspace tracking". *IEEE Transactions on Signal Processing*, 40(3):571–577, 1992.

[11] Edward J. Dudewicz and Satya N. Mishra. *Modern Mathematical Statistics*. John Wiley & Sons, 1988.

[12] Donald L. Duttweiler, James E. Mazo, and David G. Messerschmitt. "An upper bound on the error probability in decision-feedback equalization". *IEEE Transactions on Information Theory*, 20(4):490–497, 1974.

[13] A. Mark Earnshaw and Steven D. Blostein. "Unbiased estimation of camera translation direction from optical flow using linear constraints". In *1994 Canadian Conference on Electrical and Computer Engineering*, volume I, pages 392–395, 1994.

[14] A. Mark Earnshaw and Steven D. Blostein. "An error analysis of camera translation direction estimation from optical flow using linear constraints". In *1995 International Conference on Image Processing*, pages 394–397, 1995.

[15] A. Mark Earnshaw and Steven D. Blostein. "A chip-level IS95-compliant cellular CDMA simulator: Design, implementation, and analysis". Technical report, Department of Electrical and Computer Engineering, Queen's University, 1996. Available from `http://ipcl.ee.queensu.ca`.

[16] A. Mark Earnshaw and Steven D. Blostein. "Investigating the effects of imperfect digital beamforming on cell capacity in a cellular CDMA communication system". In *1996 International Conference on Universal Personal Communications*, pages 458–462, 1996.

[17] A. Mark Earnshaw and Steven D. Blostein. "The performance of camera translation direction estimators from optical flow: Analysis, comparison, and theoretical limits". *IEEE Transactions on Pattern Analysis and Machine Intelligence*, 18(9):927–932, 1996.

[18] A. Mark Earnshaw and Steven D. Blostein. "A combined soft-decision deinterleaver/decoder for the IS-95 uplink", 1997. Submitted to *IEEE Transactions on Vehicular Technology.*

[19] A. Mark Earnshaw and Steven D. Blostein. "A perturbation analysis and performance bound for the estimation of 3-D camera translation direction", 1997. Submitted to the *Canadian Journal of Electrical and Computer Engineering.*

[20] Alper T. Erdogan, Ayman F. Naguib, and Arogyaswami Paulraj. "The effect of directional antennas in CDMA wireless local loop systems". In *MPRG Wireless Personal Communications Symposium*, 1995.

[21] Robert M. Fano. "A heuristic discussion of probabilistic decoding". *IEEE Transactions on Information Theory*, 9:64–74, 1963.

[22] David D. Feldman. "An analysis of the projection method for robust adaptive beamforming". *IEEE Transactions on Antennas and Propagation*, 44(7):1023–1030, 1996.

[23] David D. Feldman and Lloyd J. Griffiths. "A projection approach for robust adaptive beamforming". *IEEE Transactions on Signal Processing*, 42(4):867–876, 1994.

[24] Paul G. Flikkema. "Spread-spectrum techniques for wireless communications". *IEEE Signal Processing Magazine*, 14(3):26–36, 1997.

[25] G. David Forney, Jr. "The Viterbi algorithm". *Proceedings of the IEEE*, 61(3):268–278, 1973.

[26] Gerard J. Foschini. "Layered space-time architecture for wireless communication in a fading environment when using multi-element antennas". *Bell Labs Technical Journal*, 1(2):41–59, 1996.

[27] D. Gerlach and A. Paulraj. "Base-station transmitting antenna arrays with mobile to base feedback". In *27th Asilomar Conference on Signals, Systems and Computers*, pages 1432–1436, 1993.

[28] Filippo Giannetti. "Capacity evaluation of a cellular CDMA system operating in the 63-64 GHz band". *IEEE Transactions on Vehicular Technology*, 46(1):55–64, 1997.

[29] Klein S. Gilhousen, Irwin M. Jacobs, Roberto Padovani, Andrew J. Viterbi, Jr. Lindsay A. Weaver, and Charles E. Wheatley III. "On the capacity of a cellular CDMA system". *IEEE Transactions on Vehicular Technology*, 40(2):303–312, 1991.

[30] John D. Gorman and Alfred O. Hero. "Lower bounds for parametric estimation with constraints". *IEEE Transactions on Information Theory*, 36(6):1285–1301, 1990.

[31] John Doolin Gorman. *Error Bounds in Constrained Estimation.* PhD thesis, Dept. of Electrical Engineering, University of Michigan, 1991.

[32] Stephen V. Hanly. "An algorithm for combined cell-site selection and power control to maximize cellular spread spectrum capacity". *IEEE Journal on Selected Areas in Communications*, 13(7):1332–1340, 1995.

[33] Philip Harley. "Short distance attenuation measurements at 900 MHz and 1.8 GHz using low antenna heights for microcells". *IEEE Journal on Selected Areas in Communications*, 7(1):5–11, 1989.

[34] Jack M. Holtzman. "A simple, accurate method to calculate spread-spectrum multiple-access error probabilities". *IEEE Transactions on Communications*, 40(3):461–464, 1992.

[35] Chih-Lin I, Charles A. Webb III, Howard C. Huang, Stephan ten Brink, Sanjiv Nanda, and Richard D. Gitlin. "IS-95 enhancements for multimedia services". *Bell Labs Technical Journal*, 1(2):60–87, 1996.

[36] Garrick T. Irvine and Peter J. McLane. "Symbol-aided plus decision-directed reception for PSK/TCM modulation on shadowed mobile satellite fading channels". *IEEE Journal on Selected Areas in Communications*, 10(8):1289–1299, 1992.

[37] Ahmad Jalali and Paul Mermelstein. "Effects of diversity, power control, and bandwidth on the capacity of microcellular CDMA systems". *IEEE Journal on Selected Areas in Communications*, 12(5):952–961, 1994.

[38] Louay M. A. Jalloul and Jack M. Holtzman. "Performance analysis of DS/CDMA with non-coherent M-ary orthogonal modulation in multipath fading channels". *IEEE Journal on Selected Areas in Communications*, 12(5):862–870, 1994.

[39] Michel G. Jansen and Ramjee Prasad. "Capacity, throughput, and delay analysis of a cellular DS CDMA system with imperfect power control and imperfect sectorization". *IEEE Transactions on Vehicular Technology*, 44(1):67–75, 1995.

[40] F. Jelinek. "Fast sequential decoding algorithm using a stack". *IBM Journal of Research and Development*, 13(6):675–685, 1969.

[41] Akihiro Kajiwara. "Effects of cell size, directional antenna, diversity, and shadowing on indoor radio CDMA capacity". *IEEE Transactions on Vehicular Technology*, 46(1):242–247, 1997.

[42] J.G. Kalbfleisch. *Probability and Statistical Inference*, volume 1: Probability. Springer-Verlag, 1985.

[43] Chamroeun Kchao and Gordon L. Stüber. "Analysis of a direct-sequence spread-spectrum cellular radio system". *IEEE Transactions on Communications*, 41(10):1507–1516, 1993.

[44] J.Y. Kim and J.H. Lee. "Effect of imperfect power control on acquisition performance in a DS/CDMA system". *Electronics Letters*, 32(14):1255–1256, 1996.

[45] Hamid Krim and Mats Viberg. "Two decades of array signal processing research". *IEEE Signal Processing Magazine*, 13(4):67–94, 1996.

[46] C.-C. Lee and R. Steele. "Closed-loop power control in CDMA systems". *IEE Proceedings – Communications*, 143(4):231–239, 1996.

[47] Cheng-Chou Lee and Ju-Hong Lee. "Robust adaptive array beamforming under steering vector errors". *IEEE Transactions on Antennas and Propagation*, 45(1):168–175, 1997.

[48] William C.Y. Lee. "Overview of cellular CDMA". *IEEE Transactions on Vehicular Technology*, 40(2):291–302, 1991.

[49] James S. Lehnert. "An efficient technique for evaluating direct-sequence spread-spectrum multiple-access communications". *IEEE Transactions on Communications*, 37(8):851–858, 1989.

[50] James S. Lehnert and Michael B. Pursley. "Error probabilities for binary direct-sequence spread-spectrum communications with random signature sequences". *IEEE Transactions on Communications*, 35(1):87–98, 1987.

[51] Khaled Ben Letaief. "Efficient evaluation of the error probabilities of spread-spectrum multiple-access communications". *IEEE Transactions on Communications*, 45(2):239–246, 1997.

[52] Khaled Ben Letaief, Khurram Muhammad, and John S. Sadowsky. "Fast simulation of DS/CDMA with and without coding in multipath fading channels". *IEEE Journal on Selected Areas in Communications*, 15(4):626–639, 1997.

[53] Yiu-Wing Leung. "Power control in cellular networks subject to measurement error". *IEEE Transactions on Communications*, 44(7):772–775, 1996.

[54] Jen-Wei Liang and Arogyaswami J. Paulraj. "On optimizing base station antenna array topology for coverage extension in cellular radio networks". In *1995 IEEE 45th Vehicular Technology Conference*, pages 866–870, 1995.

[55] Joseph C. Liberti, Jr. and Theodore S. Rappaport. "Analytical results for capacity improvements in CDMA". *IEEE Transactions on Vehicular Technology*, 43(3):680–690, 1994.

[56] Chun Loo. "A statistical model for a land mobile satellite link". *IEEE Transactions on Vehicular Technology*, 34(3):122–127, 1985.

[57] Ruxandra Lupas and Sergio Verdú. "Linear multiuser detectors for synchronous code-division multiple-access channels". *IEEE Transactions on Information Theory*, 35(1):123–136, 1989.

[58] Ruxandra Lupas and Sergio Verdú. "Near-far resistance of multiuser detectors in asynchronous channels". *IEEE Transactions on Communications*, 38(4):777–781, 1990.

[59] Peter S. Maybeck. *Stochastic Models, Estimation, and Control*, volume 1. Academic Press, Inc., 1979.

[60] Michael J. Miller, Branka Vucetic, and Les Berry, editors. *Satellite Communications: Mobile and Fixed Services*. Kluwer Academic Publishers, 1993.

[61] Laurence B. Milstein, Theodore S. Rappaport, and Rashad Barghouti. "Performance evaluation for cellular CDMA". *IEEE Journal on Selected Areas in Communications*, 10(4):680–689, 1992.

[62] Robert A. Monzingo and Thomas W. Miller. *Introduction to Adaptive Arrays*. John Wiley & Sons, Inc., 1980.

[63] Shimon Moshavi. "Multi-user detection for DS-CDMA communications". *IEEE Communications Magazine*, 34(10):124–136, 1996.

[64] Ayman F. Naguib. *Adaptive Antennas for CDMA Wireless Networks*. PhD thesis, Dept. of Electrical Engineering, Stanford University, 1995.

[65] Ayman F. Naguib. "Power control in wireless CDMA: Performance with cell site antenna arrays". In *1995 Global Communication Conference*, pages 225–229, 1995.

[66] Ayman F. Naguib and Arogyaswami Paulraj. "Effects of multipath and base-station antenna arrays on uplink capacity of cellular CDMA". In *1994 Global Communication Conference*, pages 395–399, 1994.

[67] Ayman F. Naguib and Arogyaswami Paulraj. "Performance of CDMA cellular networks with base-station antenna arrays". In *1994 International Zurich Seminar on Digital Communications*, pages 87–100, 1994.

[68] Ayman F. Naguib and Arogyaswami Paulraj. "Performance enhancement and trade-offs of smart antennas in CDMA cellular networks". In *1995 IEEE 45th Vehicular Technology Conference*, pages 40–44, 1995.

[69] Ayman F. Naguib and Arogyaswami Paulraj. "Performance of DS/CDMA with M-ary orthogonal modulation cell site antenna arrays". In *1995 International Conference on Communications*, pages 697–702, 1995.

[70] Ayman F. Naguib and Arogyaswami Paulraj. "Recursive adaptive beamforming for wireless CDMA". In *1995 International Conference on Communications*, pages 1515–1519, 1995.

[71] Ayman F. Naguib and Arogyaswami Paulraj. "Performance of wireless CDMA with M-ary orthogonal modulation and cell site antenna arrays". *IEEE Journal on Selected Areas in Communications*, 14(9):1770–1783, 1996.

[72] Ayman F. Naguib, Arogyaswami Paulraj, and Thomas Kailath. "Capacity improvement of base-station antenna arrays: Cellular CDMA". In *27th Asilomar Conference on Signals, Systems and Computers*, pages 1437–1441, 1993.

[73] Ayman F. Naguib, Arogyaswami Paulraj, and Thomas Kailath. "Capacity improvement with base-station antenna arrays in cellular CDMA". *IEEE Transactions on Vehicular Technology*, 43(3):691–698, 1994.

[74] Ayman F. Naguib, Arogyaswami Paulraj, and Thomas Kailath. "Performance of CDMA cellular networks with base-station antenna arrays: The downlink". In *1994 International Conference on Communications*, pages 795–799, 1994.

[75] John Panicker and Surinder Kumar. "Effect of system imperfections on BER performance of a CDMA receiver with multipath diversity combining". *IEEE Transactions on Vehicular Technology*, 45(4):622–630, 1996.

[76] Athanasios Papoulis. *Probability, Random Variables, and Stochastic Processes*. McGraw-Hill, Inc., 1984.

[77] Bernard Picinbono. "On circularity". *IEEE Transactions on Signal Processing*, 42(12):3473–3482, 1994.

[78] Bernard Picinbono. "Second-order complex random vectors and normal distributions". *IEEE Transactions on Signal Processing*, 44(10):2637–2640, 1996.

[79] Bernard Picinbono and Pascal Bondon. "Second-order statistics of complex signals". *IEEE Transactions on Signal Processing*, 45(2):411–420, 1997.

[80] Raymond L. Pickholtz, Laurence B. Milstein, and Donald L. Schilling. "Spread spectrum for mobile communications". *IEEE Transactions on Vehicular Technology*, 40(2):313–322, 1991.

[81] Raymond L. Pickholtz, Donald L. Schilling, and Laurence B. Milstein. "Theory of spread-spectrum communications – A tutorial". *IEEE Transactions on Communications*, 30(5):855–884, 1982.

[82] S. Unnikrishna Pillai. *Array Signal Processing*. Springer-Verlag, 1989.

[83] R. Prasad, A. Kegel, and M.G. Jansen. "Effect of imperfect power control on cellular code division multiple access system". *Electronics Letters*, 28(9):848–849, 1992.

[84] John G. Proakis. *Digital Communications*. McGraw-Hill, Inc., 1989.

[85] Qualcomm Inc. "An overview of the application of code division multiple access (CDMA) to digital cellular systems and personal cellular networks", 1992.

[86] Qualcomm Inc. "Mobile station-base compatibility standard for dual-mode wideband spread system", 1993.

[87] Gregory Raleigh, Suhas N. Diggavi, Ayman F. Naguib, and Arogyaswami Paulraj. "Characterization of fast fading vector channels for multi-antenna communication systems". In *28th Asilomar Conference on Signals, Systems and Computers*, pages 853–857, 1994.

[88] Richard Roy and Thomas Kailath. "ESPRIT – Estimation of signal parameters via rotational invariance techniques". *IEEE Transactions on Acoustics, Speech, and Signal Processing*, 37(7):984–995, 1989.

[89] Ron Rudokas. "Capacity losses in sector and microcell cellular systems". *IEEE Communications Letters*, 1(2):43–45, 1997.

[90] Jack Salz and Jack H. Winters. "Effect of fading correlation on adaptive arrays in digital wireless communications". In *1993 International Conference on Communications*, volume 3, pages 1768–1774, 1993.

[91] Jack Salz and Jack H. Winters. "Effect of fading correlation on adaptive arrays in digital mobile radio". *IEEE Transactions on Vehicular Technology*, 43(4):1049–1057, 1994.

[92] Ralph O. Schmidt. "Multiple emitter location and signal parameter estimation". *IEEE Transactions on Antennas and Propagation*, 34(3):276–280, 1986.

[93] Wan Yi Shiu and Steven D. Blostein. "Adaptive digital beamforming in cellular CDMA systems using noniterative signal subspace tracking". In *1997 International Conference on Communications*, pages 652–656, 1997.

[94] Bernard Sklar. "Rayleigh fading channels in mobile digital communication systems – Part I: Characterization". *IEEE Communications Magazine*, 35(7):90–100, 1997.

[95] Bernard Sklar. "Rayleigh fading channels in mobile digital communication systems – Part II: Mitigation". *IEEE Communications Magazine*, 35(7):102–109, 1997.

[96] Peter J. Smith, Mansoor Shafi, and Hongsheng Gao. "Quick simulation: A review of importance sampling techniques in communications systems". *IEEE Journal on Selected Areas in Communications*, 15(4):597–613, 1997.

[97] Essam A. Sourour and Masao Nakagawa. "Performance of orthogonal multicarrier CDMA in a multipath fading channel". *IEEE Transactions on Communications*, 44(3):356–367, 1996.

[98] Gordon L. Stüber and Chamroeun Kchao. "Analysis of a multiple-cell direct-sequence CDMA cellular mobile radio system". *IEEE Journal on Selected Areas in Communications*, 10(4):669–679, 1992.

[99] Simon C. Swales, Mark A. Beach, David J. Edwards, and Joseph P. McGeehan. "The performance enhancement of multibeam adaptive base-station antennas for cellular land mobile radio systems". *IEEE Transactions on Vehicular Technology*, 39(1):56–67, 1990.

[100] Michail K. Tsatsanis and Georgios B. Giannakis. "Optimal decorrelating receivers for DS-CDMA systems: A signal processing framework". *IEEE Transactions on Signal Processing*, 44(12):3044–3055, 1996.

[101] Barry D. Van Veen and Kevin M. Buckley. "Beamforming: A versatile approach to spatial filtering". *IEEE ASSP Magazine*, pages 4–24, April 1988.

[102] Sergio Verdú. "Minimum probability of error for asynchronous Gaussian multiple-access channels". *IEEE Transactions on Information Theory*, 32(1):85–96, 1986.

[103] A.J. Viterbi and J.K. Omura. *Principles of Digital Commmunication and Coding.* McGraw-Hill, 1979.

[104] Andrew J. Viterbi. "Error bounds for convolutional codes and an asymptotically optimum decoding algorithm". *IEEE Transactions on Information Theory*, 13(2):260–269, 1967.

[105] Andrew J. Viterbi. *CDMA: Principles of Spread Spectrum Communication.* Addison-Wesley, 1995.

[106] Andrew J. Viterbi, Audrey M. Viterbi, and Ephraim Zehavi. "Performance of power-controlled wideband terrestrial digital communication". *IEEE Transactions on Communications*, 41(4):559–569, 1993.

[107] Audrey M. Viterbi and Andrew J. Viterbi. "Erlang capacity of a power controlled CDMA system". *IEEE Journal on Selected Areas in Communications*, 11(6):892–900, 1993.

[108] Yiping Wang and J.R. Cruz. "Adaptive antenna arrays for cellular CDMA communication systems". In *1995 International Conference on Acoustics, Speech, and Signal Processing*, pages 1725–1728, 1995.

[109] Mati Wax and Yosef Anu. "Performance analysis of the minimum variance beamformer". *IEEE Transactions on Signal Processing*, 44(4):928–937, 1996.

[110] Mati Wax and Yosef Anu. "Performance analysis of the minimum variance beamformer in the presence of steering vector errors". *IEEE Transactions on Signal Processing*, 44(4):938–947, 1996.

[111] Juyang Weng, Thomas S. Huang, and Narendra Ahuja. "Motion and structure from two perspective views: Algorithms, error analysis, and error estimation". *IEEE Transactions on Pattern Analysis and Machine Intelligence*, 11(5):451–476, 1989.

[112] J.H. Wilkinson. *The Algebraic Eigenvalue Problem.* Oxford University Press, 1965.

[113] Jianming Wu and Ryuji Kohno. "A wireless multimedia CDMA system based on transmission power control". *IEEE Journal on Selected Areas in Communications*, 14(4):683–691, 1996.

[114] Qiang Wu and Kon Max Wong. "Blind adaptive beamforming for cyclostationary signals". *IEEE Transactions on Signal Processing*, 44(11):2757–2767, 1996.

[115] Qiang Wu, Wei-Ling Wu, and Jiong-Pan Zhou. "Centralised power control in CDMA cellular mobile systems". *Electronics Letters*, 33(2):115–116, 1997.

[116] Howard H. Xia, Henry L. Bertoni, Leandro R. Maciel, Andrew Lindsay-Stewart, and Robert Rowe. "Microcellular propagation characteristics for personal communications in urban and suburban environments". *IEEE Transactions on Vehicular Technology*, 43(3):743–752, 1994.

[117] Roy D. Yates and Ching-Yao Huang. "Integrated power control and base station assignment". *IEEE Transactions on Vehicular Technology*, 44(3):638–644, 1995.

[118] Shiann-Jeng Yu and Ju-Hong Lee. "The statistical performance of eigenspace-based adaptive array beamformers". *IEEE Transactions on Antennas and Propagation*, 44(5):665–671, 1996.

[119] Shiann-Jeng Yu and Ju-Hong Lee. "Design of two-dimensional rectangular array beamformers with partial adaptivity". *IEEE Transactions on Antennas and Propagation*, 45(1):157–167, 1997.

[120] Norman Yuen and Benjamin Friedlander. "Asymptotic performance analysis of ESPRIT, higher order ESPRIT, and virtual ESPRIT algorithms". *IEEE Transactions on Signal Processing*, 44(10):2537–2550, 1996.

[121] Jens Zander. "Distributed cochannel interference control in cellular radio systems". *IEEE Transactions on Vehicular Technology*, 41(3):305–311, 1992.

[122] Jens Zander. "Performance of optimum transmitter power control in cellular radio systems". *IEEE Transactions on Vehicular Technology*, 41(1):57–62, 1992.

Vita

A. Mark Earnshaw

EDUCATION

Queen's University	Ph.D.	Electrical and Computer Engineering	1991–97
University of Waterloo	M.A.Sc.	Systems Design Engineering	1989–91
University of Waterloo	B.A.Sc.	Systems Design Engineering	1984–89

EXPERIENCE

Radio System Designer (1997–), Nortel, Nepean, Ontario

Adjunct Instructor (1995,1996), Electrical and Computer Engineering, Queen's University

Research Assistant (1991–1997), Electrical and Computer Engineering, Queen's University

Teaching Assistant (1991–1994), Electrical and Computer Engineering, Queen's University

Research Assistant (1989–1991), Systems Design Engineering, University of Waterloo

Teaching Assistant (1989–1991), Systems Design Engineering, University of Waterloo

PUBLICATIONS

A. Mark Earnshaw and Steven D. Blostein (1997), "An Error Analysis of Feedback Correlation Beamforming for the IS-95 Reverse Link", Submitted to *1998 International Conference on Communications.*

A. Mark Earnshaw and Steven D. Blostein (1997), "Efficient Evaluation of Adaptive Digital Beamforming for Multi-Service Provision in a Cellular CDMA System", Submitted to *1998 Vehicular Technology Conference.*

A. Mark Earnshaw and Steven D. Blostein (1997), "A Combined Soft-Decision Deinterleaver/Decoder for the IS-95 Uplink", Submitted to *IEEE Transactions on Vehicular Technology.*

A. Mark Earnshaw and Steven D. Blostein (1997), "A Perturbation Analysis and Performance Bound for the Estimation of 3-D Camera Translation Direction", To appear in the *Canadian Journal of Electrical and Computer Engineering.*

A. Mark Earnshaw and Steven D. Blostein (1996), "Investigating the Effects of Imperfect Digital Beamforming on Cell Capacity in a Cellular CDMA Communication System", *1996 International Conference on Universal Personal Communications.*

A. Mark Earnshaw and Steven D. Blostein (1996), "A Chip-Level IS95-Compliant Cellular CDMA Simulator: The Reverse Link", Submitted to *IEEE Journal on Selected Areas in Communications.*

A. Mark Earnshaw and Steven D. Blostein (1996), "A Chip-Level IS95-Compliant Cellular CDMA Simulator: Design, Implementation, and Analysis", Technical Report, Department of Electrical and Computer Engineering, Queen's University.

A. Mark Earnshaw and Steven D. Blostein (1996), "The Performance of Camera Translation Direction Estimators from Optical Flow: Analysis, Comparison, and Theoretical Limits", *IEEE Transactions on Pattern Analysis and Machine Intelligence.*

A. Mark Earnshaw and Steven D. Blostein (1995), "An Error Analysis of Camera Translation Direction Estimation from Optical Flow Using Linear Constraints", *1995 IEEE International Conference on Image Processing.*

A. Mark Earnshaw and Steven D. Blostein (1995), "The Performance of Camera Translation Direction Estimators", Technical Report, Department of Electrical and Computer Engineering, Queen's University.

A. Mark Earnshaw and Steven D. Blostein (1994), "Unbiased Estimation of Camera Translation Direction from Optical Flow Using Linear Constraints", *1994 Canadian Conference on Electrical and Computer Engineering.*

A. Mark Earnshaw and Andrew K. C. Wong (1991), "3-D Object Model Synthesis in a Monocular Imaging System", Advances in Machine Vision – Strategies and Applications.

A. Mark Earnshaw and Andrew K. C. Wong (1991), "3-D Object Model Synthesis in a Monocular Imaging System", *Vision Interface 91.*